HAL
open science

Déformation des unités métamorphiques de haute pression de la subduction à l'exhumation. (Exemple des Cyclades, Grèce)

Melody Philippon

▶ **To cite this version:**

Melody Philippon. Déformation des unités métamorphiques de haute pression de la subduction à l'exhumation. (Exemple des Cyclades, Grèce). Sciences de la Terre. Universite Rennes 1, 2010. Français. NNT : . tel-01137796

HAL Id: tel-01137796

https://insu.hal.science/tel-01137796v1

Submitted on 31 Mar 2015

HAL is a multi-disciplinary open access archive for the deposit and dissemination of scientific research documents, whether they are published or not. The documents may come from teaching and research institutions in France or abroad, or from public or private research centers.

L'archive ouverte pluridisciplinaire **HAL**, est destinée au dépôt et à la diffusion de documents scientifiques de niveau recherche, publiés ou non, émanant des établissements d'enseignement et de recherche français ou étrangers, des laboratoires publics ou privés.

Déformation des unités métamorphiques de haute pression de la subduction à l'exhumation.

(Exemple des Cyclades, Grèce)

Mélody Philippon

18 Octobre 2010

Alternance Marbres Schistes de l'unité de Kastri (37°29'11,58''N, 24°53'55,44''E)

Directeur de thèse Jean-Pierre Brun
Co-Directeur de thèse : Frédéric Gueydan

Sommaire

Résumé 6
Abstract 7
Introduction 9

PARTIE 1/ INTRODUCTION ET PROBLEMES 11

Chapitre 1: Métamorphisme et zone de Subduction 13
1.1. Les faciès métamorphiques 15
1.2. Les « Paired Metamorphic Belts» 16
1.3. Deux types de frontières de plaques 17

Chapitre 2: Les roches métamorphiques : observables géologiques 21
2.1. Pétrologie, géochronologie et rhéologie 23
2.2. Structures et déformation interne des unités métamorphiques 27

Chapitre 3: Les processus d'exhumation des roches métamorphiques 31
3.1. Dynamique des frontières de plaque en convergence : évolution des concepts 33
3.2. Les modèles d'exhumation 33

Chapitre 4 Les schistes bleus Cycladiques 48
4.1. L'âge de l'extension Egéenne : une brève revue 50
4.2. L'exhumation des schistes bleus cycladiques : évolution des concepts. 52

PARTIE 2/ DEFORMATION D'UNE UNITE HP-BT LORS DE LA SUBDUCTION ET DE L'EXHUMATION: EXEMPLE DE L'ILE DE SYROS 65

Chapitre 5 : Les pseudomorphes de Lawsonites : une jauge de non déformation des schistes bleus. 67
Abstract 69
5.1. Introduction 69
5.2. Regional Geology 70
5.3. Ductile deformation and Lawsonite pseudomorphs 71
5.4. Discussion 74
5.5. Conclusions 75

Chapitre 6 : Des données de terrain au modèle 3D 82
Abstract 84
6.1. Introduction 85
6.2. Geological background 88
6.3. Available data and 3-D methodology 91
6.4 Structural pattern 93
6.5. Discussion and conclusions 102
6.6. Interpolation of foliation 111
6.7. Building 3-D geological surfaces from field data using implicit functions 111

Chapitre 7 : Histoire tectonique de l'île de Syros : de la subduction à l'extension Egéenne. 115
Abstract 117
7.1. Introduction 118
7.2. Geological setting 119
7.3. General structure 120

7.4. Ductile deformation 124
7.5. Flat & Ramp extensional system 129
7.6. Discussion-Conclusions 137

PARTIE 3/ UN NOUVEAU MODELE D'EVOLUTION TECTONIQUE POUR LES SCHISTES BLEUS CYCLADIQUES. 152

Chapitre 8 : Enregistrement de la subduction et de l'exhumation dans les schistes bleus cycladiques (Mer Egée, Grèce). 154
Abstract 156
8.1. Introduction 156
8.2. The Cycladic Blueschists Unit 157
8.3. Kinematics of extension and subduction 165
8.4. Segmentation of the Cycladic Blueschists Unit since middle Miocene 168
8.5. Map restoration of the post-Serravalian deformation 177
8.6. Ductile shearing related to subduction 183
8.7. Discussion 186
Conclusion 189

Chapitre 9: L'extension Egéenne et extrusion de l'Anatolie depuis 15 Ma. 208
Abstract 210
9.1. Introduction 210
9.2. Effect of Input Parameters 212
9.3. Aegean extension since Tortonian 218
9.4. Appendix 219

PARTIE 4/ CONCLUSIONS GENERALES 225
10.1 Méthodologie d'analyse structurale 227
10.2 Tectonique Egéenne 230
10.3. L'extension Egéenne et l'extrusion de l'Anatolie depuis 15 Ma. 238
Références 243

ANNEXE A : Estimations PT 277

ANNEXE B : Tentative de datation des sphènes 286

ANNEXE C : Philippon et al., 2009 289

ANNEXE D : Carte géologique de l'île de Syros 1 :50000 305

Annexe E : Coupes géologiques de l'île de Syros 1 :50000 307

Annexe F : Dimensionnement des expériences analogiques 309

Résumé

Les roches métamorphiques de haute pression – basse température sont des témoins du fonctionnement des zones de subduction à l'échelle de la lithosphère. Lors de leur enfouissement ces roches subissent un métamorphisme prograde, puis retrograde pendant leur exhumation, et une évolution des déformations de ductiles à fragiles. Cette thèse présente une analyse des déformations successives enregistrées par l'unité des Schistes Bleus Cycladiques (SBC) en Grèce pendant un cycle subduction-exhumation, dans le cadre de l'extension arrière-arc du Domaine Egéen.

L'étude des déformations ductiles enregistrées par les SBC a permis de distinguer celles associées à l'enfouissement, pendant la subduction, de celles synchrones de l'exhumation et de caractériser leur cinématique dans le contexte dynamique de l'extension égéenne. Une restauration des déformations postérieures à 12 Ma montre que l'extension Miocène inférieur à moyen n'est due qu'à un seul détachement, le Détachement Nord Cycladique, contrôlant le développement d'un seul dôme extensif, le Core Complex des Cyclades Centrales.

Des expériences de laboratoire sur modèles réduits ont permis d'argumenter que la déformation égéenne, depuis 12 Ma, résultait d'une interaction entre le retrait vers le SW de la subduction Hellenique et le déplacement vers l'ouest de l'Anatolie, au moins 7 Ma plus tôt qu'on le pensait jusqu'à présent. La zone plissée du centre des Cyclades en est un témoin géologique direct. Les expériences ont aussi montré que la suture du Vardar a joué un rôle important dans ce processus, en tant que zone de faiblesse mécanique.

Mots Clés : unités métamorphiques de haute pression, subduction Hellenique, exhumation des roches de haute pression, core complexes, cinématique de la déformation.

Abstract

High pressure-low temperature metamorphic rocks are witness of the behaviour of subduction zones at lithosphere scale. These rocks undergo prograde and retrograde metamorphism during burial and exhumation, respectively. During exhumation, deformation evolves from ductile to brittle. The present thesis consists in an analysis of the successive deformations recorded by the Cycladic Blueschist Unit (CBU) in Greece during a subduction-exhumation cycle, in the frame of the Aegean back-arc extension.
The study of ductile deformations recorded by the CBU was used to separate those associated to burial, during subduction, from those related to exhumation and to characterise their kinematics in the frame of the Aegean extension dynamics. A restoration of post-12 Ma deformations shows that in early to middle Miocene deformation is due to only one detachment (the North Cycladic Detachment) controlled only one core complex (the Central Cyclades Core Complex).

Laboratory experiments on small-scale models have been used to argue that Aegean extension, since 12 Ma, resulted from an interaction between the Hellenic subduction retreat toward the SW and the westward displacement of Anatolia at least 7 years earlier than what was thought up to now. The folded domain of the central Cyclades is a direct witness of this interaction. The experiments also show that the Vardar suture has played an important localising role in this process as a pre-existing weak zone.

Keywords : high pressure metamorphic units, Hellenic subduction, HP rocks exhumation, core complexes, kinematic of deformation.

Introduction

Les zones de subduction sont une particularité géologique propre au système Terre. Elles participent pour une grande part à la tectonique des plaques en fournissant 90% de l'énergie nécessaire au déplacement des plaques tectoniques (Slab pull) et ont pour conséquence l'enfouissement les roches à plus ou moins grande profondeur. En résumé, les zones de subduction sont à l'origine des déplacements horizontaux des roches à la surface terrestre à grande échelle (échelle globale) mais également des déplacements verticaux des roches à plus petite échelle (échelle régionale).

L'objectif de ce travail de thèse était de comprendre la manière dont les unités métamorphiques Haute Pression - Basse Température générées au sein des zones de subduction sont déformées lors de leur enfouissement et de leur exhumation afin d'apporter des contraintes mécaniques concernant leur genèse (en profondeur) et leur mise en place (en surface).

Pour ce faire, nous avons choisi de mener une étude de terrain sur les îles de Syros et Sifnos, appartenant à l'Unité des Schistes Bleus Cycladiques. Ces îles des Cyclades (Mer Egée, Grèce) sont des objets d'étude idéaux car elles présentent une préservation exceptionnelle des paragénèses de Haute Pression/Basse Température.

La démarche adoptée lors de ces trois ans de thèse a été pluri disciplinaire : travail de terrain, modélisation 3D, modélisation analogique, pétrologie et géochronologie.

Afin:

(1) de caractériser les déformations progrades et rétrogrades affectant les unités métamorphiques de haute pression basse température.

(2) de comprendre quelle(s) interface(s) participent à l'exhumation des roches métamorphiques de HP/BT.

(3) de comprendre comment la dynamique du panneau plongeant influe sur les derniers incréments de déformation.

Le plan de ce mémoire de thèse se compose de quatre parties :

- ***La première partie*** consiste en une synthèse bibliographique rappelant brièvement les problématiques tectoniques générales qui se posent quant aux mécanismes d'exhumation des unités métamorphiques HP/BT. La fin de cette partie présente le contexte géologique régional de l'étude de terrain menée dans le cadre de ce travail de thèse, et pose les questions régionales.
- ***La deuxième partie*** est basée sur l'étude de terrain. L'analyse microstructurale couplée à la pétrologie permet de caractériser les déformations ductiles pro et rétrogrades au sein des schistes bleus des îles de Syros. L'obtention d'un schéma structural cohérent en 3D est un premier pas indispensable vers la compréhension des déformations affectant les unités de haute pression basse température. Enfin, l'évolution tectonique de l'île de Syros peut être approchée.
- ***La troisième partie*** consiste en une synthèse géologique à l'échelle des Cyclades, elle apporte un éclairage nouveau sur la compréhension régionale de la tectonique en mer Égée. Les modèles analogiques réalisés durant cette thèse ont permis de tester la contribution respective des principaux paramètres contrôlant la structure de l' Egée, a savoir: 1) déplacements aux limites : l'extrusion de l'Anatolie, Le Slab Roll back et la 2) La rhéologie de la croûte Egéeenne (non uniforme car elle présente des zones sutures océaniques).
- ***La quatrième partie*** de ce manuscrit synthétise les apports de ce travail de thèse d'une part méthodologiques et d'autre part concernant la compréhension du domaine Egéen.

Partie 1/ Introduction et problèmes

Chapitre 1: Métamorphisme et zone de Subduction

1.1. Les faciès métamorphiques

Pour de faibles gradients thermiques (150 à 350°C/GPa), les faciès métamorphiques rencontrés sont ceux des schistes bleus et des éclogites (Fig. I-1). Le faciès des schistes bleus tiens son nom du Glaucophane ou amphibole bleu (Eskola, 1939). La limite inférieure du faciès des schistes bleus est la réaction métamorphique Albite → Jadéite + Quartz (Fig. I-1, aire en bleu ciel). Le champ de stabilité du faciès des schistes bleus est compris entre 0,5 et 2,5 GPa et 200 et 650°C. A plus haute pression, la limite supérieure du faciès des éclogites est la réaction quartz → coésite (Fig. I-1, aire en violet), le champ de stabilité des Eclogites est compris entre 1,5 à 3 GPa pour des températures supérieures à 400°C. Le faciès des éclogites est caractérisé par des paragénèses contenant l'assemblage Grenat + Omphacite.

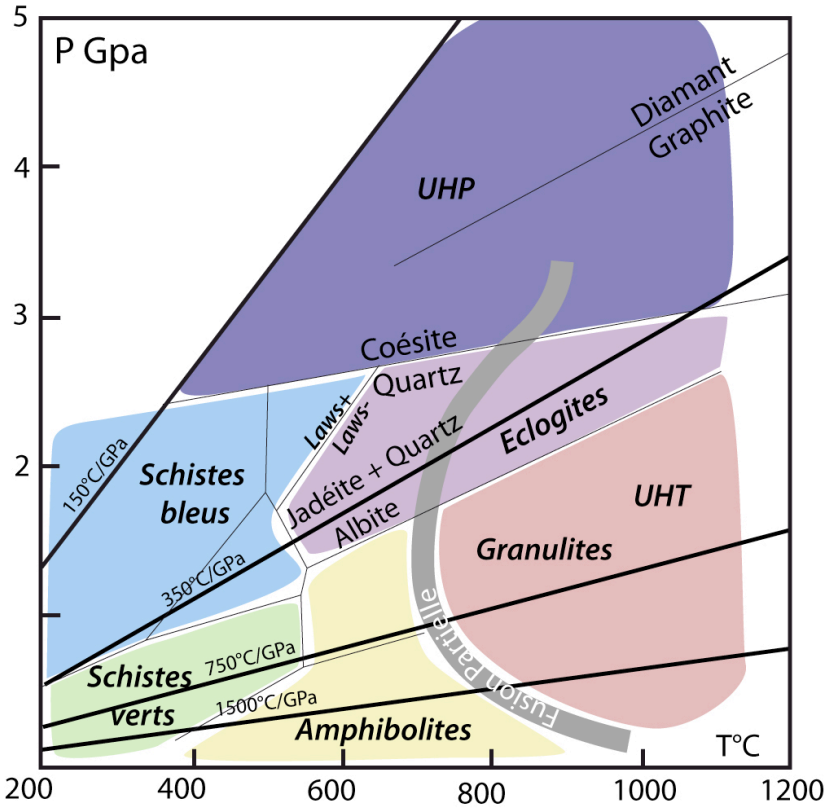

Fig. I-1 Diagramme montrant les principaux faciès métamorphiques dans l'espace Pression/Température. Quatre gradients thermiques sont indiqués. Les principales réactions qui limitent les faciès métamorphiques sont aussi indiquées (Bousquet et al., 1997).

Pour de forts gradients thermiques (750 à 1500°C/GPa), les faciès rencontrés sont ceux des amphibolites et granulites. Les roches entrent dans le faciès des granulites lorsque elle passent la réaction de fusion partielle. Ces roches sont de haute température – basse pression.

1.2. Les « Paired Metamorphic Belts»

Miyashiro (1961) décrit les Paired Metamorphic Belts ou «paire de ceintures métamorphiques », sur la base d'observation de ceintures métamorphiques régionales parallèles, de mêmes âges mais présentant des caractéristiques métamorphiques différentes qui affleurent au Japon. L'une des ceintures est de type basse pression - haute température, l'autre de type haute pression - basse température. La formation des Paired Metamorphic Belts est le résultat de l'enfouissement d'une plaque océanique sous un arc insulaire ou une marge continentale en frontière de plaque convergente (Miyashiro, 1961) (Fig. I-2).

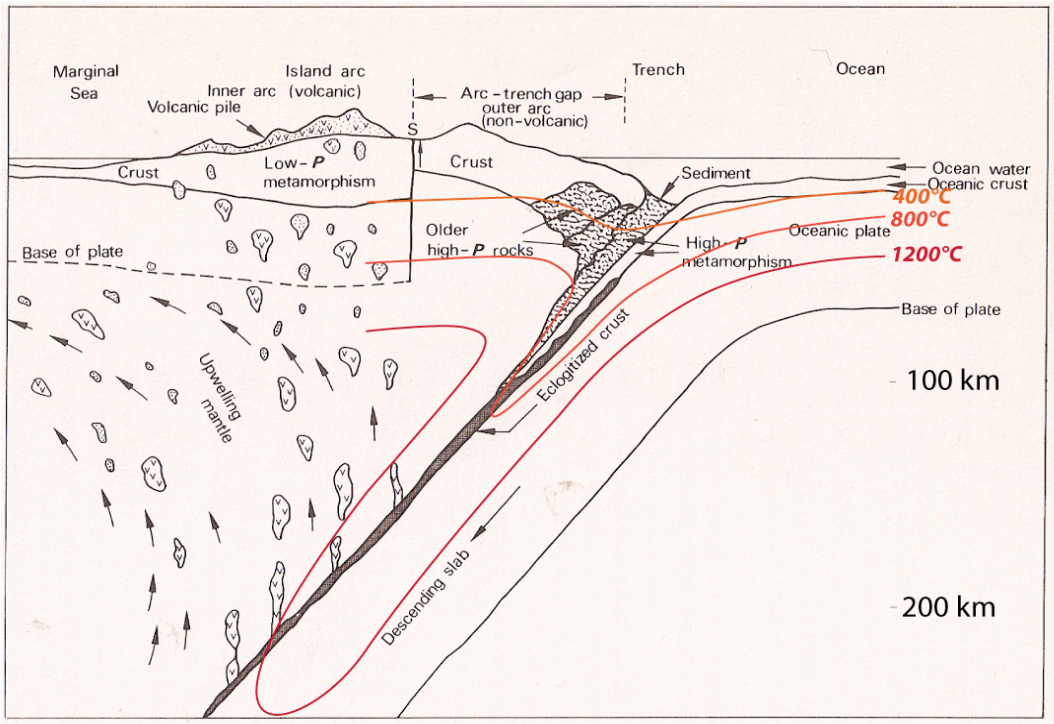

Fig. I-2 Schéma représentant l'origine des Paired Metamorphic Belts, en prenant comme référence l'évolution de l'arc Nord-Est du Japon du Miocène au présent (Miyashiro, 1965), superposé au modèle thermique de la

zone de subduction du Sud Ouest du Japon, montrant les isothermes déviés le long du panneau plongeant. Isotherme tout les 400°C. (D'après Peacock et Wang, 1999).

1.2.1. Ceinture de haute pression

Le modèle thermique de zone de subduction proposé par Peacock et Wang (1999), montre que le panneau plongeant entraîne du matériel froid à grande profondeur perturbant ainsi les isothermes et induisant un faible gradient géothermique (Fig. I-2). Les roches ainsi subduites subissent un métamorphisme haute pression mais aussi basse température.

1.2.2. La ceinture de haute température

La ceinture de basse pression est aussi de haute température, elle résulte d'une activité magmatique intense se traduisant par la mise en place de nombreux plutons granitiques dont les chaînes de volcans andésitiques d'arc insulaire ou de marge sont la manifestation en surface. Les observations globales montrent que l'arc plutonique/volcanique est situé à une distance de 100±20 km de la fosse, la déshydratation de la croûte océanique hydratée favorise la fusion du coin de manteau et la genèse d'un volcanisme de type calco-alcalin.

1.3. Deux types de frontières de plaques

Deux types de frontières de plaques convergentes sont distinguées : (1) La subduction océanique où des milliers de kilomètres de lithosphère océanique sont subduits (Fig. I-3a) et (2) la collision continentale où la fermeture d'un bassin océanique aboutit à une collision continentale (Fig. I-3b) (Lallemand, 1999 ; Liou et al., 2004 ; Ernst 2010). La plaque plongeante entraîne des lithologies mafiques et felsiques à 35-120 km, produisant selon le type de frontière convergente du métamorphisme haute pression (HP) voir ultra-haute pression (UHP).

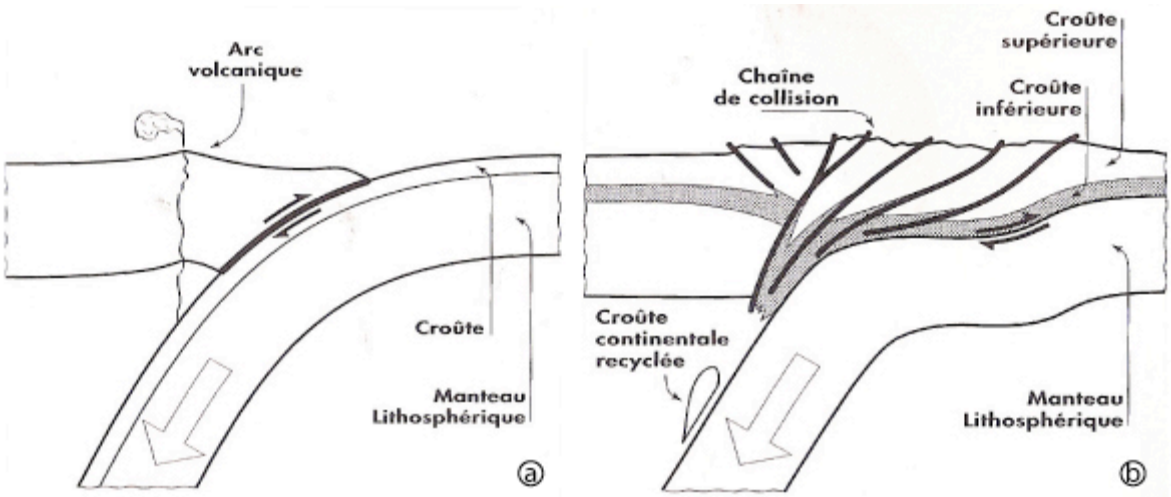

Fig. I-3 Les deux types de frontières de plaques convergentes (Lallemand, 1999).

À chaque type de roches métamorphiques correspond un gradient thermique qui lui est propre (Fig. I-1). La synthèse de Brown (2010), montre la dépendance entre régime thermique et le contexte tectonique. Le concept original des paired metamorphic belts de Miyashiro est ainsi élargi au-delà des ceintures métamorphiques des prismes d'accrétion Circum Pacifique, permettant de faire la relation entre régime thermique et contexte tectonique.

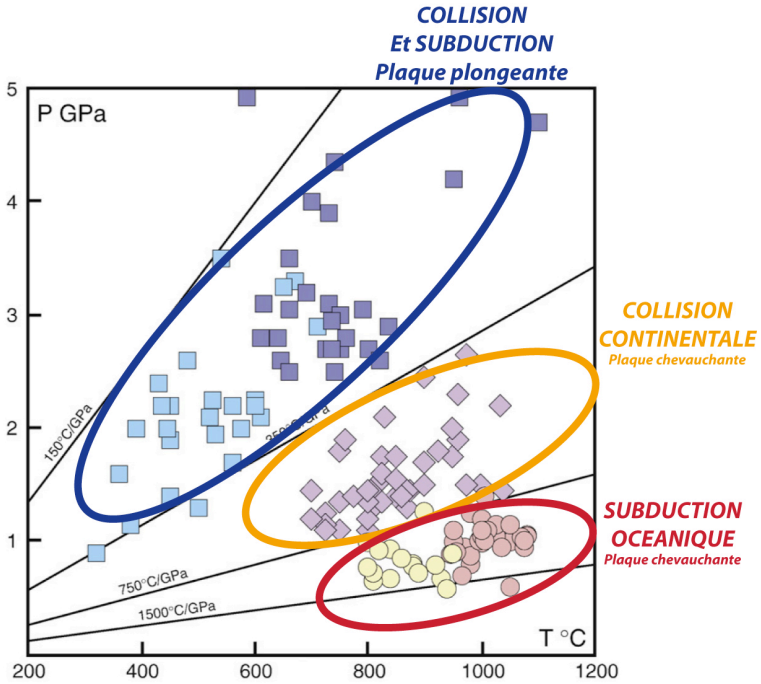

Fig I-4. Pics de pression-température de 140 Paired Metamorphic Belts et leur relation avec le gradient géothermique. Carrés Bleu ciel et violet foncé : métamorphisme HP et UHP, cercles jaunes et rouge métamorphisme HT et UHT, et losanges violets métamorphisme intermédiaire (Brown, 2010)

1.3.1. La subduction océanique

Dans le cas d'une subduction océanique, on observe une « paired metamorphic belt» classique. La plaque plongeante est soumise à des régimes thermiques bas à intermédiaires (dT/dP= 150 à 350°C/GPa, carrés bleus et violets, Fig. I-4), et la plaque chevauchante, dans le même temps, est soumise à des régimes thermiques élevés (dT/dP=750 à 1500°C/GPa, ronds Jaunes et rouges, Fig. I-4) et des granites se mettent en place dans la croûte de la plaque chevauchante. Les subductions océaniques produisent et recyclent la croûte continentale. Les pressions qui y sont enregistrées traduisent des profondeurs d'enfouissement comprises entre 35 et 70 km (Ernst, 1971; Aoya et al., 2001; Agard et al., 2008).

1.3.2. La collision continentale

Lorsque le système orogénique passe de la subduction à la collision, la suture et les matériaux de la plaque plongeante enregistrent des régimes thermiques bas à intermédiaires (dT/dP= 150 à 350°C/GPa, carrés bleus et violets, Fig. I-4) et la plaque chevauchante enregistre, dans le même temps, des régimes thermiques intermédiaires, (dT/dP= 350 à 750°C/GPa, losanges roses, Fig. I-4). Ces ceintures qui présentent un métamorphisme intermédiaire associé à un métamorphisme de haute pression -basse température, sont les « unpaired metamorphic belts» décrites par Miyashiro (1973).

Les pressions enregistrées au niveau de zones de collision continentale sont hautes à ultra haute pression (HP à UHP) (Chopin, 1984; Smith, 1984; Sobolev et Shatsky, 1990; Coleman et Wang, 1995). Le recensement mondial de la coésite –polymorphe de haute pression du quartz-, du diamant –polymorphe de haute pression du graphite- et des assemblages à Lawsonite –le champ de stabilité de la Lawsonite est compris entre 2,1 à 2,5 GPa 350 et 450°C : traduisant des pressions hautes pour de très faibles températures - met en évidence les endroits du globe où les mouvements verticaux sont les plus importants (Fig. I-5). On trouve les roches UHP majoritairement au niveau des zones de collision continentale.

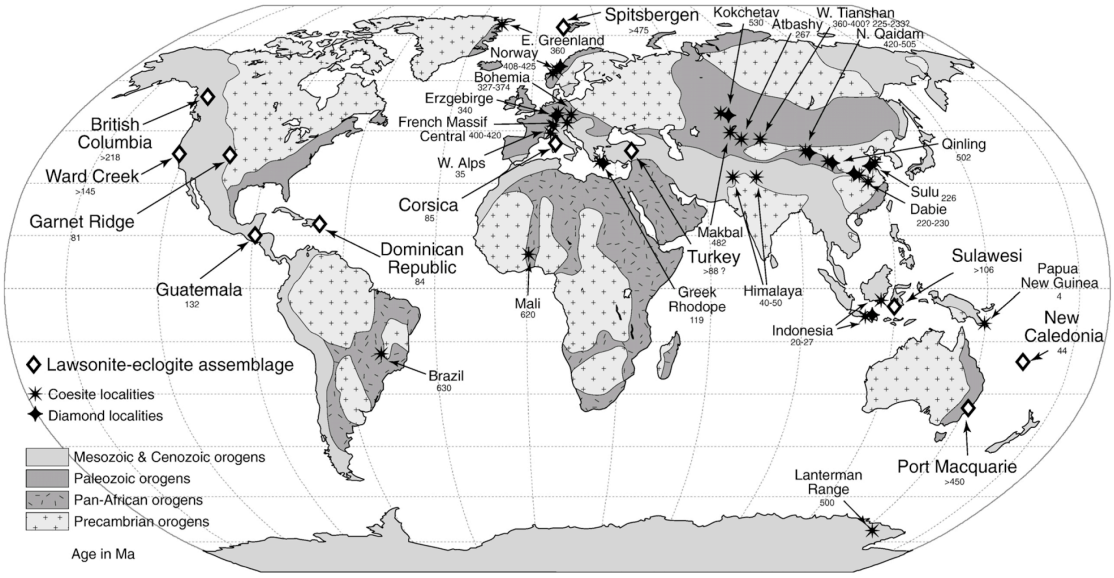

Fig. I-5 Mappemonde montrant les affleurements à Lawsonite (losanges), signant un gradient géothermique froid et à Coésite (Croix) et Diamant (Etoile noire) qui sont les marqueurs de la ultra haute pression (Tsujimori et al., 2006).

On distingue deux types de roches métamorphiques générées au sein des zones de subduction. Ces deux types de roches générés dans le même contexte tectonique requièrent pourtant des gradients thermiques très différents lors de leur exhumation. Le chapitre qui suit traite des observables géologiques concernant ces deux types de roches.

Chapitre 2: Les roches métamorphiques : observables géologiques

2.1. Pétrologie, géochronologie et rhéologie

2.1.1. Roches métamorphiques de haute pression – basse température.

- Les vitesses d'exhumation des roches HP-UHP sont différentes selon la nature du matériel exhumé.

Les vitesses d'exhumation sont comprises entre 3,6 et 0,5 cm/an pour Dora Maira massif cristallin interne UHP des Alpes (Rubatto et Hermann 2001). Une majeure partie de l'exhumation du massif de Dora Maira (68%) se fait à une vitesse de 3,6 cm/an - des profondeurs de 117 à 37 km- (Fig. II-1a). En revanche, le Zermatt-Saaz -constitué de matériel océanique- s'exhume à des vitesses plus faibles allant de 1 à 2,6 cm/an au maximum pour les trois quarts du trajet ascendant (Fig. II-1b, Amato et al.,. 1999). En revanche quelle que soit la nature du matériel, la dernière partie de l'exhumation se fait à des vitesses comparables, de l'ordre de quelques mm/an.

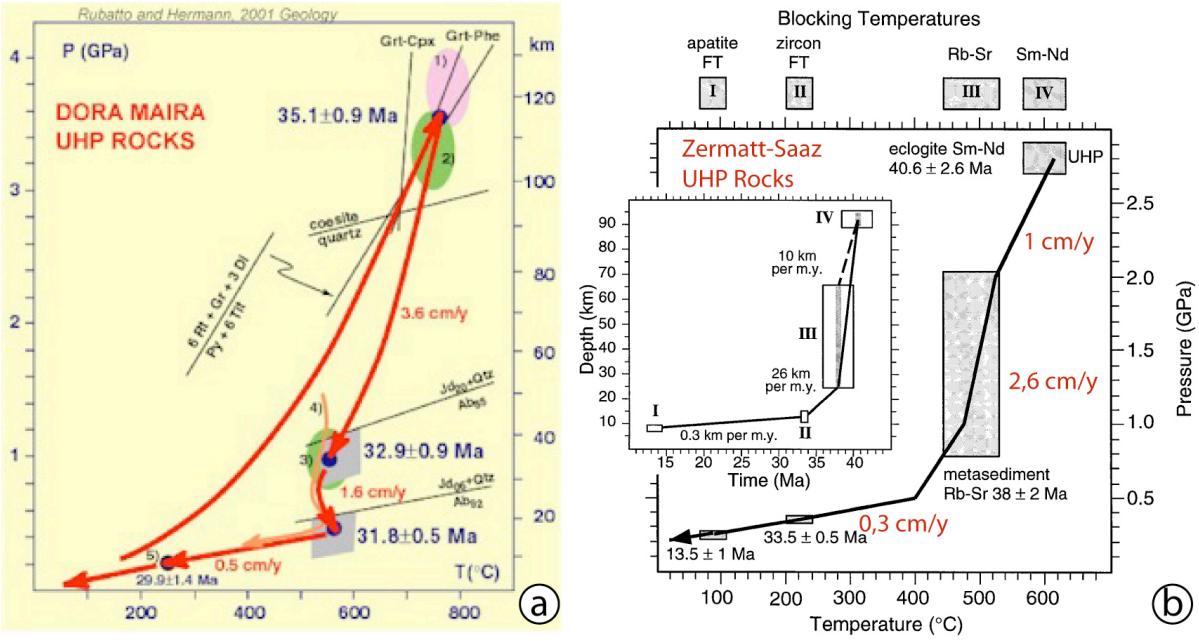

Fig. II-1. Chemins pression température temps (PTt) pour les unités Alpines de Dora Maira (a) et du Monviso (b). Les vitesses d'exhumation de ces deux unités sont caractéristiques de l'exhumation de croûte continentale (a) et de croûte océaniques (b). (Rubatto et Hermann 2001 ; Amato et al.,. 1999).

Les taux d'exhumation de la croûte continentale sont du même ordre de grandeur (cm.an -1) que celui des vitesses de subduction (Rubatto et Hermann 2001). Le contraste de densité entre le manteau environnant, 3300kg/m3, et la croûte

continentale, 3100kg/m3, est tel que la croûte continentale a une flottabilité positive. Les vitesses d'exhumation élevées sont attribuées au fait que le retour à la surface de la croûte continentale est facilité par sa flottabilité positive (Ernst et al., 1997; Ranalli 2000).

- Les vitesses d'exhumation des roches HP-UHP sont différentes selon la profondeur à laquelle se trouve le matériel en cours d'exhumation.

Quelle que soit la nature du matériel exhumé, les deux diagrammes PTt présentés ici montrent que les roches s'exhument avec une vitesse élevée durant les deux tiers de leur exhumation (de l'ordre du cm/an) puis sur le dernier tiers leur vitesse d'exhumation est relativement faible (de l'ordre du mm/an) (Fig. II-1). Les vitesses d'exhumation sont différentes selon que le matériel en cours d'exhumation se trouve dans le chenal de subduction -espace pincé entre plaques plongeante et chevauchante ou dans le prisme d'accrétion (Guillot et al., 2009).

- Taux d'érosion élevés et présence de roches métamorphiques de haute pression.

Les plus forts taux d'érosion sont mesurés aux endroits de forte topographie. Les endroits présentant de forts reliefs sont localisés au niveau des chaînes de montagnes actives qui présentent à l'affleurement des roches métamorphiques HP voir UHP. Parmi les exemples les plus discutés on retrouve ceux de l'Himalaya et de Taiwan (Fig. II-2). Les taux d'érosion sont de l'ordre du mm/an et dépassent exceptionnellement le cm/an (Duchêne et al., 1997; Ring et al., 1999). Ils ne peuvent donc en aucun cas êtres invoqués comme étant des deux premiers tiers de l'exhumation dont les vitesses sont supérieure au cm/an.

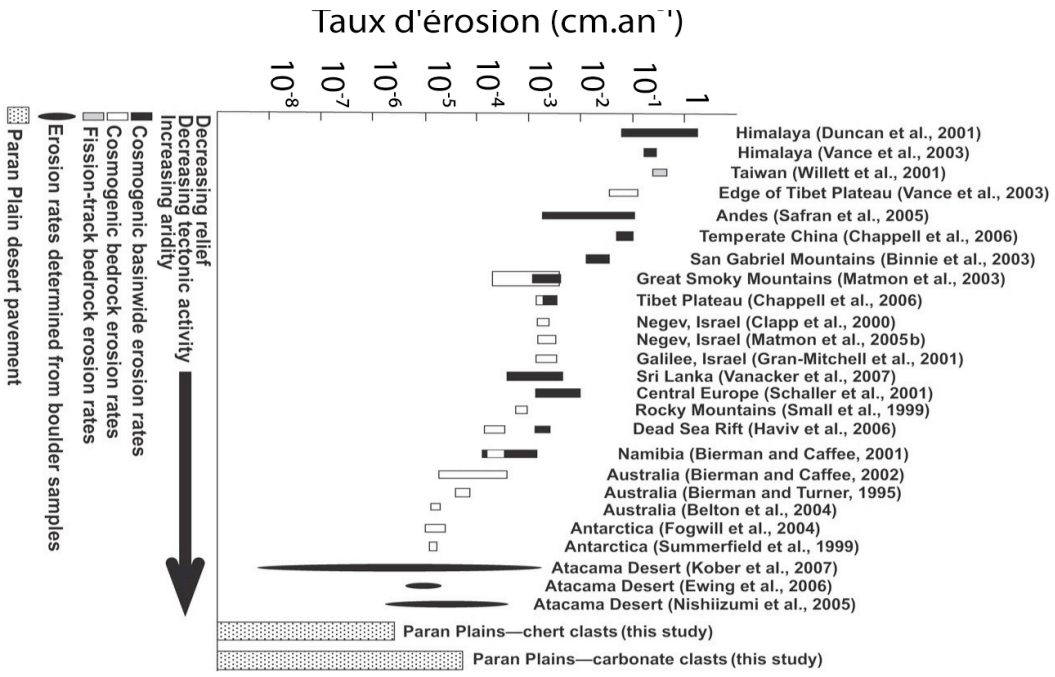

Fig. II-2. Taux d'érosion observés au niveau de différentes localités. Les taux d'érosion diminuent avec le relief et l'activité tectonique. (Matmon et al., 2009).

La rhéologie des unités subduites est dépendante de la température et de la vitesse de déformation qui leur est appliquée, mais dépend également d'autres paramètres comme la présence de fluides. Les observations de terrains montrent, de façon non systématique, que certaines unités métamorphiques UHP sont enveloppées dans de la serpentinite. La serpentinite est le produit d'altération des péridotites, a une viscosité faible et une densité peu élevée, elle est supposée avoir facilité l'exhumation des unités qu'elle enveloppe (Fig. II-3, Guillot et al., 2001). Dans le cas de matériel mafique ayant une densité plus forte que celle du manteau environnant (flottabilité négative), seule la présence de serpentinite peut expliquer leur exhumation (3300kg/m3 contre 3500kg/m3) (Hermann et al., 2000, Guillot et al., 2000, Guillot et al., 2001).

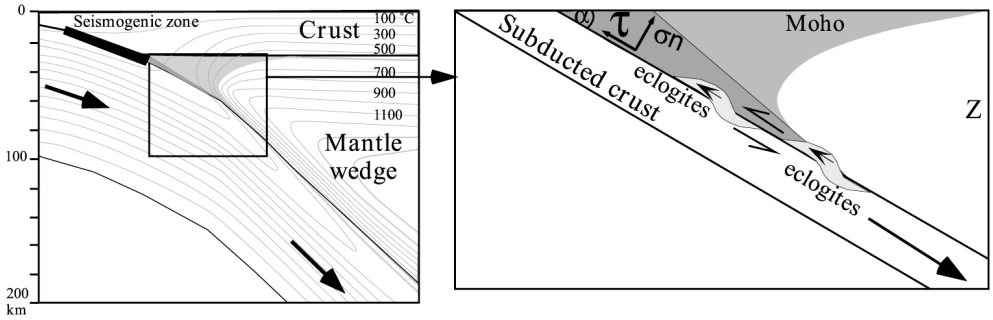

Fig. II-3. Hydratation du coin de manteau qui se serpentinise et permet aux éclogites mafiques, malgrés leur flottabilité négative d'être exhumées. Modifiée d'après Guillot et al., 2001.

Cependant, les roches de haute pression ne sont pas systématiquement associées à de la serpentine. L'exhumation de ces unités s'est donc faite de manière différente.
À partir des observations de terrain, trois paramètres sont donc évoqués concernant l'exhumation des roches de haute pression -basse température : les forces de volumes (e.g. flottabilité), l'érosion et la rhéologie des roches de haute pression – basse température.

2.1.2. Roches métamorphiques de haute température - basse pression

On retrace l'histoire de refroidissement plutôt que leur histoire pression température car ces roches contiennent des paragénèses minérales pour lesquelles l'estimation de la pression est difficile. Les taux de refroidissement sont de l'ordre de la dizaine de degrés Celsius par million d'années et sont estimés grâce aux datations effectuées sur une série de minéraux dont la température de fermeture décroît (Fig. II-4).

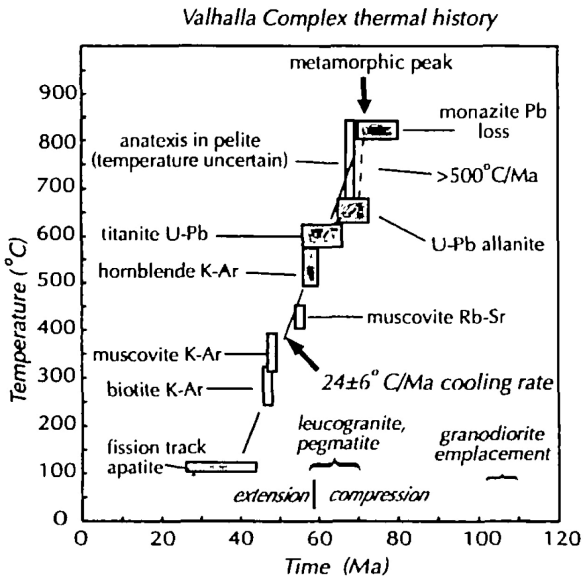

Fig. II-4. Diagramme température – temps montrant le taux de refroidissement du dôme métamrophique du Valhalla (Colombie Britannique, Canada)(Spear et Parrish 1996)

Le développement de ces dômes nécessite une température au moho élevée (>800°C) et que la croûte soit soumise à de l'extension (Buck 1991, Tirel et al., 2009). L'origine de cette anomalie thermique reste discutée. Afin de l'expliquer, on invoque soit l'épaississement de la croûte et le doublement de la concentration d'éléments radiogéniques ou bien la remontée d'asthénosphère (i) via le découplage croûte – manteau lithosphérique (Brun et Faccenna 2008) ou (ii) grâce à un amincissement d'échelle lithosphérique (Lister et Forster 2009).

2.2. Structures et déformation interne des unités métamorphiques

2.2.1. Roches métamorphiques de haute pression – basse température.

La géométrie observable des nappes métamorphiques à l'affleurement correspond à la déformation totale, c'est-à-dire la somme des déformations ductiles et fragiles subies par l'unité. Les unités métamorphiques sont souvent appelées nappes métamorphiques, faisant passer l'idée d'une géométrie particulière, en l'occurrence un rapport surface - épaisseur très grand. En effet, les unités métamorphiques affleurent sur une grande surface (Voir carte des Alpes, Fig. II-5). Ces unités sont de relativement faible épaisseur et ont un pendage faible, comme l'illustre la coupe présentée en figure

II-5. La géométrie en nappe est acquise lorsque l'unité se détache du panneau plongeant (Carry et al., 2009).

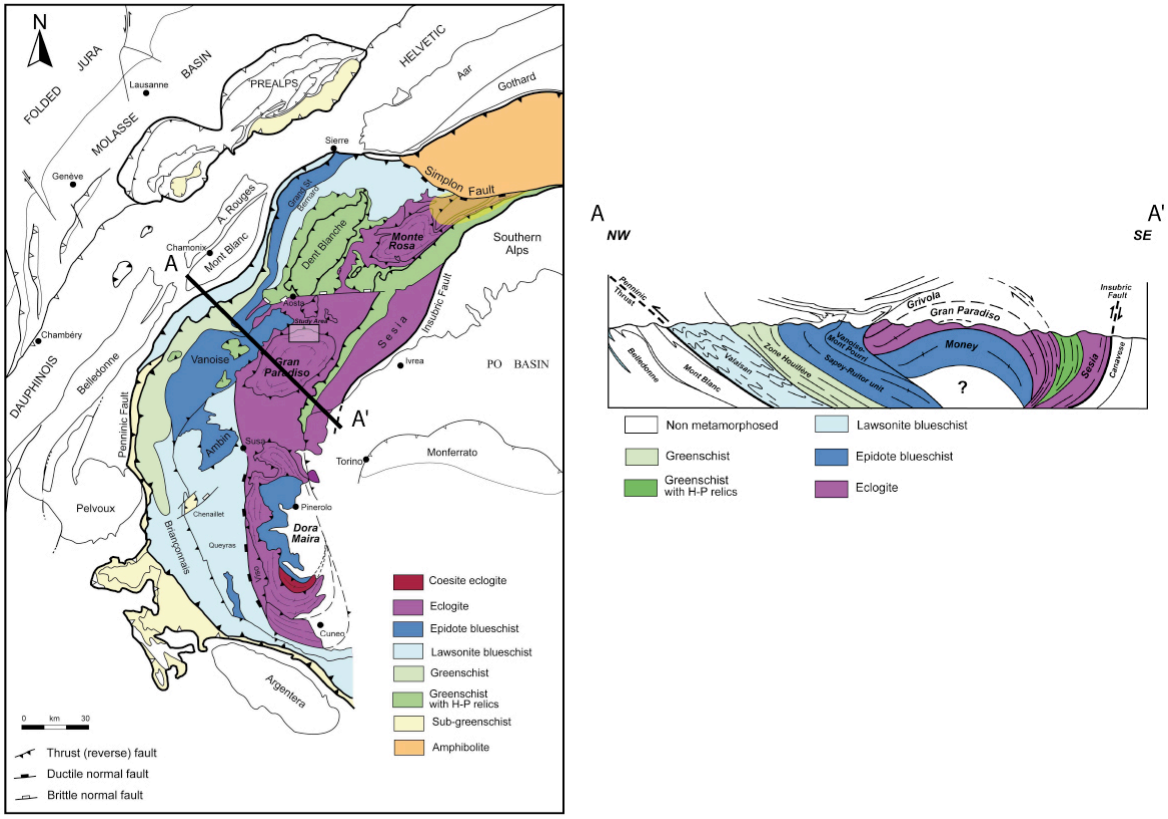

Fig. II-5. Carte (a) et coupe (b) métamorphique(s) des Alpes. (Le Bayon 2005).

La déformation ductile observée dans les unités de haute pression - basse température est caractérisée par la présence d'une foliation régionale pénétrative qui est parallèle aux contacts tectoniques (Voir Coupe Fig. II-5a). La foliation porte une linéation régionale perpendiculaire aux chevauchements d'échelle crustale (Voir coupe Fig. II-5). La linéation régionale porte deux critères de cisaillements opposés (Voir Carte Fig. II-5b) (Egée Gautier et Brun 1994a ; Alpes Ganne et al., 2006, Corse ; Jolivet et et al., 1990). La présence de deux critères de cisaillement portés par la même linéation à l'échelle régionale a été reportée dans plusieurs unités de haute pression (Gautier et Brun 1994a ; Ganne et al., 2006; Philippon et al., 2009). Ils sont soit décrits comme synchrones et attribués à l'enfouissement et à l'exhumation synchrone au sein de la zone de subduction» (Ganne et al., 2006; Huet et al., 2009; Jolivet et al., 2009).

Enfin, malgré leur remontée vers la surface, ces unités métamorphiques conservent leurs paragénèses de haute pression, deux hypothèses sont avancées :

- Les réactions métamorphiques de rétromorphose ne peuvent pas se faire pour des raisons cinétiques ou bien parce que toute l'eau disponible dans le système a été consommée lors des réactions progrades.
- La déformation accompagnée par une rétromorphose est localisée sur les interfaces accommodant les grands mouvements conduisant à une hétérogénéité de la déformation. D'autres témoins attestent de la localisation de la déformation, par exemple les fossiles retrouvés dans des unités de schistes bleus (Pohl, 1999).

2.2.2. Roches métamorphiques de haute température - basse pression

Les roches métamorphiques de haute température affleurent sous forme de dômes (Fig. II-6). Décrits historiquement dans le Bassin & Range sous l'appellation de metamorphic core complexes (MCCs) ou « noyau métamorphiques complexes » dans les années 80 (Davis et Coney, 1979, Crittenden et al.,1980). Structuralement il s'agit d'un dôme de roche métamorphique de haute température exhumée le long d'un détachement à faible pendage (décollement, Fig. II-6). Ce détachement crustal sépare le dôme de roches métamorphiques de haute température d'une unité supérieure non métamorphique. Au toit du détachement, l'unité supérieure est soumise à de l'extension cassante formant des grabens remplis de dépôts synchrones de la déformation extensive.

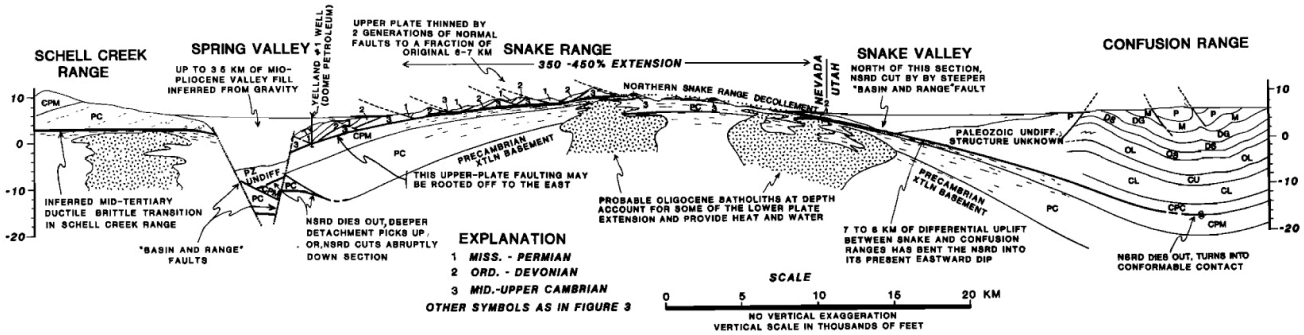

Fig. II-6. Coupe du Snake Range, montrant la géométrie en dôme des unités de haute température (Miller et al., 1983).

La déformation ductile observée dans les unités métamorphiques est caractérisée par la présence d'une linéation d'étirement parallèle à l'extension, portant deux sens de cisaillements opposés (Fig. II-7). Ces sens de cisaillements sont synchrones et attribués à

l'exhumation du dôme métamorphique de haute température lors de l'amincissement homogène de la croûte (Brun et Van den Driessche 1994).

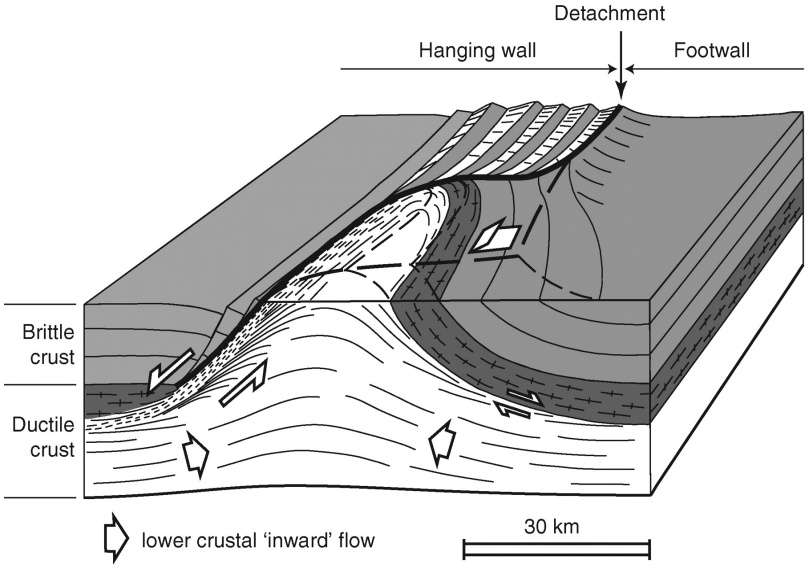

Fig. II-7. Bloc diagramme d'un dôme métamorphique montrant la cinématique de la déformation ductile observée dans les roches exhumées (Brun et Van den Driessche 1994).

Les roches métamorphiques de haute pression et de haute température se forment à plus ou moins grande profondeur dans les zones de subduction et affleurent à la surface. Les observables géologiques apportent de fortes contraintes concernant leur origine (pétrologie, géochronologie) et les mécanismes qui les ont amenés à la surface (structure et déformation interne). Le chapitre qui suit traite des modèles proposés pour expliquer leur exhumation au sein d'une zone de subduction active.

Chapitre 3: Les processus d'exhumation des roches métamorphiques

3.1. Dynamique des frontières de plaque en convergence : évolution des concepts

La compréhension du fonctionnement des frontières de plaques en convergence a évolué au cours du temps.

Le concept en deux temps qui consiste en (1) collision (épaississement de la croûte), formation des roches métamorphiques puis (2) extension post orogénique (Effondrement gravitaire, changement de conditions aux limites), exhumation des roches métamorphiques au sens large (Coney et Harms 1984). Ce concept d'exhumation par extension post orogénique ne fait pas de distinction entre exhumation des roches haute température et haute pression (Gautier et Brun 1994a).

Fin des années 1980, celui d'extension syn orogénique est né : lors de la collision - épaississement, l'extension est active perpendiculairement à la compression et participe à l'exhumation des roches métamorphiques, c'est l'extension syn orogénique (Dewey 1988). Concernant les roches exhumées lors de l'extension syn orogénique on parle de l'exhumation syn orogénique, ce sont des roches de haute pression. Avigad et al., 1997).

Actuellement un nouveau concept émerge: celui de l'extension syn convergence, il n'implique pas qu'il y est d'épaississement - collision préalable à l'exhumation des roches métamorphiques. Les roches sont enfouies, acquièrent leur métamorphisme de haute pression et sont exhumées dans l'espace libéré par l'extension syn convergence, l'extension est accommodée par l'exhumation des roches métamorphiques de haute pression (Brun et Faccenna 2008).

3.2. Les modèles d'exhumation

Les deux mécanismes géologiques qui permettent d'expliquer l'exhumation des roches métamorphiques sont l'érosion et l'extension (Platt 1987). La flottabilité positive des roches métamorphiques est un paramètre sur lequel s'appuient tous les modèles d'exhumation. J'ai choisi de distinguer les nombreux modèles d'exhumation selon qu'ils expliquent l'exhumation des roches métamorphiques de haute pression sans considérer celle des roches de haute température ou bien qu'ils fassent intervenir des mécanismes distincts pour expliquer l'exhumation des roches haute pression et haute température.

Je me suis limitée aux modèles d'exhumation des roches métamorphiques au sein d'une zone de subduction active. Je ne traiterais donc pas les modèles d'exhumation post orogénique des roches métamorphiques (se référer à Brun et Van den Driessche 1994).
Dans le contexte de la tectonique des plaques, le référentiel correct pour estimer les mouvements horizontaux des plaques est le manteau asthénosphérique (Fig. III-1, Heuret et Lallemand, 2005). Heuret et Lallemand posent Vup=Vd+Vt, avec Vup : vitesse de la plaque supérieure, Vd : taux de déformation arrière arc et Vt : vitesse de la fosse. Le schéma présenté ici (Fig. III-1), montre la structure d'une zone de subduction, l'espace entre la plaque plongeante et la plaque supérieure est dénommée l'arc.

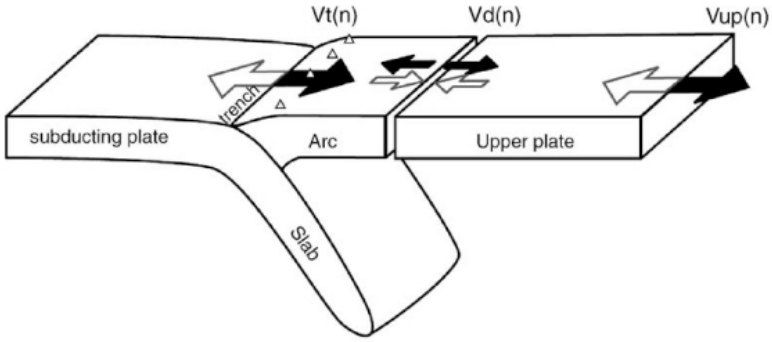

Fig. III-1. Structure d'une zone de subduction : Vup vitesse absolue de la plaque supérieure, Vt vitesse absolue de la fosse et Vd taux de déformation arrière arc (Heuret et Lallemand, 2005).

J'ai donc également choisi de distinguer les nombreux modèles d'exhumation selon qu'ils font intervenir les zones de subductions ayant un taux de déformation arrière arc absolu nul ou non (un arc ayant un volume relativement constant ou non). Le taux de déformation arrière arc Vd, est nul si |Vup|=|Vt|, cela implique un bilan nul entre matériel sortant et entrant dans «l'arc ». Par contre si |Vt| > |Vup|, ce bilan devient non nul s'il implique plus de matériel entrant que sortant, dans l'arc.

3.2.1. Expliquant l'exhumation des roches métamorphiques lato sensu, taux de déformation arrière arc nul.

- Corner Flow : modèle originel et dérivés, fondés sur le concept de prisme d'accrétion (Tableau I-1).

Le début des années 80 voit éclore le premier modèle conceptuel d'exhumation des roches haute pression - basse température. Cloos (1982) proposent sous

l'appellation de « corner flow », un chenal prismatique et étroit pincé entre la plaque chevauchante et la plaque plongeante dans lequel s'enfouissent et s'exhument les roches de haute pression/basse température (Fig. III-2).

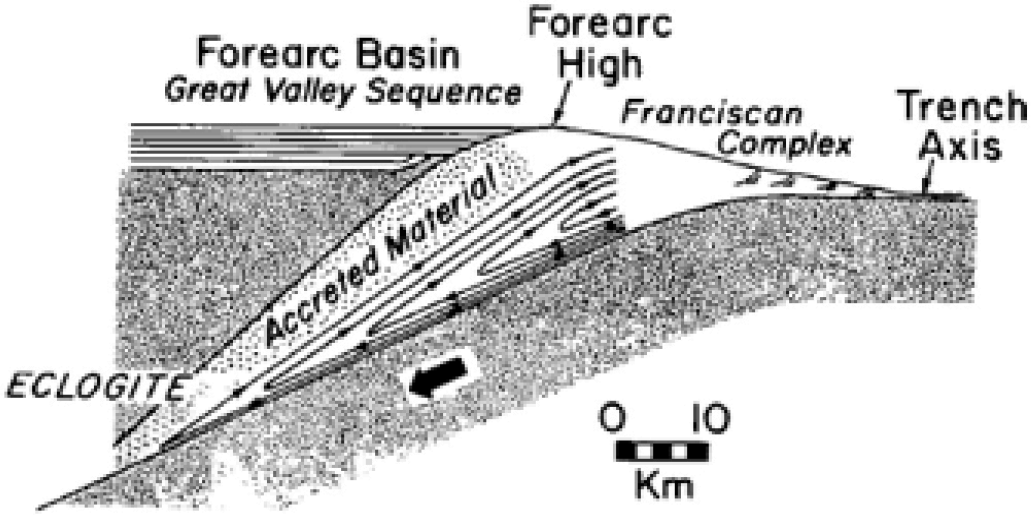

Fig. III-2. Chenal de subduction (Modifié d'après Cloos and Shreve 1988a et b).

Les processus physiques en compétition dans ce chenal sont le gradient de pression (directement dépendant de la largeur du chenal) qui est maximal au centre du chenal et minimal sur les bordures, et le cisaillement induit par la plaque plongeante maximale au toit de celle-ci et nulle au mur de la plaque chevauchante (Fig. III-3, England and Holland 1979). De la somme de ces deux champs de vitesse résulte un champs de vitesse dont les vecteurs sont colinéaires du mouvement de la plaque subduite): dans sa partie inférieure le matériel s'enfouit avec la plaque plongeante, dans sa partie supérieure le matériel remonte vers la surface sous la plaque supérieure.

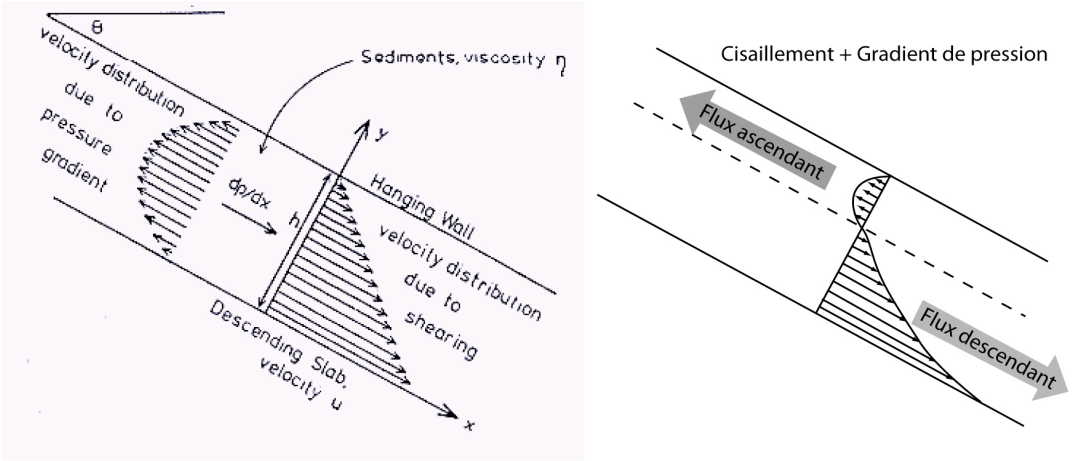

Fig. III-3. Cinématique du chenal de subduction (England et Holland, 1979).

On distingue plusieurs variantes :

Les modèles de « corner flow » dans lesquels L'exhumation des roches métamorphiques résulte d'un couplage processus tectonique et érosion. Dans le modèle de Platt (1987), l'érosion est couplée à l'extension et participe à l'exhumation des roches métamorphiques (Fig. III-4., Platt 1987). Or, le prisme d'accrétion à une largeur fixe ce qui pose problème : il ne peut pas ou peu être soumis à de l'extension.

Dans le modèle analogique de Malavieille et al., 2010, l'érosion est couplée à l'empilement de nappes métamorphiques (Fig. III-4., Malavieille 2010). Ce modèle analogique est purement fragile et d'échelle crustale, il nécessite également que les taux d'érosion soient égaux au taux d'exhumation des roches métamorphiques ce qui n'est pas le cas.

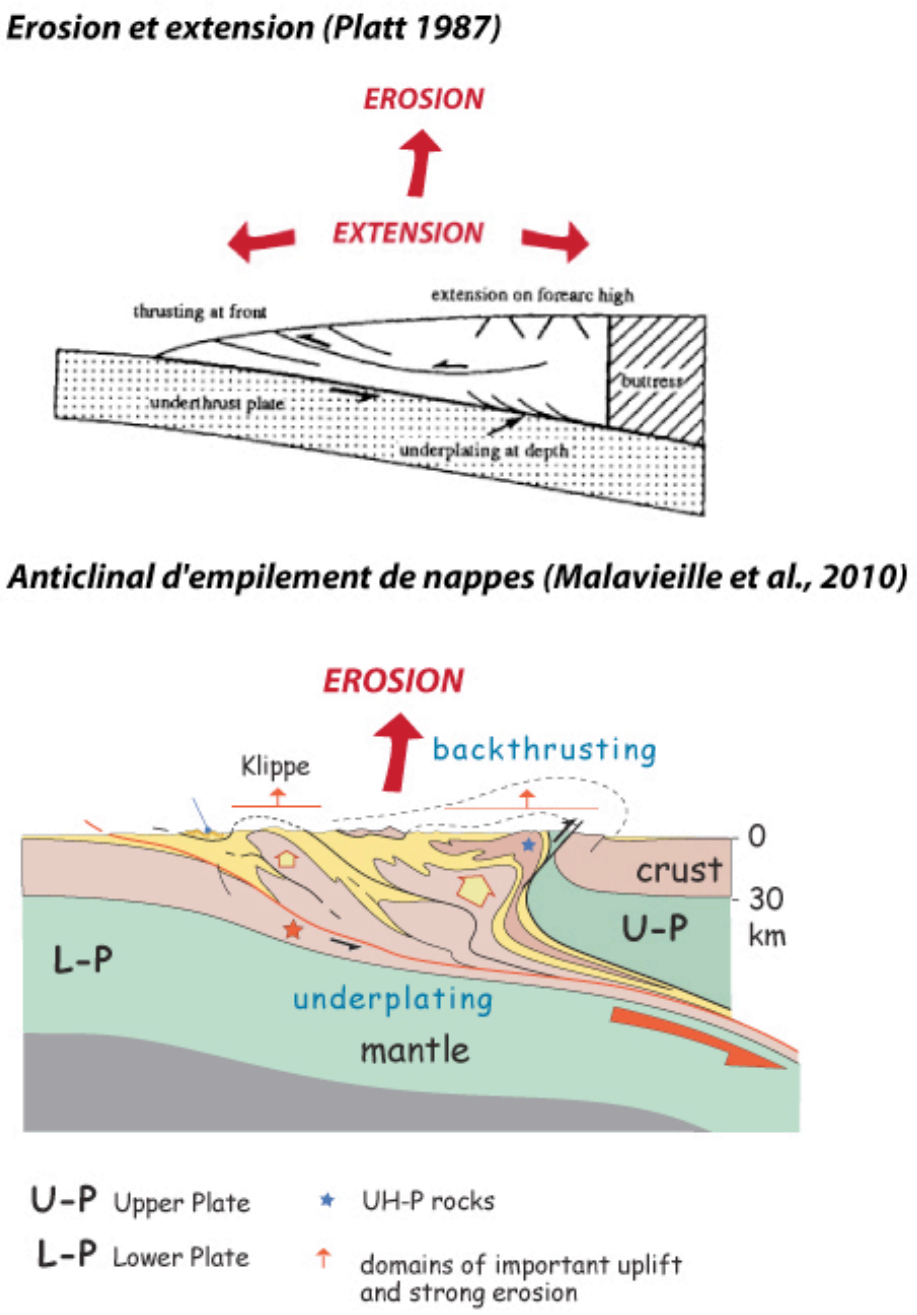

Fig. III-4. Deux modèles d'exhumation contrôlés principalement par l'érosion. L'érosion est couplée soit à l'extension (Platt 1987), soit à la compression (Malavieille 2010).

Le slab break-off ou détachement du slab, induit un rebond isostatique. Le pop up formé par l'accrétion de terrains lors de la subduction subit alors un soulèvement qui, couplé à l'érosion, permet l'exhumation des roches métamorphiques (Davies et Blanckenburg, 1995) (Fig. III-5, Tableau I-1)

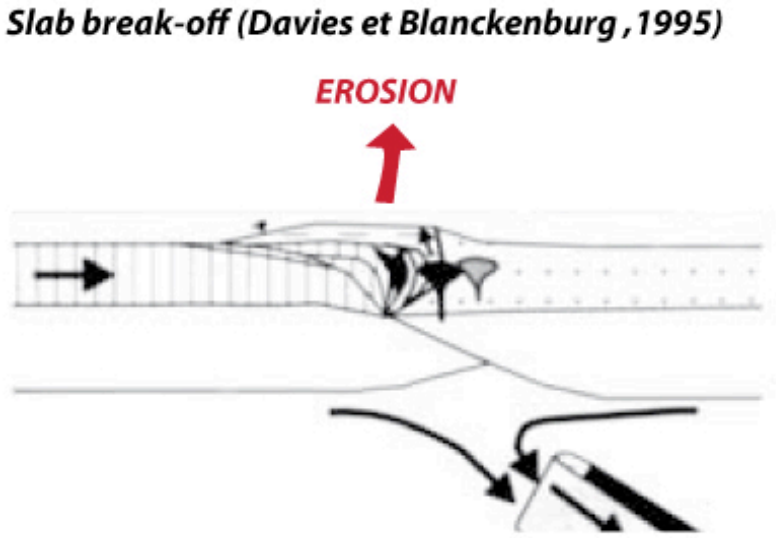

Fig. III-5. Modèles d'exhumation contrôlé par l'érosion, déclenché par le détachement du panneau plongeant (Davies et Blanckenburg 1995).

La fermeture du chenal de subduction se situe à approximativement à 45 km de profondeur (Cloos 1982; Shreve et Cloos 1986 ; Cloos et Shreve 1988 a et b). Cette profondeur est insuffisante pour expliquer l'exhumation des roches d'ultra-haute pression provenant de profondeurs pouvant atteindre 90 à 100 km. Le « corner flow » requiert que le matériel en exhumation ait une faible viscosité, ce modèle convient pour expliquer l'exhumation des sédiments du prisme d'accrétion mais pas pour expliquer l'exhumation de croûte continentale ou océanique détachés du panneau plongeant. Tous les modèles de corner flow nécessitent de fort taux d'érosion pour exhumer les roches métamorphiques. Ces modèles sont quelque peu statiques et représentent un instant du fonctionnement d'une zone de subduction mais pas son évolution dans le temps car ils s'appuient sur l'analogie avec la géométrie actuelle observée sur le terrain.

- Le modèle du chenal de subduction tente d'expliquer l'exhumation d'unités métamorphiques HP voir UHP : ce chenal se ferme à plus grande profondeur, cependant il fonctionne de la même façon que le corner flow (Jolivet et al., 2003, Ganne et al., 2006, Huet et al.,2009) (Fig. III-6, Tableau I-1).

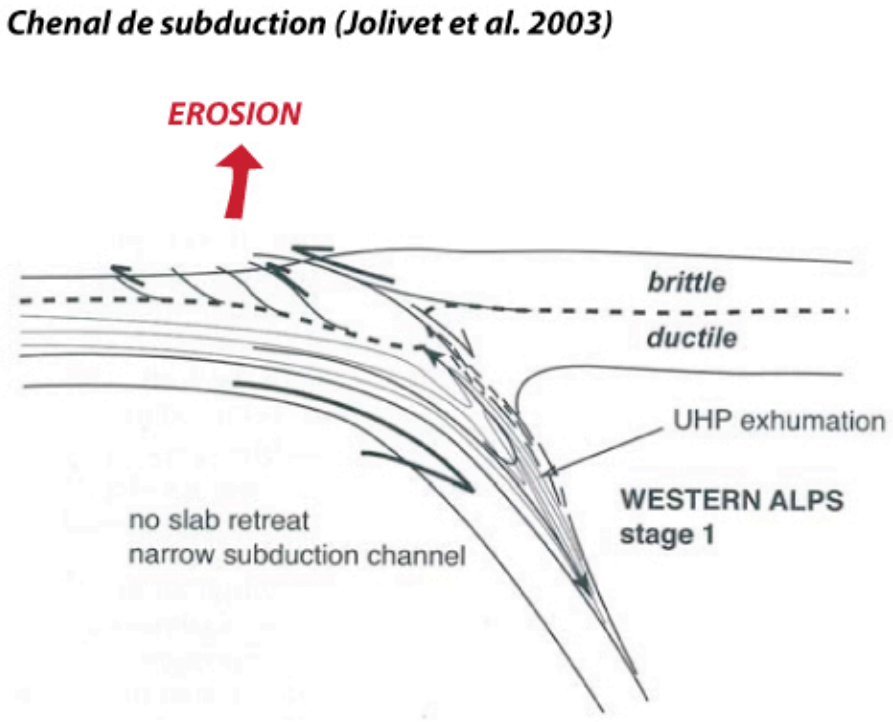

Fig. III-6. Le chenal de subduction (Jolivet et al., 2003)

- L'individualisation d'une écaille de croûte supérieure (Tableau I-1). Ce modèle est basé sur la flottabilité positive de la croûte qui se détache grâce à un niveau de faible résistance lorsque les forces de flottabilités deviennent supérieures aux forces de couplages (Chemenda et al., 1995, 1996). L'exhumation est accommodée par de l'érosion en surface (Fig. III-7). Le détachement de la croûte continentale intervient lorsque la résistance du matériel est inférieure aux forces extérieures appliquées (Carry et al., 2009). Le modèle conceptuel de l'extrusion wedge (Ring et Reischmann 2002) n'est rien d'autre que le modèle de Chemenda et al., (1995).

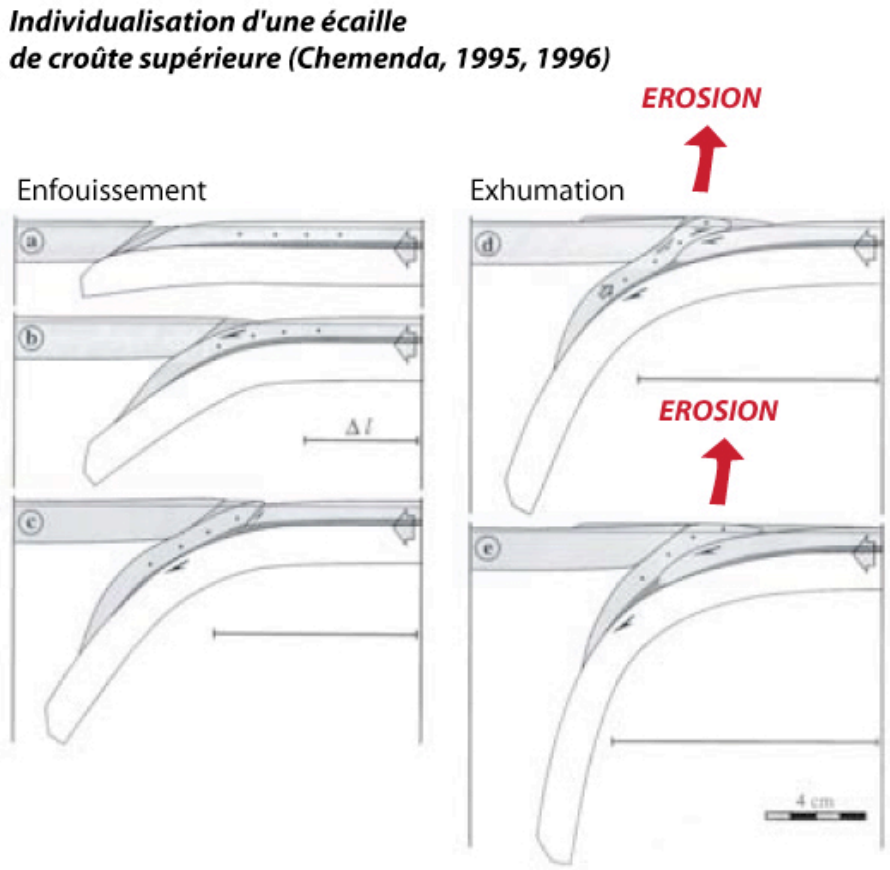

Fig. III-7. Modèles d'exhumation d'une unité de croûte continentale, découplée du panneau plongeant et remontant par flottabilité (Chemenda et al., 1995).

Ces deux variantes du «corner flow» visent à expliquer l'exhumation des roches de haute pression dans un chenal de subduction, mais requièrent des rhéologies très différentes pour fonctionner. Le chenal de subduction fait intervenir un fluide visqueux alors que l'extrusion wedge permet à un bloc rigide, donc peu visqueux d'être exhumé entre un chevauchement basal et une faille normale sommitale.

Récemment, plusieurs modèles numériques combinant des concepts de « corner flow » et de chenal de subduction ont été proposés (Stöckhert et Gerya, 2005 ; Burov 2001; Yamato et al., 2008). Le modèle numérique de Stöckhert et Gerya (2005) exhume uniquement la croûte continentale appartenant à la plaque chevauchante, et la géométrie des unités exhumées forment un dôme (Fig. III-8). Le modèle de Yamato et al., 2008 rend compte des chemins PT observés dans les différentes unités métamorphiques des Alpes qu'elles soient océaniques ou continentales (Fig. III-8). Les calculs de chemins

PT permettent d'estimer des vitesses d'exhumation à 3 mm/an pour le matériel océanique (Monviso, Zermaat Saaz), compatibles avec les observations de terrain (Fig. I-6b).

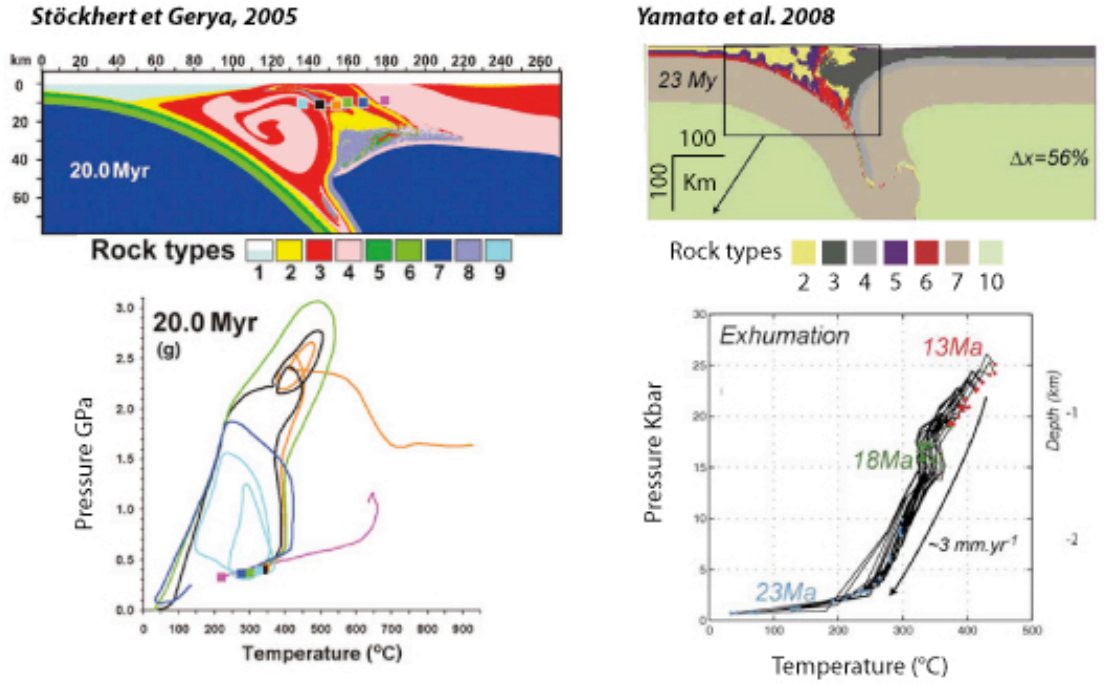

Fig. III-8. Modèles numériques permettant d'estimer les trajets PT suivis par le matériel en exhumation. Légende : (1) air ou eau, (2) sédiments, (3) croûte continentale supérieure, (4) croûte continentale inférieure, (5) croûte océanique supérieure, (6) croûte océanique inférieure,(7) manteau lithosphèrique, (8) manteau serpentinisé, (9) manteau hydraté et (10) manteau asténosphèrique.(Stöckert et Gerya, 2005; et Yamato et al., 2008).

Les modèles numériques sont performants pour expliquer les chemins PT des unités métamorphiques de haute pression. Cependant, la géométrie en nappe de ces unités métamorphiques, observée sur le terrain n'est pas obtenue.

Les différents modèles proposés ci-dessus:

1/ requièrent tous de très forts taux d'érosion (Vexhumation=Vérosion) pour fonctionner (Tableau I-1). Hors les observables géologiques montrent que les taux d'érosion les plus élevés sont de l'ordre du cm.an-1 au maximum, alors que les vitesses d'exhumation des roches de haute pression sont supérieures au cm.an-1.

2/ ont pour résultat une géométrie obtenue qui est différente de la structure des unités métamorphiques observée.

	Références	Echelle		Conditions recquises		Géométrie des unités Métamorphiques	Origine des unités Métamorphiques		Déformation Ductile	Interfaces accomodant l'exhumation
		Croûte	Lithosphère	Erosion	Viscosité		Plaque plongeante	Plaque Chevauchante		
Corner Flow	Cloos 1982, Shreve and Cloos 1986, Cloos and Shreve 1988, Platt 1986, Malavielle 2010	x		Forte	Faible	Largeur d'affleurement = épaisseur de l'unité	x		Deux sens de cisaillements synchrones et opposés	Bordure de la plaque chevauchante
	Stöckhert et Gerya 2005					En dôme		x		Détachments dans la plaque chevauchante ??
Subduction Channel	Jolivet 2003a et b		x			Largeur d'affleurement = épaisseur de l'unité	x			Bordure de la plaque chevauchante
	Burov 2001, Yamato 2007									
Slab Break Off	Davies et Blackenburg 1995								Localisée en bordure d'unité exhumée	Toit et mur de l'unité exhumée
Extrusion Wedge	Chemenda 1995, Chemenda 1996		x		Forte					
	Ring et al 2007	x								

Tableau I-1 Récapitulatif des modèles d'exhumation des roches métamorphiques de haute pression (sans considérer l'exhumation des roches de haute température associées)

3.2.2. Distinguant l'exhumation des roches métamorphiques de haute pression et de haute température. Taux de déformation arrière arc non nul.

Ces deux modèles sont d'échelle lithosphèrique et ne font pas intervenir l'érosion pour expliquer l'exhumation des roches métamorphiques haute pression et haute température.

- *Switch tectonics (Tableau I-2).* Le mode tectonique raccourcissement ou extension peut changer abruptement durant une convergence continue. Lister et Forster (2010) décrivent deux cycles: l'épaississement post-amincissement et l'amincissement post épaississement, permettant d'expliquer l'exhumation des roches haute température et haute pression (Fig. III-9).

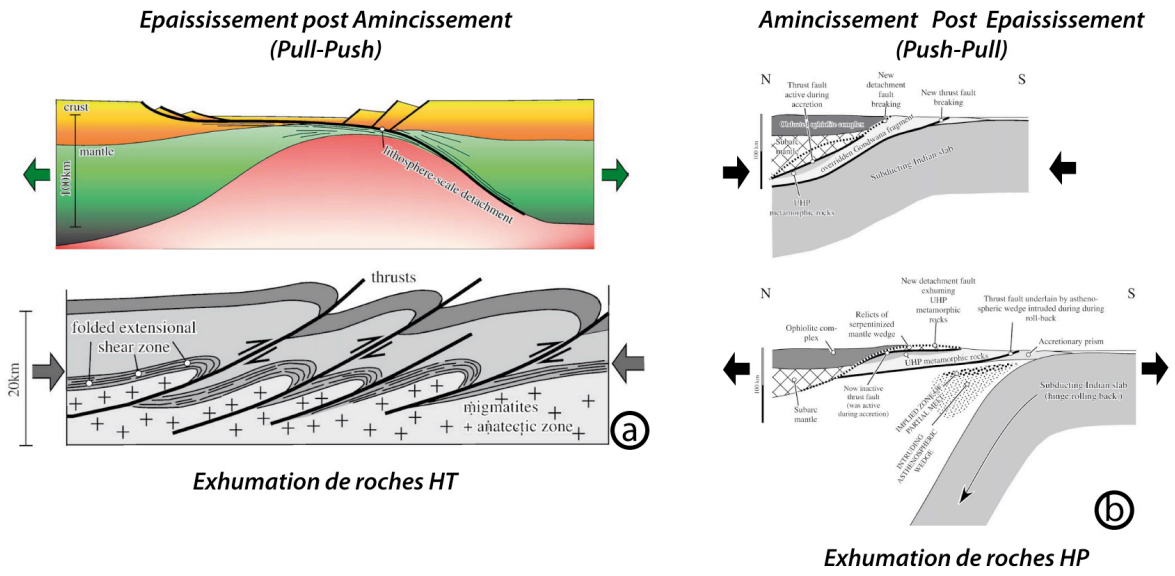

Fig. III-9. Les deux modes tectoniques qui sont actifs dans les chaînes de montagnes a) l'épaississement post amincissement qui permet l'exhumation de roches de haute température et b) l'amincissement post épaississement qui lui permet l'exhumation de roches de haute pression (Lister et Forster, 2010).

Pull-Push ou épaississement post-amincissement (Fig. III-9a): on passe de l'extension horizontale caractérisée par l'amincissement de la lithosphère entière et la remontée d'asthénosphère générant une forte anomalie thermique. Un détachement se localise dans le manteau lithosphérique et vient connecter à la limite litho – asthénosphère qui est activée en extension. L'extension laisse place à la compression horizontale et l'exhumation se fait en raccourcissement. La croûte ductile inférieure s'exhume au cœur de plis. Ce mode permet d'exhumer des roches de haute température et génère également le magmatisme et l'anatexie grâce à la forte anomalie thermique.

Push-Pull ou amincissement post-épaississement (Fig. III-9b): comparable au modèle de Rawling et Lister 1999. À noter que, dans ces modèles, les roches métamorphiques de haute pression - basse température sont exhumées via des structures en dômes. Les interfaces qui participent à l'exhumation des roches HP sont différentes de celles qui exhument les roches haute température.

Pourquoi le mode tectonique change ?

Rawling et Lister (1999) décrivent ces changements dans le mode tectonique au cours d'un orogène sans pour autant en décrire la cause. Lister et al., (2001), apportent un élément de réponse: le changement de mode tectonique de la compression (lorsque que l'on est en collision continentale) à l'extension est due au roll back, au recul du panneau plongeant sans décrire pourquoi la subduction recule. Le recul de la subduction suite à l'entrée d'un bloc continental (Brun et Faccenna, 2008), d'un plateau océanique ou d'un arc insulaire entraîne le changement de mode tectonique Lister et Forster (2009).

- *Roll-back (Tableau I-1).* Le roll-back déclenché par l'entrée de blocs continentaux dans la zone de subduction (Fig. III-10), fondé sur l'exemple de la Méditerranée où l'on observe plusieurs ceintures de roches métamorphiques associées à une seule zone de subduction. L'exhumation des unités métamorphiques de haute pression -basse température est spatialement et temporellement associée à l'entrée de bloc continentaux dans la subduction qui déclenche le roll back de la subduction et crée ainsi l'espace nécessaire à l'exhumation des roches métamorphiques de haute pression/basse température (Brun et Faccenna, 2008). Lors de son enfouissement, la croûte se découple du panneau plongeant (en partie grâce à sa flottabilité). Une fois détachée, l'unité est accrétée à la plaque supérieure. La vitesse d'exhumation de l'unité est directement dépendante de la vitesse de retrait de la fosse –Vt- (les vitesses des plaques sont rapides, de l'ordre du cm/an). L'unité nouvellement accrétée est chauffée par l'asthénosphère qui s'engouffre dans le coin de manteau, la croûte est découplée du manteau lithosphérique. Cela déclenche un nouveau stade d'exhumation de type core complex pour lequel les vitesses d'exhumation dépendent de l'extension horizontale et sont

relativement faibles (mm/an). Cela correspond aux observables géologiques (Fig. I-12) qui font apparaître une exhumation en deux temps.

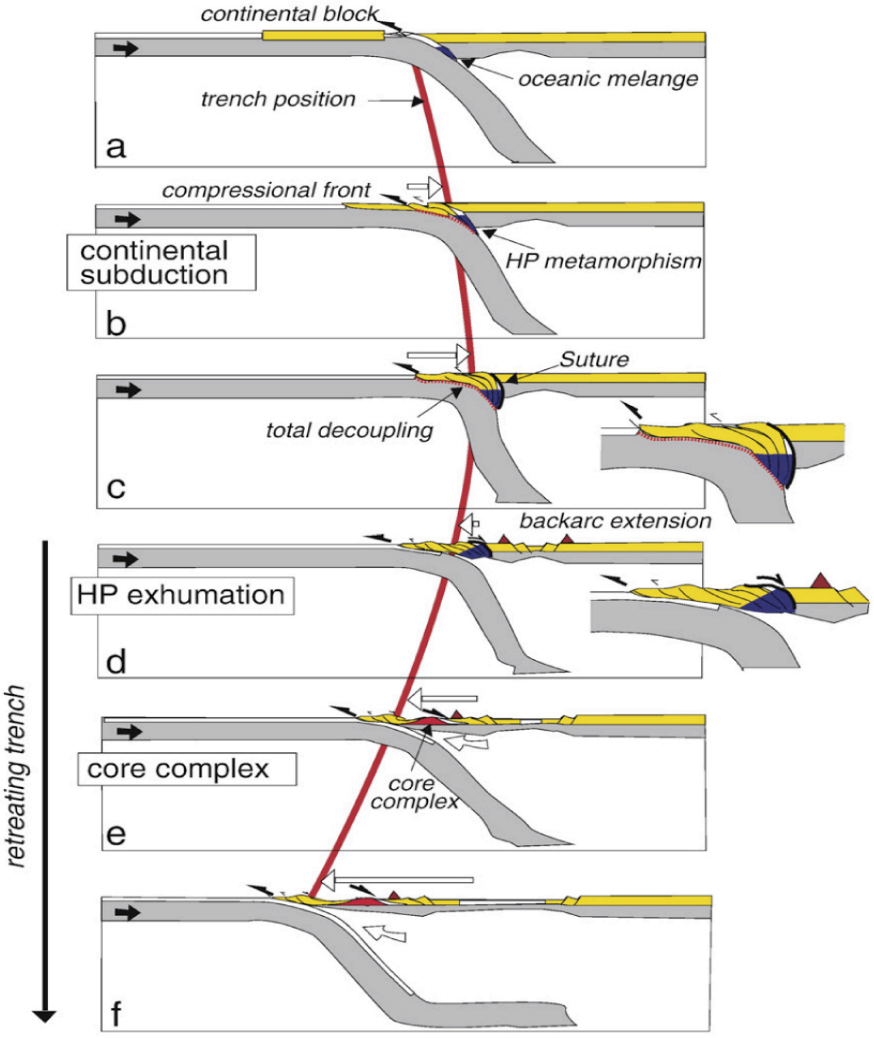

Fig. III-10. Modèle du Roll back, dans lequel l'entrée dans la zone de subduction de blocs continentaux fait reculer le slab et déclenche l'exhumation des unités métamorphiques de haute pression-basse température (Brun et Faccenna, 2008).

Ces modèles ont l'avantage de ne pas nécessiter de forts taux d'érosion pour fonctionner, les géométries observées sont semblables à celles qui sont obtenues. Aussi, ces modèles sont à même d'expliquer la formation des unités de haute pression sans passer par le modèle classique épaississement → HP : on peut avoir de l'HP sans épaississement relaxation thermique de la croûte → HT, on peut avoir de l'HT autrement.

	Références	Conditions recquises	Unités Métamorphiques HP				Unités Métamorphiques HT				Relations structurales entre unités HP et HT
			Origine	Géométrie	Déformation Ductile	Interfaces accomodant l'exhumation	Origine	Géométrie	Déformation Ductile	Interfaces accomodant l'exhumation	
Roll back	Brun et Facenna 2008	Extension syn convergence	Plaque plongeante	Pendage faible	localisée lors du découplage de l'unité, sens de cisaillement précoce associé au paragénèses HP	Bordure de la plaque chevauchante, Toit et mur de l'unité HP	Plaque chevauchante	Dôme	Linéation parallèlle à la direction d'extension, sens de cisaillement tardif associé à la rétromorphose	Détachement Crustal type MCC	Détachement recoupant l'unité HP. Deux sens de cisaillements asynchrones
Switch Tectonic	Lister et Forster 2010	Changement Extension <=> compression (et vice versa) syn convergence	Plaque plongeante	Dôme	Non précisé	Chevauchements réactivés en détachments, détachements néoformés	Non précisé (probablement plaque chevauchante)	Affleurent au cœur de plis au toit de chevauchements	Non précisé	Détachement lithosphèrique	Non précisé

Tableau I-2 Récapitulatif des modèles d'exhumation qui distinguent l'exhumation des roches métamorphiques de haute pression de celles de haute température.

Les zones de subduction exhument deux types de roches métamorphiques via des mécanismes distincts. Lors de ce travail de thèse, je me suis concentrée sur l'étude structurale d'une unité métamorphique de haute pression. Plusieurs points doivent être éclaircis afin de comprendre les tenants et aboutissants de la manière dont les roches métamorphiques de haute pression sont déformées lors de leur enfouissement et de leur exhumation.

1/ Comprendre la géométrie 3D d'un objet géologique est une étape essentielle à la compréhension des mécanismes mis en jeu lors de sa déformation.

2/ Alors que la déformation ductile est localisée sur des interfaces conduisant à une grande hétérogénéité de la déformation, les unités métamorphiques présentent une déformation ductile cisaillante, pénétrative… Il est donc impératif d'identifier la signification des déformations cisaillantes observées.

Concernant l'exhumation des roches métamorphiques, les interfaces des plaques, plongeante et chevauchante, sont celles qui accommodent les plus grands déplacements.

3/Les structures accommodant la subduction qui constituent des niveaux de faiblesse sont elles réactivées lors de l'exhumation ?

PROBLEMES GENERAUX

Déterminer des critères d'identification, sur le terrain, des structures et des déformations associées à la subduction, car il y a superposition des déformations associées à la subduction à celles qui sont associées à l'exhumation

Identifier si la subduction et l'exhumation des roches haute -pression sont accommodées par les mêmes interfaces.

Le terrain choisi afin de répondre à ces questions est l'unité des schistes bleus Cycladiques (Grèce). Cette unité de haute pression présente des conditions d'affleurement idéales. Le chapitre suivant fait état des débats qui agitent les Cyclades, auxquels ce travail de thèse apporte quelques éléments de réponses.

Chapitre 4 Les schistes bleus Cycladiques

4.1. L'âge de l'extension Egéenne : une brève revue

De l'avènement de la théorie de la tectonique des plaques jusqu'à nos jours, la Mer Egée a été et reste très étudiée. Au fil du temps, l'âge avancé pour le début de l'extension Egéenne n'a cessé d'augmenter avec l'évolution des concepts tectoniques. Je propose ici une brève synthèse retraçant cette évolution.

4.1.1. Extension arrière arc cassante, lié à la subduction

En mer Egée et en Grèce continentale la géologie anté-miocène est comparable, cependant la sismique réfraction montre que l'épaisseur de croûte en Egée est de 30km contre 50 km pour la Grèce. Sur cette base, McKenzie (1978) suggère que l'épaisseur de la croûte Egéenne à été divisé par deux depuis le Miocène (5 Ma). Les études néotectoniques montrent que le début de l'extension est Tortonien à Langhien (Angelier 1979; Mercier, 1979)

L'interaction entre le panneau plongeant et l'arc Hellénique crée de l'extension (Le Pichon et Angelier, 1979). Ils attribuent donc le début de l'extension à l'âge du panneau plongeant. Les séismes qui donnent une indication sur la profondeur maximale du panneau plongeant sous l'arc volcanique et de son pendage. Ils estiment que l'âge des magmas les plus vieux dans l'arc Egéen sont de 2,7 Ma (Fitykas et al., 1976). Avec ces informations, on peut déduire la longueur de panneau plongeant, l'âge de l'arc volcanique vient contraindre le taux d'enfouissement. A partir de la longueur du slab et du taux d'enfouissement, Le Pichon et Angelier (1979) estiment un age 13-12 Ma Serravalien- Tortonien pour le début de la subduction Hellénique.

La croûte continentale en position de plaque chevauchante dans les zones de subduction est soumise de façon prédominante à de l'extension Mercier (1981). Lorsque la subduction est active, la croûte est soumise à de l'extension générale et des chevauchements localisés au niveau de la fosse. Quand la subduction se bloque, la déformation compressive se propage dans le domaine arrière arc.

4.1.2. Extension post-Epaississement

Lister et al., (1984) sont les premiers à décrire un metamorphic core complex dans les Cyclades. Les îles d'Ios et Naxos sont des dômes allongés qui sont affectés par une linéation de direction N à NE. La direction d'extension ductile indiquée par ces linéations d'étirement est compatible avec la direction d'étirement cassante (Fig. IV-1, Angelier et al., 1982). Les sens de cisaillement indiquent un mouvement vers le Sud. Ces auteurs estiment le début de la déformation ductile à 25 Ma, âge de l'évènement métamorphique dans les Cyclades (Kreutzer et al., 1978 et Andriessen et al., 1979). La déformation cassante observée en Crète est datée à 11 Ma (Drooger et Meulenkamp, 1973), c'est l'âge du début de l'extension cassante retenue par Lister et co-auteurs.

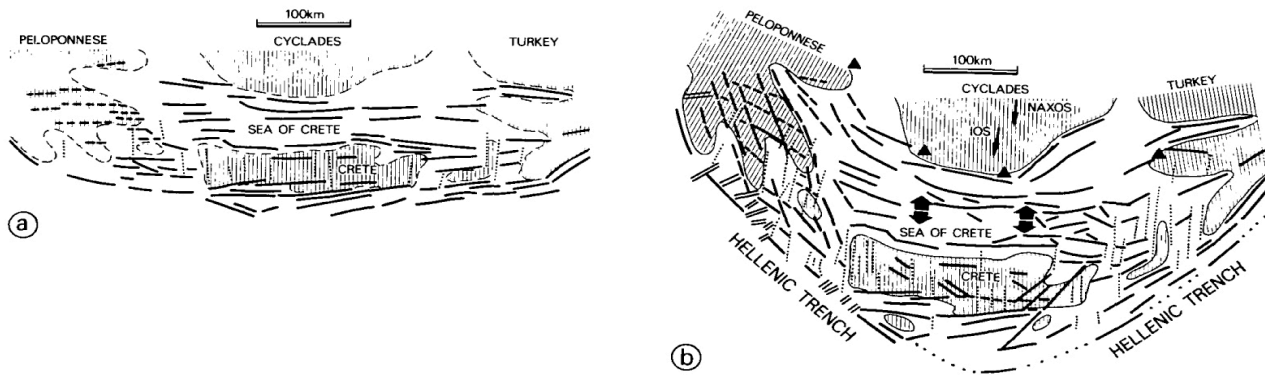

Fig. IV-1. Modèle d'extension d'Angelier et al., (1982), a) restauration anté-Tortonien (13 Ma), b) Structures actuelles, combiné avec les données de sens de cisaillement (Lister et al., 1984).

Gautier et al., 1993, estiment que l'âge de l'extension est au minimum Aquitanienne (25 Ma), âge donné par les sédiments se déposant dans les hémi-grabens au toit du détachement. Gautier et Brun (1994a) démontrent que l'extension est Oligocène, 35 Ma, en corrélant les âges de l'extension observée dans le Rhodope, l'Eubée, la Crète mais également en prenant en compte que l'extension est post-épaississement. Elle débute donc une fois que les chevauchements les plus jeunes cessent de fonctionner. Les derniers chevauchements sont datés au début de l'Oligocène (Bizon et al., 1976; Sotiropoulos et al., 2003; Van Hinsbergen et al., 2005).

4.1.3. Extension syn-convergence.

La subduction Hellénique est continue du Jurassique, fermeture de l'Océan du Vardar, à l'actuel. L'épaississement est Crétacé à Eocène inférieur dans les Cyclades (ou du moins l'âge des roches métamorphiques de haute pression est Crétacé à Eocène). L'extension commence à l'Eocène Moyen (45 Ma) dans le massif du Rhodope (Burchfield et al., 2003, Brun et Sokoutis 2007, Kounov et al., 2004) et les derniers chevauchements sont d'âge Eocène (42 Ma, Liati 2005). À l'Eocène, des chevauchements se développent à l'avant de la chaîne, (i.e. dans les Cyclades) et l'extension affecte le domaine arrière arc (i.e. dans le Rhodope).

4.2. L'exhumation des schistes bleus cycladiques : évolution des concepts.

Les modèles d'exhumation s'inspirent directement des concepts tectoniques en usage et sont dépendants de l'âge attribué à l'extension Egéenne.

4.2.1. Exhumation post orogénique

- De dômes métamorphiques «chauds»

À l'échelle régionale, les sens de cisaillements opposés portés par la linéation régionale NE et les sens de cisaillement co-axiaux sont supposés synchrones et associés à l'exhumation des metamorphic core complexes. Les sens de cisaillements vers le NE sont associés au déplacement sur le détachement à pendage NE et le sens de cisaillement vers le SW est synchrone et associé au mouvement sur le flanc arrière des dômes (Fig. IV-2). L'inversion des sens de cisaillements à lieu au milieu du dôme où l'on trouve des indicateurs de co-axialité (Gautier et Brun 1994a).

Fig. IV-2. Coupe schématique de la paire de dômes Naxos/Ios, montrant les zones affectée par un cisaillement vers le Nord, Le Sud et Coaxial (Gautier et Brun 1994a).

Jolivet et al., (2010), montrent que les détachements responsables de l'exhumation post orogénique des roches de haute température réactivent des zones de faiblesse préexistantes comme les chevauchements ayant contribués à l'empilement de nappes, ou encore la suture du Vardar (Fig. IV-3).

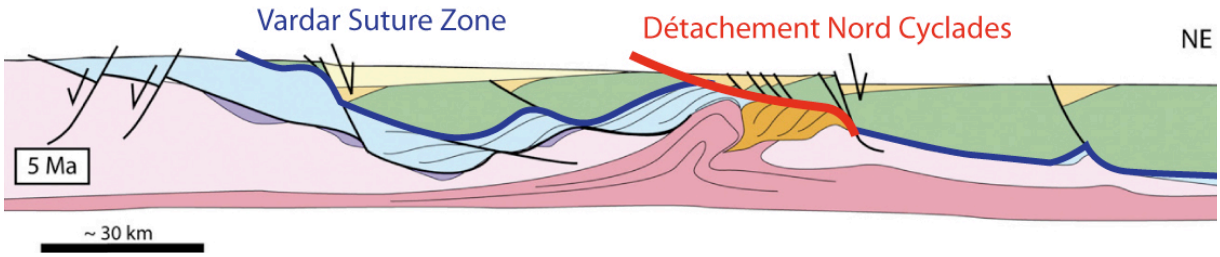

Fig. IV-3. Coupe des Cyclades montrant la géométrie de la suture du Vardar et du détachement Nord Cyclades (Jolivet et al., 2010).

- D'un Dôme métamorphique «froid»

L'unité des schistes bleus cycladiques est un «core complex froid» qui s'exhume en extension (Fig. IV-4, Huet 2010). Ces modèles numériques montrent que la rhéologie particulière de la lithosphère Egéenne hérité de l'empilement de nappes métamorphiques est un paramètre prépondérant car il permet de développer des «metamorphic core complexes» dit froids car ils se développent malgré une température au Moho faible (TMoho<800°C).

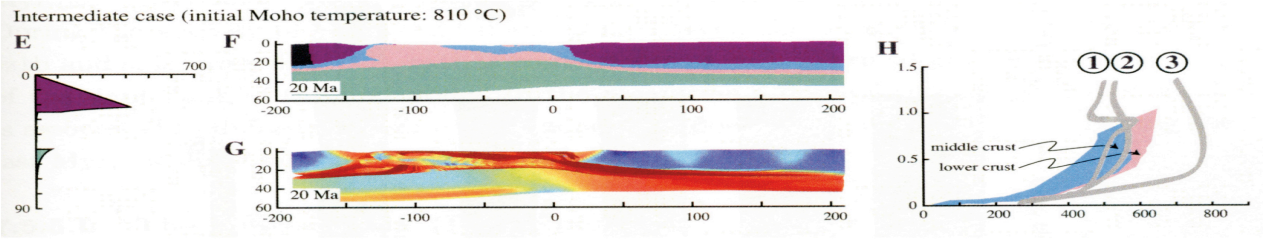

Fig. IV-4. Résultats du modèle thermomécanique, expliquant l'exhumation de l'unité des schistes bleus cycladiques .D'après Huet 2010.

Attention, car ces deux modèles d'exhumations post orogénique ne font pas de différence entre exhumation des roches de haute pression et celle des roches de haute température, contrairement aux suivants.

- De dômes métamorphiques «froids et chauds»

Jolivet et al., 2004, proposent qu'il existe deux types de dômes métamorphiques extensifs (Fig. IV-5). Les dômes de « type b » sont allongés perpendiculairement à la direction d'étirement nord-sud et correspondent à l'exhumation de la croûte moyenne le long de détachements à pendage Nord (Tinos, Andros), ils exhument les roches de haute pression. Les dômes de « type a » sont allongés parallèlement à la direction d'etirement nord sud et exhument des roches de haute température. Chronologiquement, les dômes de « type b » se forment en premier et exhument les roches de haute pression, puis les dôme de « type a » exhument les roches de haute température, recoupant les dômes de « type b» précédemment formés. Il se forme alors deux linéations d'étirement asynchrone et perpendiculaires, comme on peu l'observé dans les Cyclades ou deux directions perpendiculaires de linéations sont observées NE à Tinos et E à Syros.

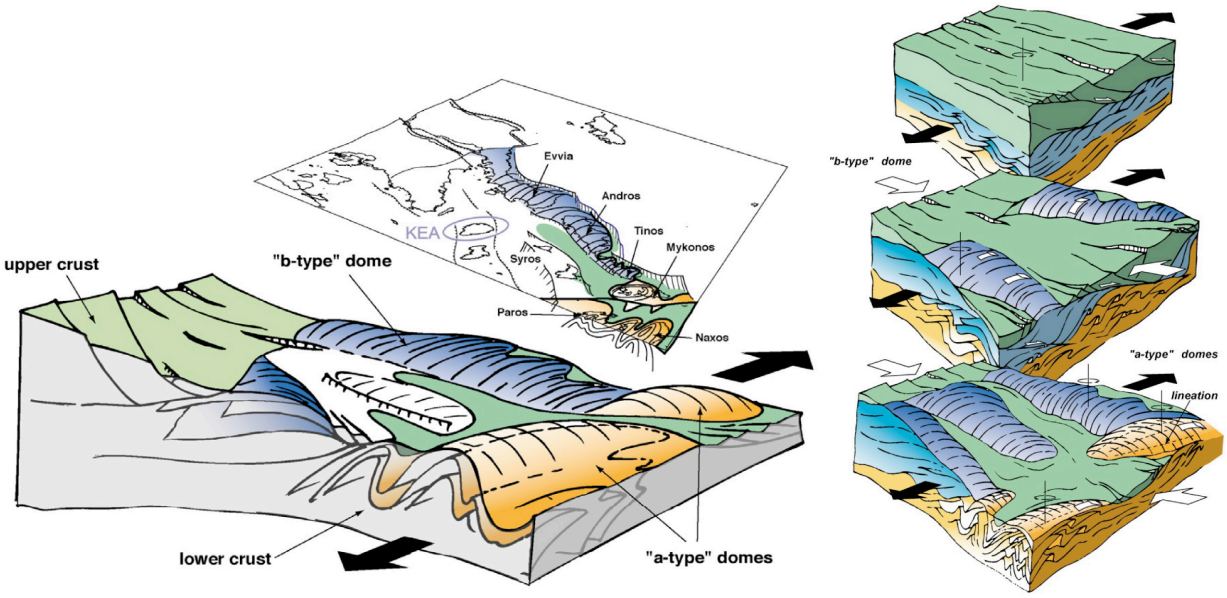

Fig. IV-5. Carte et bloc diagramme des Cyclades montrant les dômes de type a en orangé et de type b en bleu. A droite, coupes évolutives montrant l'exhumation successive des dômes de types a puis b (Jolivet et al., 2004).

Van Hinsbergen et al., (2005) distinguent des core complexes froids et chauds. Le «core complex chaud» exhume des roches de haute température, est limité par deux détachements l'un à son toit, l'autre à son mur. Le détachement sommital permet l'exhumation du core complex sensu stricto, le détachement basal permet d'exhumer du

matériel chaud sous le core complex (Fig. IV-6). Le «core complex froid» présente un seul détachement sommital, qui participe à l'exhumation de celui-ci sans superposition de haute température. Pour ces auteurs, la paire Cyclades - Crète est une paire de dômes métamorphiques froid et chaud contemporains.

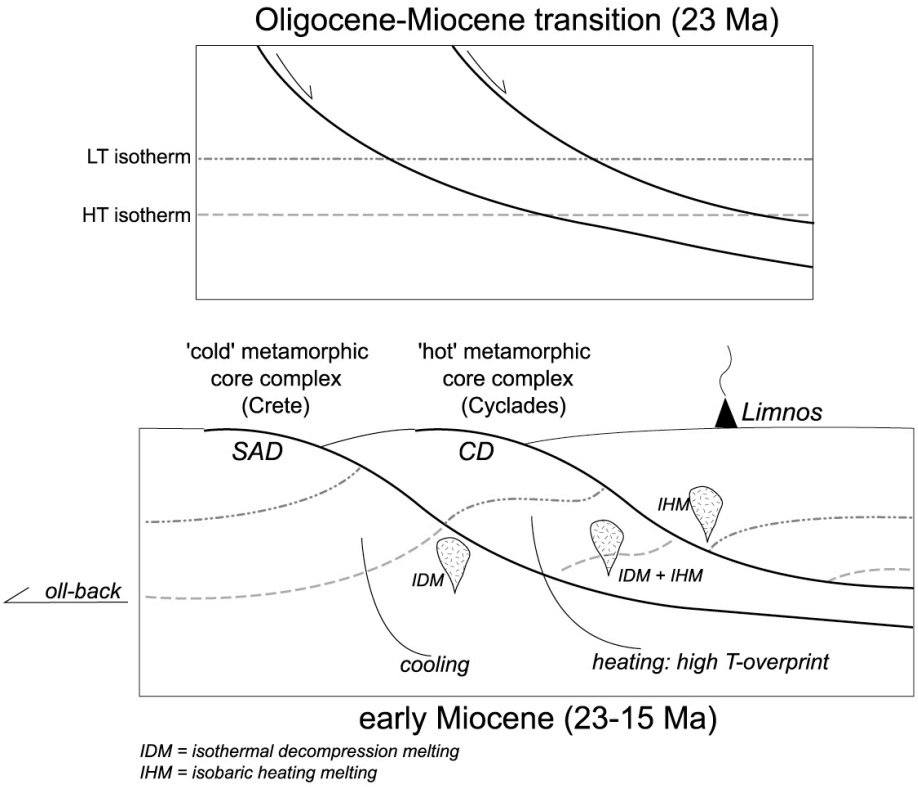

Fig. IV-6. Transition de la compression à l'extension estimée à la transition Oligo-Miocène Le core complex chaud des Cyclades, délimité par deux détachements et le core complex froid de Crète délimité par un seul détachement (Van Hinsbergen et al., 2005).

4.2.2. Exhumation syn-orogénique

Plusieurs dizaines de kilomètres de croûte ont été enlevés au-dessus des éclogites avant l'Oligocène supérieur - Miocène inférieur, i.e. avant le début de l'extension (Avigad et al., 1997). Les structures extensives associées à l'extension arrière arc jouent un rôle limité lors de l'exhumation des éclogites. Avigad et al., (1997) ont proposés qu'entre l'Eocène et l'Oligo-Miocène, des chevauchements sont actifs dans le domaine arrière arc. Les unités éclogitiques sont exhumées via des chevauchements qui fonctionnent dans un prisme d'accrétion actif. L'extension syn-orogénique ne laisse pas de structures mais pourtant elle participe, couplée aux chevauchements, à l'exhumation des éclogites (Fig. IV-7).

D'autres auteurs proposent qu'une partie de l'exhumation de l'unité des schistes bleus cycladiques a eut lieu au sein d'un chenal de subduction (Huet et al., 2009 ; Jolivet et al., 2009 et Jolivet et al., 2010,) ou grâce à l'individualisation d'une écaille de croûte supérieure sous l'appellation d'« extrusion wedges » (basé sur Chemenda et al., 1995) (Fig. III -7). La déformation ductile observée consiste en deux sens de cisaillements opposés portés par une linéation régionale résultant de l'enfouissement et de l'exhumation synchrone de l'unité métamorphique au sein d'un chenal de subduction.

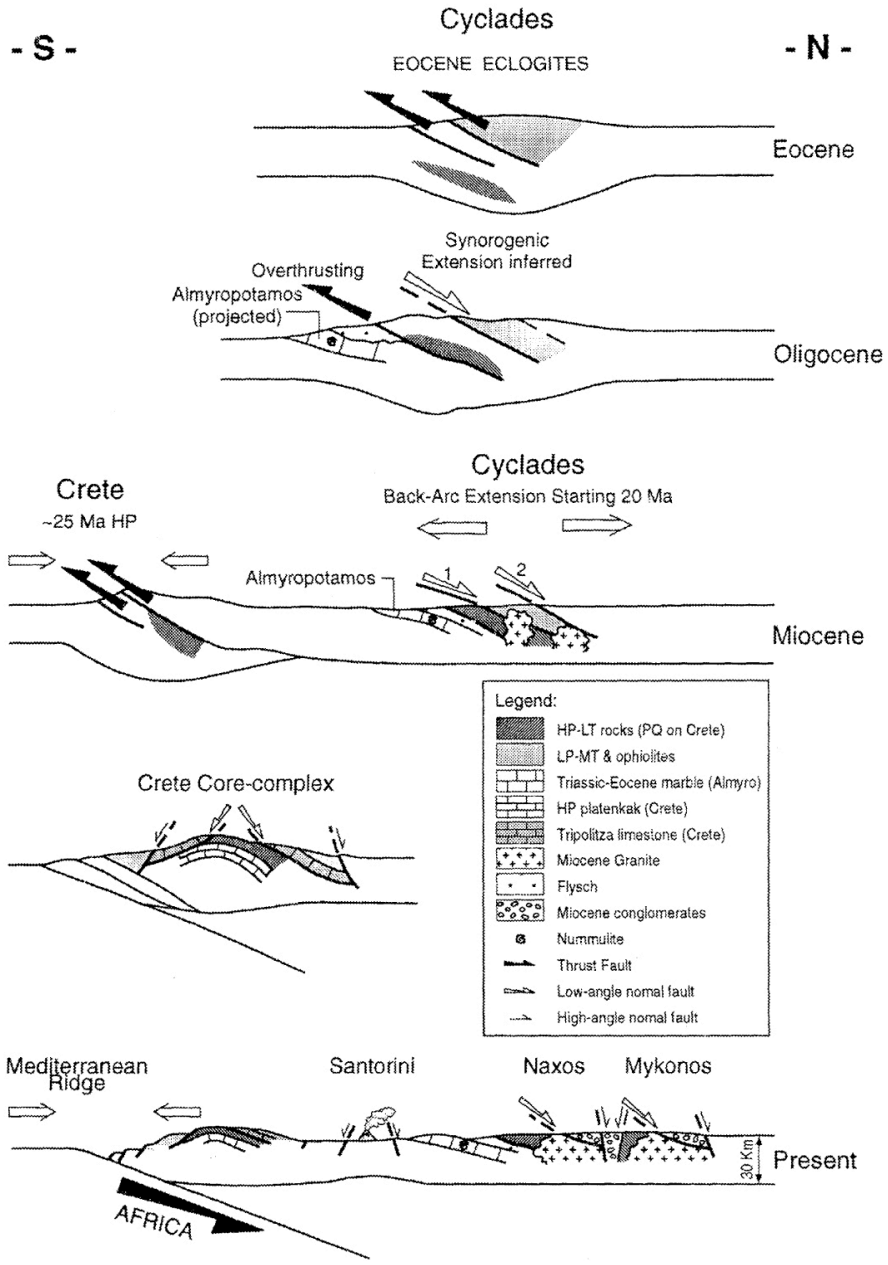

Fig. IV-7. Evolution schématique des Cyclades et de la Crète de l'Eocène a l'actuel. Une bonne part de l'exhumation des éclogites se fait entre l'éocène et le Miocène Inférieur. Les structures extensive syn orogéniques ne sont pas décrites participent à l'exhumation des éclogite dans les premiers stades de l'exhumation (Avigad et al., 1997).

4.2.3. Extension syn-convergence accommodée par l'exhumation des unités haute pression.

L'idée de la réactivation de la suture pour expliquer l'exhumation des roches de haute pression - basse température est également évoquée dans les modèles d'exhumation syn-orogénique. Le modèle du roll-back fait intervenir la réactivation de la suture lors de l'extension arrière-arc (Fig. IV-8d).

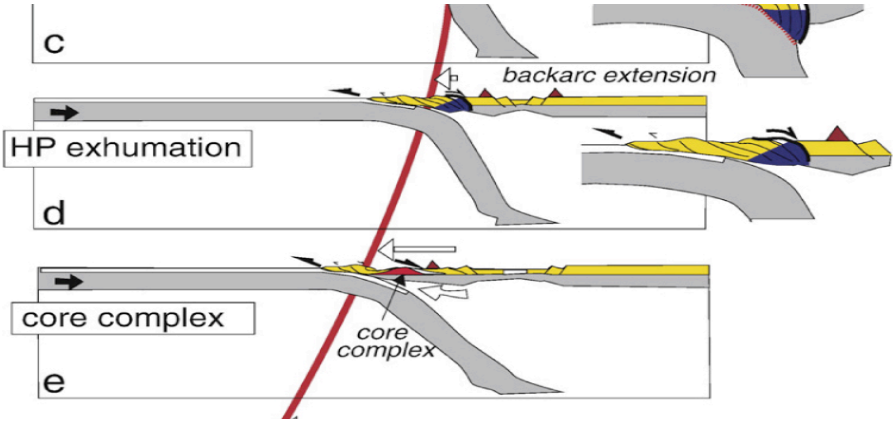

Fig. IV-8. Figure montrant l'exuhmation syn convergence des unités métamorphiques de haute pression - basse température (Brun et Faccenna 2008).

Dans ce modèle, les structures participant à l'exhumation des roches métamorphiques de haute pression et haute température sont différentes. L'exhumation des deux types de roches est liée au retrait du panneau plongeant de lithosphère africaine vers le sud lors du verrouillage de la subduction crée par l'entrée du bloc Pélagonien dans la subduction(Fig. IV -9e et f).

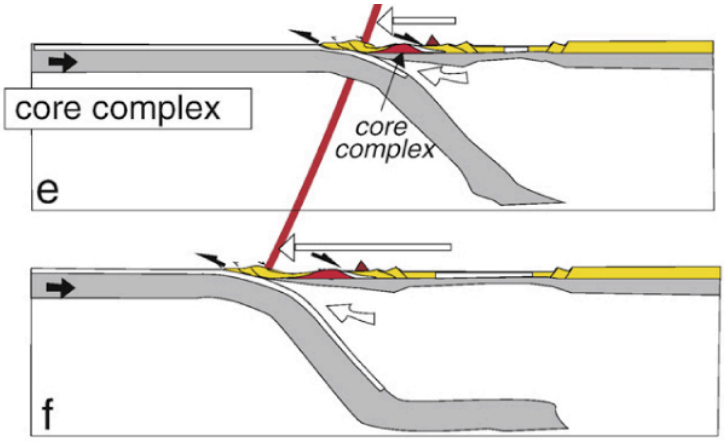

Fig. IV-9. Figure montrant l'exhumation syn convergence des unités métamorphiques de basse pression-haute température (Brun et Faccenna 2008).

Quelle est la signification des sens de cisaillements observés à l'échelle de l'unité des schistes bleus cycladiques ?

Selon les modèles d'exhumation proposés pour expliquer l'exhumation des schistes bleus cycladiques, la déformation ductile (Fig. IV-10) est interprétée de différentes manières:

Deux sens de cisaillements opposés portés par une linéation régionale soit résultant de l'amincissement homogène de la lithosphère (Gautier et Brun 1994a), soit de l'enfouissement et de l'exhumation synchrone au sein d'un chenal de subduction (Huet et al., 2009 ; Jolivet et al., 2009 et Jolivet et al., 2010,).

Deux linéations régionale asynchrones et perpendiculaires (Jolivet et al., 2004).

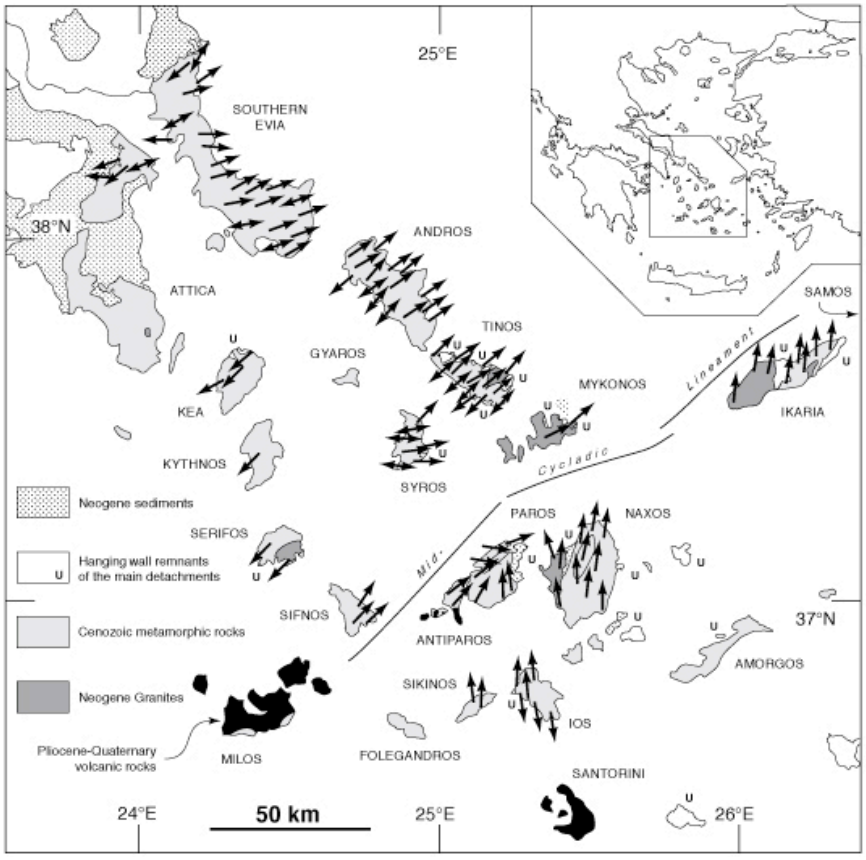

Fig. IV- 10 Carte géologique simplifiée des Cyclades. Les flèches indiquent la cinématique de la déformation extensive (Gautier et Brun 1994 a; Tirel et al., 2009).

L'un des objectifs de ce travail de thèse est donc de lever l'ambiguïté concernant les déformations ductiles observées dans l'unité des schistes bleus cycladiques et ainsi de distinguer la déformation liée à la subduction de celle liée à l'extension Egéenne.

Que signifient les contacts plats affleurant dans les Cyclades ?

Au moins trois détachements affleurent dans les Cyclades et sont décrits comme étant responsables de l'exhumation des roches haute température et haute pression constituant l'unité des schistes bleus Cycladiques (Jolivet et al., 2010). Les relations structurales entre la plaque chevauchante, l'unité haute pression des schistes bleus Cycladiques et les MCCs sont fondamentales pour comprendre si se sont les mêmes interfaces qui sont responsables de l'exhumation des roches haute pression et haute température.

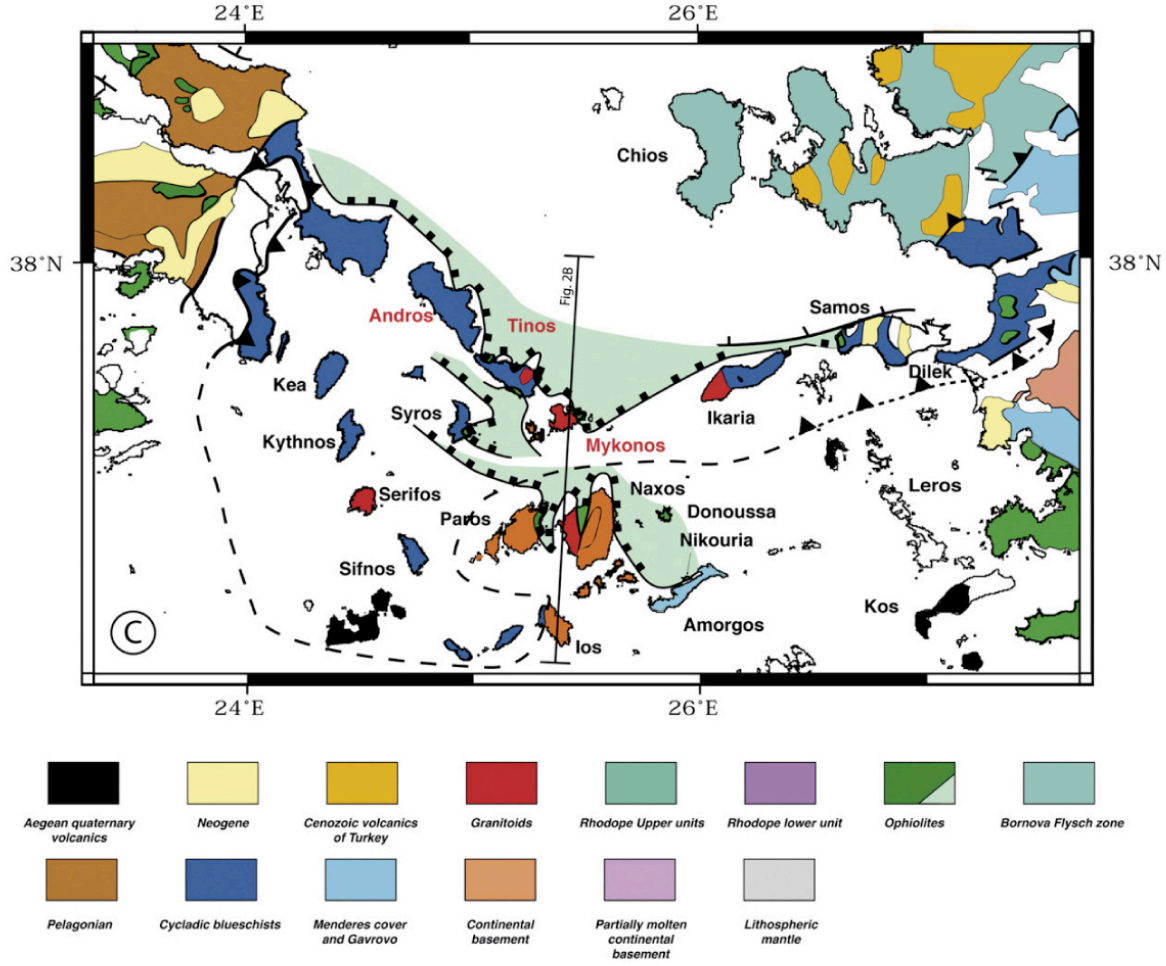

Fig. IV-11 Carte de Cyclades montrant les nombreux détachements exhumant l'unité des schistes bleus cycladiques (Jolivet et al., 2010).

L'un des objectifs de cette thèse est de contraindre au mieux la structure de l'unité des schistes bleus cycladiques. Ceci afin d'analyser le rôle des contacts plats dans l'exhumation de l'unité des schistes bleus Cycladiques.

Comment se comporte la lithosphère Egéenne lorsqu'elle est soumise à l'extension ?

Parmis les modèles cinématiques proposés pour expliquer l'extension Egéenne, on distingue deux types de modèles qui se basent sur les observables géologiques.
Le modèle de blocs rigides dans lesquels la déformation est localisée en bordure de blocs (Mc Kenzie 1972, 1978) est basé sur la propagation de la faille nord Anatolienne.

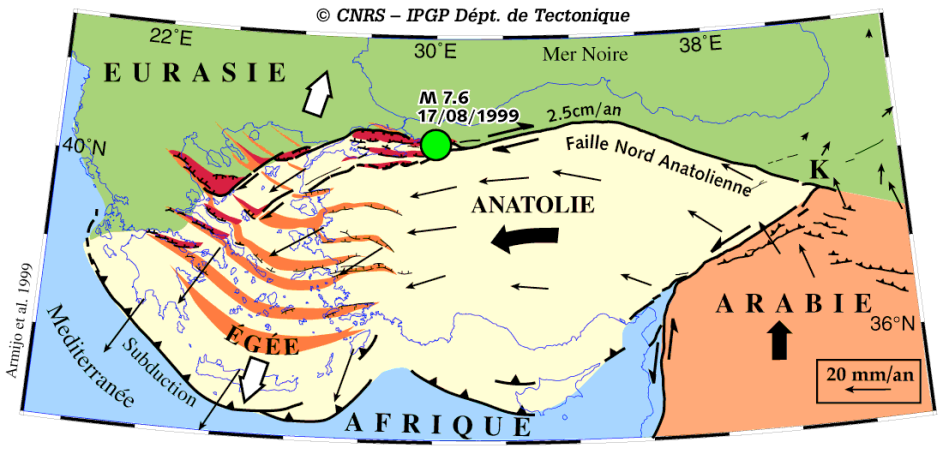

Fig. IV-13 Carte régionale montrant la propagation de la faille nord anatolienne (Armijo et al. 1999)

Dans l'autre modèle classiquement proposé, le flux de croûte ductile contrôle la déformation de la croûte fragile (Gautier et al.,1999, Hatzfeld 1995).

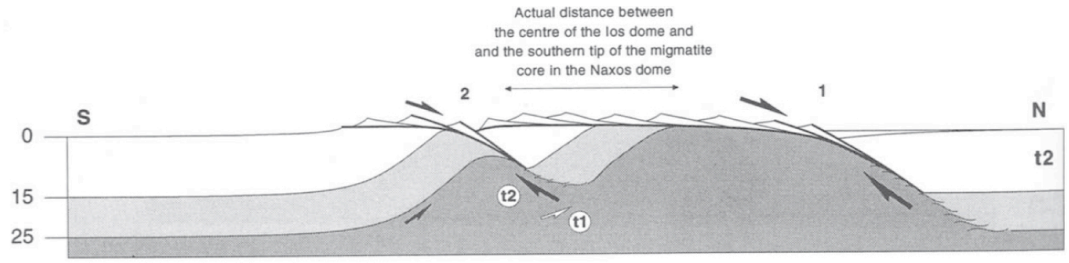

Fig. IV-12 Coupe de la croûte Egéenne au niveau du core complex des Cyclades (Gautier et Brun 1994 a)

Ces deux modèles se basent sur des comportements mécaniques très différents : la propagation de la Faille Nord Anatolienne et l'exhumation de « metamorphic core complexes ». L'objectif de L'ANR EGEO, qui a financé intégralement cette thèse, était de comprendre pourquoi la lithosphère Egéenne produit des réponses mécaniques si différentes. Les modèles analogiques réalisés durant cette thèse montrent la compatibilité de ces réponses lors de la déformation de la lithosphère Egéenne : de

l'exhumation du core complex des Cyclades à la propagation de la faille nord Anatolienne.

Partie 2/ Déformation d'une unite HP-BT lors de la subduction et de l'exhumation: exemple de l'île de Syros

Chapitre 5 : Les pseudomorphes de Lawsonites : une jauge de non déformation des schistes bleus.

LAWSONITE PSEUDOMORPHS: A STRAIN-FREE GAUGE IN EXHUMING BLUESCHISTS.

Melody Philippon, Frédéric Gueydan and Jean Pierre Brun

Géosciences Rennes UMR 6118 CNRS, Université de Rennes 1, 35042 Rennes cedex, France

Submitted to Geology

Abstract

The kinematics records of subduction and exhumation in Blueschists rocks of Syros (Cyclades; Greece) can be deciphered thanks to Lawsonite pseudomorphs. Since Lawsonite is a hydrous HP mineral that crystallizes along prograde rock paths and undergoes breakdown during decompression, Lawsonite pseudomorphs consist in a useful strain-free gauge to identify deformation that occurred before its destabilization. The preservation of lawsonite crystal shape despite complete retrogression indicates that the blueschist host rock has not been affected by penetrative deformation during exhumation. Using this strain-free indicator as a tool, it is shown that in the Cyclades, subduction related deformation occurred with a sense of shear top to S or SW, prior to 52 Ma and is followed by exhumation with a top to NE sense of shear.

5.1. Introduction

High-Pressure/Low-Temperature (HP/LT) metamorphic rocks represent part of the crustal material first buried in subduction zones and then exhumed. Several models have been proposed to explain exhumation processes involving different kinematics patterns (Ring and Layer, 2003, Jolivet et al., 2003, Brun and Faccenna, 2008). Deciphering in blueschists between deformations due to subduction and exhumation, respectively, is thus essential to ultimately provide constrains on those models, but remains a difficult task. Lawsonite is a hydrous HP mineral that crystallizes during the burial/prograde path of the rock inside the subduction zone (Poli and Schmidt, 1995). The metamorphic reaction of lawsonite breakdown (i.e. Lws+=WM+Ab+Ep) occurs as soon as the rock undergoes decompression and/or heating. In the Cyclades (Greece), in spite of superposed deformations linked to subduction and exhumation processes, HP units have surprisingly conserved (1) their initial sedimentary or magmatic geometry and even their stratigraphy with fossils giving ages from Visean to Eocene (Pohl, 1999;

Dubois and Bignot, 1979) and (2) evidence of prograde HP/LT metamorphism –e.g. lawsonite and aragonite pseudomorphs. Since two decades, ductile deformations in blueschists terranes have been attributed to exhumation up to the brittle/ductile transition (Jolivet and Goffé, 2000). The exceptional preservation of lawsonite pseudomorphs in Syros rocks and in blueschists terranes in general, (for worldwide occurrences see Tsujimori et al., 2006), offers a powerful tool to identify deformations that occurred in the lawsonite stability field located in the HP/BT part of the PT path, at least partly, if not entirely, related to subduction.

5.2. Regional Geology

The Cycladic blueschists Unit (CBU) corresponds to an ophiolitic unit, made of metagabbros, metavolcanites and serpentinites, thrust on top of a basement-cover margin sequence that were then metamorphosed under blueschists facies conditions during the Eocene (Fig. IV- 1). Despite their round trip across lithosphere and related deformation, the Cycladic blueschists have conserved lawsonites and aragonites pseudomorphs (Trotet et al., 2001a; Keiter et al., 2004; Brady et al., 2004) that are both witness of prograde high-pressure metamorphism (For PT path see Annexe A). The CBU unit displays a NE trending stretching lineation at regional-scale that is associated to either top to the NE or SW senses of shear. Top to S or SW are systematically observed where lawsonite pseudomorphs are preserved, (Fig. IV- 1). Syros, where the glaucophane was discovered (Hausmann, 1845), displays the largest outcropping area of well-preserved lawsonite pseudomorphs. From base to top, the two main tectonic units of Syros are: (1) a continental margin unit made of a the 300Ma gneissic basement intruded by a 240-243Ma pluton (U/Pb on Zircon SHRIMP, Keay 1998; Tomaschek et al., 2003; Tomaschek and Ballhaus, 1999 ; Tomaschek et al., 2008) and of a sedimentary cover sequence ranging from 330 to 45 Ma (Pohl, 1999; Dürr et al., 1978; Dubois and Bignot, 1979) and (2) the 240 to 80 Ma oceanic crust (Bulle et al., 2010) (Fig. IV- 1). The conditions of Eocene metamorphism are estimated from 8-17 kbar and 350-500 °C for the continental unit (Dixon and Ridley, 1987; Okrusch and Bröcker, 1990; Trotet et al., 2001a; Schumacher et al., 2008) to19-24 kbar and 500-580°C for the oceanic unit (Trotet et al., 2001a; Gitahi, 2004; Holley et al., 2004).

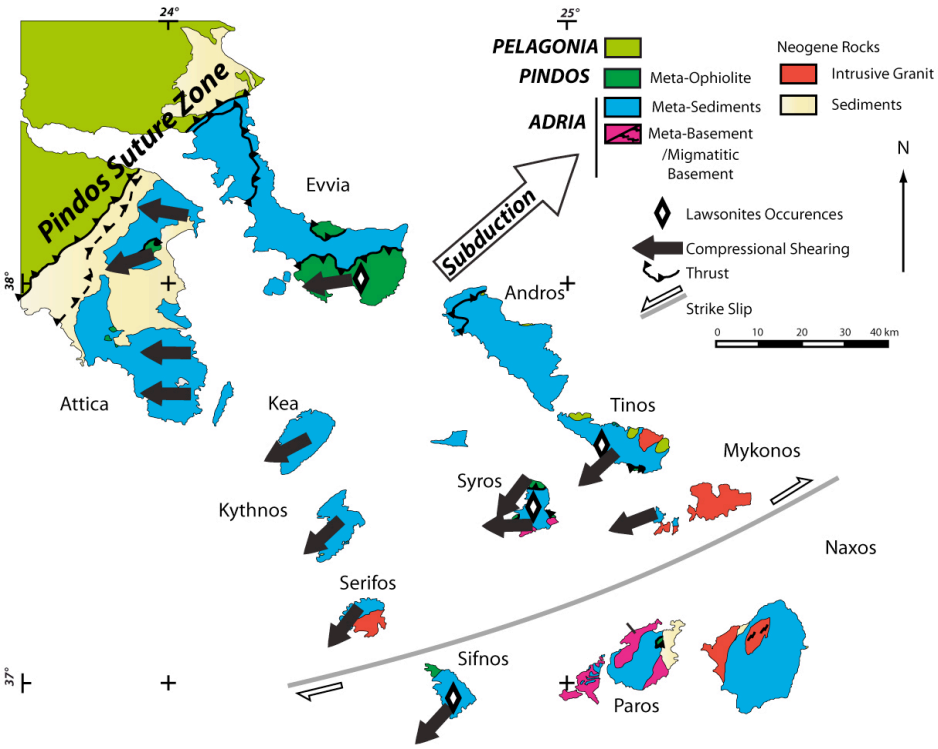

Fig. V- 1 Map of the Cyclades showing the upper Pelagonian plate, and the subducted material consisting of Pindos oceanic crust and Adria continental margin, top to the SW sense of shear and Lawsonites pseudomorphs occurrences.

5.3. Ductile deformation and Lawsonite pseudomorphs

Microprobe analyses of lawsonite pseudomorphs from Syros fine-grained blueschists have been performed with a Cameca SX50 (Microsonde Grand Ouest, 15Kv accelerating voltage, 20 nA sample current and 20 sec counting time). Figure 2a shows the titanite, glaucophane and white micas foliation, idioblastic garnets and euhedral lozenge shaped lawsonite pseudomorphs consisting of zoïsite, albite and white micas. X-Rays elements maps for TiO2 and MnO are important constraints for the lawsonite history. Intact hourglass distribution of TiO2 inside the lawsonite pseudomorph indicates that Ti was not mobile inside the fresh lawsonite and that the pseudomorph has not been deformed after the lawsonite breakdown. A late growth of lawsonite is indicated by the similar MnO distribution of garnets inside and outside the lawsonite pseudomorph (Fig. IV- 2c) and by the relationship between lawsonite pseudomorph and the titanite foliation (red elongated minerals in Fig. IV- 2b, we try to date the Titanite, see Annexe B).

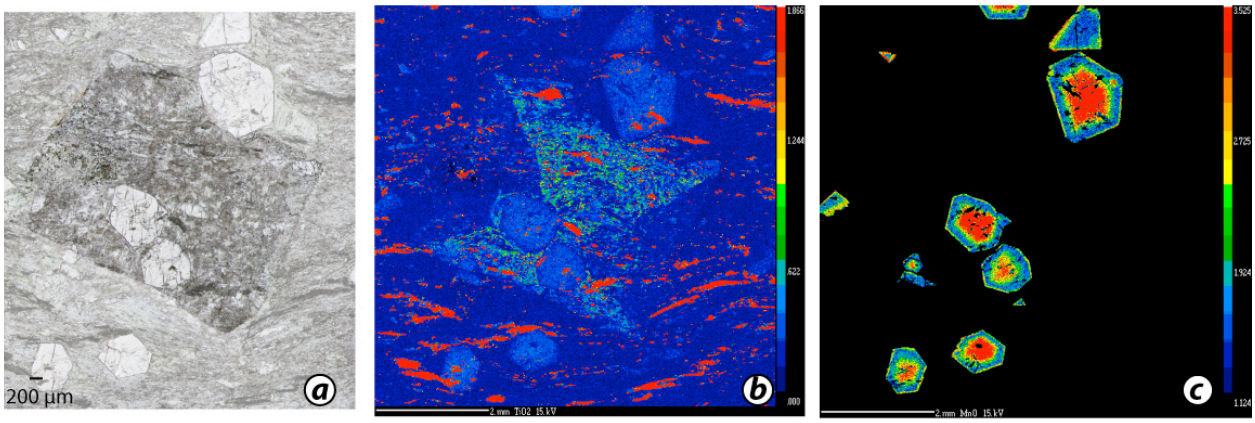

Fig. V- 2 Thin section containing Lawsonite pseudomorph (a) and X-Ray map showing the distribution of TiO2 (b) and MnO (c)

In Syros, lawsonite pseudomorphs are observed only in the oceanic unit. In the north of the island (Fig. IV- 3), where the pseudomorphs are especially well exposed, the base of the oceanic unit corresponds to metagabbros and highly deformed serpentinite schists thrust on top of marbles (Fig. IV- 3) (Ridley, 1982; Keiter et al., 2004; Bond et al., 2007) with a stretching lineation trending N-S and an associated sense of shear top to S (Fig. IV- 1).

In the thrust footwall, a second event of top-to-NE shearing that is coeval with metamorphic retrogression, from eclogite to greenschist facies (Trotet et al., 2001a) is linked to the exhumation of the CBU up to the brittle-ductile transition. During exhumation, the lawsonite crosscut the breakdown boundary and is destabilized giving the pseudomorphs.

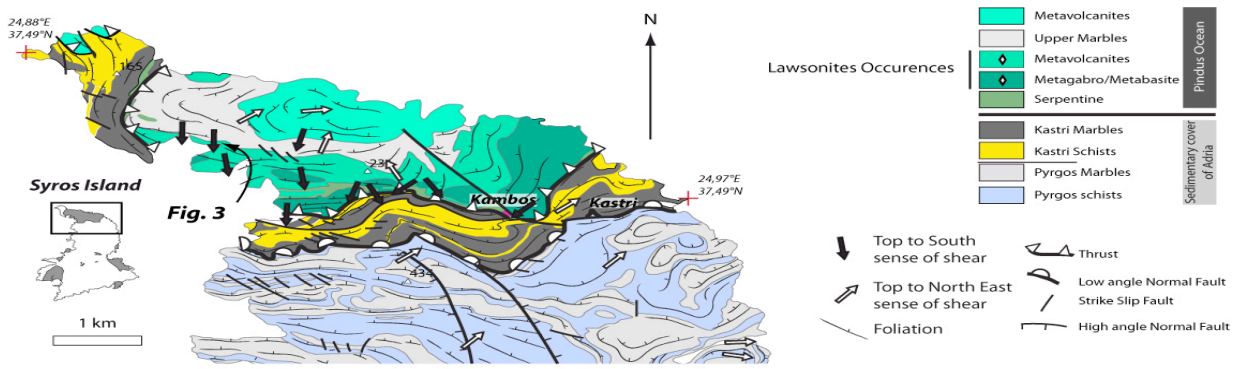

Fig. V- 3.Detailed map of North Syros illustrating the relationship between Lawsonite pseudomorphs and top to S-SE sense of shear. Top to NE sense of shear is only observed in the underlying sedimentary cover consisting of schists and marbles.

The destruction of lawsonite pseudomorphs by shear strain is well demonstrated in the small unit of lawsonite pseudomorphs-bearing rocks, located at Finikas in the southwest of the island (Fig. IV- 4) that has been affected by shear zones in greenschist facies conditions, after the destabilization of lawsonite. At outcrop-scale, between shear zones, cm-scale lawsonite pseudomorphs are numerous with well preserved shapes whereas, inside shear zones, they almost entirely disappear (Fig. IV- 4). Thin sections, between shear zones, show a foliated rock matrix made of chlorite, calcite, zoïsite, albite and white mica and lawsonite pseudomorphs composed of zoïsite+white micas+albite (Fig. IV- 4). Pressure shadows containing calcite fibers around lawsonite pseudomorphs indicate that lawsonite first acted as rigid inclusions during top to the S-SE deformation. Inside shear zone, the matrix is calcite-dominated, indicating fluid circulation, and contain stretched and folded aggregates of zoïsite, white micas and albite corresponding to strongly deformed lawsonite pseudomorphs. With the increase of strain intensity, the deformed lawsonite pseudomorphs become progressively undistinguishable from the matrix.

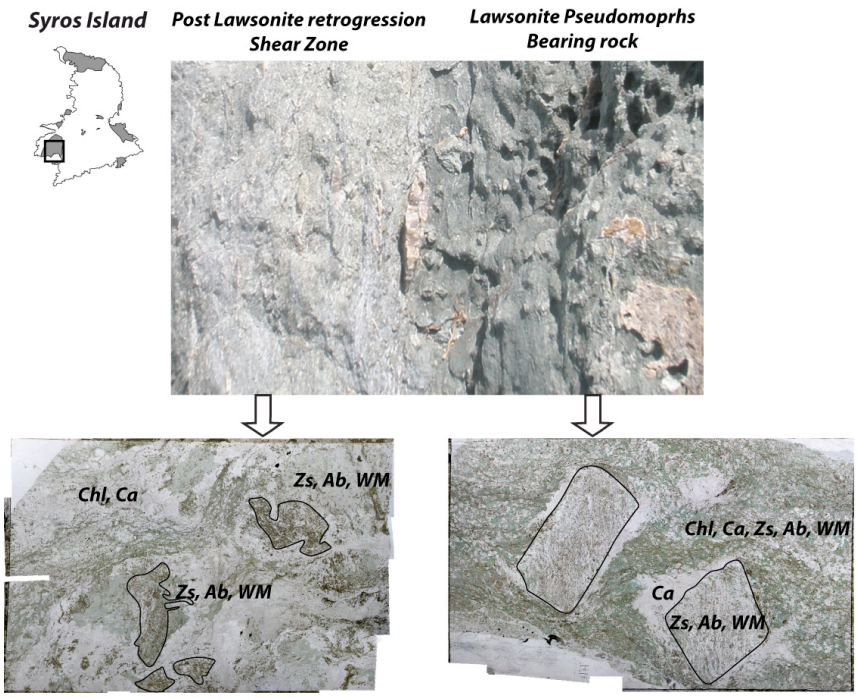

Fig. V- 4.Outcrop showing a Lawsonite pseudomorph bearing rock affected by a shear zone after the Lawsonite breakdown. Thin sections outside and inside the shear zone show the behavior of Lawsonite pseudomorph during shearing.

5.4. Discussion

The analysis of lawsonite pseudomorphs preservation combined to petrological, geochronological and kinematic data allows the identification of subduction versus exhumation effects in the evolution of the CBU:

The lawsonite stability field (Schumacher et al., 2008) is located on the prograde path of the CBU. Shearing top-to-S occurred in the lawsonite stability field, as indicated by the preservation of lawsonite pseudomorphs, and is therefore related to subduction. This event occurred prior to 52 Ma (Lagos et al., 2002, 2007).

Retrograde greenschist facies overprint associated to shearing top-to-NE (blue section of the PT path Fig. 3a) affects large volumes of the CBU from the eclogite facies to the greenschist facies (Trotet et al., 2001a) during exhumation up to the brittle/ductile transition. Lawsonite pseudomorphs are destroyed by shearing in domains affected by penetrative deformation during exhumation (see also Philippon et al., 2009, Annexe C). Aragonite crystals have a comparable behavior and give constraints on the retrograde path from their breakdown (9 Kbar) to the surface (Brady et al., 2004). Where they are preserved, rocks remain unaffected by exhumation-related penetrative deformation. The transition between the eclogite facies metamorphism (52 Ma; Lagos et al., 2002) and retrogression in the blueschists and greenschists facies is estimated at 35 Ma (Altherr et al., 1979).

Lawsonite growth occurred at deep crustal level during southward thrusting of the oceanic unit onto the margin sequence. Zack et al., (2004) advocated that lawsonite are not exhumed from normal subduction zones or that lawsonite needs a very peculiar thermal exhumation path to be preserved. From the Syros example, we show that the exceptional preservation of lawsonite and aragonite pseudomorphs only reflects the lack of penetrative deformation during exhumation, as already suggested by Keiter et al., (2004); Brady et al., (2004); Whitney and Davis, (2006) and Philippon et al., (2009). Finally, contrary to previous studies (Gautier and Brun 1994a; Rosenbaum et al., 2002; Tirel et al., 2009), the above quoted evidence shows that senses of shear, top-to-S in the

oceanic unit and the top-to-NE in the sediment/basement unit are not synchronous. This observation rules out the HP rocks exhumation models of the CBU that involve two opposite synchronous sense of shear as a result of either coaxial flattening at crustal scale (Rosembaum et al., 2002; Bond et al., 2007) or core complex-type extension (Gautier and Brun, 1994a; Tirel et al., 2009).

5.5. Conclusions

Because lawsonite pseudomorphs are composed of zoïsite + white micas + albite, any penetrative deformation makes them rapidly undistinguishable from the host rock matrix. Consequently, well-preserved lawsonite pseudomorphs with their typical euhedral lozenge-shape indicate that the host rock has not undergone any significant penetrative deformation after lawsonite destabilization. For this reason they consist in a useful strain-free gauge to identify deformations that occurred before the destabilization of lawsonite. In blueschists, this provides a very efficient tool to decipher between subduction and exhumation related deformations, as lawsonite is a hydrous HP mineral that crystallizes along prograde rock paths during subduction and that undergoes breakdown during decompression and/or heating. As exemplified in the blueschists of Syros and extended at the whole Cyclades scale (Greece), subduction related deformation that is sealed by lawsonite pseudomorphs occurred with a sense of shear top to S or SW, prior to 52 Ma. The following exhumation of the Cycladic Blueschists Unit must be re-investigated in this light.

Acknowledgments

The present work was financially supported by the ANR-EGEO project. We are extremely grateful to L. Jolivet for having introduced us to Syros geology. We alos thanks Pavel Pitra for his patience with thermocalc (and myself) and Marc Poujol for the titanites dating attempt. Discussions at various stages of the project with L. Jolivet, P. Agard, B. Huet, and L. Labrousse, in particular within the framework of the ANR-EGEO project, have been very useful and stimulating. However, the data and interpretations presented here are our entire our own.

References

Altherr, R., Schliestedt, M., Okrusch, M., Seidel, E., Kreuzer, H., Harre, W., Lenz, H., Wendt, I. & Wagner, G. A., 1979, Geochronology of high-pressure rocks on Sifnos (Cyclades, Greece): Contributions to Mineralogy and Petrology, v. 70, p. 245-255.

Bond, C., Bulter, R.W.H. and Dixon J.E, 2007, Co-axial horizontal stretching within extending orogens: the exhumation of HP rocks on Syros (Cyclades) revisited: Geological Society of London, Special publication, v. 272, p. 203-222,.

Brady, J. B., Markley, M. J., Schumacher, J. C., Cheney, J. T. & Bianciardi, G. A., 2004, Aragonite pseudomorphs in high-pressure marbles of Syros, Greece: Journal of Structural Geology, v. 26, p. 3-9.

Brun, J.P. and Faccenna, C., 2008, Exhumation of high-pressure rocks driven by slab rollback: Earth and Planetary Science Letters, v. 272, p. 1–7.

Bulle, F., Bröcker, M., Gärtner, C., Keasling, A., 2010, Geochemistry and geochronology of HP mélanges from Tinos and Andros, Cycladic Blueschists blet, Greece: Lithos, v. 117, i. 1-4, p 61-81.

Dixon, J. E. & Ridley, J., 1987, Syros. In:Helgeson, H. C. (ed.) Chemical Transport in Metasomatic Processes. Dordrecht: D. Reidel, pp. 489-518.

Dubois, R. & Bignot, G., 1978, Présence d'un "hardground" nummulitique au sommet de la série crétacée d'Almyropotamos (Eubee meridionale, Grece): Paris, Academie des Sciences Comptes Rendus, v. 289, p. 993–995.

Dürr, ST., Altherr, R., Keller, J., Okrusch, M. and Seidel, E., 1978, The median Aegean Crystaline Belt: Stratigraphy, structure, metamorphism, magmatism, In Alp, Appenines, Hellenides (eds H. Cloos, D. Roeder and K. Schmidt), p. 455–77.

Gautier, P. & Brun, J-P., 1994a, Crustal-scale geometry and kinematics of late-orogenic extension in the central Agean (Cyclades and Evvia Island): Tectonophysics, v. 238, p. 399–424.

Gitahi, N., 2004, Geochemistry and metamorphic evolution of éclogites on Syros island, Greece: Extended Abstracts, Seventeenth Annual Keck Research Symposium in Geology Proceedings, Lexington, VA, P.81-4.

Hausmann, J. F. L.,1845, Beiträge zur Oriktographie von Syra und ein neues Mineral, der Glaukophan: Gottinger geol Anzeigen, p. 193-198.

Holley, E. A., Ross, T. & Cheney, J. T., 2004, Pressure-température conditions of metamorphism in eclogites, Syros, Greece: Geological Society of America, Abstracts with Programs 36(1), A67. 2004

Jolivet, L., Faccenna, C., Goffé, B., Burov, E., Agard, P., 2003, Subduction tectonics ans exhumation of high-pressure metamorphic rocks in the Mediterranean orogens: American Journal of Science, v. 303, p. 353- 409.

Jolivet, L., and Goffé, P., 2000, Les dômes métamorphiques extensifs: Comptes rendus de l'académie des Sciences, v. 320, p. 739-751.

Keay, S., 1998, The geological evolution of the Cyclades, Greece: constraints from SHRIMP U–Pb geochronology. Ph.D. thesis, Australian National University, Canberra, pp. 335.

Keiter, M., Piepjohn, K., Ballhaus, C., Lagos, M. and Bode, M., 2004, Structural development of high-pressure metamorphic rocks on Syros Island (Cyclades, Greece): Journal of Structural Geology, v. 26, p. 1433-1445.

Lagos, M., Münker, C., Tomaschek, F. anf Ballhaus, C., 2002 Geochemistry and Lu-Hf geochronology of the metavolcanic Grizzas sequence in northern Syros (Cyclades, Greece): European Journal of Mineralogy, v. 14(1), p. 97.

Lagos, M., Scherer, E.E., Tomaschek, F., Münker, C., Keiter, M., Berndt, J. and C. Ballhaus, 2007, High précision Lu-Hf geochronology of Eocene éclogite facies rocks from Syros, Cyclades, Greece: Chemical geology, v. 243, n° 1-2, p. 16-35. doi:10.1016/j.chemgeo.2007.04.008.

Okrusch, M. and Bröcker, M., 1990, Eclogites associated with highgrade blueschists in the Cyclades archipelago, Greece: a review: European Journal of Mineralogy, v. 2, p. 451-478.

Philippon, M., Brun, J.P., Gueydan, F., 2009, Kinematic records of subduction and exhumation in the Ile de Groix Blueschist (Hercynian belt; Western france): Journal of structural geology, v. 31, n°. 11, p. 1308-1321. doi: 10.1016/j.jsg2009.07.003.

Pohl, J., 1999, Geologie und Hochdruckgesteine der Insel Syros, Griechenland. Diploma thesis, Geologisches Institut, Albert-Ludwigs Universität, Freiburg, pp. 107.

Poli, S., and Schmidt, M.W., 1995, H2O transport and release in subduction zones—Experimental constraints on basaltic and andesitic systems: Journal of Geophysical Research, v. 100, p. 22,299–22,314, doi: 10.1029/95JB01570.

Ridley, J., 1982, Arcuate lineation trends in a deep level, ductile thrust belt, Syros, Greece: Tectonophysics, v. 88, n° 3-4, p. 347-360. doi:10.1016/0040-1951(82)90246-3.

Ring, U. and Layer, P.W., 2003, High-pressure metamorphism in the Aegean eastern mediterranean : Underplating and exhumation from the late cretaceous until the Miocene to Recent above the retrreating Hellenic subduction zone. Tectonics, v. 22, n° 3, 1022, doi:10.1029/2001TC001350.

Rosenbaum, G., Avigad, D. & Sanchez-Gomez, M., 2002, Coaxial flattening at deep levels of orogenic belts: evidence from Blueschists and eclogites on Syros and Sifnos (Cyclades, Greece), Journal of Structural Geology, v. 24, p. 1451-1462.

Schumacher, J.C.B., Brady, J.B., Cheney, J.T., and Tonnsen R.R., 2008, Glaucophane bearing Marbles on Syros, Greece, Journal of Petrology, v. 49, p. 1667-1686.

Tirel C., Gautier P., van Hinsbergen D. J. J. and Wortel M. J. R., 2009, Sequential development of interfering metamorphic core complexes: numerical experiments and comparison with the Cyclades, Greece. Geological Society, London, Special Publications, v. 311, p. 257-292.

Tomaschek, F., Kennedy, A. K.,Villa, I.M., Lagos,M. and Ballhaus, C., 2003, Zircons from Syros, Cyclades, GreeceçRecrystallization and mobilization of zircon during high-pressure metamorphism. Journal of Petrology, v. 44, p. 1977-2002.

Tomaschek, F. and Ballhaus, C., 1999, TheVari Unit on Syros (Aegean Sea) and its relation to the Attic-Cycladic Crystalline Complex. Journal of Conference Abstracts, v. 4, p. 72.

Tomaschek, F., Keiter, M., Kennedy, A.K. and Ballhaus, C., 2008, Pre-Alpine basement within the Northern Cycladic Blueschist Unit on Syros Island, Greece. - Zt. dt. Ges. Geowiss. 159/3, 11 pp., DOI: 10.1127/1860-1804/2008/0159-0000.

Trotet, F., L. Jolivet, and O. Vidal, 2001a, Tectono-metamorphic evolution of Syros and Sifnos islands (Cyclades, Greece), Tectonophysics, v. 338, p. 179-206.

Tsujimori, T., Sisson, V.B., Liou, J.G., Harlow, G.E, Sorensen, S.S, 2006, Very-low-temperature record of the subduction process: A review of worldwide lawsonite éclogites. Lithos, v. 92, p. 609–624

Whitney, D.L, Davis, P.B., 2006, Why is lawsonite eclogite so rare? Metamorphism and préservation of lawsonite eclogite, Sivrihisar, Turkey, Geology , v. 34; no. 6; p. 473–476; doi: 10.1130/G22259.1.

Zack, T., Rivers, T., Brumm, R., and Kronz, A., 2004, Cold subduction of oceanic crust: Implications from a lawsonite eclogite from the Dominican Republic: European Journal of Mineralogy, v. 16, p. 909–916, doi: 10.1127/0935-1221/2004/0016-0909.

Chapitre 6 : Des données de terrain au modèle 3D

FROM FIELD DATA TO 3-D MODEL IN SYROS HP TERRAINS (CYCLADES, GREECE): A TOOL FOR CHARACTERIZING POST-METAMORPHIC DEFORMATION.

Mélody Philippon[1], Christian Le Carlier de Veslud[1], Frédéric Gueydan[1], Jean-Pierre Brun[1] and Guillaume Caumon[2]

[1]Université Rennes 1, Géosciences Rennes, bat. 15 - Campus de Beaulieu, 263 Av du général Leclerc, BP 74205, 35042, Rennes Cedex, France.
[2]CRPG, Nancy Université, CNRS. ENSG, rue du doyen Marcel Roubault, BP 40, 54501 Vandoeuvre-lès-Nancy, France.

To be submitted to Journal of structural Geology

Abstract

3-D modeling of the geometry and relationships of the High-Pressure metamorphic units is a way to understand the mechanism of exhumation bringing such rocks from depth to surface. For that purpose, we investigated Syros Island's blueschists (Aegean Sea) coupling extensive fieldwork and 3-D modeling. The island displays three units (1) a meta-ophiolite, (2) a marble/schists sequence lying on top of (3) a gneissic basement. An approach combining field studies and 3-D geometrical modelling was used to document the geometry of Syros.

Published data and data collected in the field were assembled in a 3D data base, which allowed us to test their coherency before building a 3D surface model. The construction of 3-D models from field data required the development of specific methodologies. Integrated data are: the DEM (20 m isoaltitude line), geological maps, extensive mapping of metamorphic units and around 1,000 measurements of foliations and stretching lineations. The approach is four-stages: (1) data are integrated in 3-D (2) a fault network is built, (3) foliations are interpolated in 3-D, (4) the structure of marble layers is interpolated from structural data using implicit function modeling.

A tectonic contact occurs inside the sedimentary pile, defining two units: the above Kastri unit and the underlying Pyrgos unit. We named this contact the Kastri basal fault. The 3-D model highlights two kinds of geometrical relationships between the Kastri basal fault and the foliation of the underlying units (units 2 and 3). (a) in the north of the island, foliations, contacts and the Kastri basal fault are parallel ("concordant"). (b) in

the south of the island, the Kastri basal fault contact is oblique to the underlying units ("discordant"). The evolution of relationships between the units, from North to South, is interpreted as a flat & ramp extensional system.

Results suggest two exhumation-related deformations modes: (1) a distributed ductile deformation, as evidenced by the streching lineations pattern, (2) localized ductile to brittle deformation illustrated by the flat & ramp geometry.

6.1. Introduction

In the Cyclades area, the metamorphic nappes stacking results from the Pindus closure and the continental collision between Adria Plate and Pelagonian Plate (Fig. VI-1). This collision led to the formation of the well-known Cycladic Blueschists Unit (CBU). Understanding the mechanism of deformation of HP-LT metamorphic units is a first step to reach before discussing the exhumation mechanism that brought such rocks from high depth to surface.

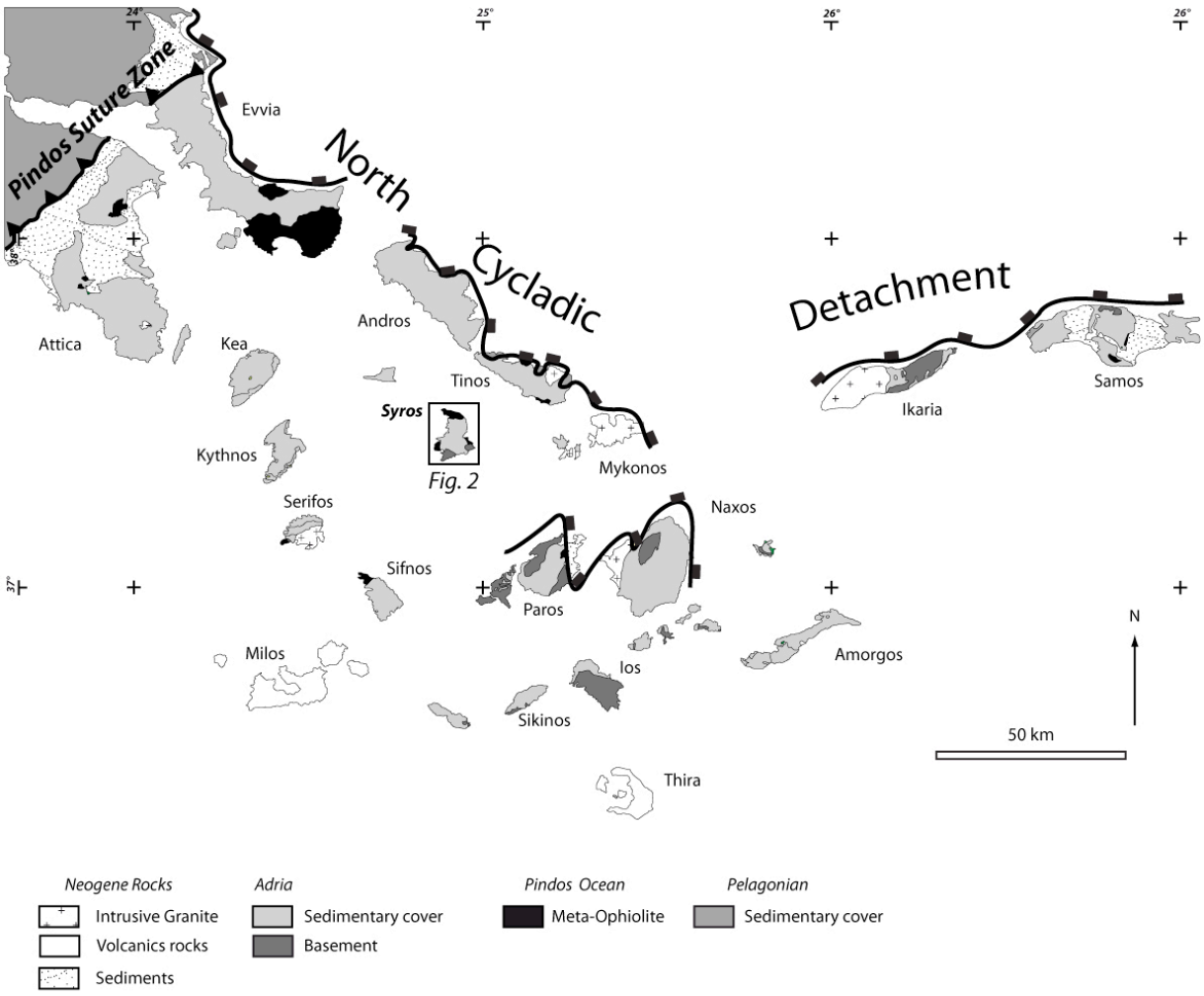

Fig. VI-1: General map of the Cyclades, showing the different lithologies outcropping in the Aegean Sea. The island of Syros is located in the central Cyclades and the three rock-types of the CBU are outcropping in the island.

Syros Island's blueschists and eclogite facies rocks are relatively poorly retrogressed and thus the island presents one of the the best-preserved HP parageneses of the CBU. It is therefore a key area to understand the relationship between the constitutive units of the CBU and the way they were deformed because it gathers in the same area continental and oceanic units, with good exposure conditions. However, many aspects of the structure and geological history of the Island, and more generally of the Aegean area are still discussed (Ridley, 1982, 1984; Trotet et al., 2001 a and b; Rosenbaum et al., 2002; Keiter et al., 2004; Bond et al., 2007; Jolivet et al., 2010; Ring et al., 2010).

In particular, three issues are of special interest:

(1) The relationships between the units. They are complex, with structures (and particularly shallow dipping faults sometimes considered as "detachments") whose geometry and role are still discussed. For instance, Trotet et al. (2001a) propose that HP units reflects the juxtaposition by major detachments of units derived from different structural levels, and subsequently overprinted at greenschist facies. In contrast, Bond et al. (2007) suggest that the conservation of HP is allowed by a heterogeneous metamorphic overprint through the decompression history.

(2) The deformation distribution: broadly distributed or strongly localized along shear zone. How/Why detachment can localized whereas a pervasive deformation in affecting the whole pile?

(3) Outcrop to map scale deformation versus large scale tectonic.

In order to bring some elements of discussion, this paper proposed a new tectonic pattern of the whole island in the light of extensive field investigation and structural mapping, including measurement of foliations, fold axis, fault orientation. Accurately mapping and representing geological structures, particularly taking into account their 3-D geometry, is of particular importance. Thus, all the data were vizualized in a 3-D modeler. A modeling by implicit function (Frank et al., 2007; Calcagno et al., 2008) appears to be very efficient because of it can provide rapidly a consistent 3-D model in area where imaging in depth is poor, integrating orientation measurements and structural constraints.

A first result of this study is to provide a consistent 3-D model of the island, integrating all available data. This model highlights two kinds of geometrical relationships between the basal contact of the meta-ophiolite and the foliation of the underlying units: (a) in the north and south of the island, foliations and basal contact are parallel ("concordant"). (b), in the central part of the island, the basal contact is oblique to the underlying units ("discordant"). The evolution of relationships between the units, from North to South, is interpreted as a flat & ramp extensional system.

Our results also suggest two exhumation-related deformations modes: (1) a distributed ductile deformation, as evidenced by the arcuate streching lineations pattern, (2) localized ductile to brittle deformation illustrated by the flat & ramp geometry.

Finally, this study highlights the interest of 3-D modelers for studying frontier domains, where imaging in depth is poor a central role, because they allow to integrate different kinds of data, ensure consistency between data and models and test hypothesis, in a back-and-forth process between geological interpretation and a 3-D models.

6.2. Geological background

6.2.1. Overview

The CBU results from the burial and exhumation of the Pindus Ocean in a northward dipping subduction zone during Eocene times (Bonneau and Kienast 1982). Since 45 Ma roll back is active in the area, and generates two episodes of metamorphic core complexe emplacement coupled with HP metamorphism: a 45 Ma Rhodope core complexe synchronous with HP metamorphism is the Cyclades and a 20 Ma Cycladic core complexe, synchronous with HP metamorphism in the Phyllades Nappes (Crete and Peloponnesus, Jolivet et al., 2009). Jolivet and Brun (2010), have estimated that the trench has undergone 700 km of retreat since 45 Ma. The CBU, mainly outcropping in Aegean Sea, is described as a structural pile composed of three units, from bottom to top: (1) Pre Alpine granitic basement, (2) margin sediments sequence: marbles and schists -at the bottom, serpentine's intercalation can outcrop-, with a decreasing metamorphism from blueschist facies to greenschist facies trough the pile, (3) a meta-ophiolitic mélange. This unit affected by high-pressure metamorphism is structurally below non-metamorphosed Cretaceous to Paleogene limestones and ophiolites belongings to the Pelagonian overriding plate. The island of Syros is the place where the HP metamorphism of the CBU is the best preserved.

6.2.2 Lithology

Syros displays the complete lithological and structural pile constituting the Cycladic Blueschists Unit from Hercynian basement and overlying sedimentary sequence to the overthrusted pindus oceanic crust (Fig. VI-2).

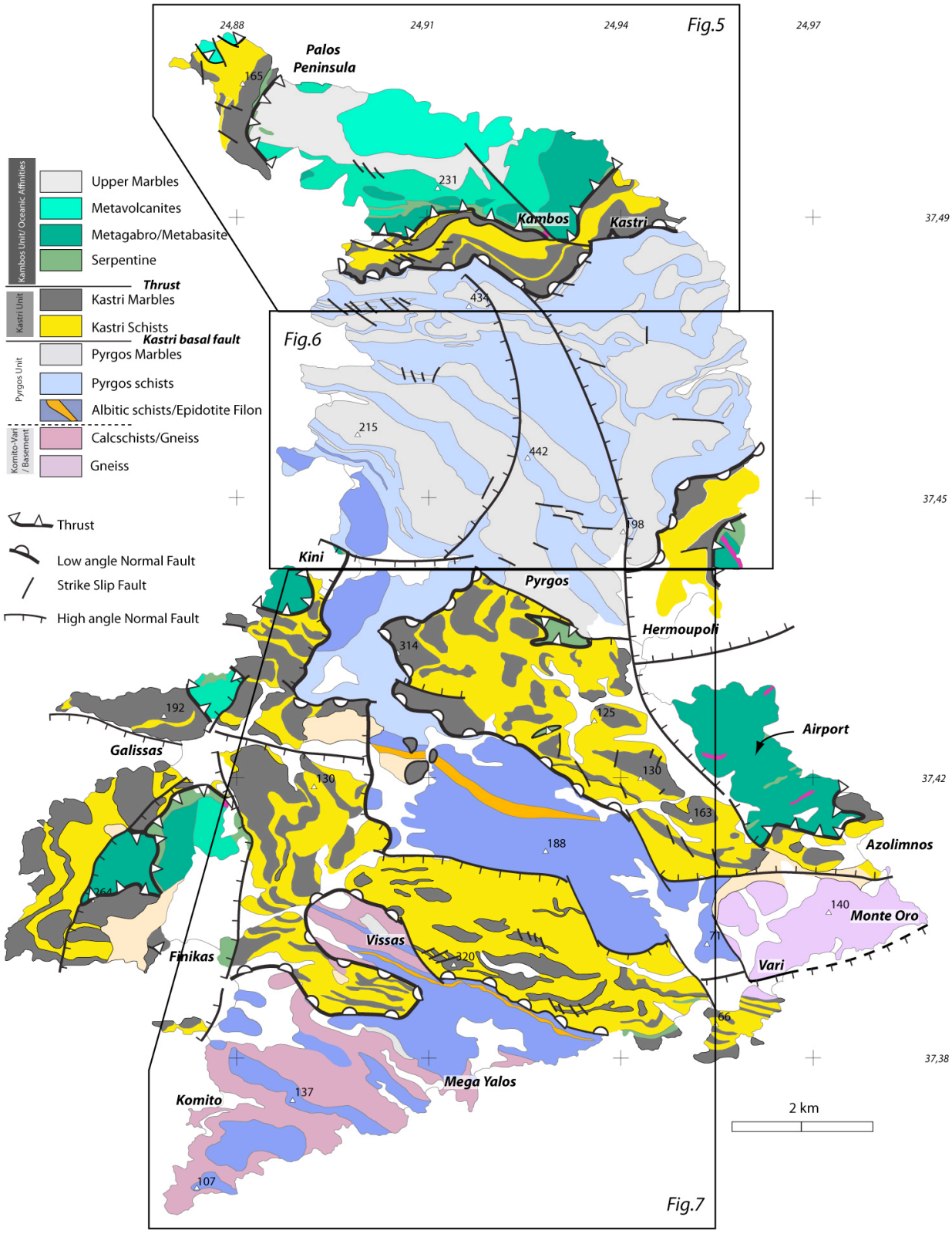

Figure VI-2: Map of Syros showing the four different units pointed out by our structural study. The main tectonic contacts are the thrusts (triangle symbols), steeply dipping normal fault (barbed lines) and the low-angle fault system (hemispheric symbols). (See Annexe D for the 1 :50000 Map of Syros)

- Basement

Two basement outcrops are kown in the island: the Vari and the Komito gneisses. For the Vari orthogneiss (W of the island, Fig. VI-2), P-T conditions have been estimated from greenschists facies condition (Phengite Si substitution, Maluski et al., (1987) to 15kbar, 500°C (Tomaschek and Ballhauss 1999). SHRIMP analyses gave an age of 240-243 Ma for the emplacement of the pluton in the Vari orthogneiss (U/Pb on Zircon, Keay 1998, Tomaschek et al., 2003).

Tomaschek et al., (2008) shows that the Komito gneiss (SW of the island, Fig. VI-2) is part of the Cycladic pre-alpine basement and SHRIMP analyses yield an age of 300 Ma for theses rocks. Age of metamorphism has been estimated from 53.5 ± 1.3 to 37.3 ± 1.3 Ma Blueschist facies, and 30.3 ± 0.9 for the Greenschist facies (40Ar/39Ar on phengites, Maluski et al., 1987) and are the same as those obtained for the overlying sedimentary sequence and oceanic unit (Pulitz et al., 2005).

On the basis of a single cretaceous age, obtain by Maluski et al., 1987 (40Ar/39Ar on phengites), the Vari unit has been interpreted as a piece of overriding Pelagonian plate, above the CBU via a flat-lying contact and then is structurally the uppermost part of the lithological pile. However, geochronological data from Tomaschek and Ballhaus, (1999) and Tomaschek et al., (2008) Keay, (1998) suggest that Komito and Vari outcrops may belong to the same unit: a ca. 300 Ma unit, locally intruded by a ca. 240 Ma. pluton. These results confirm the original interpretation of Bonneau et al. (1980 a) linking the Komito and Vari orthogneisses as a piece of the lowermost part of the Cycladic basement. Thus, and following Philippon et al., (chap. 7), field observations suggest that there is no detachment between Vari and the CBU and that the Vari unit is a piece of orthogneissic material outcropping as a window below the CBU.

- Metasedimentary sequence

The volcano-sedimentary sequence lies on top of the basement (Fig. VI-2). This sequence may be subdivided into two subsunits: (i) the Pyrgos unit, characterized by glaucophane schist, greenschists, dolomitic marbles and cherts and the Kastri unit, characterized by glaucophane schists and marbles (Schumacher et al., 2008). The difference between Pyrgos and Kastri units results from a differences in the metamorphic grade and in the sedimentary material: Pyrgos shows Greenschists,

Blueschists facies rocks and dolomitic marbles whereas Kastri present Blueschists facies rocks and marbles.

Both sedimentary units are metamorphosed under Blueschists facies from 8 to 17 kbar, 350-500 °C (Trotet et al., 2001b; Schumacher et al., 2008). The presence of microfossils (Foraminiferous Forschiidae), gave a deposition age of Pyrgos unit marbles estimated at 330-350 Ma (Pohl 1999, see Schumacher et al., 2008). SHRIMP analyses gave an age of 243 ± 2 Ma for Kastri unit's metatuffites outcropping not far from the top of the sequence (Keay, 1998, Tomaschek et al., 2003).

- *Ophiolitic mélange*

The rocks outcropping at the top of the series, the Kambos unit, are affiliated to the Oceanic crust (Fig. VI-2). They consist of coarse-grained metagabbros, fine-grained metabasalts and metavolcanites and serpentinic schists. Metamorphism for this unit has been estimate eclogite faciès from 19-24 kbar, 500-580°C (Gitahi, 2004, Holley et al., 2004, Trotet et al., 2001b). U/Pb SHRIMP age of magmatic zircons are comprised between 240 Ma and 80 Ma giving estimation for the age of the basic protolith (Tomaschek et al., 2008, Bulle et al., 2010). High-pressure metamorphism is estimated to have occurred at 52 Ma, (Lu/Hf on Garnet, Lagos et al., 2007).

6.3. Available data and 3-D methodology

A mapping of the geological units of the island was established following 4 months of extensive field investigations, covering the whole island. As a result of these investigations, a structural map and about 1,000 measurements of foliations and stretching lineations were obtained.

In parallel with these investigations, a 3-D model of Syros was built using the gOcad 3-D modeller, that allows a discrete representation of geological objects through regular (grid) or irregular meshes (polygonal curves, triangulated surfaces, and tetrahedralized solids, Mallet, 2002). 3D reconstruction of geological objects (e.g. faults or stratigraphic contacts) from data is based on the Discrete Smooth Interpolation (DSI, Mallet, 2002). A wide range of constraints was used to take into account the different types of data, but also to ensure geometrical and geological consistency between objects (Mallet, 2002; Caumon, 2010).

Integrated field data are: the high-resolution DEM (20 m isoaltitude line), geological and structural maps and measurements of foliations and stretching lineations. It is however clear that there is, in one hand, a dense set of field and structural data, associated with a strong topographic relief, but on the other hand, no data for constraining geometry of geological structures in depth. The construction of complex 3-D geometrical models from field data and scarce subsurface data is currently an important research topic motivated in part by increasing exploration in frontier domains, where seismic imaging is poor. In this case, the 3-D model is used iteratively for integrating data, checking their consistency and comparing proposed model with field evidences. A specific workflow may be proposed (Fig. VI-3) for a 3-D reconstruction as accurate as possible of Syros, a characterization of the geometrical and geological relationships between units, and finally the characterisation of the deformation chronology.

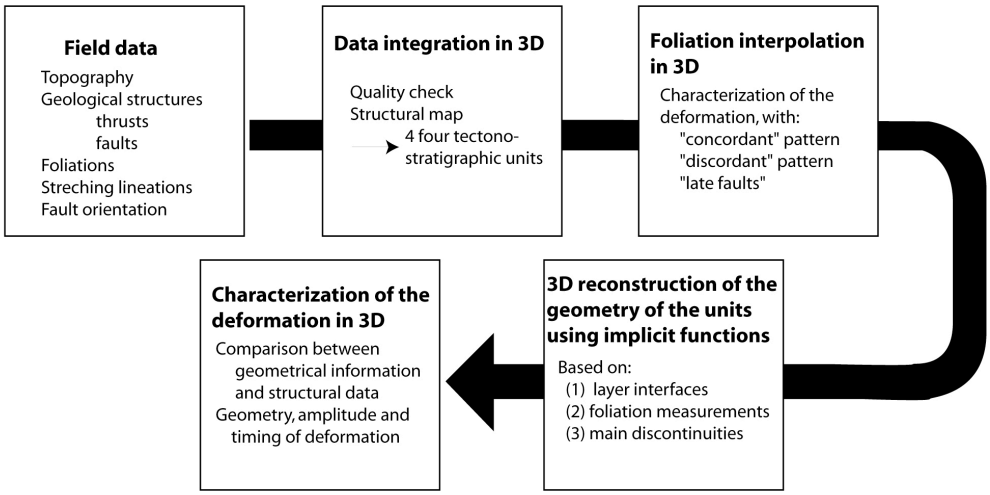

Figure VI-3: Proposed workflow for a 3-D characterization of Syros from field data.

More in detail:

- A Digital Terrain Model (DTM) is built, associating the topography, the geological boundaries, the foliation and streching lineations. The DTM is particularly interesting because the high topographic relief allows a direct observation of geological structures in 3-D.
- A foliation map is built in 2D for characterizing the geological and geometrical relationships between units (see Annexe 1). The main results of this stage is to identify the different type of major discontinuities in the studied area;

- Several surfaces representing the geometry of the geological structures are built. Because this model is based on a dense surface field data but on scarce subsurface data, the implicit surfaces approach was chosen (see Annexe 2 and Fig. VI-4, Franck et al., 2007; Caumon, 2010).

6.4 Structural pattern

We decide to investigate three key areas of the island to illustrate the specific relationships between the units. These areas have been chosen according to the amount of field data able to constrain 3D geometry. The other areas are not fully investigated here because they are underconstrained, and display second order structures.

6.4.1. The Palos peninsula

The Palos peninsula shows the uppermost part of the pile (Fig. VI-5a). A first prominent structural feature in this area is the thrust of mafic and ultramafic rocks of the Kambos unit onto the metasedimentary unit. This thrust is EW oriented close to Kambos and becames NS oriented close to Palos (Fig. VI-2 and VI-5a and c), suggesting a sigmoid shape with a N45° directed fold axe (Stereonet Fig. VI-5c). The metamorphic grade across the Kambos contact shows no sharp boundary (Keiter et al., 2004). South of Kambos, a layer-parallel fault occurs inside the sedimentary unit between the Kastri and Pyrgos units, at the base of the Kastri unit: the Kastri basal fault. At the outcrop scale, the Kastri basal fault is a metric semi brittle décollement fault. A second prominent feature is that the thrust, the Kastri basal fault and the foliations are parallel, thus defining a "concordant" structural pattern.

In the Kambos area, some kilometric to hectometric, N160, late normal-dextral faults are observed (Keiter et al., 2004). One of the most significant is the Finikia fault, east dipping late extensional fault roots in the area (see also § 5.2). The thrust and the décollement are affected by this fault as shown by their sigmoïdal shape (Fig. VI-5a adn c). This specific pattern attests that the Finikia fault is a transtensional fault.

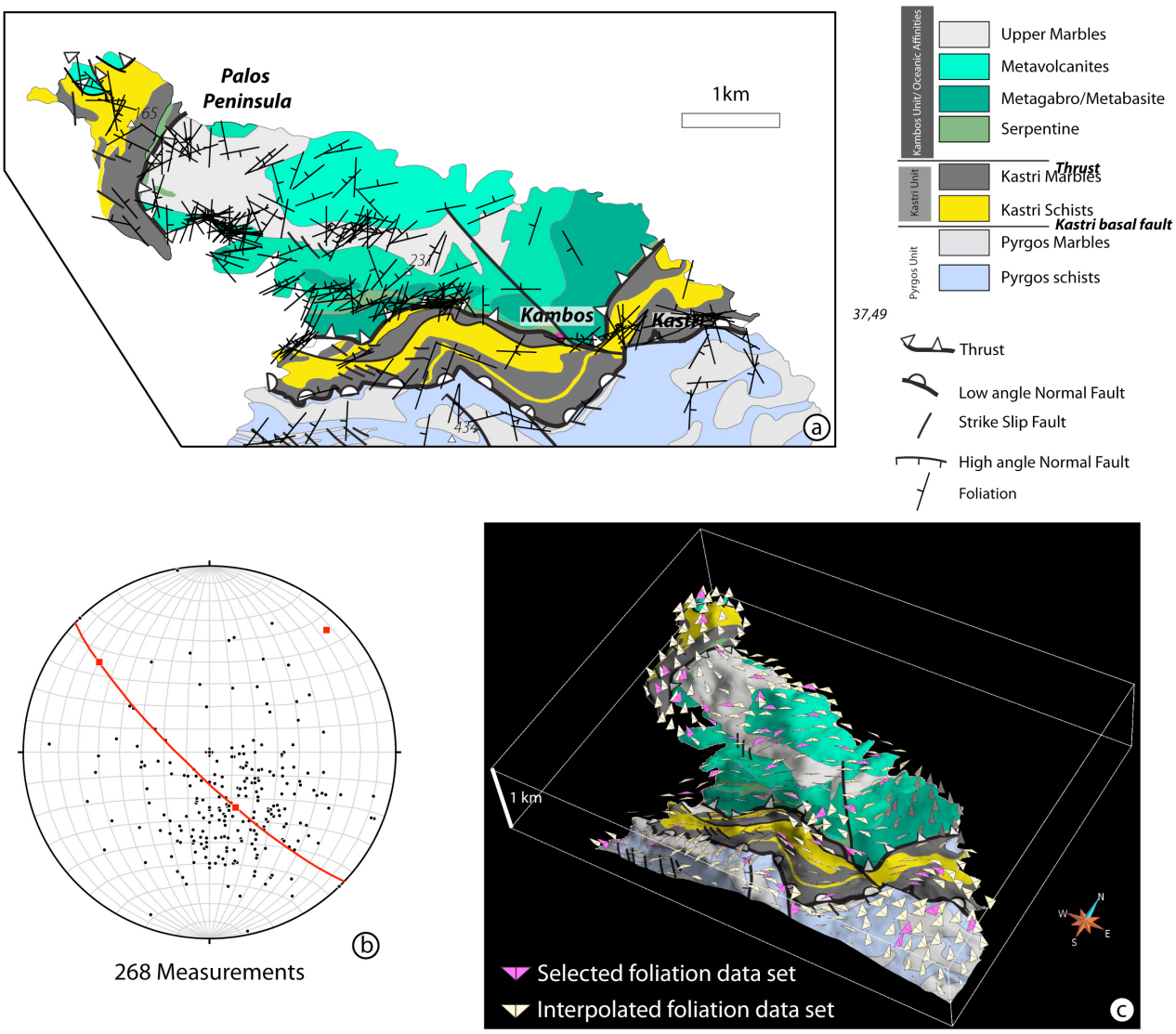

Fig. VI-5: The Palos peninsula area. (a) Lithological map, main tectonic contacts and foliation measurements (b) Stereonet showing the foliation poles –black dots- and the fold axes obtained thanks to a cylindrical best fit - red square- (c) 3D view of the model: the DTM, selected foliation data set and interpolated foliation data set. (a) and (c) clearly show that thrust, the Kastri basal fault and the foliations are parallel, and that they display an arcuate pattern.

6.4.2. The Kini-Kastri area

The Kini-Kastri area is marked by a continuous sequence of marble/schist interlayered lithologies of the Pyrgos unit, with no change in metamorphic grade (Bond et al., 2007) (Fig. VI-6a). Two opposite normal faults/ transtensional, the Finikia and the Kini fault, may be observed, thus defining a horst. They are slightly arcuate, but roughly NS oriented, and rooted in the Kastri basal fault to the N. The Kini fault is a minor fault

only inducing a limited offset of the marble/schist layers. It is connected to the Delphini fault. The Finikia fault displays a dextral offset of the marble/schist layer that increases toward the South, its southern extremity cannot be observed because located offshore. This fault network defines three blocks from W to E. In the western and center blocks, the foliation is roughly parallel to the bedding and is arcuate (Fig. 6b and c). Indeed, the foliation orientation turns from N90 in the NW, where it is parallel to the Kastri basal fault, to N150 to the SE defining the Kini fold which have a N60°directed axe (Fig. VI-6b). In the easternmost blocks, the foliation is also parallel to Kastri basal fault to the N. Toward the S, it displays a more complex pattern, with a global N30 orientation, but affected by secondary folds of N45 axis (Fig. VI-6c).

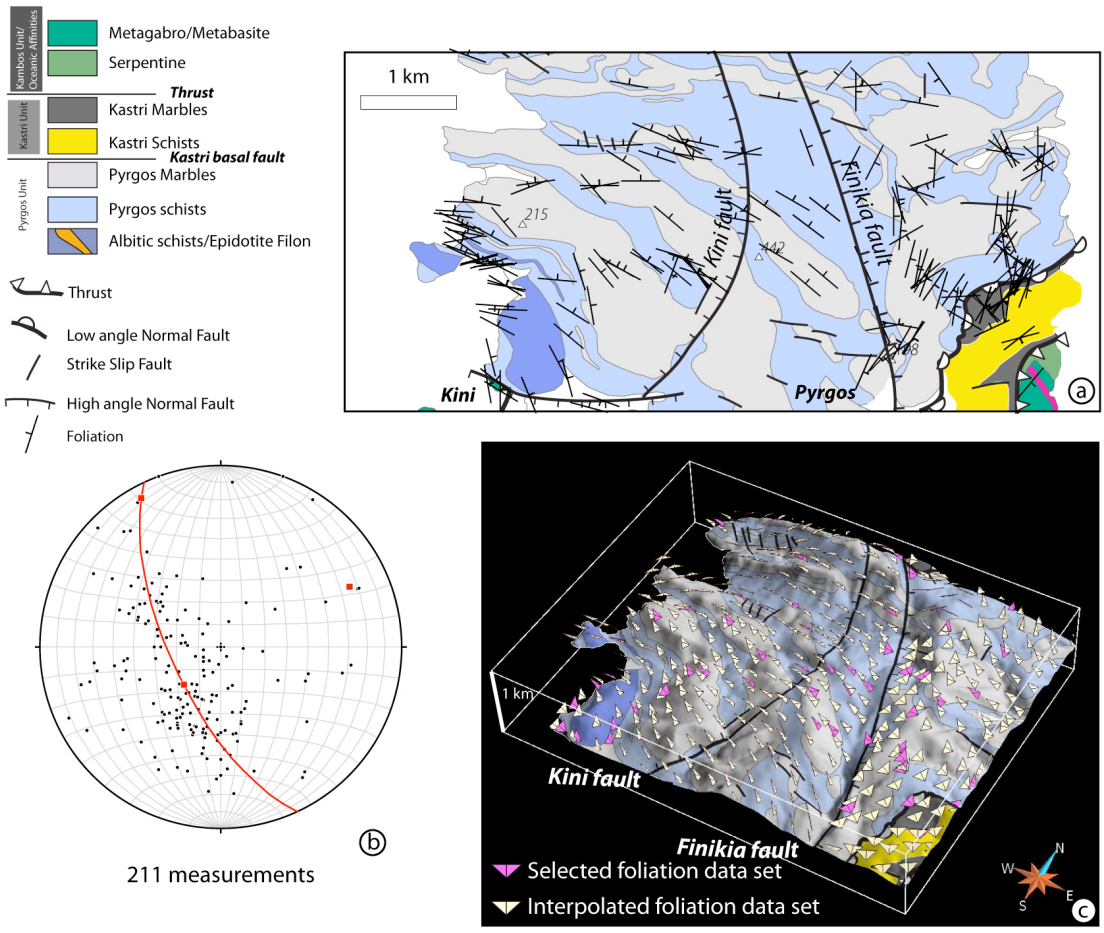

Fig. VI-6: Kini Kastri area (a) Lithological map, main tectonic contacts and foliation measurements (b) Stereonet showing the foliation poles –black dots- and the fold axes obtained thanks to a cylindrical best fit - red square- (c) 3D view of the model: the DTM, selected foliation data set and interpolated foliation data set. W of the Finikia fault, The foliation has a sigmoid shape, and turns from N90 in the NW, where it is parallel to the Kastri basal fault, to N150 to the SE. E of this fault, the foliation display a global N30 orientation, but affected by secondary folds.

6.4.3. The Hermoupoli-Komito area

The southern part of the Syros map (Fig. VI-2 and VI-7a) shows two large klippes of the Kambos and Kastri units, dismembered by kilometrics E-W trending steeply dipping normal faults: the Delphini and the Xroussa faults, respectively to the north and south. These klippes are lying unconformably on top of the Pyrgos unit. From Hermoupoli to the southern coast, the Kastri basal fault hangingwall is lying with a southward shallow dip on top of the NE dipping foliation of the footwall (Fig. VI-7b). In the hangingwall the foliation also dips to the NE, displaying angular relationship with the Kastri basal fault of about 30°, as illustrated by the field picture (Fig. VI-7c). Cross-cutting relationships show that the hangingwall comes into contact with deeper footwall levels toward the south. At late stage of its evolution, the Kastri basal fault was cut by two sets of steeply dipping faults trending either E-W or sub-meridian. The dip of E-W trending normal faults changes from northward to the east of the Finikia Fault to southward to the west (See Hermoupoli vicinity, Fig. VI-7). The mean foliations trend is WNW-ESE (N99° directed). The Kastri basal fault is are E-W directed either gently dipping south or north. The steeply dipping normal fault displays two direction trend a N-S (dominant) and a E-W one (minor).

It should also be noted that in the southern extremity of the island, the foliation becomes nearly horizontal and present folds with a N120 axis (Fig. VI-7a).

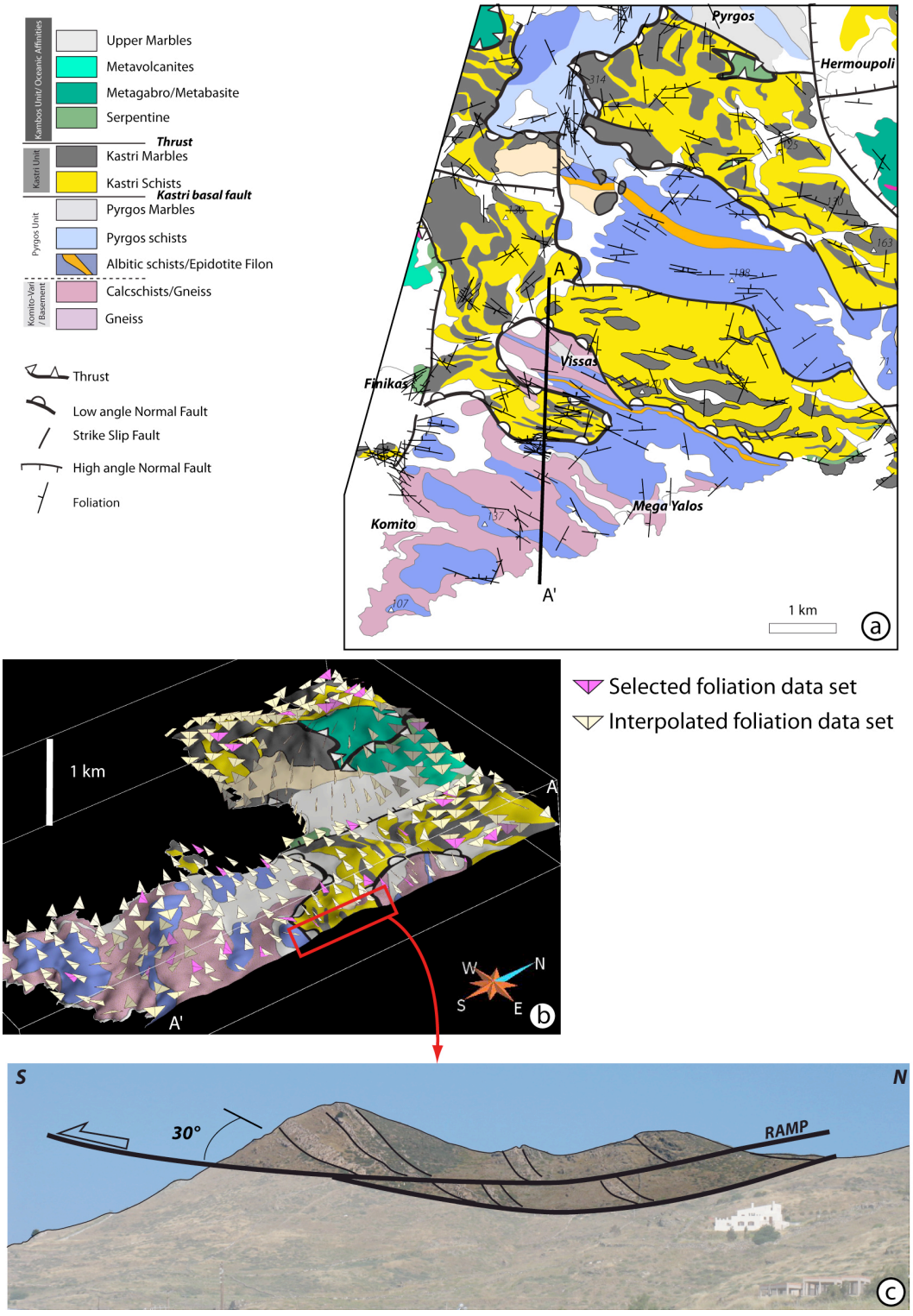

Fig. VI-7: Hermopouli-Komito area (a) Lithological map, main tectonic contacts and foliation measurements (b) 3D view of the model: the DTM, selected foliation data set and interpolated foliation data set (c) Field pictures of the Kastri basal contact in the vicinity of the Vissas area. An angular discordance of ca. 30° may be observed between the foliation and the Kastri basal.

6.4.4. Structural map

From the above description we propose a new structural schema (Fig. VI-8). The most significant steeply dipping faults, displaying a major throw, are the N-S oriented Finikia fault, and the E-W oriented Xroussa and Delphini faults. The Finikia fault roots in the Kastri marbles, north of the island and dead in the area of Azolimnos (Southeast of Syros) and displays a component of strike slip decreasing from north to south. In its northern extremity it's a strike slip fault having a vertical dip whereas going through the south, it becomes a transtensional and then normal fault displaying a 60° of dip.

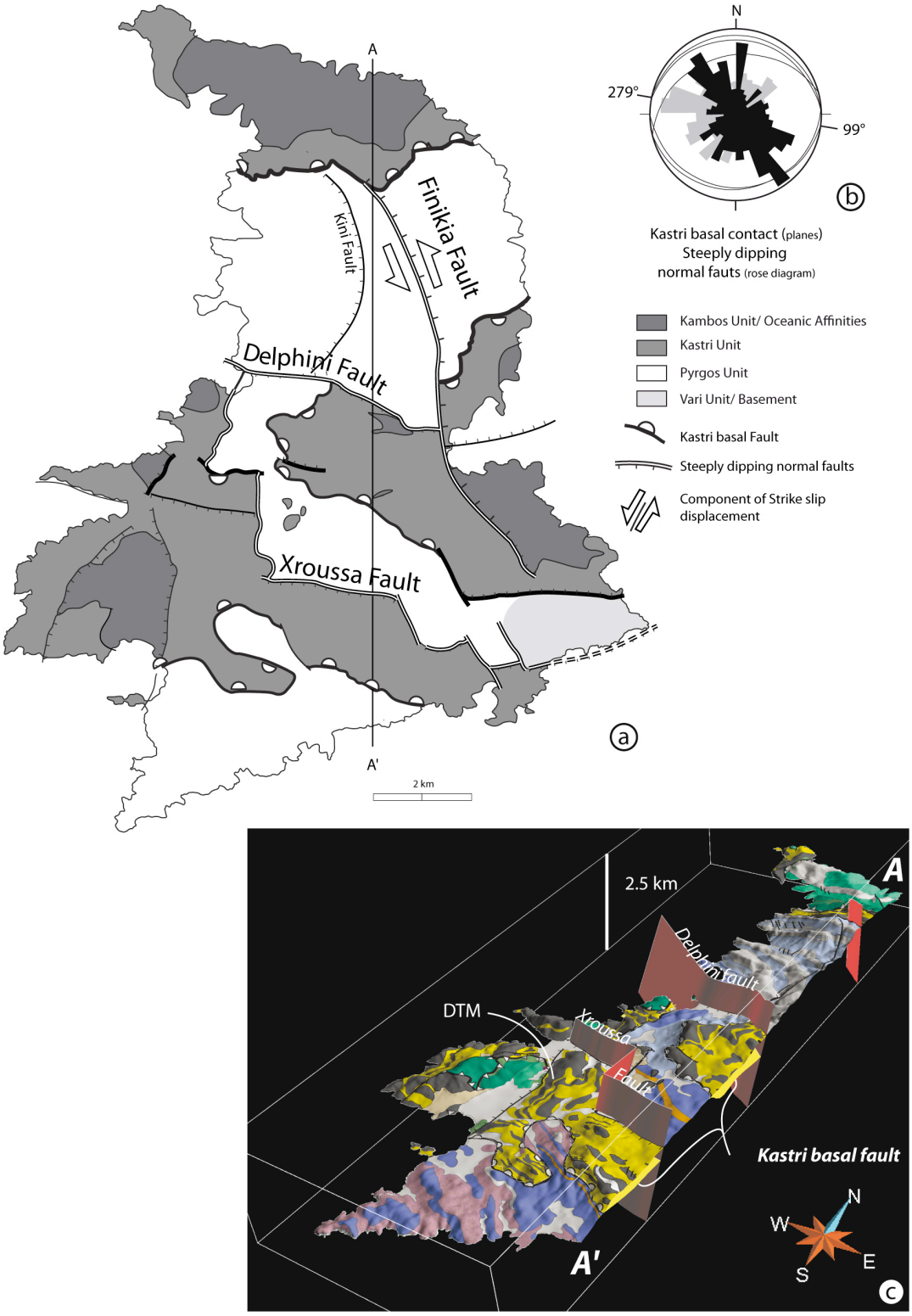

Fig. VI-8: Simplified structural pattern proposed for Syros. The main features controlling the geometry are: the steeply dipping normal faults of Finikia, Delphini and Xroussa and the Kastri basal fault, which is a flat lying contact.

In the north of the island, the Kastri basal fault is parallel to the foliation and the bedding, the lithological sequence is not modified thus this fault a decollement. In the south of the island, the Kastri basal faut display angular relationship with its footwall, it is a detachment. This evolution from decollement to the north to detachment to the south is a flat and ramp system that occurred at the base of the Kastri marbles. Two types of tectonic features structure the island: the steeply dipping normal faults and the Kastri basal fault, which is a flat lying contact. The structural relationships between these two features show their chronology. The Kastri basal fault is cross cut by the steeply dipping normal fault network leading to the dismemberment of allochtonous units of Kastri and Kambos. The steeply dipping normal fault network is a late feature that cross cut the Kastri basal contact.

6.4.5. 3D modeling with implicit surfaces

The study area is marked by a continuous or faulted sequence of interlayered lithologies. This provide a good opportunity to build a consistent 3D geometric model of the lithological interfaces using an implicit surface approach (see Annexe for further details).

The outcrop contour of each interface was picked in 3D on the DTM. Then, each contour was given a scalar value, here corresponding to the average thickness to a reference interface. Four main discontinuities were considered: the Finikia, Xroussa, Delphini steepy normal faults and the Kastri basal fault. The area N of the Delphini fault is well constrained by a dense set of data curves. In the block between the Delphini and Xroussa faults, it was only possible to correlate two data curves with those of N; this block is clearly underconstrained. South of Xroussa fault, three curves were defined, using an estimate of Xroussa fault throw (ca. 1000m) proposed by Philippon et al., (chap. 7, see cross sections) Due to a lack of data in a highly deformed zone, the region above the Kastri basal fault (i.e. two large klippes of the Kambos and Kastri units) were not considered.

Then, a tetraedralized solid (ca. 250 000 tetrahedra), cut by the main discontinuities was built (Fig. VI-9a and b). A scalar function was interpolated in 3-D in this solid, constrained by the value of each contour, orientation data and indirectly by the faults. Finally, an isovalue surface corresponding to each interface was extracted from the

tetraedralized solid. Globally, once a tetrahedralized solid is built, the two last stages together (interpolation s.s. and surface extraction) require less then 15 minutes to be completed.

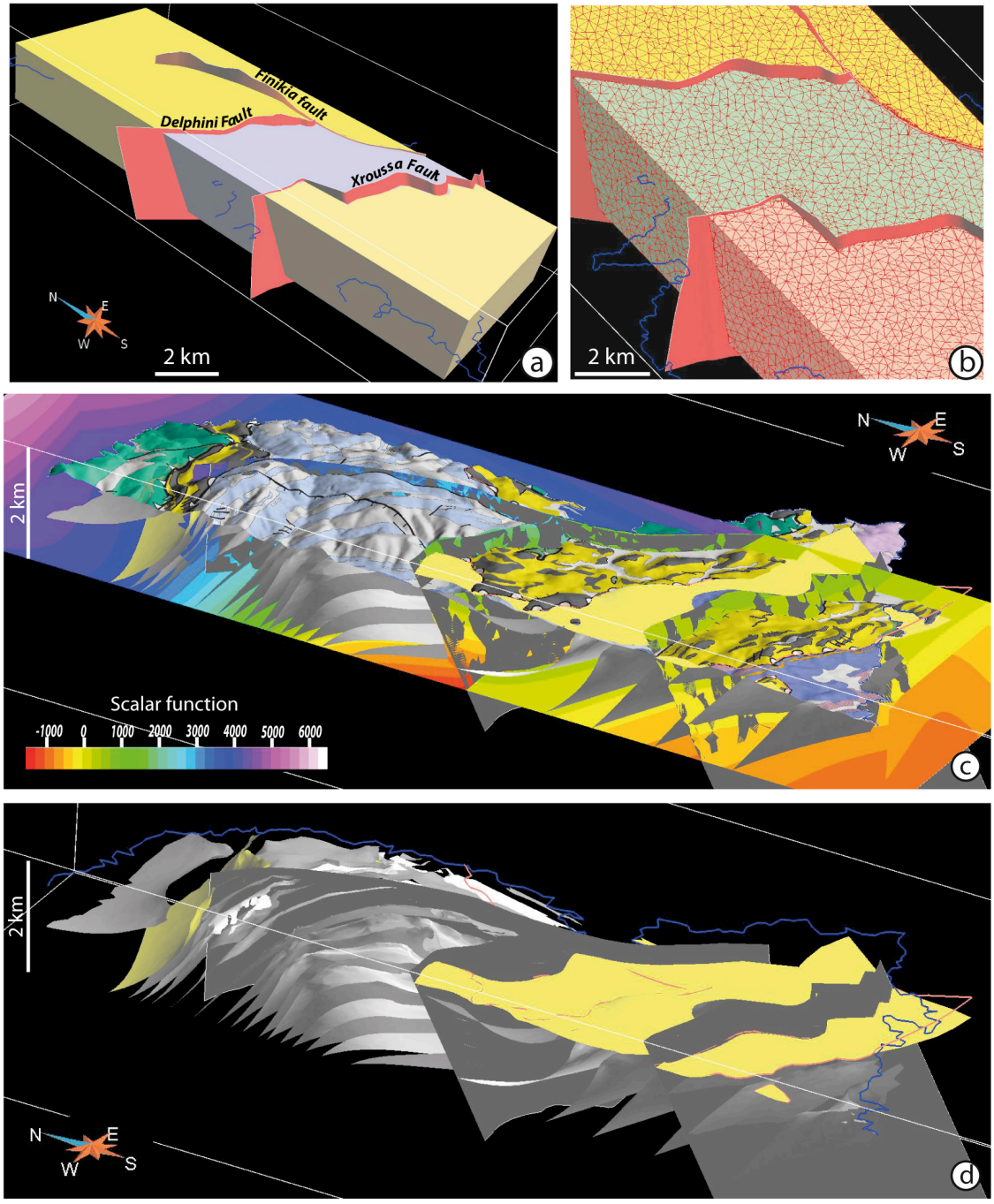

Figure VI-9: Implicit 3D modelling, a) Tetrahedralized volume cut by the mains faults ()(b) (c) and (d) Main results of the 3-D modeling: the interpolated marble/schists layer (in light gray/medium gray), the nappe contact (in yellow) and the main fault (in brown).

The obtained surfaces are in good agreement with surface data (contours and dips, Fig. VI-9c), but further document the geometry of layers in depth. Globally, and apart from the two large klippes, the island presents a complex sigmoidal shape. To the N, the oceanic unit turns from a NS to a N80 orientation, close to Kambos, where it becomes parallel to the Kastri unit. Close to Kastri, the Pyrgos and the Kastri unit are parallel, although been separated by the Kastri basal fault. In the center of the island, the Pyrgos marble and schists layers display a sigmoidal shape with a EW orientation close to Kastri, a N150 one close to Pyrgos, a N30 one close to Kini and finally a N100 one between the two klippes (Fig. VI-9). In the Kini-Kastri area, the complex outcrop contour may be simply explained by the fact that to the W, the topography roughly cross cuts the foliation at high angle whereas to the E, it is sub parallel to the bedding and thus, the same marble or schist layer may be cut several times.

Except in areas where secondary faults or folds are present, the dip of the layers remains relatively constant at ca. 30-50° over the island. However, it seems to decrease to ca. 30° on the N, whereas it is almost horizontal in the southern extremity (Fig. VI-9d).

6.5. Discussion and conclusions

6.5.1. Deformation pattern and lineation distribution

As note previously, foliation trajectories display a sigmoidal shape illustrating the folding of the whole pile (Fig. VI-10a and c). The Komito/Vari basement and the overlying Pyrgos sedimentary unit are autochthonous relatively to rhe Kastri sedimentary unit and the Kambos oceanic unit. Therefore the sigmoidal shape of the foliation observed in these two units more likely reflects the folding event with N30° trending axes. The two orientations of steeply dipping normal fault network combined with their associated strike slip component suggest a mean N30° direction of stretching and a mean N 120° shortening (Stereonet, Fig. VI-10b). compatible with the observed deformation pattern. It is interesting to note that in the Palos peninsula and Kini-Kastri area, the stretching lineation, mainly corresponding to retrograde history of rocks (Philippon et al., chap. 7), are roughly perpendicular with both the foliations and the lithological layers (Fig. VI-10a). Contrary to Ridley (1982), who argue that the arcuate pattern of the stretching lineations was due to a "ductile wrenching at deep level of the

crust", we suggest that this folding event may have initiated the passive reorientation of the stretching lineations in post metamorphic conditions (Philippon et al., chap. 7).

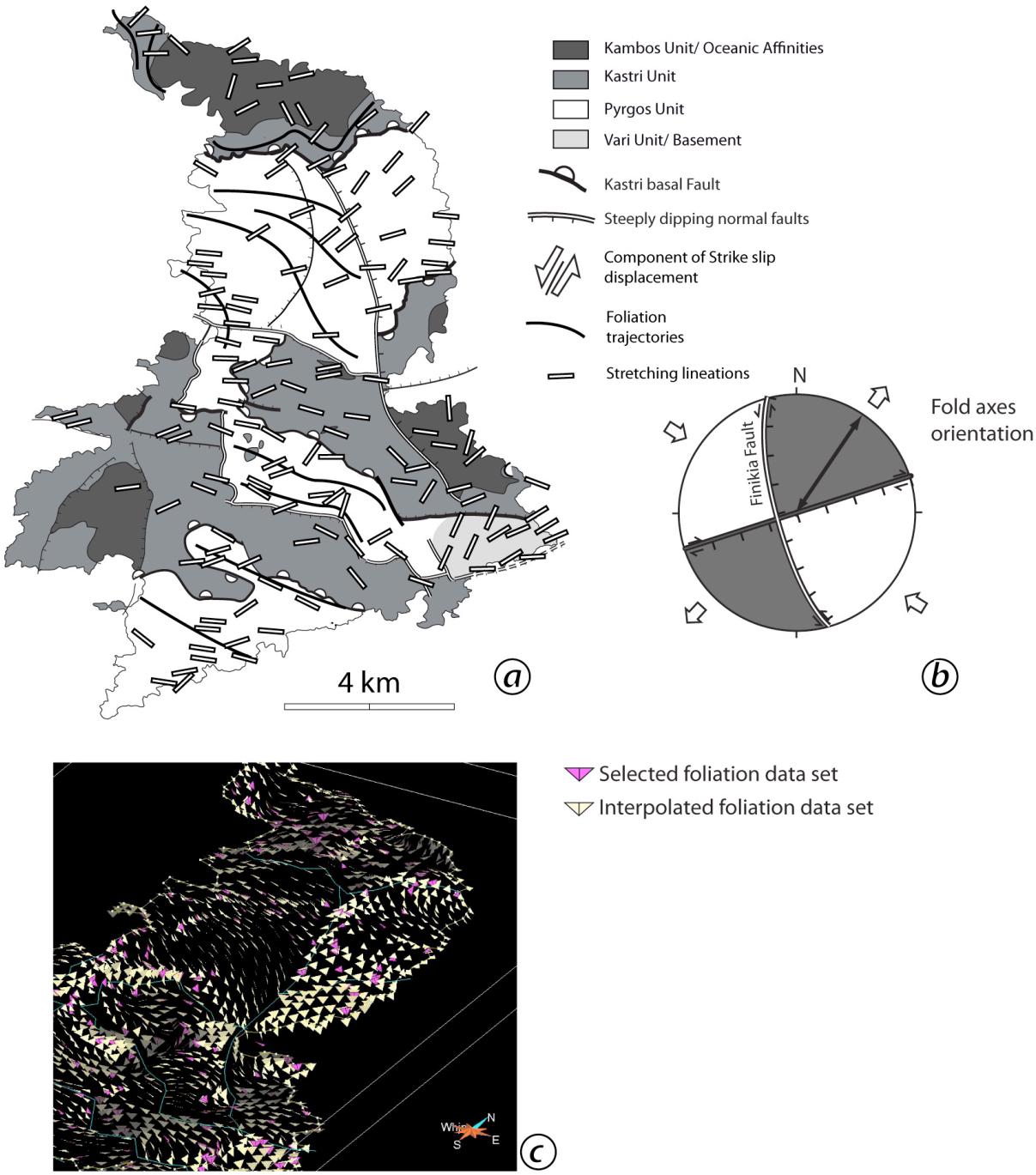

Fig. VI-10: Deformation pattern a) Structural schema of the Syros, with the simplified foliation trend (black lines) and the stretching lineations b) Schematic stereonet that illustrates the relationship between the observed normal faults and the development of N45° trending axes folds and c) 3D view of the interpolated foliation pattern also illustrating the 3D geometry.

6.5.2. Flat lying contact in Cyclades

Flat lying contacts in the Cyclades are described to be responsible for the exhumation of the Cycladic blueschits unit below the Pelagonian plate. Simple 3D geometrical modeling of the CBU lithological pile outcropping in Syros coupled with new petrological data (from Schumacher et al., 2008) shows that the flat lying contacts previously describes as syn metamorphic interfaces triggering the differential exhumation of the constitutives units of the islands are a single interface: the Kastri basal fault. The Kastri basal fault is 1) post metamorphic, 2) occurred inside the pile and therefore is not a detachment, 3) is a subtractive contact as in the southeastern of the island, the oceanic unit is almost lying on the basement, 4) the constitutives units of the islands have the same PT path. A detachment separates high grades rocks in the footwall from upper plate or syn deformation sedimentary deposits in the hangingwall. With this straightforward definition, only one detachment is outcropping in the Cyclades: above the Naxos/Paros metamorphic core complexes. Other flat lying contacts described within the CBU should be re examined in the light of preliminary this structural study.

6.5.2. Interest of 3D modeling from scarce data

When only field data are available, a 3-D geomodeler represents a first-order tool for integrating different kinds of data and ensuring consistency between data and models. However, and due to the lack of data in depth, the construction of good quality models is usually a labour-intensive procedure requiring constant checks on quality and geological validity. Therefore, a new approach, combining 2-D interpolation of orientation (identification the main discontinuities) and 3-D interpolation with implicit surfaces was developed to construct rapidly a geologically consistent (Caumon et al., 2004, 2009) set 3-D surfaces from field data only. In addition, this approach allows the 3-D model to be updated simply if new data are available. However, the most limiting factor is the availability of a faulted tetraedralized model. This is especially true if a complex set of fault is present, and in this case, a simplification may be required.

It is clear that while the 3D surfaces produced by this method match outcrop data and are geologically consistent, they can, at best, provide only consistent and reasonable estimates in poorly constrained areas. And because several interpretations are possible

in underconstrained areas, the proposed approach is interesting for testing geological and geometrical scenarios and obtain rapidly a consistent model. From that point of view, this approach may be considered as "3-D cartography" rather than 3-D modeling s.s. (Mallet, 2002). And because all 3D variations in the original data are integrated and respected, this reconstruction can be therefore considered as a more valid representation of the true geometry of Syros than can be produced by traditional cross section construction.

The next step to improve this model will be to perform a 3-D balanced restoration. Balanced restoration, which aims at unfolding and unfaulting a stack of layers, could provide help in checking model consistency, reducing structural uncertainties and quantifying extension/shortening and deformation.

References

Bonneau, M., Blake, M.J.C., Gueyssant, J., Kienast, J.R., Lepvrier C., Maluski H. and D. Papanikolaou, D., (1980a), Sur la signification des séries métamorphiques (schistes bleus) des cyclades (Héllènides, Grèce). L'exemple de l'île de Syros. Comptes rendus de l'académie des sciences Paris 290, 1463-1466.

Bonneau, M.B., Kienast, J.R., 1982. Subduction, collision et schistes bleu: exemple de l'Egée, Grèce. Bulletin de la Société Géologique de France 7, 785-791.

Bond, C., Butler, R., Dixon, J., 2007. Co-axial horizontal streching within extending orogens: the exhumation of HP rocks of Syros (Cyclades) revisited. In: Ries, A., Butler, R. and Graham, R. (Eds), Deformation of the continental crust: The legacy of Mike Coward. Geological Society, London Special Publications, 272. pp. 203-222.

Bulle, F., Bröcker M., Gärtner C., Keasling, A., 2010. Geochemistry and geochronology of HP mélanges from Tinos and Andros, cycladic blueschist belt, Greece. Lithos, 117, 61-81,

Calcagno, P., Chiles, J.-P., Courrioux, G., Guillen, A., 2008. Geological modelling from field data and geological knowledge Part I. Modelling method coupling 3-D potential-field interpolation and geological rules. Physics of the Earth and Planetary Interiors 171, 1-4:147-157.

Caumon, G., Lepage F., Sword C., Mallet, J.L., 2004. Building and Editing a Sealed Geological Model. Mathematical Geology 36, 4., 405-424.

Caumon, G., Collon-Drouaillet, P., Le Carlier de Veslud, C., Viseur, S., Sausse, J., 2009. Teachers aide: Surface-based 3D modeling of geological structures. Mathematical Geosciences 41, 8, 927-945.

Caumon G. (2010), Towards Stochastic Time-Varying Geological Modeling. Mathematical geosciences, 42 (5), 555-569. doi: 10.1007/s11004-010-9280-y

Chilès, J.-P., Aug, C., Guillen, A., Lees, T., 2004. Modelling the geometry of geological units and its uncertainty in 3-D from structural data: The potential field method. In Proc. Orebody Modelling and Strategic Mine Planning, 313-320.

Cowan, E. J., Beatson, R. K., Ross, H. J., Fright, W.R., McLennan, T. J., Evans, T. R.J., Carr, C., Lane, R.G., Bright, D.V., Gillman, A.J., Oshust, P.A., Titley, M., 2003. Practical implicit geological modeling. In S. Dominy, editor, Proc. 5th International Mining Conference, Australian Inst. Mining and Metallurgy, pp. 89-99.

De Donatis, M., 2001. Three-dimensional visualisation of the Neogene structures of an external sector of the Northern Apennines, Italy. AAPG Bulletin 95: 419-431.

De Kemp, E., 2000. 3-D visualization of structural field data: examples from the Archean Caopatina Formation, Abitibi greenstone belt, Québec, Canada. Computers and Geosciences 26, 509-530.

Fernández, O.. Muñoz, J.A., Arbués, P., Falivene, O. and Marzo, M., 2004. Three-dimensional reconstruction of geological surfaces: An example of growth strata and turbidite systems from the Ainsa basin (Pyrenees, Spain). AAPG Bulletin 88, 1049-1068.

Frank, T., Tertois, A.L., Mallet, J.-L., 2007. 3-D-reconstruction of complex geological interfaces from irregularly distributed and noisy point data. Computers and Geosciences 33, 932-943.

Gautier, P., Brun, J.P., 1994. Ductile crust exhumation and extensional detachments in the central Aegean (Cyclades and Evvia islands), Geodin. Acta 7, 57 – 85.

Gitahi, N., 2004. Geochemistry and metamorphic evolution of éclogites on Syros island, Greece. Extended Abstracts, Seventeenth Annual Keck Research Symposium in Geology Proceedings, Lexington, VA, P.81-4.

Gumiaux, C., 2004 Geostatistics applied to the best fit interpolation of orientation data. Tectonophysics 376, 364, 241-259.

Holley, E. A., Ross, T., Cheney, J. T., 2004. Pressure-température conditions of metamorphism in eclogites, Syros, Greece. Geological Society of America, Abstracts with Programs 36(1), A67.

Jolivet L. and Brun J.P., 2010. Cenozoic geodynamic evolution of the Aegean. International Journal of Earth Sciences 99, 1, 109-138.

Jolivet, L., Trotet, F., Monié,P., Vidal, O., Goffé, B., Labrousse,L., Agard, P. and Ghorbal B., 2009. Along-strike variations of P–T conditions in accretionary wedges and syn-orogenic extension, the HP–LT Phyllite–Quartzite Nappe in Crete and the Peloponnese. Tectonophysics 480, 1-4, 133-148.

Jolivet, L., Lecomte, E., Huet, B., Denèle, Y., Lacombe, O., Labrousse, L., Le Pourhiet, L., Mehl, C., 2010. The North Cycladic Detachment System. Earth and planetary Science Letters 289, 87–104.

Keay, S., 1998. The geological evolution of the Cyclades, Greece: constraints from SHRIMP U–Pb geochronology. Ph.D. thesis, Australian National University, Canberra, 335p.

Keiter, M., Piepjohn, K., Ballhaus, C., Lagos, M. and Bode M., 2004. Structural development of high-pressure metamorphic rocks on Syros Island (Cyclades, Greece). Journal of Structural Geology 26, 8, 1433-1445.

Lagos, M., Scherer, E.E., Tomaschel, F., Münker, C., Keiter, M., Berndt, J., Ballhaus, C., 2007. High précision Lu-Hf geochronology of Eocene éclogite facies rocks from Syros, Cyclades, Greece. Chemical Geology 243, 16-35.

Mallet, J.L., 2002. Geomodeling. Applied Geostatistics. Oxford University Press, New York, NY, 624 p.

Maluski, H., Bonneau, M., Kienast, J.R., 1987. Dating the metamorphic events in the Cycladic area: 40Ar/39Ar data from metamorphic rocks of the island of Syros (Greece), Bulletin de la Société géologique de France III, 833-841.

Pohl, J., 1999. Geologie und Hochdruckgesteine der Insel Syros, Griechenland. Diploma thesis, Geologisches Institut, Albert-Ludwigs Universitat, Freiburg, 107 p.

Putlitz, B., Cosca, M. A. & Schumacher, J. C., 2005. Prograde mica 40Ar/39Ar growth ages recorded in high pressure rocks (Syros, Cyclades, Greece). Chemical Geology 214, 1-2, 79-98.

Ridley, J., 1982. Arcuate lineation trends in a deep level, ductile thrust belt, Syros, Greece. Tectonophysics 88, 3-4, 347-360.

Ridley, J., 1984. Listric normal faulting and the reconstruction of the synmetamorphic structural pile of the Cyclades. In: Ries, A., Butler, R. and Graham, R. (Eds), Deformation of the continental crust: The legacy of Mike Coward. Geological Society of London, Special Publication 17,pp 755-761.

Ring, U., Thomson, S.N., Bröcker, M., 2003. Fast extension but little exhumation : the Vari detachment in the Cyclades, Greece. Geological magazine 140, 3, 245-252.

Ring U., Glodny J., Thomas W., Thomson S., 2010, The Hellenic Subduction System: High-Pressure Metamorphism, Exhumation, Normal Faulting, and Large-Scale Extension. Annual Review of Earth and Planetary Sciences 38, 45-76.

Rosenbaum, G., Avigad D. and Sánchez-Gómez, M., 2002. Coaxial flattening at deep levels of orogenic belts: evidence from blueschists and eclogites on Syros and Sifnos (Cyclades, Greece), Journal of Structural Geology 24 (9), 1457-1462.

Tomaschek, F. & Ballhaus, C., 1999. TheVari Unit on Syros (Aegean Sea) and its relation to the Attic-Cycladic Crystalline Complex. Journal of Conference Abstracts 4, 72.

Tomaschek, F., Kennedy, A. K.,Villa, I.M., Lagos,M. & Ballhaus, C. Zircons from Syros, Cyclades, Greece, 2003. Recrystallization and mobilization of zircon during high-pressure metamorphism. Journal of Petrology 44, 1977-2002.

Tomaschek, F., Keiter, M., Kennedy, A.K., Ballhaus, C., 2008. Pre-Alpine basement within the Northern Cycladic Blueschist Unit on Syros Island, Greece. - Zt. dt. Ges. Geowiss 159/3, 11 pp.

Trotet, F., Jolivet, L., Vidal, O., 2001a.Tectono-metamorphic evolution of Syros and Sifnos islands (Cyclades, Greece), Tectonophysics 338, 179-206.

Trotet, F., Vidal, O., Jolivet L., 2001b. Exhumation of Syros and Sifnos metamorphic rocks (Cyclades, Greece). New constraints on the P-T paths. European Journal of Mineralogy 13 (5), 901 – 920. doi: 10.1127/0935-1221/2001/0013/0901.

Schumacher, J.C.B., J.B.; Cheney, J.T.; Tonnsen R.R., 2008. Glaucophane bearing Marbles on Syros, Greece, Journal of Petrology 49, 1667-1686.

Annexe:

6.6. Interpolation of foliation

The method for interpolation foliation data follows that proposed by Gumiaux et al., (2004), with the difference that the interpolation is performed with the DSI method (Mallet, 2002) instead of geostatistics. It may be summarized as follows:

Each dip and azimuth data point is transformed into an unit vectors through its direction cosines,

These direction cosines are not circular and may be interpolated on a map, with a range of [-1, +1] constraint. Discontinuities, representing faults, or thrusts, may be taken into account during this stage,

After interpolation, each vector is normalized to an unit vector (which is not the case after interpolation, due to the linear behavior of the interpolation).

The dip and azimuth angles corresponding to the direction cosines are calculated on the map,

This method has been applied to a 1000 foliation dataset measured in the field. The Figure 5 to 7 show the good agreement between the data and the interpolation. Because the method is 2D, it provides simply first draft results for which several hypothesis can be tested. In particular, the influence of hypothetical faults may be investigated easily in order to decipher between continuous or discontinuous deformation patterns. Similarly, the possibility that the foliations could locally become parallel to faults in their early history (ductile proto-faults) may also be investigated.

6.7. Building 3-D geological surfaces from field data using implicit functions

Complex geometries, such as in Syros, are best represented using a 3-D modeling approach. The classical surface-based modeling process (e.g. Mallet, 2002), where interfaces are built individually, is efficient if the data density is high (e.g. 2-D or 3-D seismic survey). However, when only sparse data are available, this process provides sometimes spurious results, requiring time-consumming quality check and post-editing. For this reason, the construction of complex 3-D geometrical models from field data and scarce subsurface data is currently an important research topic motivated in part by increasing exploration in frontier domains, where imaging in depth is poor (e.g. de

Kemp, 2000; De Donatis, 2001; Cowan et al., 2003; Chiles et al., 2004; Fernández et al., 2004; Frank et al., 2007; Calcagno et al., 2008). However, some of the proposed methods were not found to be fully appropriate for Syros study. For instance, the use of multiple cross-sections (e.g. De Donatis, 2001) is difficult, because it uses already interpreted data as constraints from the beginning of the modelling process. Similarly, the dip-domain approach proposed by Fernández et al. (2004) could not be used due to the complexity of the foliation patterns in metamorphic rocks. By contrast, implicit function approach (Chiles et al., 2004; Cowan et al., 2003; Calcagno et al., 2008; Frank et al., 2007) appears to be very attractive because of it can provide rapidly a consistent 3-D model (Caumon et al., 2004, 2009).

Implicit methods may be applied when one has to model a succession of interfaces (e.g. stratigraphic horizons or a stack of layers in metamorphic rocks). They consider geological interfaces not as explicit surfaces but as equipotentials of some scalar 3-D function. Using such a volumetric representation in the model building process directly enforces a real consideration of the 3-D geometry of the studied structures, but also some basic structural consistency rules (e.g., no interfaces cross-over, or termination of interfaces onto faults).

From a technical point of view, the implicit modeling program (details of which may be found in Franck et al., 2007; Caumon, 2010), is a plug-in of the gOcad 3-D modeller (Mallet, 2002). In a first step (Fig. 4a), datapoints corresponding to stratigraphic horizons have to be assigned a constant scalar value, that should respect some convention, for instance being proportional to the average thickness between the each interface and a reference interface. Orientation data are specified by a 3-D vector that is used to constrain the gradient of the scalar function in each tetrahedron where each point lies. In a second step (Fig. 4b), a 3-D tetrahedralized solid enclosing the volume of interest of the studied area is built. Handling of faults is currently achieved by using a tetrahedral mesh conforming to, and discontinuous accross faults and other discontinuities. This allows two scalar values to be represented at the same geometric location, corresponding respectively to the hanging wall and the footwall on the fault surface. Then (Fig. 4b), the scalar function is interpolated on each node of the tetrahedralized solid, taking into account the available data with the Discrete Smooth

Interpolation method (DSI, Mallet, 2002). In a final step (Fig. 4c), isovalue surface corresponding to values of each interface are computed from the tetrahedralized solid.

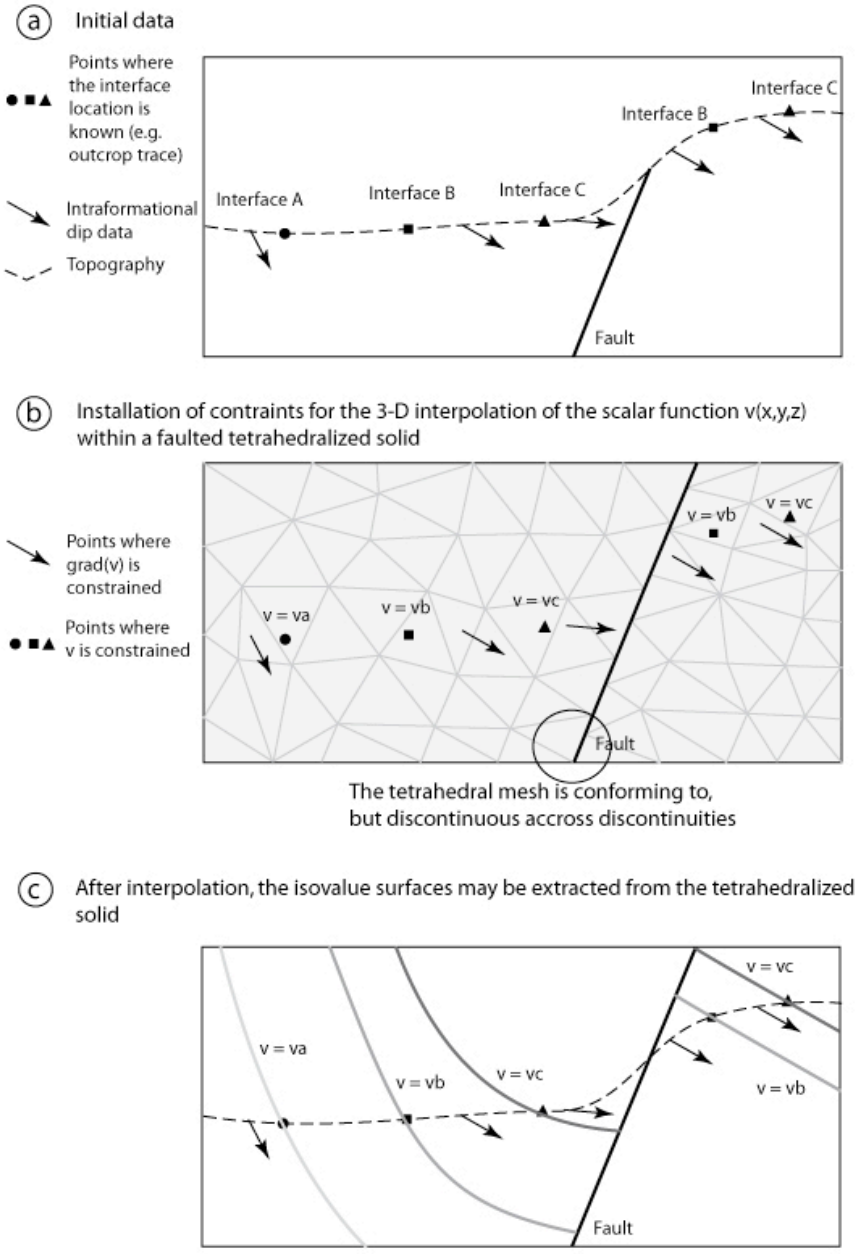

Fig. VI-4: Schematic description of 3-D geological modeling with an implicit function approach. a) Initial dataset, with 3 interfaces outcrop data (A to C), some intraformational orientation data and one fault. b) A tetrahedralized solid enclosing the volume of interest is built and several constraints are installed linking the scalar function to be interpolated v(x,y,z) to the data. c) The scalar function v(x,y,z) is interpolated on the solid, and isovalues corresponding to the interfaces (va to vc, stored as triangulated surfaces) are computed from the solid. The obtained results is both geometrically and geologically consistent because it honors outcrop data, orientation data (including intraformational ones) and takes into account the fault.

This method is very attractive for structural modeling, especially in poorly constrained settings for the following reasons (Caumon, 2010):

- built-in structural consistency of interface (no cross-over, conforming to faults, Caumon et al., 2004; 2009),
- possibility to integrate intraformational orientation measurements, without need for projections,
- possibility to account for folding orientation and folding style,
- rapid to build, as soon as a consistent tetrahedralized solid, eventually faulted, is available.

The implicit method however presents several drawbacks or limitations. Firstly, and apart from accessibility to 3-D modeling software, the need of a faulted tetrahedralized solid is a limiting factor. Indeed, in spite of meshing progresses, the tetrahedralization is still a difficult process and subject to limited numerical accuracy. This is particularly true in the presence of intersecting faults. Secondly, the obtained result, although geometrically consistent, remains underconstrained in poorly documented areas. In these area, the result is highly dependent on the interpolation method used. Here, the Discrete Smooth Interpolation method (Mallet, 2002) allows to take into account different types of constraints, and may enforce the quality of the result. For instance, global or local fold axis may be provided, yielding sub-cylindrical folds. Similarly, the scalar function may be constrained to be higher or lower than a given threshold ("inequality constraint"). Finally, a roughness constraint (Franck et al., 2007) may be imposed to smooth the variation of the gradient of the scalar function. Although this constraint may be conflicting with the other constraints, it ensures the convergence of the interpolation and prevent spurious oscillations to appear.

Chapitre 7 : Histoire tectonique de l'île de Syros : de la subduction à l'extension Egéenne.

TECTONICS OF THE SYROS BLUESCHISTS (CYCLADES, GREECE): FROM SUBDUCTION TO AEGEAN EXTENSION

Mélody Philippon, Jean Pierre Brun and Frédéric Gueydan

Géosciences Rennes UMR 6118 CNRS, Université de Rennes 1, 35042 Rennes cedex, France

Submitted to Tectonics

Abstract

In Syros, high-pressure metamorphism affects a lithological pile that is comprised of, from base to top: i) the Komito-Vari granitic basement, ii) a margin sedimentary sequence that is predominantly made of marbles and schists (the Pyrgos and Kastri units) and iii) the Kambos meta-ophiolitic mélange. The tectonic history occurred in three main stages. During the first stage, in the mid-Eocene, the Kambos oceanic unit was thrust southward on top of the sedimentary pile. Top-to-the South southwest ductile senses of shear are synchronous with prograde high-pressure metamorphism and associated with this thrusting event. The second stage corresponds to a top-to-the-northeast ductile shear that affects the whole metamorphic pile and is synchronous with the metamorphic retrogression from eclogite to greenschist facies. However, the Kambos oceanic unit remained partly undeformed, as shown by significant volumes containing undeformed lawsonite pseudomorphs. No major extensional detachment related to this exhumation event outcrops in the island. The localised semi-brittle to brittle deformation of the third stage is associated with the post-metamorphic development of: i) a flat-ramp extensional system at the island scale, whose southward minimum displacement is estimated at approximately 7 km and ii) two sets of steeply dipping normal faults, either E-W or sub-meridian indicating that the mean stretching and shortening directions are trending NNE-SSW and ESE-WNW, respectively. This sequence of major tectonic events and their relationship to metamorphism are interpreted within the framework of the subduction of the Pindus Ocean and then of the Adria continental passive margin. Stage 1, in the mid-Eocene, corresponds to the thrusting of the Pindus oceanic unit on top of the Adria margin sediments. During stage 2, from late Eocene to early Oligocene, the Adria crust was decoupled from the underlying lithospheric mantle and exhumed up to the mid-lower crustal level. In stage

3, in the mid-late Miocene, the Syros high-pressure units underwent Aegean brittle extension at upper-crust levels, resulting in a southward flat-ramp extensional system and steeply dipping normal faulting.
Key words: Cyclades, blueschists, eclogite, subduction, exhumation, flat-ramp extension, detachment.

7.1. Introduction

The outcropping of high-pressure rocks is commonly thought to be the result of burial in subduction zones followed by exhumation back to the surface. Deformation associated with exhumation is often intense and consequently, earlier deformations are either erased or obscured and therefore difficult to recognise. This could explain why most of the recent structural studies focus on the processes of high-pressure (HP) rock exhumation. For this same reason, deciphering between subduction and exhumation-related deformations obviously remains a scientific challenge with respect to two main aspects: i) designing concepts and techniques to identify and characterise subduction-related deformations and ii) describing and quantifying the whole subduction-exhumation cycle.

Syros Island (Cyclades, Greece) presents well-preserved eclogites and blueschist rocks and displays an exceptional preservation of pseudomorphs of HP minerals, such as lawsonite [Keiter et al., 2004] and aragonite [Brady et al., 2004] in particular. Specific mechanisms of exhumation must have contributed to the exceptional preservation of these minerals that attest to the earlier tectonic history of the Syros blueschists. The purpose of the present study was to identify these mechanisms and their significance in order to understand the subduction-exhumation cycle in the Cyclades. Because of its mineralogical variety, Syros has been the focus of numerous studies in geology, petrology, geochronology and structural geology. Using this exceptional background, we carried out extensive structural mapping that allowed to distinguish between three main deformation events whose geometry and kinematics are characterised. The results are discussed within the framework of the evolution of the Hellenic subduction.

7.2. Geological setting

The Cycladic Blueschists unit (CBU) mainly outcrops in the central Aegean Sea, Evvia and Attica [Bonneau and Kienast, 1982] (Fig. VII-1). Within this framework, Syros and Sifnos Islands display the best-preserved evidence of the high-pressure metamorphism. The CBU is a structural pile composed of three units, from bottom to top: (1) a Pre-Alpine granitic basement, (2) a margin sedimentary sequence principally made of marbles and schists, and (3) a meta-ophiolitic mélange with a decreasing metamorphism from blueschist facies to greenschist facies through the pile [Bonneau et al., 1980a and b, Ridley 1984]. The CBU units are seated below non-metamorphosed Cretaceous to Palaeogene limestones and ophiolites belonging to the Pelagonian overriding plate. These units underwent a prograde high-pressure metamorphism in the Eocene [Bonneau and Kienast, 1982; Pulitz et al., 2005]. From late Oligocene to late Miocene, the blueschists were overprinted by a high temperature metamorphic event that was responsible for the commonly observed greenschist facies retrogression [Wijbrans et al., 1990] and that culminated in basement migmatisation in the centre of the Cyclades (Mykonos, Paros and Naxos Islands) [Lister et al., 1984; Gautier et al., 1993]. Finally, this metamorphic evolution finished with the emplacement of several granite plutons in the CBU between 18 and 10 Ma [Altherr et al., 1982].

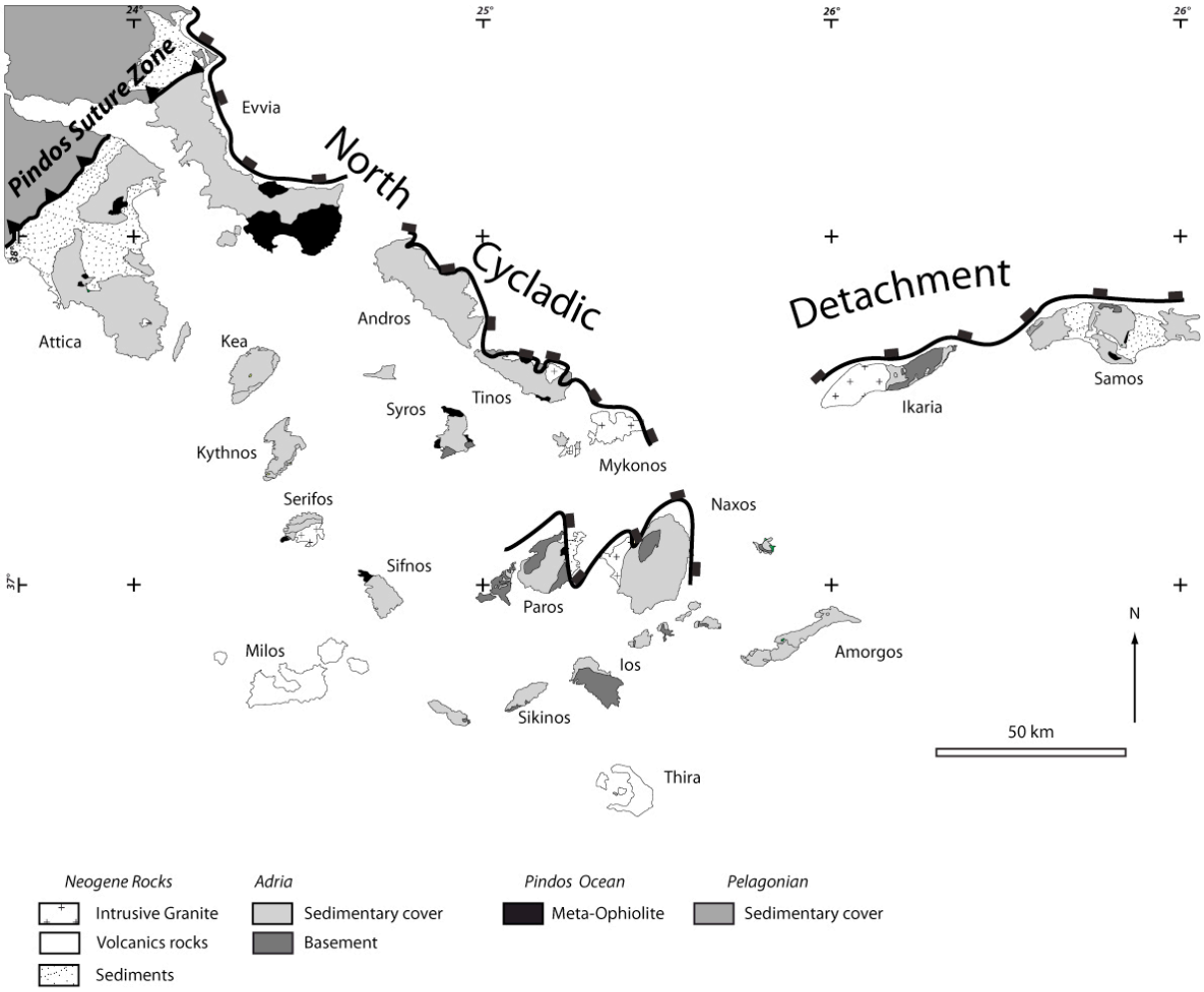

Fig. VII- 1: General map of the Cyclades, showing the different lithologies outcropping in the Aegean Sea: the Cycladic blueschists unit is sensu stricto composed of the Adria plate sedimentary cover and basement and the Pindus Ocean. The Pelagonia plate lies above the CBU. The Neogene rocks are either intrusives or deposed on top of the CBU and Pelagonia (granites, volcano and sediments). Syros Island is located in the central Cyclades and the tree rock-types of the CBU are out cropping in the island.

7.3. General structure

Our structural map of Syros Island (Fig. VII-2) integrates Hetch's [1984] geological map and our extensive structural mapping. The geological pile is composed of four structural units, from bottom to top: (1) the Komito-Vari basement unit, (2) the Pyrgos volcanic and sedimentary sequence (3) the Kastri volcanic and sedimentary sequence (Schumacher et al., 2008), and (4) the Kambos oceanic series. Bedding-parallel foliation trajectories in Figure VII-2 were drawn from 866 foliations measurements. On average, foliations dip to the NE with a mean NW-SE trend. However, in the Kini area, they define an anticline with a NE plunging axis. At the island scale, the initial lithological sequence

is well preserved and kept its original continuity on top of the crystalline basement up to the Triassic, below an allochtonous slice made of the Kastri and Kambos units to the south.

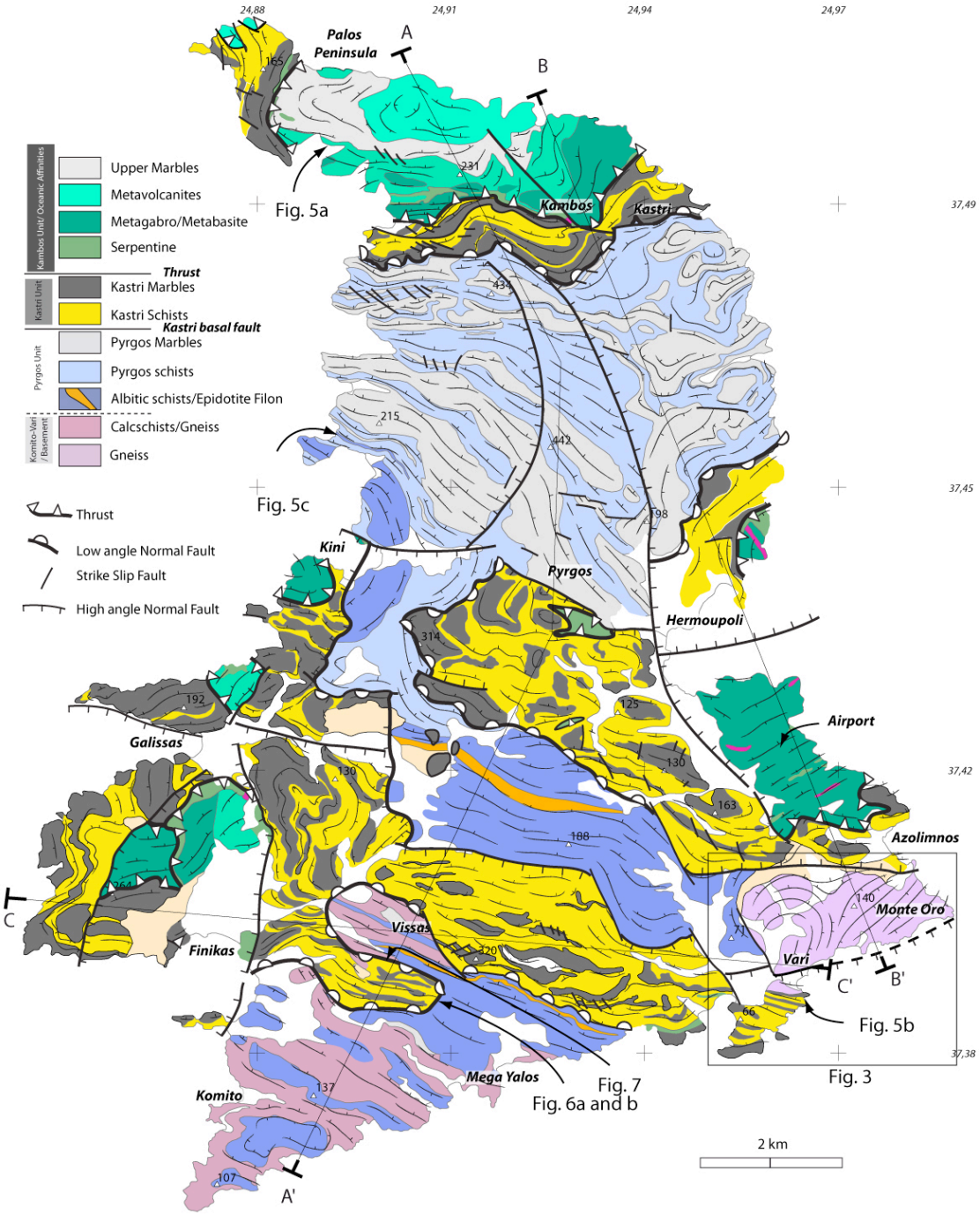

Fig. VII-2: Detailed map of Syros showing the four different units pointed out by our structural study. The main tectonic contacts are a thrust (triangle symbols) and a low-angle fault system (hemispheric symbols). Foliations trajectories have been drawn from 866 foliation measurements and show the 3D structure of the island.

7.3.1. The Komito-Vari basement

The Vari orthogneisses in southeastern Syros and the southwestern Komito orthogneisses (Fig. VII-2) were initially interpreted as the basement of the CBU, on the basis of structural mapping [Bonneau et al., 1980a and b]. The protolith of the Vari orthogneiss is a granite pluton whose crustal emplacement is dated at 240-243 Ma [SHRIMP analyses of U/Pb on zircon; Keay 1998; Tomaschek et al., 2003]. The Komito gneiss (Fig. VII-2) yields an age of 300 Ma [SHRIMP analyses of U/Pb on zircon; Tomaschek et al., 2008].

PT conditions in the Vari unit have been estimated from greenschist facies conditions (Phengite Si substitution; Maluski et al. [1987]) at 15 kbar and 500°C [Dixon and Ridley, 1987; Okrusch and Bröcker, 1990]. The age of the blueschist facies metamorphism has been estimated from 53.5 ± 1.3 to 37.3 ± 1.3 Ma and 30.3 ± 0.9 for the greenschist facies (40Ar /39Ar on phengites; Maluski et al., [1987]). The same metamorphism ages are found in the above sedimentary sequence and oceanic unit [Pulitz et al., 2005].

Our mapping of foliations in the Vari unit defines an upright anticline, trending NE-SW that is cut to the north and to the south by steeply dipping normal faults trending E-W (Fig. VII-3). To the west, the foliation of the anticline is parallel to the basal schists of the Pyrgos unit. In agreement with Bonneau et al. [1980 a and b], Tomaschek and Ballhaus [1999], Ballhaus et al. [1999] and Tomaschek et al. [2008], this structural pattern shows that the Vari unit is located at the base of the CBU. It must be noted that in addition to previous data, careful field observation has not revealed any evidence for a flat-lying detachment that would separate the Vari unit from a supposedly underlying CBU, as previously proposed by Gautier [1995], Trotet et al. [2001a] and Ring et al. [2003].

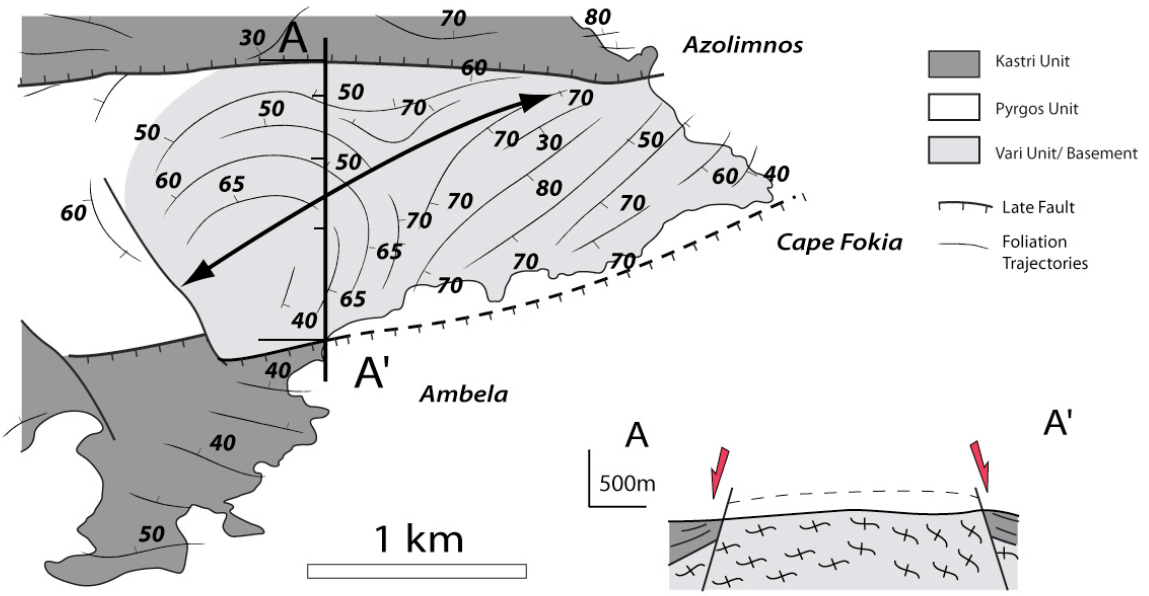

Fig. VII-3: Detailed work on the Vari unit. Map of the Vari orthogneiss foliation trajectories have been drawn form 89 foliations measurements. Cross section AA' is N-S directed and shows the geometry of the northern and southern contacts of the Vari unit with the other lithologies of the island.

The Komito gneiss, which makes up most of the southwestern part of the island, is a lateral equivalent of the Vari unit. Both define the Komito-Vari Hercynian gneissic basement of the new structural pile proposed in this study (Fig. VII-2).

7.3.2. The volcano-sedimentary sequences of Pyrgos and Kastri

From base to top, the two volcano-sedimentary and marbles sequences lying on top of the Komito-Vari basement (Fig. VII-2) are the Pyrgos and Kastri units. They mainly differ by the presence of dolomitic marbles in the Pyrgos unit. The presence of microfossils (Foraminiferous Forschiidae) give a deposition age of 330-350 Ma for the marbles of the Pyrgos unit(Pohl, 1999; see Schumacher et al., 2008). Metatuffites close to the top of the Kastri unit have been dated as 243 ± 2 Ma (SHRIMP analyses of U/Pb on zircon; Keay, 1998; Tomaschek et al., 2003). The whole volcano-sedimentary sequence, as well as the intercalated marbles, have been metamorphosed in the blueschist facies from 8 to 17 kbar at 350-500°C (Trotet et al., 2001b; Schumacher et al., 2008). Contrary to the Kastri unit, the Pyrgos unit is retromorphosed almost everywhere in the greenschist facies

(Trotet et al., 2001b). Breccias and gouges indicate that the Kastri-Pyrgos flat-lying contact (white hemispheric symbols; Fig. VII-2) is a movement surface.

7.3.3. Ophiolite

The rocks have an oceanic crust affinity at the top of the lithological pile. They consist of coarse-grained metagabbros (Kambos and Kini areas), fine-grained metabasalts and metavolcanites (Palos Peninsula, Airport, Galissas and Kini) and serpentinic schists (Finikas, base of the Kambos gabbros). A marble sequence has been tectonically intercalated in this igneous rock unit (Palos Peninsula). Eclogite metamorphism has been estimated in the range of 19-24 kbar and 500-580°C [Gitahi, 2004; Holley et al., 2004; Trotet et al., 2001b]. The U/Pb SHRIMP age of magmatic zircons are between 240 Ma and 80 Ma, providing an age estimate of the basic protolith [Ballhaus et al., 1999; Tomaschek et al., 2008; Bulle et al., 2010]. High-pressure metamorphism is estimated at 52 Ma (Lu/Hf on garnet; Lagos et al., 2007).

Syros Island displays a complete lithological pile of the Cycladic Blueschists unit, from the Hercynian basement to its overlying sedimentary sequence up to the Triassic [Keay, 1998; Tomachek et al., 2003], on top of which the Pindus oceanic crust was thrust.

7.4. Ductile deformation

Most rocks display a stretching lineation on foliation surfaces that are more frequently marked by glaucophane in blueschists, assemblages of quartz and chlorite in greenschists and fine corrugations and streaks on bedding planes of marbles. At the island scale, stretching lineations display an "arcuate pattern" from a mean N30° trend to the north to a mean N90° trend to the south [Ridley, 1982; Fig. VII-4].

7.4.1. Top-to-the-southwest shear, prograde blueschist metamorphism and thrusting of the ophiolites

To the north of the island, the Kambos unit (ophiolites), with serpentinite at the base, is thrust on top of the meta-sedimentary Kastri unit (white triangular symbols in Fig. VII-4). The thrusting was interpreted by Bonneau et al. [1980a and b] as related to

ophiolite emplacement prior to high pressure metamorphism. Schumacher et al. [2008] also argued that the stacking of thrust units was completed before the metamorphic climax using P-T estimates in glaucophane-bearing marbles. Along the thrust plane, folding indicates thrusting toward the south [Ridley, 1982]. Our mapping of shear criteria (black arrows in Fig. VII-4) shows top-to-the-south or -southwest senses of shear, in agreement with the conclusions of Ridley [1982] and Keiter et al. [2004]. The occurrence of sheath folds indicates an increase in strain intensity close to the thrust zone.

The Kambos unit is characterised by the widespread occurrence of lawsonite porphyroblast pseudomorphs whose development was synchronous with a top-to-the-south sense of shear (Fig. VII-5a), showing that thrusting was not prior to but instead synchronous with metamorphism, contrary to the results published by Bonneau et al. [1980a and b] and Schumacher et al. [2008]. As the lawsonite stability field corresponds to a narrow range of low temperatures, located on the prograde path of the Syros blueschist rocks (Fig. 12 in Schumacher et al., 2008), the top-to-the- south sense of shear occurred during prograde metamorphism –i.e. subduction. The preservation of lawsonite pseudomorphs indicates that shearing stopped prior to their destabilisation [Keiter et al., 2004; Philippon et al., 2009].

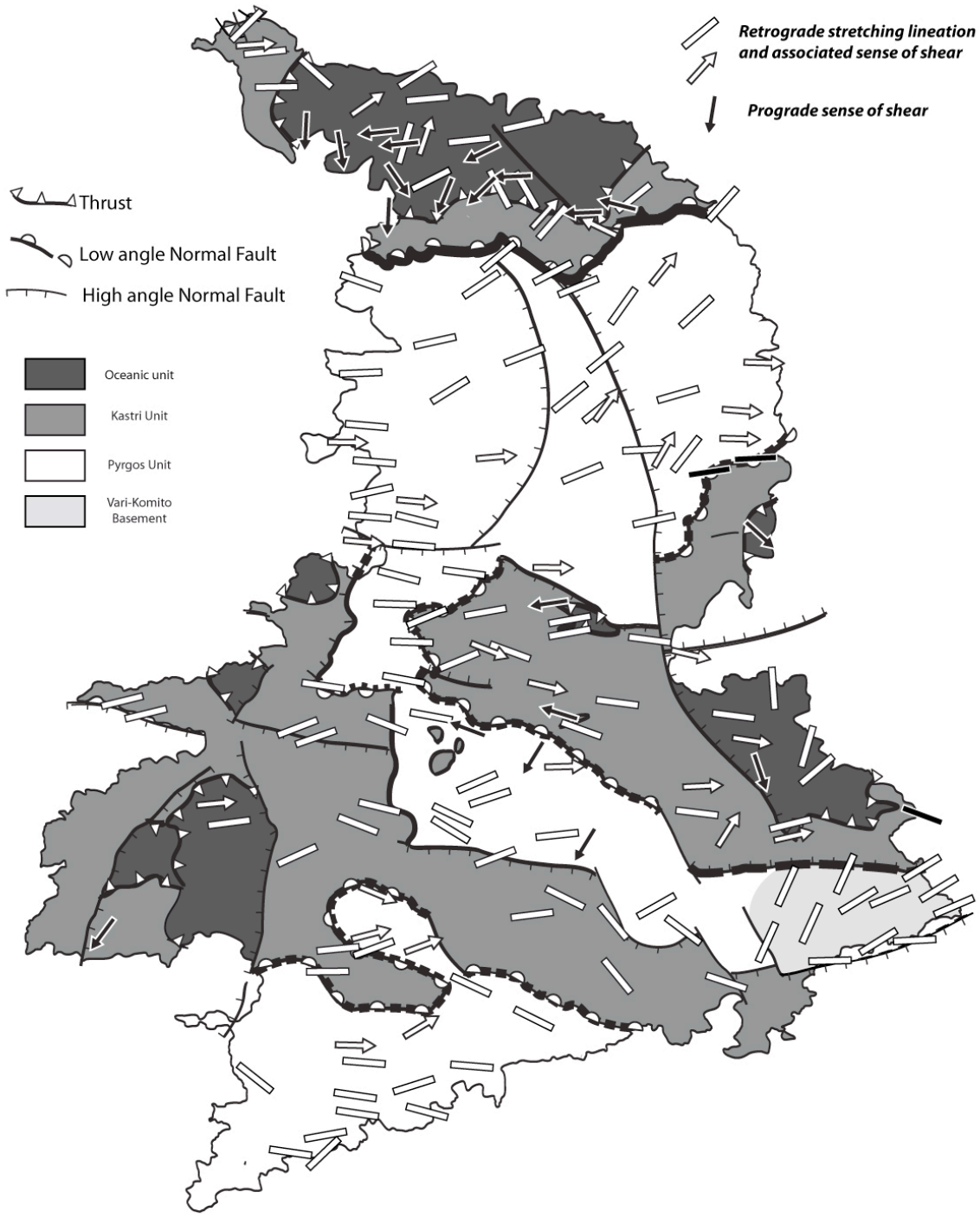

Fig. VII-4: Structural schema of Syros island showing the four main units that constitute the island shown in coulours ranging from dark grey to white: Kambos oceanic units, Kastri unit, Vari unit, and Pyrgos unit. The deformations observed in the field consist of prograde shearing associated with Lasonite pseudomorphs, shown by black arrows, and the white bars and arrows show the retrograde stretching lineation and associated sense of shear, respectively.

7.4.2 Top-to-the-northeast shear, retrograde greenschist metamorphism and exhumation

Top-to-the-northeast shear affects the four constitutive units of the island (white arrows in Fig. VII-4), whereas top-to-the-southwest shear is mostly preserved in the oceanic unit and seldom in the meta-sedimentary units. The top-to-the-northeast shear, as observed in the transition from eclogites and blueschists (Fig. VII-5b) to greenschists (Fig. VII-5c), indicates that it occurred during retrograde metamorphism, i.e. decompression (Trotet et al., 2001b). This pervasive deformation is linked to the exhumation of the unit from its maximum depth of burial up to the mid-lower crustal levels and has been described as a continuum of ductile extensive deformation from eclogite facies to greenschists facies (Trotet et al., [2001b]; Figs. VII-5b and c). Geochronological data indicate that the eclogite facies occurred at 52 Ma (Lagos et al., [2007]; Lu/Hf on garnet), the blueschist facies is dated from 53 to 35 Ma and finally, the greenschist facies is known to occur at 30 Ma (Maluski et al., [1987]; 40Ar /39Ar on phengites).

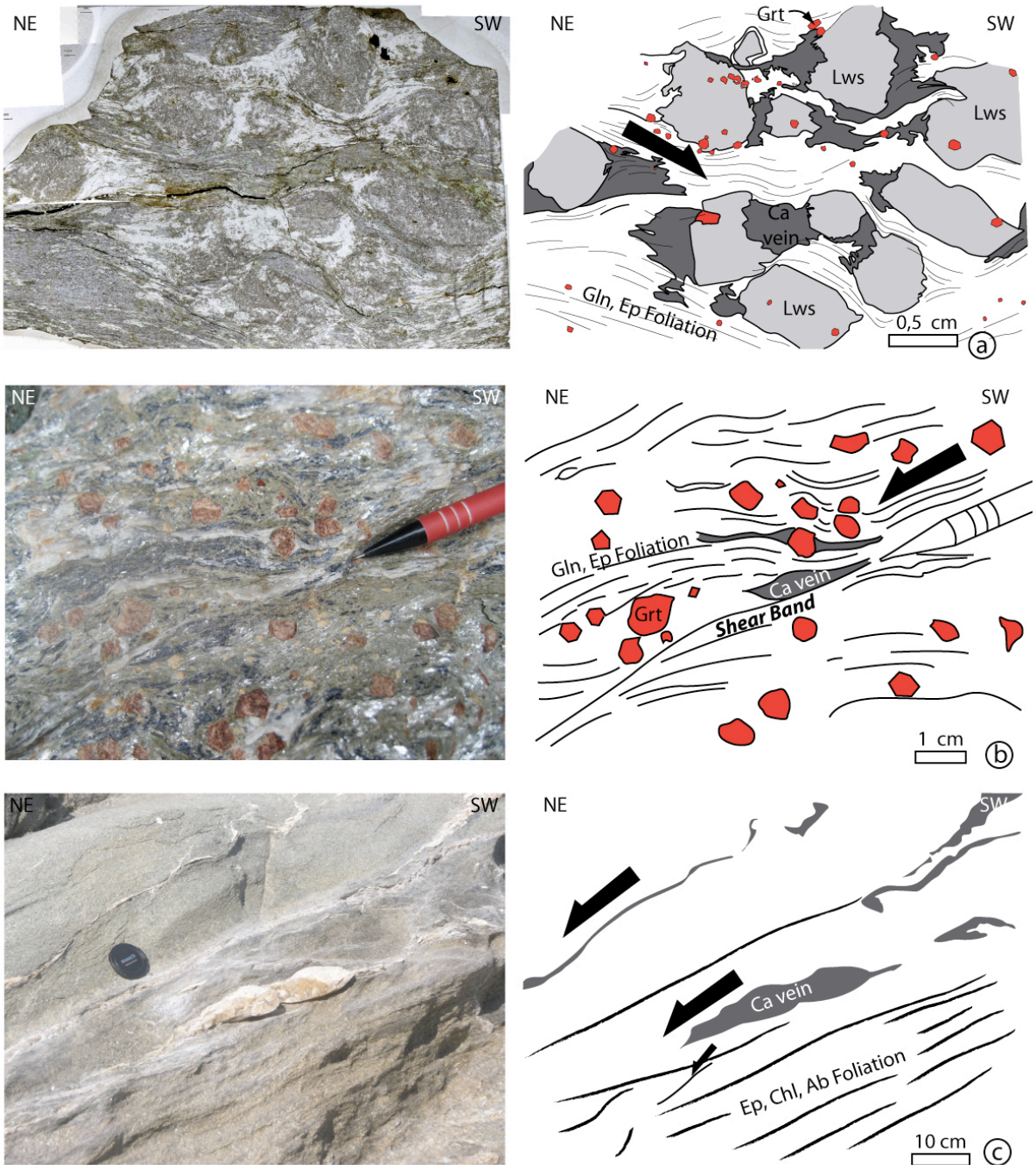

Fig. VII-5: Micro- and macrostructures observed in the Syros rocks. a) Thin-section showing top-to-the-SW sense of shear in Lawsonite bearing blueschists (belonging to the Kambos unit, north of the island). b) Field photograph of a garnet, glaucophane and epidote-bearing rock, recognised as eclogite facies rocks by Trotet et al., [2001b] (Ormo Ambelos area), displaying top-to-the-NE sense of shear. c) Greenschist facies rocks with a ab, chl, ep and ca paragenesis, showing a top-to-the-NE sense of shear.

7.5. Flat & Ramp extensional system

The southern part of the Syros map (Fig. VII-2) shows two large klippes of the Kambos and Kastri units lying unconformably on top of the Pyrgos unit. Conversely, to the north, the Kambos and Kastri units lie conformably on top of the Pyrgos unit. This island-scale structural pattern results from a predominantly post-metamorphic flat-ramp-type extension.

7.5.1. The Kastri basal fault

Where it can be observed directly, the major flat-lying basal contact of the Kastri unit displays metre-thick gouges and breccias that reworked the metamorphic rocks in a brittle fashion the metamorphic rocks. This indicates that displacement along this tectonic contact took place in the brittle crust. At the outcrop scale, southward senses of motion are marked by semi-brittle shear zones, pull-apart-type Ca-Qz veins and series of Riedel-type small faults.

Figure VII-6a is a landscape view of an area in the vicinity of Vissas, showing the Kastri unit lying on top of the Pyrgos unit. Inside the Kastri unit, marble layers dip northward and are cut by a low angle normal fault dipping gently southward. The offset of marble layers along this fault indicates a top-to-the-south sense of displacement.

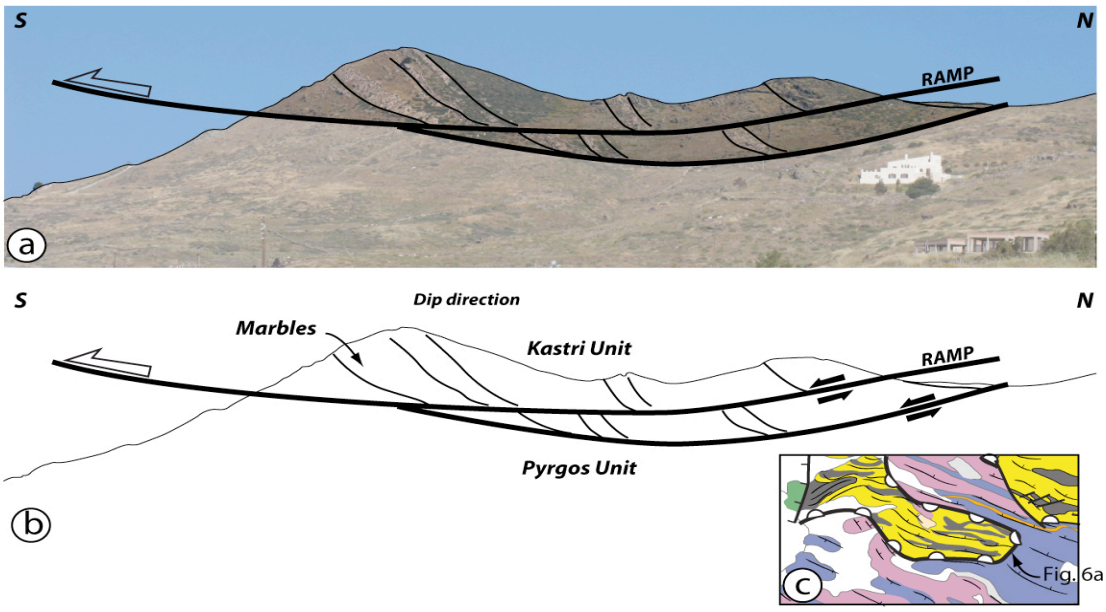

Fig. VII-6: Field evidence of displacement along the flat and ramp system. The kastri basal contact between the Kastri marbles and underlying Pyrgos marbles (in the vicinity of Vissas). A top-to-the-S displacement is shown by the offset of the marble layers in the Kastri unit.

At the outcrop scale, close to the basal contact, semi-brittle shear zones associated with calcite-filled tension gashes (Fig. VII-7) also indicate a top-to-the-south sense of shear. Two mean directions of displacement are reported in Figure VII-8 for the two main klippes in the south of the island.

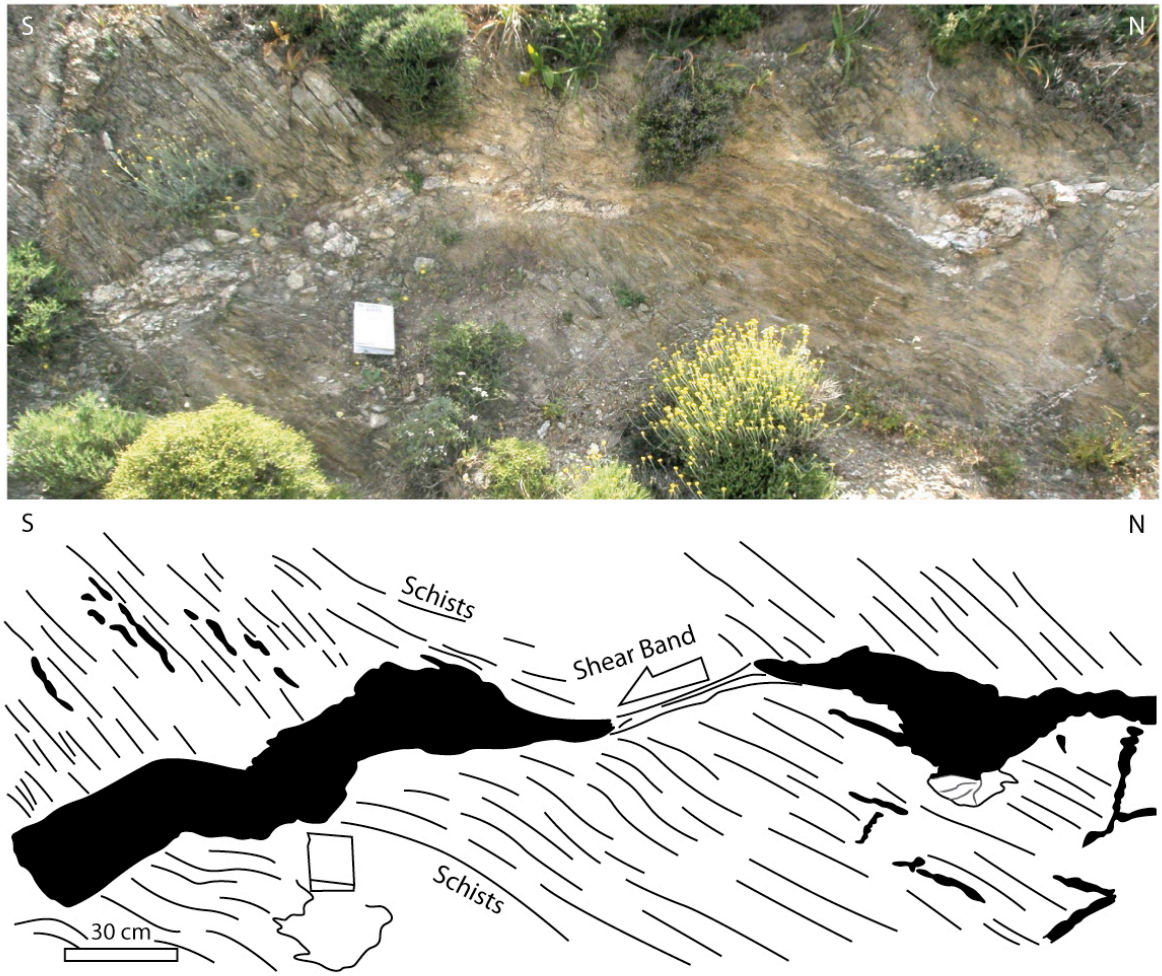

Fig. VII-7: The schists-schists contact still observed in the vicinity of Vissas. The deformation is located on a shear band filled by fluids and indicating a top-to-the-S sense of shear.

7.5.2. Cross-sections

The flat-ramp geometry of the Kastri basal fault at the island scale is illustrated by three cross-sections (see location in Figs. VII-2 and VII-8). Cross-sections AA' and BB' are nearly parallel to the N-S direction of displacement (Fig. VII-8). From base to top, the fault hanging wall is made up by the Kastri sedimentary unit, the Kambos oceanic units, the footwall by the Komito-Vari basement unit and the Pyrgos sedimentary unit.

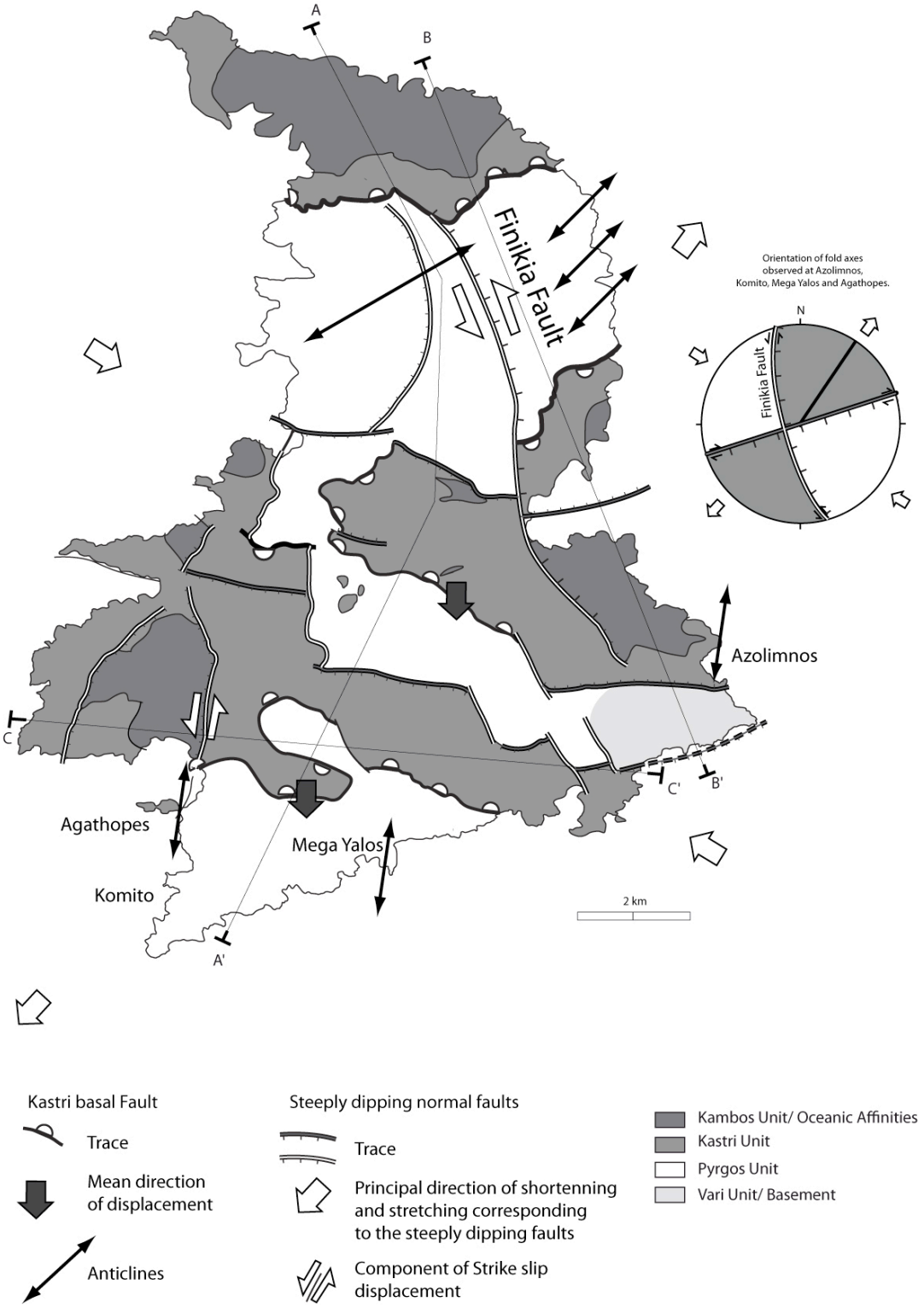

Fig. VII-8: Structural map of Syros Island showing the main tectonic features related to extension: the flat & ramp extensional system (hemispheric symbols) cross-cut by the steeply dipping normal fault network. This network shows two orientations: N-S, which is accompanied by a strike-slip motion on the faults in white lines and an E- network, either south- or north-dipping, in dark grey lines. White arrows show the principal direction of shortening and stretching corresponding to the steeply dipping faults. Black arrows show the mean direction of displacement along the kastri basal fault.

Sections AA' and BB' show that in the north of the island, in vicinity of Kambos, the Kastri basal fault is parallel to the foliation-parallel lithological layering of the Kastri and Pyrgos units that are gently dipping to the north. In other words, it is a décollement. In the southern part of the island, from Hermoupoli to the southern coast, the fault hanging wall is lying with a southward shallow dip on top of the NE-dipping foliation of the footwall. Cross-cutting relationships show that the hanging wall comes into contact with deeper footwall levels toward the south. These geometrical hanging wall-footwall relationships, the southward sense of displacement and associated brittle deformation indicate that the Kastri basal fault is a regional-scale extensional detachment dipping southward that developed at a late stage of the island evolution, in post-metamorphic conditions. Sections AA' and BB' also show that the whole pile is affected by the Kini anticline (Fig. VII-2), which has an half-wavelength of approximately 5 km. A few of the short wavelength folds with a NE-SW axis trend (Fig. VII-8) are likely to be related to basement faulting at a deeper level (Section AA'; Fig. VII-9).

Cross-section CC', which is close to perpendicular to the direction of displacement, shows the flat-lying attitude of the detachment systems along strike.

At a late stage of evolution, the Kastri basal fault was cut by two sets of steeply dipping faults trending either E-W or sub-meridian (Figs. VII-8 and VII-9). The dip of E-W trending normal faults changes from northward to the east (Section AA'; Fig. VII-9) of the Finikia fault (Fig. VII-8) to southward to the west (Section BB'; Fig. VII-9). The Finikia fault, which is dipping to the east, combines normal and sinistral strike-slip components. The observed strike-slip component along the Finikia fault is kinematically compatible with the change of dip of the EW trending normal faults in its hanging wall and footwall. This strongly suggests that the two sets of steeply dipping normal faults are at least partly contemporaneous.

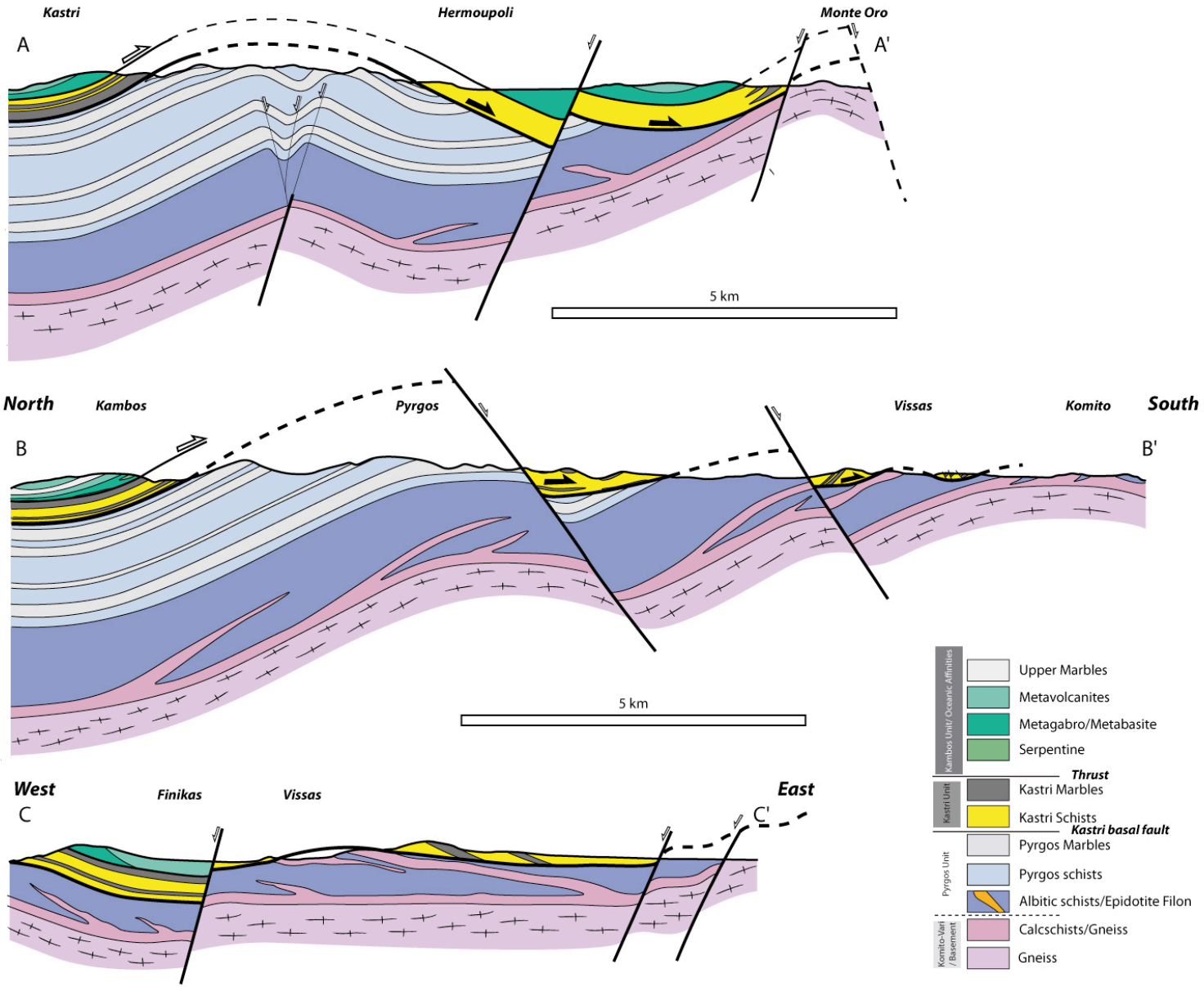
Kastri
Hermoupoli
Monte Oro
A
A'
5 km
North
Kambos
Pyrgos
Vissas
Komito
South
B
B'
5 km
West
Finikas
Vissas
East
C
C'
Kambos Unit/ Oceanic Affinities
Upper Marbles
Metavolcanites
Metagabro/Metabasite
Serpentine
Thrust
Kastri Unit
Kastri Marbles
Kastri Schists
Kastri basal fault
Pyrgos Unit
Pyrgos Marbles
Pyrgos schists
Albitic schists/Epidotite Filon
Komito-Vari / Basement
Calcschists/Gneiss
Gneiss

Fig. VII- 9: Cross-sections of Syros Island showing the geometry and relationship between the constitutive units of the island. The AA' and BB' cross-sections show the evolving relationship of the flat and ramp system from north to south: north of the island, a flat contact is observed and the oceanic/kastri units are lying on Pyrgos marbles, the central part of the island presents a ramp-type contact and finally, the southern part of the island shows a flat contact between the oceanic/kastri units and the basement. The E-W CC' cross-section shows the lateral behaviour of the flat and ramp system. (See Annexe E for the cross section at 1:50000).

In addition to the two sets of large normal faults described in the previous section and shown in both the structural map (Fig. VII-8) and cross-sections (Fig. VII-9), some local observations deserve to be added here. In N-S trending strain corridors in Komito, the Agathopes and Azolimnos folds and crenulation of foliation, with N30 trending axes, also indicate a sinistral strike-slip component, such as along the faults trending like the large Finikia fault (Fig. VII-9). This late extensional system developed in response to the mean directions of stretching and shortening trending NNE-SSW and ESE-WNW, respectively (stereo-diagram in Fig. VII-9). The southward direction of displacement along the flat-ramp extensional system is slightly oblique to the principal axis of stretching mentioned above. However, it is likely that this obliquity could simply result from a dextral component of block rotation during these late stages of semi-brittle to brittle deformation (post-metamorphic) recorded in Syros. In particular, this would explain the mean rotation of the stretching lineations observed at the island scale from N30° in the north to E-W in the south.

The Komito-Vari unit is the deepest exposed level of the Syros lithological pile in the core of a broad anticline, as portrayed in sections AA' and BB'. Late E-W trending normal faults affect the anticline in the Vari area but do not change the whole polarity of units as observed in the detailed mapping (Fig. VII-3). Therefore, both the local-scale structural study of Vari and the coherence between the regional-scale cross-sections AA' and BB' confirm the basement position of the Komito-Vari unit (Bonneau 1980a and b). This is contrary to allochtonous-type interpretations that consider the Vari orthogneisses as the hanging wall of a detachment (the so-called Vari detachment) dipping to the NE [Ridley, 1984; Maluski et al., 1987; Gautier, 1995; Trotet et al., 2001a; Ring et al., 2003; Jolivet et al., 2010].

7.5.3. Cross-section restoration

The development of flat-ramp extensional systems is summarised in two steps in Figure VII-10, on the basis of analogue experiments by McClay and Scott [1991] and Roure et al. [1992]. The hanging wall forms a rollover anticline that is not observed in Syros but which should likely occur offshore. Because the rollover is not observed, the total displacement cannot be fully evaluated. Therefore, from the geometry observed in Syros, only a minimum value of the displacement can be estimated.

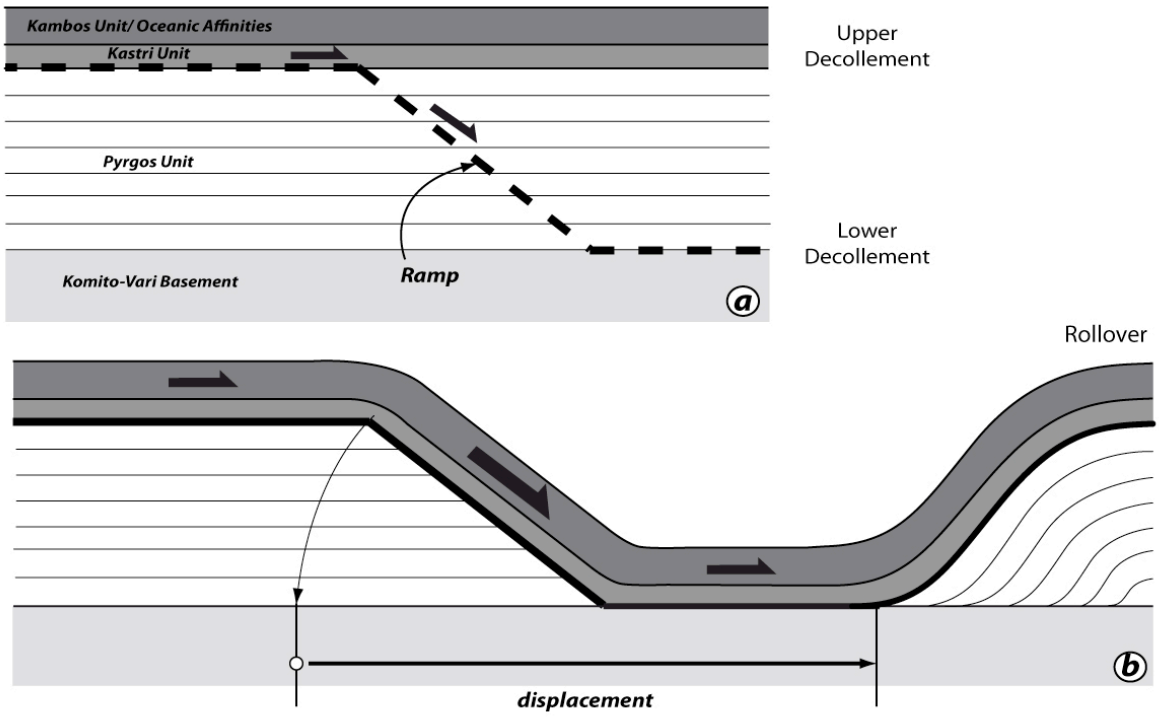

Fig. VII-10: Schematic sketch showing the development of the flat and ramp system from its initiation inside the metamorphic pile (a) to the displacement of the unit along the flat and ramp contact (b).

Figure VII-11 shows a two-step restoration of cross section AA' (Fig. VII-11a). In the first step, displacements along the steeply dipping faults are removed (Fig. VII-11b). The second step consists in i) unfolding the Kini anticline and ii) moving back the most southern extremity of the hanging wall (Kambos and Kastri units) to the upper end of the ramp (Fig. VII-11c). This gives a minimum displacement of approximately 7 km.

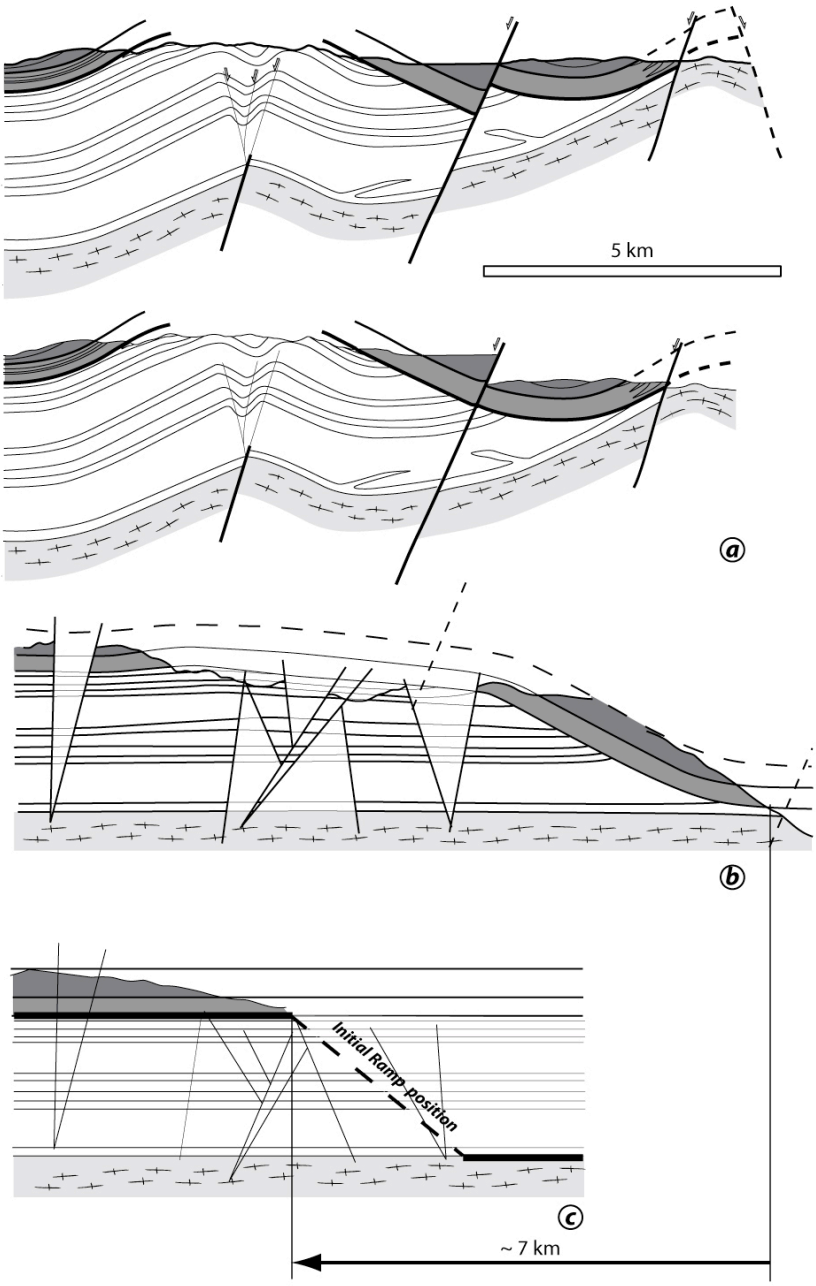

Fig. VII-11: Restoration of cross-section B: a) removing the displacement along the steeply dipping normal faults, b) unfolding and c) annealing the displacement along the ramp. The initial position of the ramp is found by cancelling the space obtained during the unfolding of the Kini anticline.

The restoration illustrates that this detachment system used two décollement layers that are, from top to base: i) the interface between the Kastri and Pyrgos units, suggesting that a weaker layer existed at this level in the sedimentary pile and ii) the interface between the Pyrgos sedimentary unit and the Komito-Vari orthogneissic basement. The two décollements were connected by a southward dipping ramp cross-

cutting the Pygos unit with a restored angle of about 45°. During flat-ramp extension, the unloading of the footwall by 4 km of hanging wall led to a flexuration that brought the movement surface into a flat-lying attitude.

7.6. Discussion-Conclusions

7.6.1. A three-stage tectonic history

The structural analysis presented in this paper shows that the tectonic history of the Syros blueschists unit can be summarised in three major stages.

The first stage corresponds to the thrust emplacement of the Kambos oceanic unit on top of the Kastri unit [Bonneau et al., 1980a and b, Ridley 1982, Keiter et al., 2004]. The oceanic units show evidence of pervasive ductile shear synchronous with prograde high-pressure metamorphism with a top-to-the-south-southwest sense of shear, indicating a southward direction of thrust emplacement. The age of thrusting cannot be directly constrained in Syros as the sediments of the Kastri unit are attributed to the Triassic [Keay 1998]. However, as demonstrated by palaeontological evidence from Evvia [Dubois and Bignot 1979] and Attica [Katsikatsos et al., 1986a,b] the youngest sediments of the CBU are nummulitic flysch, giving a mid-Eocene age for the thrusting [Shaked et al., 2000]. This is in agreement with the 52 Ma age obtained for eclogite facies metamorphism in Syros [Lagos et al., 2007].

The second stage corresponds to a pervasive top-to-the-northeast ductile shear affecting the whole metamorphic pile. However, this second major deformation event, which is synchronous with the metamorphic retrogression from eclogite to greenschist facies [Trotet et al., 2001b], left some volumes of the Kambos oceanic unit almost undeformed, as shown in particular by the undeformed lawsonite pseudomorphs. The same is seen for some marbles, where aragonite pseudomorphs also remained undeformed [Brady et al., 2004]. No major detachment related to this event outcrops in the island.

The third stage corresponds to semi-brittle to brittle deformation. It started with a flat-ramp extension using two décollement levels: i) the interface between the Kastri and Pyrgos sedimentary units and ii) the interface between the Pyrgos sedimentary unit and the underlying Komito-Vari orthogneiss basement. The southward minimum displacement along this late detachment is approximately 7 km. During the late

evolution of this deformation event, two sets of steeply dipping normal faults trending either E-W or sub-meridian indicate the mean directions of stretching and shortening trending NNE-SSW and ESE-WNW, respectively.

Figure VII-12 presents our interpretation of the three-stage Syros evolution at the lithosphere scale within the framework of the Hellenic subduction retreat (cross-sections simplified from Jolivet and Brun [2010]) and refers to the PT path of Schumacher et al. [2008]. Stage 1 shows the thrusting of the oceanic unit on top of the subducting Adria passive margin in the mid-Eocene. During stage 2, the upper plate of the subduction is submitted to core complex-type extension (Southern Rhodope Core Complex; Brun and Sokoutis, [2007]) and the Adria crust that is decoupled from thesubducting lithospheric mantle [Brun and Faccenna, 2008] is exhumed up to the mid-lower crustal level. The CBU exhumation that started soon after stage 1 is accommodated by trench retreat. Stage 3 is dominated by core complex-type extension in the central Cyclades (Naxos-Paros-Mykonos) which is controlled by 1) the North Cycladic Detachment [Jolivet et al., 2010] and 2) distributed normal faulting at the regional scale. During this stage, Syros underwent southward flat-ramp extension, giving a detachment internal to the CBU, followed by steeply dipping normal faulting.

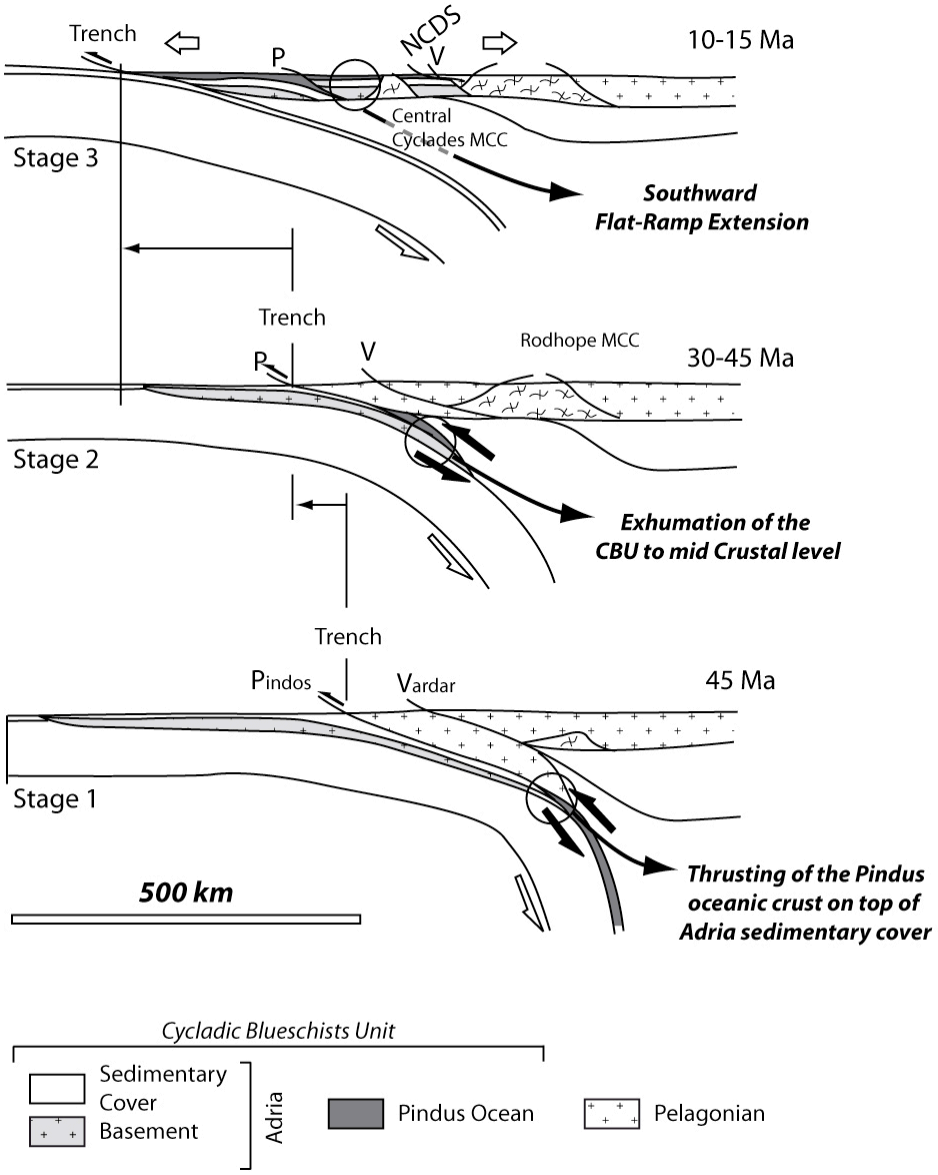
Trench
P
NCDS
V
10-15 Ma
Central
Cyclades MCC
Stage 3
Southward
Flat-Ramp Extension
Trench
P
V
Rodhope MCC
30-45 Ma
Stage 2
Exhumation of the
CBU to mid Crustal level
Trench
Pindos
Vardar
45 Ma
Stage 1
500 km
Thrusting of the Pindus
oceanic crust on top of
Adria sedimentary cover
Cycladic Blueschists Unit
Sedimentary
Cover
Basement
Adria
Pindus Ocean
Pelagonian

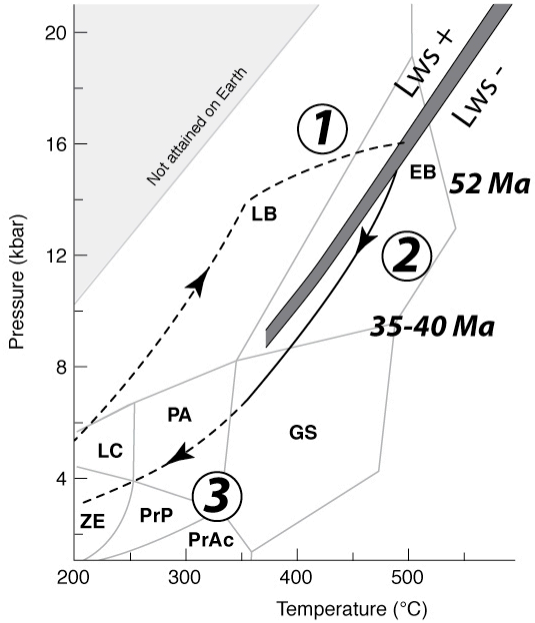
Pressure (kbar)
Temperature (°C)
Not attained on Earth
LWS +
LWS -
1
2
3
52 Ma
35-40 Ma
EB
LB
PA
GS
LC
ZE
PrP
PrAc

Fig. VII-12: PT path of Syros blueschists from Schumacher et al. [2008; Fig. 12]. The three cross-sections show the tectonic history of the Syros blueschists. From 1) burial to Lws-Blueschists facies accompanied by a top-to-the-S sense of shear, 2) Exhumation along the inverted suture with a top-to-the-N sense of shear, and finally 3) a N-S back arc Aegean extension.

7.6.2. Structural record of subduction in the Cyclades

This study shows that the occurrence of lawsonite pseudomorphs is an extremely useful tool to identify deformations related to prograde metamorphism and therefore attributable to subduction. Senses of shear prior to lawsonite destabilisation are top-to-the-S-SW. It is not unlikely that similar senses of shear described at many different places in the Cyclades could also be related to subduction. In particular, the SW directed shear observed in the southern Cyclades could be re-examined in this way (Serifos, Kea and Kythnos: Iglseder et al., [2009]; Kythnos: our own observations). Interestingly, the top-to-the-southwest shearing in Ios is interpreted as related to either a SW-dipping extensional detachment [Foster and Lister 2009] or to thrusting toward the SW [Huet et al., 2009].

7.6.3. No syn-metamorphic detachment in Syros

Ridley [1984; Fig. 6] interpreted the Vari orthogneiss as the "roof of the convergence zone in which the blueschist metamorphism took place" and later put on top of the CBU by a low angle normal fault. Since Maluski et al. [1987] obtained a Cretaceous age for the Vari unit, it has been described as a klippe of the upper Pelagonian block lying on top of the CBU. Consequently, and as initially suggested by Ridley [1984], a detachment is supposed to separate the orthogneisses from the underlying CBU (Gautier [1995], Fig. 2.8, p. 293;), the so-called Vari detachment [Trotet et al., 2001a, Ring et al., 2003], and is considered to locally represent the North Cycladic Detachment System [Jolivet et al., 2010].

Three lines of argument show that the hypothesis of the so-called Vari detachment cannot be maintained and confirm the basement interpretation of Bonneau et al. [1980 a and b], Tomaschek and Ballhaus [1999] and Tomaschek et al., [2008]. First,

not a single field evidence has been found in favour of a shallow dipping detachment separating the Pyrgos and Vari units. Second, detailed mapping of the Vari shows that the Vari unit appears as an anticline seated below the Pyrgos unit, in agreement with Bonneau et al. [1980 a and b], Tomaschek and Ballhaus [1999] and Tomaschek et al. [2008]. Third, the construction of two cross-sections passing through Komito to the west and Vari to the east, separated by a distance of more than 5 km, both display the same cover-basement relationship. This last evidence is responsible for the use of the term Komito-Vari unit.

7.6.4. Top-to-the-northeast shearing

As the Vari detachment cannot be maintained, the tectonic significance of shearing top-to-the-northeast must be reconsidered.

It is noteworthy that the bedding-parallel foliation bears two opposite and non-synchronous shear indicators. Shear top-to-the-south-southwest is prograde while shear top-to-the-north-northeast is retrograde. Thus, the foliation that was created during top-to-the-south-southwest shear was reactivated by a top-to-the-north-northeast shear during metamorphic retrogression in the less competent lithologies. This suggests that shearing related to both subduction and exhumation was controlled by the same mechanical boundary, namely the Pindus suture zone. At the regional scale, the Pindus suture zone, which separates the CBU from the Pelagonian block, trends NNE-SSW and is cut at a right angle by the North Cycladic Detachment System? (Fig. VII-1). This suggests that exhumation accommodated by top-to-the-northeast shearing corresponds to the reactivation of the Pindus Suture Zone prior to the development of the North Cycladic Detachment.

7.6.5. Opposite senses of shear

The existence of opposite senses of shear in the CBU, which has been identified a long time ago (e.g. Gautier and Brun, [1994a and b]), is interpreted in various ways.

In Syros, as well as in other Cyclades islands, they are considered to develop synchronously either i) resulting from convergent ductile flow from below the opposite limbs of a core complex [Gautier and Brun, 1994a and b, Jolivet and Patriat, 1999; Tirel

et al., 2009] or ii) as conjugate shear zones in a coaxial deformation [Rosenbaum et al., 2002 and Bond et al., 2007]. On the basis of these observations, Bond et al. [2007] concluded that "it is "symmetrical" pure-shear-dominated configuration [Malavieille 1993; Fig. 16a] that provides a better description of the crustal-scale deformation". The evidence in Syros for top-to-the-S-SW shear related to thrusting of the oceanic unit on top the sediments of the Adria margin prior to top-to-the-northeast shear related to exhumation suggests that the synchronism of shear indicators development must be checked carefully. Co-axial deformation giving rise to conjugate shear bands can develop on a small scale if, in particular, viscosity contrasts between layers favour strain partitioning. Indeed some good examples of this exist in Syros. However, transposing this type of kinematic pattern to the crustal-scale (e.g. at the whole Cyclades scale) would also require a careful check of the synchronism of shearing events at the regional scale.

At the scale of the whole Cyclades Islands, opposite senses of shear, top-to-the-southwest to the south and top-to-the-northeast to the north, were recently interpreted as being synchronous and reflecting both downward (subduction) and upward (exhumation) ductile flow within a NE-dipping subduction channel [Huet et al., 2009; Jolivet et al., 2009]. Here again the synchronism of shear indicators development must be checked carefully but, in addition, it would be necessary to show that top to S-SW shear is located in the lower part of the CBU and top to NE in the upper part. This is not in agreement with the fact that in Syros, to the north as well as in the south Cyclades islands, the part of the CBU that is observed corresponds to the base of the sedimentary cover lying on top of the Adria basement.

7.6.6. Flat & Ramp extension

During flat-ramp extension in Syros, the footwall unloading by the removal of 4 km of hanging wall led to a flexuration that brought the movement surface into a flat-lying attitude. It is noteworthy that if the flat-ramp origin of the extensional system is not noticed, it could lead to the conclusion that the detachment was originally dipping at a low angle. In our opinion and experience, this more likely applies to other so-called low angle detachments in the Cyclades realm. A second important inference is the fact

that such detachments are post-metamorphic. Of course, they may significantly contribute to the whole exhumation process of metamorphic rocks but as they develop in the semi-brittle to brittle crust, they are not directly related with the metamorphic history proper. In addition, the southward sense of displacement is opposite to the top-to-the-northeast ductile sense of shear associated with the retrogressive metamorphism. Therefore, using the top-to-the- south sense of shear as an indicator of the dominant kinematic of metamorphic rock exhumation would be misleading. This upper crust low-angle faulting is only a late feature of Aegean extension. As they likely occur at other places in the Cyclades their identification is necessary to avoid wrong conclusions concerning the history of blueschists exhumation.

Acknowledgements

The present work was financially supported by the ANR-EGEO project. We are extremely grateful to L. Jolivet for having introduced us to Syros geology and for the field trip that he organised especially for us in Tinos and Mykonos. Great thanks are due to A. Eude and L. Tual, who helped with the structural mapping. Discussions at various stages of the project with L. Jolivet, P. Agard, B. Huet, and L. Labrousse, in particular within the framework of the ANR-EGEO project, have been very useful and stimulating. However, the data and interpretations presented here are our entire our own.

References

Altherr, R., Kreuzer, H., Wendt, I., Lenz, H., Wagner G.A., Keller, J., Harre W. and Höhndorf A (1982), A late Oligocene/Miocene high temperature belt in the Attic-Cycladic crystalline complex (SE Pelagonian, Greece). Geol. Jb. E23, 67-164.

Ballhaus, C., Tomaschek, F., Keay, S (1999), Stratigraphy and Age Relations on the Island of Syros, Cyclades. Journal of Conference Abstracts 4 (1), 72.

Bond, C., Bulter, R.W.H. and Dixon J.E. (2007), Co-axial horizontal stretching within extending orogens: the exhumation of HP rocks on Syros (Cyclades) revisited. Geological Society of London, Special publication, 272, 203-222. doi: 10.1144/GSL.SP.2007.272.01.12

Bonneau, M.B., C., Gueyssant, J., Kienast, J.R., Lepvrier, C., Maluski, H., Papanikolaou, D. (1980a), Sur la signification des séries métamorphiques (schistes bleus) des cyclades (Héllènides, Grèce). L'exemple de l'île de Syros. Comptes rendus de l'académie des sciences Paris 290, 1463-146..

Bonneau, M.B., Gueyssant, J., Kienast, J.R., Lepvrier, C., Maluski, H. (1980b), Tectonique et métamorphisme Haute pression d'âge Eocène dans les Hellénides : exemple de l'île de Syros (Cyclades, Grèce). Comptes rendus de l'académie des sciences Paris 291, 171-174.

Bonneau, M.B. and Kienast, J.R. (1982), Subduction, collision et schists bleu: exemple de l'Egée, Grèce. Bulletin de la société Géologique de France 7, 785-791.

Brady, J. B., Markley, M. J., Schumacher, J. C., Cheney, J. T. & Bianciardi, G. A. (2004), Aragonite pseudomorphs in high-pressure marbles of Syros, Greece. Journal of Structural Geology 26 (1), 3-9. doi:10.1016/S0191-8141(03)00099-3

Bröcker, M. & Enders, M. (1999), U-Pb zircon geochronology of unusual eclogite-facies rocks from Syros and Tinos (Cyclades, Greece). Geological Magazine 136, 111-118.

Brun, J.P. and Faccenna, C. (2008), Exhumation of high-pressure rocks driven by slab rollback. Earth and Planetary Science Letters 272, 1–7. doi:10.1016/j.epsl.2008.02.038

Brun, J.P. and Sokoutis, D. (2007), Kinematics of the Southern Rhodope Core Complex (North Greece). International Journal of Earth Sciences 96 (6), 1079-1099. doi:10.1007/s00531-007-0174-2

Bulle,F., Bröcker M., Gärtner C., Keasling, A. (2010), Geochemistry and geochronology of HP mélanges from Tinos and Andros, Cycladic blueschist belt, Greece. Lithos 117 (1-4), 61-81. doi:10.1016/j.lithos.2010.02.004

Dixon, J. E. & Ridley, J., (1987), Syros (field trip excursion). In: Chemical transport in metasomatic processes (ed Helgeson, H. C.) Nato Advanced Study Institutes Series. Series C, pp. 489-500, D. Reidel Publishing Company, Dordrecht.

Dubois, R. and Bignot, G. (1979), Presence d'un "hardground" nummulitique au de la serie crétacée d'Almyropotamos (Eubee meridionale, Grece). Paris, Academie des Sciences Comptes Rendus 289, 993–5.

Forster M.A. and G.S. Lister (2009), Core complex related extension of the Aegean lithosphere initiated at the Eocene-Oligocene transition. Journal of Geophysical Research (Solid Earth), 114, B02401, 36 PP. doi:10.1029/2007JB005382.

Gautier, P., Brun, J.P. , Jolivet, L. (1993), Structure and kinematics of Upper Cenoizoic extensional detachment on Naxos and Paros (Cyclades Islands, Greece). Tectonics 12, 1180-1194.

Gautier, P., and J. P. Brun. (1994 b), Ductile crust exhumation and extensional detachments in the central Aegean (Cyclades and Evvia islands). Geodinamica Acta 7, 57 – 85.

Gautier, P. (1995), Géométrie crustale et cinématique de l'extension tardi-orogénique dans le domaine centre-égéen. Ïles des Cyclades et D'eubée (Grèce). PhD Thesis. Mémoire de Géosciences Rennes 61, 417 pp. ISBN 2-905532-60-2

Gitahi, N. (2004), Geochemistry and metamorphic evolution of éclogites on Syros island, Greece. Extended Abstracts, Seventeenth Annual Keck Research Symposium in Geology Proceedings, Lexington, VA, P.81-4.

Hecht, J. (1984), Geological map of Greece 1:50 000, Syros island. Athens: Institute of Geology and Mineral Exploration.

Holley, E. A., Ross, T. & Cheney, J. T. (2004), Pressure-température conditions of metamorphism in eclogites, Syros, Greece. Geological Society of America, Abstracts with Programs 36 (4), 91.

Huet, B., Labrousse, L., Jolivet, L. (2009), Thrust or detachment? Exhumation processes in the Aegean: Insight from a field study on Ios (Cyclades, Greece). Tectonics 28, TC3007. doi:10.1029/2008TC002397

Iglseder, C., B. Grasemann, D. A. Schneider, K. Petrakakis, C. Miller, U. S. Klötzli, M. Thöni, A. Zàmolyi, and C. Ramboussek. (2009), I and S-type plutonism on Serifos (W-Cyclades, Greece), Tectonophysics, doi:10.1016/j.tecto.2008.09.021

Jolivet L., and Patriat. M. (1999), Ductile extension and the formation of the Aegean Sea. Geological Society, London, Special Publications 156, 427-456. doi: 10.1144/GSL.SP.1999.156.01.20

Jolivet L. and Brun J.P. (2008), Cenozoic geodynamic evolution of the Aegean. International Journal of Earth Sciences 99 (1), 109-138. doi:10.1007/s00531-008-0366-4

Jolivet, L., Trotet, F., Monié,P., Vidal, O., Goffé, B., Labrousse,L., Agard, P. and Ghorbal B. (2009), Along-strike variations of P–T conditions in accretionary wedges and syn-orogenic extension, the HP–LT Phyllite–Quartzite Nappe in Crete and the Peloponnese. Tectonophysics 480 (1-4), 133-148. doi:10.1016/j.tecto.2009.10.002

Jolivet, L., Lecomte, E., Huet, B., Denèle, Y., Lacombe, O., Labrousse, L., Le Pourhiet, L., Mehl, C. (2010), The North Cycladic Detachment System. Earth and planetary Science Letters. 289, 87–104. doi:10.1016/j.epsl.2009.10.032

Katsikatsos, G., Migiros, G., Triantafillis, M., Mettos, A., (1986a), Geological structure of Internal Hellenides (E. Thessaly — SW Macedonia, Euboa–Attica–Northern Cyclades Islands and Lesvos). Geological and Geophysical Research, Special Issue 191–212.

Katsikatsos, G., Dounas, A., Gaitanakis, P., (1986b), Geological Map of Greece, Athinai–Elefsis Sheet 1.50.000, I.G.M.E., Athens.

Keay, S., (1998), The geological evolution of the Cyclades, Greece: constraints from SHRIMP U–Pb geochronology. Ph.D. thesis, Australian National University, Canberra, pp. 335.

Keiter, M., Piepjohn, K., Ballhaus, C., Lagos, M. and Bode M. (2004), Structural development of high-pressure metamorphic rocks on Syros Island (Cyclades, Greece). Journal of Structural Geology 26 (8), 1433-1445. doi:10.1016/j.jsg.2003.11.027

Lagos, M., Scherer, E.E., Tomaschel, F., Münker, C., Keiter, M., Berndt, J., Ballhaus, C. (2007), High précision Lu-Hf geochronology of Eocene éclogite facies rocks from Syros, Cyclades, Greece. Chemical geology 243 (1-2), 16-35. doi:10.1016/j.chemgeo.2007.04.008

Lister, G. S., Banga, G. and A. Feenstra, A. (1984), Metamorphic core complexes of cordilleran type in the Cyclades, Aegean Sea, Greece. Geology., 12, 221-225. doi:10.1130/0091-7613(1984)12<221:MCCOCT>2.0.CO,2

Malavieille J. (1993), Late orogenic extension in Mountain belts : Insights from the Basin and Range and the Late Paleozoic Variscan belt. Tectonics 12, 1115-1130.

Maluski, H., Bonneau, M., Kienast, J.R. (1987), Dating the metamorphic events in the Cycladic area: 40Ar/39Ar data from metamorphic rocks of the island of Syros (Greece), Bulletin de la Société géologique de France III, 833-841.

McClay and Scott. (1991), Experimental models of hangingwall deformation in ramp-flat listric extensional fault systems. Tectonophysics 188 (1-2), Pages 85-96. doi:10.1016/0040-1951(91)90316-K

Okrusch, M. & Bröcker, M. (1990), Eclogites associated with high grade blueschists in the Cyclades archipelago, Greece: a review. European Journal of Mineralogy 2, 451-478.

Pe-Piper, G., and Piper, D. J. W. (2007),. Neogene back-arc volcanism of the Aegean: new insights into the relationship between magmatism and tectonics. in Cenozoic Volcanism in the Mediterranean Area, edited by L. Beccaluva and G. Bianchini, Geological Society of America, pp. 17–31. doi: 10.1130/2007.2418(1102)

Philippon, M., Brun, J.P., Gueydan, F. (2009), Kinematic records of subduction and exhumation in the Ile de Groix Blueschist (Hercynian belt, Western france). Journal of structural geology 31 (11), 1308-1321. doi: 10.1016/j.jsg2009.07.003.

Pohl, J. (1999), Geologie und Hochdruckgesteine der Insel Syros, Griechenland. Diploma thesis, Geologisches Institut, Albert-Ludwigs Universitat, Freiburg, 107 pp.

Putlitz, B., Cosca, M. A. & Schumacher, J. C. (2005), Prograde mica 40Ar/39Ar growth ages recorded in high pressure rocks (Syros, Cyclades, Greece). Chemical Geology 214 (1-2), 79-98. doi:10.1016/j.chemgeo.2004.08.056

Ridley, J. (1982), Arcuate lineation trends in a deep level, ductile thrust belt, syros, Greece. Tectonophysics, 88, 3-4, 347-360. doi:10.1016/0040-1951(82)90246-3

Ridley, J. (1984), Listric normal faulting and the reconstruction of the synmetamorphic structural pile of the Cyclades. Geological society of London, special publication 17, 755-761.

Ring, U., Thomson, S.N., Bröcker, M. (2003), Fast extension but little exhumation : the Vari detachment in the Cyclades, Greece. Geological magazine, 140, (3), p 245-252. DOI: 10.1017/S0016756803007799.

Rosenbaum, G., Avigad D. and Sánchez-Gómez, M. (2002), Coaxial flattening at deep levels of orogenic belts: evidence from blueschists and eclogites on Syros and Sifnos (Cyclades, Greece), Journal of Structural Geology 24 (9), 1457-1462. doi:10.1016/S0191-8141(01)00143-2

Roure F., Brun J-P., Colletta B., and Van Den Driessche. (1992), Geometry and kinematics of extensional structures in the Alpine Foreland Basin of Southeastern France. Journal of Structural Geology, 14 (5), 503-519. doi:10.1016/0191-8141(92)90153-N

Schumacher, J.C.B., Brady, J., Cheney, J.T., Tonnsen R.R. (2008), Glaucophane bearing Marbles on Syros, Greece, Journal of Petrology 49 (9), 1667-1686. doi:10.1093/petrology/egn042

Shaked, Y. Avigad D. and Garfunkel Z. (2000), Alpine high-pressure metamorphism at the Almyropotamos window (southern Evia, Greece). Geological Magazine 137 (4), 367–380.

Tirel, C., Gautier, P., van Hinsbergen, D. J. J., and Wortel M. J. R. (2009), Sequential development of interfering metamorphic core complexes: numerical experiments and comparison with the Cyclades, Greece. Geological Society, London, Special Publications, 311, 257-292. doi: 10.1144/SP311.10

Tomaschek, F. & Ballhaus, C. (1999), TheVari Unit on Syros (Aegean Sea) and its relation to the Attic-Cycladic Crystalline Complex. Journal of Conference Abstracts 4, 72.

Tomaschek, F., Kennedy, A. K.,Villa, I.M., Lagos,M. & Ballhaus, C. (2003), Zircons from Syros, Cyclades, Greece Recrystallization and mobilization of zircon during high-pressure metamorphism. Journal of Petrology 44 (11), 1977-2002. doi: 10.1093/petrology/egg067

Tomaschek, F., Keiter, M., Kennedy, A.K. and Ballhaus, C. (2008), Pre-Alpine basement within the Northern Cycladic Blueschist Unit on Syros Island, Greece. - Zt. dt. Ges. Geowiss. 159/3, 11 pp. doi: 10.1127/1860-1804/2008/0159-0000

Trotet, F., Jolivet, L. and Vidal, O. (2001a),. Tectono-metamorphic evolution of Syros and Sifnos islands (Cyclades, Greece), Tectonophysics 338 (2), 179-206. doi:10.1016/S0040-1951(01)00138-X

Trotet, F., Vidal, O., Jolivet, L. (2001b), Exhumation of Syros and Sifnos metamorphic rocks (Cyclades, Greece). New constraints on the P-T paths. European Journal of Mineralogy Volume 13 (5), p. 901 – 920. doi: 10.1127/0935-1221/2001/0013/0901

Wijbrans, J.R., Schliestedt, M., York, D. (1990), Single grain argon laser probe dating of phengites from the blueschist to greenschist transition on Sifnos (Cyclades, Greece). Contribution to mineralogy and petrology 104, 582-593.

Partie 3/ Un nouveau modèle d'évolution tectonique pour les schistes bleus cycladiques.

Chapitre 8 : Enregistrement de la subduction et de l'exhumation dans les schistes bleus cycladiques (Mer Egée, Grèce).

RECORD OF SUBDUCTION AND EXHUMATION IN THE CYCLADIC BLUESCHISTS (CENTRAL AEGEAN, GREECE)

Melody Philippon, Jean-Pierre Brun and Frédéric Gueydan
Géosciences Rennes, UMR 6118. Université de Rennes 1.

To be submitted to Tectonophysics

Abstract

The Cycladic Blueschist Unit represents the northern passive margin of the Adria continental block plus some ophiolitic melange remnants representing the Pindos ocean that have been affected by a high pressure-low temperature metamorphism in the blueschist and eclogite facies, in Eocene. Prior to Lutetian, ophiolitic and margin units underwent thrusting toward the SW inside a NE-dipping subduction. Two stages of exhumation are characterized by top to NE senses of shear: i) from mantle depths to lower crustal levels before 37 Ma that was accommodated by an extensional inversion of the Vardar suture zone and ii) from deep crustal levels to near surface between 30 and 20 Ma that was accommodated by the North Cycladic Detachment. It is during this stage that the Central Cyclades Core Complex exhumed. Segmentation of the CBU by normal faults started at 12 Ma coeval with block rotation around a vertical axis and folding with NS-trending axes that were dominantly controlled by the Myrthes-Ikaria strike-slip fault in the centre of the Cyclades.

Key Words: Subduction, Exhumation, Back arc extension, Rollback.

8.1. Introduction

Since three decades the Cycladic blueschists of central Aegean became a natural laboratory for studying the exhumation processes of high-pressure metamorphic rocks. Aegean back-arc extension is controlled by a 700 km retreat of the Hellenic subduction toward the southwest since 45 Ma (Jolivet and Brun, 2010). During this process, a succession of oceanic domains and continental blocks have been subducted in the following order: Vardar ocean, Pelagonian continental block, Pindos ocean, Adria continental block and, finally, the Mediterranean oceanic lithosphere that is still subducting. In this frame, a single subducting slab, well imaged by seismic tomography

(Wortel and Spakman, 2000), whereas two oceanic suture zones, Vardar and Pindos, occur at surface. The Pelagonia and Adria continental blocks were subducted and soon after exhumed bringing high pressure rocks back to surface. This suggests that exhumation of high-pressure rocks is driven by the subduction of small continental blocks during the slab rollback of a single and continuous subduction (Brun and Faccenna, 2008).

The Cycladic Blueschist Unit (CBU) represents the northern passive margin of the Adria continental block plus some ophiolitic melange remnants representing the Pindos ocean that have been affected by a high pressure-low temperature metamorphism in the blueschist and eclogite facies, in Eocene (Bonneau and Kienast, 1982). Since 20 years, it has been argued that large parts of the CBU were affected by conjugate senses of shear top to NE and SW within core complexes (Gautier and Brun, 1994a and b). Evidence of thrusting up to middle Eocene and of early exhumation starting in middle-late Eocene lead to the conception of syn-orogenic exhumation (Avigad et al., 1997) and to the further development of the "subduction channel" concept (Jolivet et al., 2003).

The present study aims at establishing the relative timing and kinematics of subduction and exhumation-related deformations at the whole Cyclades scale. To match this goal, we attempt i) to restore the initial geometry of the CBU prior to the segmentation that affected the region since middle Miocene and 2) to identify the different processes that have contributed to the CBU exhumation.

8.2. The Cycladic Blueschists Unit

The Cycladic Blueschists Unit (CBU) dominantly outcrops in the Cyclades islands, in central Aegean Sea, but also in the Attica peninsula and in the Olympus and Ossa mountains in Greece mainland (Fig. VIII-1). Toward the NE, the CBU is cut by the North Cycladic Detachment System (Jolivet et al., 2010). Toward the NW, the Pelagonian unit is thrust on top of the CBU (Shaked et al., 2000). The occurrence of ophiolite remnants located below the thrust contact in Attica indicates that the top of the CBU is the Pindos ocean suture zone. This SW-NE trending contact continues in Evvia where it is cut but the North Cycladic detachment (Fig. VIII-1).

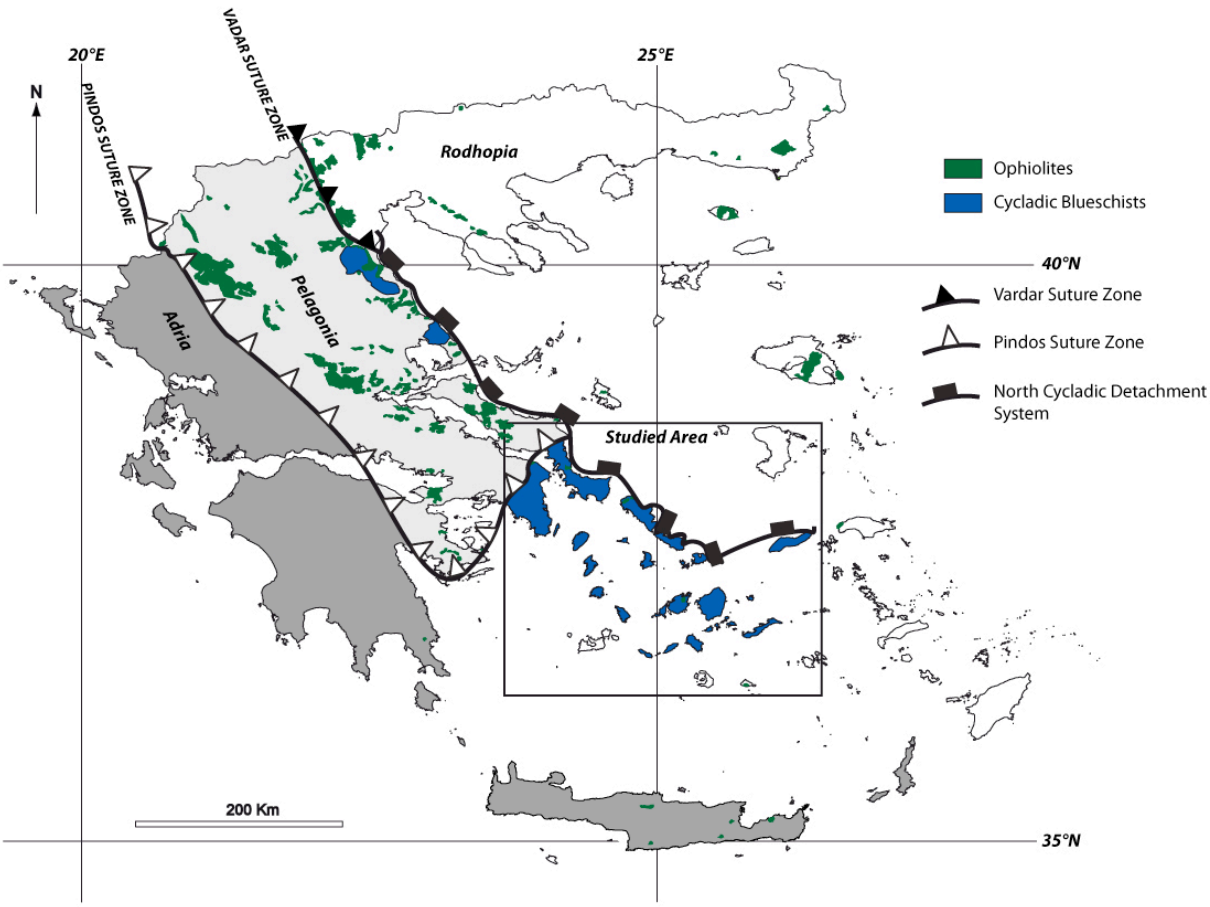

Fig. VIII-1 Regional map of Greece mainland and Aegean Sea showing the main tectonic contacts (Vardar and Pindos suture zones and North Cycladic Detachment) and the main continental blocks (Rhodopia, Pelagonia and Adria)

This regional-scale setting of the CBU shows that it corresponds to the sedimentary cover and basement units of the Adria continental block that is seated below the Pelagonian continental block (Fig. VIII-1). The presence of remnants of ophiolitic melange at many places in the Cyclades indicates that oceanic units of the Pindos ocean were the northward prolongation of the Adria passive margin (Bonneau, 1984).

8.2.1 Lithology

The CBU is constituted from base to top by three main components (Fig. VIII-2):
(1) The Hercynian basement dominantly consists of orthogneisses whose protolith has been dated in several islands by U/Pb SHRIMP on magmatic zircons : Delos : 327±4 to 295 ±4 Ma ; Paros : 325±4 to 302±2 Ma ; Antiparos : 308±3 to 292±1 Ma ; Ios : 311±2 to

302±3 Ma ; Sikinos : 325±4 to 301±2 Ma (Engels and Reischmann, 1999; Tomaschek and Ballhaus, 1999; Tomaschek et al., 2001) (Fig. VIII-3).

(2) The sedimentary cover lying on top of the basement corresponds to marbles and schist sequences whose depositional ages range from Visean to Eocene (REFS, Pohl 1999; Dubois and Bignot, 1978; Dürr et al., 1979) (Fig. VIII-3).

(3) On top of the sedimentary cover, an ophiolitic mélange mainly consist of serpentine schists with knockers of metagabbros and metabasalts of Triassic to Cretaceous ages (Lagos et al., 2007; Bulle et al., 2010) that represent relicts of the Pindos Ocean (Bonneau and Kienast, 1982). (Fig. VIII-3). Rift-related plutonic intrusions with similar ages emplaced in the Hercynian basement of several Cyclades islands. The largest pieces of the ophiolitic mélange outcrop in Evvia (western Cyclades)(Shaked et al., 2000), Syros (central Cyclades) and Ikaria (eastern Cyclades) but small klippes can also be observed in Tinos, Sifnos, Serifos, Amorgos and Attica (Fig. VIII-2).

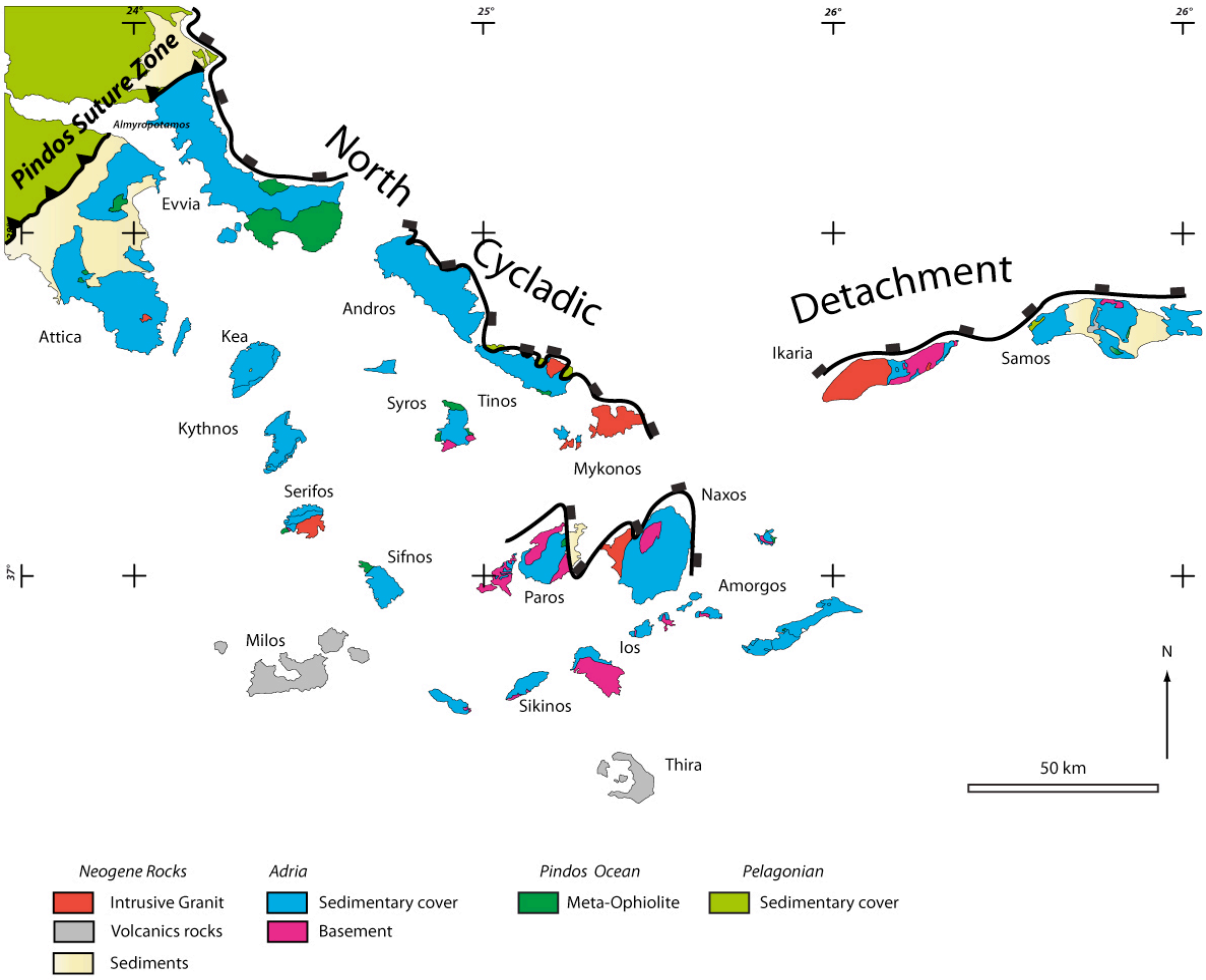

Fig. VIII-2. Simplified geological map of the Cycladic Blueschists Unit

As a whole, the basement widely outcrops in the southern Cyclades whereas sediments and oceanic rocks mainly outcrop in the north of the archipelago.

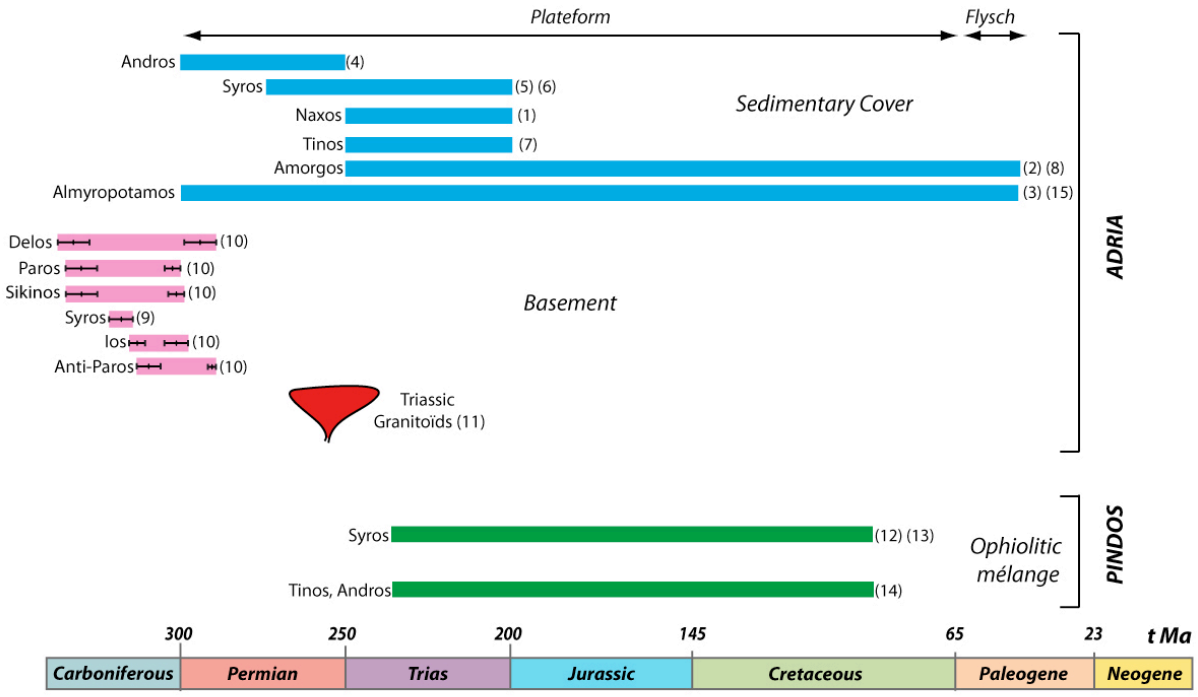

Fig. VIII-3. Ages of the main geological formations of the Cycladic Blueschist Unit. Numbers refer to source references (see Tab. 1).

		Location	Age	Reference	N° in Fig. 3
Adria	Sedimentary Cover	Naxos	Trias	Dürr et al., 1978	1
		Amorgos	Triassic to Eocène	Dürr 1985	2
		Amorgos	Middle Eocene	Dürr 1985	2
		Almyropotamos	Permian to Middle Eocene	Dubois and Bignot 1979 Katsikastos et al., 1986 b	3 and 15
		Andros	Permian	Papanikolaou 1978	4
		Syros	Viseen to Middle Trias	Pohl 1999, Keay 1998	5, 6
		Tinos (Panormos)	Trias	Avigad and Garfunkel 1989	7
		Amorgos Fysch (Top of the)	Eocene	Fytrolakis et al., 81	8
	Basement	Syros	240±3 Ma	Tomaschek et al., 2001	9
		Delos	295±4 to 327±4 Ma	Engels and Reischmann 1999	10
		Paros	302±2 to 325±4	Engels and Reischmann 1999	10
		Sikinos	301±2 to 325±4 Ma	Engels and Reischmann 1999	10
		Ios	302±3 to 311±2 Ma	Engels and Reischmann 1999	10
		Anti-Paros	292±1 to 308±3 Ma	Engels and Reischmann 1999	10
Granitoïds		Syros	Trias	Tomaschek et al .,2001	11
Pindos	Ophiolitic Melange	Syros	Trias to Cretaceous	Tomaschek et al., 2003 and Brocker and Keasling 2006	12, 13
		Tinos	Trias to Cretaceous	Bulle et al., 2010	14
		Andros	Trias to Cretaceous	Bulle et al., 2010	14

Table VIII-1: Ages of deposit or crystallization for sediments and magmatic rocks respectively, associated references for the data in the figure VIII-3

8.2.2 High pressure metamorphism

The whole CBU pile from basement to oceanic-type rocks underwent HP metamorphism with pressure/temperature (PT) conditions ranging between 6 and 22 Kbar and 350 to 650 °C (see references in Tab.2). Maximal recorded PT conditions reach 18 kbar/525°C in the basement and sedimentary cover and 22Kbar/650°C in the oceanic-type rocks (Fig. VIII-4). The overall dispersion of PT peaks could reflect i) variations in maximum depth attained by rocks as well as ii) differences in analytical methods used for different rock types and mineralogical assemblages. However, the significant difference in the maximum observed pressure ranges in oceanic-type rocks (8-22 Kbar) and in sedimentary cover and basement (6-18 Kbar) likely indicates that oceanic-type rocks have been subducted at deeper levels than the basement and sedimentary cover.

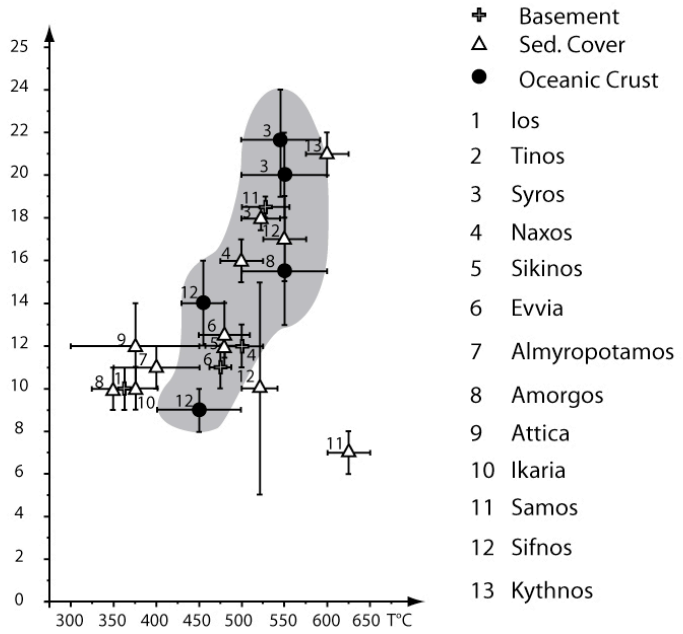

Fig. VIII-4. Diagram showing the maximum pressure and temperature conditions reached by the different lithological units of the CBU. Numbers refer to source references (see Tab. 2)

	Location	PT Peak estimation P(Kbar)	PT Peak estimation T(°C)	Method	Reference	N° in Fig. 4
Basement	Ios	9 to 11	350 to 400	Thermobarometry	Van der Maar and Jansen 1983	1
	Syros	12	550	Thermobarometry	Tomashek and Ballhaus 1999	3
	Samos	18 to 19	530		Will et al., 98	11
	Samos	18-19	510 to 530	Thermocalc	Ring et al., 2007	11
Sedimentary Cover	Tinos	17,5 to 18,5		TWEEQ	Parra et al., 2002	2
	Syros	17	500	TWEEQ	Trotet et al., 2001b; Schumacher et al., 2008	3
	Naxos	12	470		Avigad 1998	4
	Sikinos	11	475	Thermocalc	Gupta and Bickle 2004	5
	Evvia	10 to 12	350 to 450	Thermocalc	Shaked et al., 2000	6
	Almyropotamos	10	350	Thermocalc	Shaked et al., 2000	7
	Amorgos	10 to 14	300-450	PerPlex	Rosenbaum and Ring 2007	8
	Sikinos	11 to 14	460-500		Gupta and Bickle 2004	7
	Attica (corellation with Almyropotamos)	9 to 11	370		Baziotis 2008	9
	Ikaria	6 to 8	600 to 650	Thermocalc	Ring 2007	10
	Ikaria (corellation with Samos)	15	500		Ring 2007	10
	Samos (correllationwith Almyropotamos	8 to 10	350 to 400	Thermocalc	Ring et al., 2007	11
	Samos	5 to 15	500 to 540	Thermocalc	Ring et al., 2007	11
	Sifnos	17	550	Thermocalc	Schmadicke and Will 2003	12
	Kythnos	21	600	Teriak	Kostopoulos (2010 Pers. Com.)	13
	Sifnos	5	425	Stable isotope	Matthews and Schliestedt 84	12
Ophiolite	Syros	19-24	500-580	Geothermobarometrie/ Ravna and Terry (2004)	Gitahy 2004, Holley et al .,2004	3
	Amorgos	13 to 18	500-600	PerPlex	Rosenbaum and Ring 2007	8
	Samos	8 to 12	400 to 500	Thermocalc	Ring et al., 2007	11
	Sifnos	12 to 16	455	Stable isotope	Matthews and Schliestedt 84	12
	Sifnos	20	500-600	Thermocalc	Schmadicke and Will 2003	12

Table VIII-2: References concerning the PT estimation of the different lithologies of the CBU shown in figure VIII-4.

The significance of maximum pressure ranges in the two of rock types will be discussed in a further section. The ranges of metamorphism ages observed at regional-scale (Fig. VIII-5) indicate that the CBU underwent i) a metamorphism from eclogite to blueschist facies during Early Eocene (55-35 Ma) and ii) a greenschist-facies retrogression in Oligocene (35-20 Ma) (see references in Tab.3).

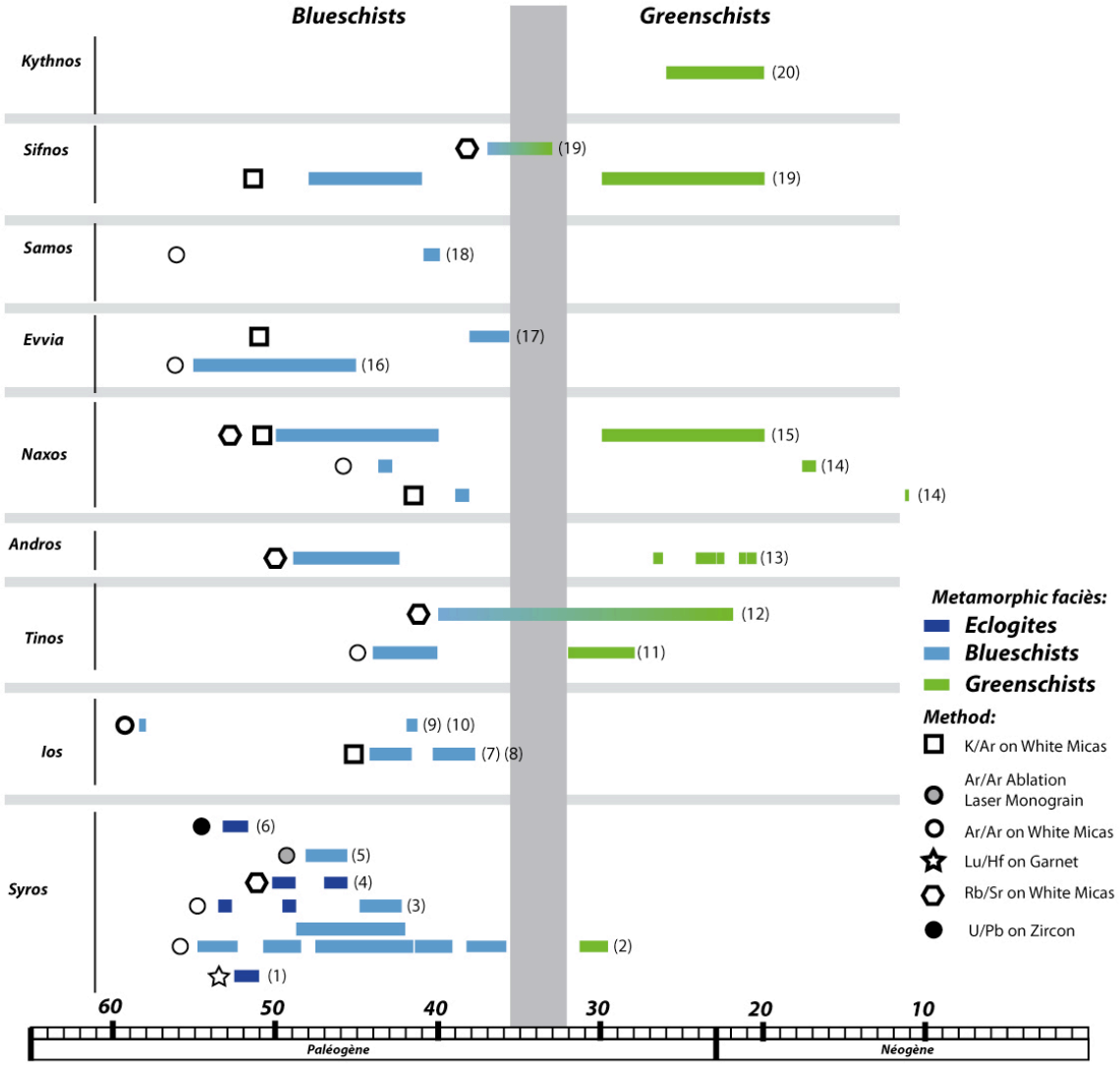

Fig. VIII-5. Ages of high-pressure metamorphism and greenschist overprint of the whole Cycladic Blueschists Unit. Numbers refer to source references (see Tab. 3).

Location	Age of metamorphic event	uncertainity	Metamorphic Faciès	Method	Reference	N° in Fig. 5
Syros	52,2	0,3	Eclogites	Lu/Hf on garnet	Lagos et al., 2002	1
Syros	51,4	0,4	Eclogites	Lu/Hf on garnet	Lagos et al., 2002	1
Syros	49,7	1,2	BS	Ar/Ar on paragonite	Maluski et al., 1987	2
Syros	40,2	1,1	BS	Ar/Ar on phengite	Maluski et al., 1987	2
Syros	53,5	1,3	BS	Ar/Ar on phengite	Maluski et al., 1987	2
Syros	44,5	3	BS	Ar/Ar on phengite	Maluski et al., 1987	2
Syros	45,3	3,4	BS	Ar/Ar on phengite	Maluski et al., 1987	2
Syros	37,1	1,3	BS	Ar/Ar on phengite	Maluski et al., 1987	2
Syros	48		GS	Ar/Ar on phengite	Maluski et al., 1987	2
Syros	30,3	0,9	GS	Ar/Ar on phengite	Maluski et al., 1987	2
Syros	49,2	0,2	Eclogites	Ar/Ar on phengite	Baldwin 1996	3
Syros	53,1	0,2	Eclogites	Ar/Ar on phengite	Baldwin 1996	3
Syros	39,6	0,1	BS	Ar/Ar on phengite	Baldwin 1996	3
Syros	43,5	0,12	BS	Ar/Ar on phengite	Baldwin 1996	3
Syros	46,3	0,7	Eclogites	Rb/Sr Phengite, Whole rock	Brocker and Enders 2001	4
Syros	49,4	0,7	Eclogites	Rb/Sr Phengite, Whole rock	Brocker and Enders 2001	4
Syros	46,3	0,7	Eclogites	Ar/Ar UV LA Phengite	Pulitz et al., 2005	5
Syros	47	1,2	Eclogites	Ar/Ar UV LA Phengite	Pulitz et al., 2005	5
Syros	52,4	0,8	Eclogites	U/Pb Zircon SHRIMP	Tomaschek et al., 2003	6
Ios	43	1,3	BS	K/Ar on Ph and Pa	Andriessen et al., 1987	7
Ios	39		BS	K/Ar on Ph and Pa	Kreutzer et al., 1978	8
Ios	39		BS		Henjes-Kunst and Kreutzer 1982	9
Ios	25,6		BS	K/Ar on Ph and Pa	Kreutzer et al., 1978	8
Ios	41,58	0,36	BS	Ar/Ar on WM (Ph,Mu,Pa)	Baldwin and Lister 1998	10
Ios	58,01	0,14	BS	Ar/Ar on WM (Ph,Mu,Pa)	Baldwin and Lister 1998	10
Tinos	44-40		BS	Ar/Ar	Brocker et al 1993	11
Tinos	32-28		GS	Ar/Ar	Brocker et al 1993	11
Tinos	40-22		BS to GS	Rb/Sr	Brocker and Franz 1998	12
Andros	45.7 ± 3.2		BS	Rb–Sr phengite	Brocker and Franz 2006	13
Andros	23.7 ± 0.4		GS	Rb–Sr phengite	Brocker and Franz 2006	13
Andros	21.3 ± 0.2		GS	Rb–Sr phengite	Brocker and Franz 2006	13
Andros	20.7 ± 0.3		GS	Rb–Sr phengite	Brocker and Franz 2006	13
Andros	23.3 ± 0.2		GS	Rb–Sr phengite	Brocker and Franz 2006	13
Andros	23.5 ± 0.3		GS	Rb–Sr phengite	Brocker and Franz 2006	13
Andros	26.5 ± 0.3		GS	Rb–Sr phengite	Brocker and Franz 2006	13
Andros	22.8 ± 0.2		GS	Rb–Sr phengite	Brocker and Franz 2006	13
Andros	23.0 ± 0.2		GS	Rb–Sr phengite	Brocker and Franz 2006	13
Naxos	38,5	0,4	BS	K-Ar/ WM	Wijbrans and McDougall 96	14
Naxos	11,3	0,1	GS	K-Ar/ WM	Wijbrans and McDougall 96	14
Naxos	43,3		BS	Ar/Ar on phengite	Wijbrans and McDougall 96	14
Naxos	17,2		GS	Ar/Ar on muscovite	Wijbrans and McDougall 96	14
Naxos	45	5	BS	Rb/Sr and K/AR Pa,Ph,Mu	Andriessen et al., 79	15
Naxos	25	5	GS	K/Ar	Andriessen et al., 79	15
Naxos	11		GS	K/Ar	Andriessen et al., 79	15
Evvia	45 to 55		BS	Ar/Ar on ph and Gln	Maluski et al., 1981	16
Evvia	37		BS	K-Ar	derived from Klein-Helmkamp et al 95	17
Samos (corellation Almyropotamos /Tinos/Kerketas)	25,2	1,6	BS	Ar/Ar on phengite	Ring and Layer 2003	18
Samos and Evvia (CBU)	40,1	0,5	BS	Ar/Ar on phengite	Ring and Layer 2003	18
Sifnos	48 to 41		BS	K - A r	Altherr et al., 79	19
Sifnos	37 to 33		BS to GS	Rb/Sr	Altherr et al., 79	19
Sifnos	25	5	GS		Altherr et al., 79	19
Ktyhnos	20-26		GS		Schliestedt et al., 94	20

Table VIII-3. References concerning the estimation of the age of the HP metamorphism shown by the figure VIII-5.

8.2.3 High temperature metamorphism and granites

In the central part of the Cyclades, high temperature metamorphism lead to partial melting in the metamorphic core complex (MCC) of Mykonos-Delos and Naxos/Paros at 20 Ma (Keay et al., 2001, U-Pb on zircon) associated to granite bodies in Miocene (22-8 Ma) (Fig. VIII-6). In the central Cyclades, the greenschist retrogression history is likely related to this late high temperature event. Few granitic plutons emplaced in the CBU, outside the MCC, during middle-late Miocene: Ikaria/18-9Ma (Ref), Serifos/8.5-9 Ma (Altherr et al., 1982), Lavrion-Attica/11.9-8.3 Ma (Liati et al., 2009). Most of granites occurrences are S-type or combine I and S-types (Pe-Piper and Piper, 2002 and 2007; Stouraiti et al., 2010).

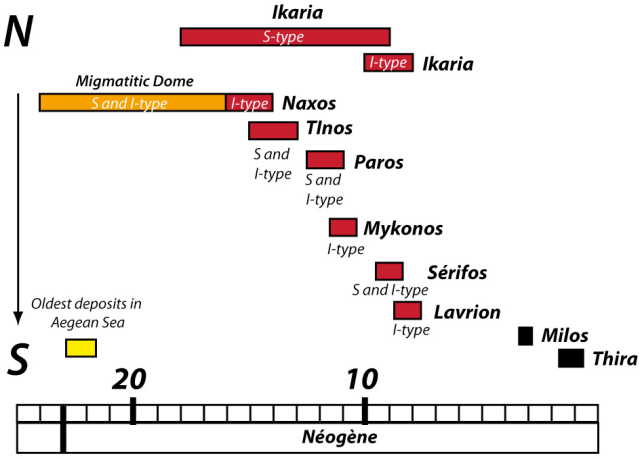

Fig. VIII-6. Ages of migmatization (Keay et al. 2001), granites (see table 1 in Stouraiti et al 2010, Pe-piper and Piper, 2002 and 2007) and volcanism (Pe-piper and piper 2002) that emplaced in the Cycladic Blueschists Unit during Miocene.

Granite emplacement associated with the development of low-angle detachment fault (Naxos-Paros (Gautier et al., 1993 ; Martin et al., 2005 ; Brichau et al.,. 2006), Mykonos (Faure and Bonneau, 1988), Serifos (Brichau et al., 2008 ; Iglseder et al., 2009), Ikaria (Ring, 2007), Lavrion (Liati et al., 2009)) and the decrease of migmatites-granite ages from North to South (Fig. VIII-6) indicates an overall southward migration of extension during Miocene, at regional-scale.

8.3. Kinematics of extension and subduction

8.3.1 Ductile extension

Since around 25 years, the ductile fabrics of the Cycladic Blueschists Unit are considered to result from i) syn to post-orogenic extension of the whole thickened crust that is responsible for the exhumation of both HP and HT metamorphic rocks (Lister et al., 1984; Gautier et al., 1990 and 1993; Avigad and Garfunkel, 1989; Gautier and Brun, 1994a and 1994b; Vandenberg and Lister, 1996; Avigad et al., 1997; Jolivet and Patriat 1999; Gautier, 1999; Jolivet and Goffé, 2000; Trotet et al., 2001 a; Ring et al., 2001, 2003, 2007 and Ring, 2007; Ring and Reischmann, 2002; Ring and Layer, 2003; Van Hinsbergen et al., 2005; Brichau et al., 2007, 2008; Katzir et al., 2008; Mehl et al., 2007; Rosenbaum and Ring, 2007; Brun and Faccenna 2008; Ring and Kumerics, 2008; Jolivet et al., 2009; 2010; Tirel et al., 2009; Brun and Sokoutis 2010; Huet et al., 2009) or ii) episodic events of shortening and extension (Forster and Lister, 2005, 2009).

Most Cycladic islands display a NE-SW trending stretching lineations (Fig. VIII-7). Exceptions are all located in a NE-SW trending corridor crossing the central Cyclades: Syros, Paros, Antiparos, Delos and Mykonos where stretching lineations also show an E-W trend.

Senses of shear associated to the NE-SW trending lineation are either top to NE or top to SW (Fig. VIII-7). In the northern islands (Evvia, Andros, Tinos, Mykonos, Syros, Paros, Naxos), close to the North Cycladic Detachment (Jolivet et al., 2010), the opposite senses of shear are most often interpreted as synchronous and conjugate (Gautier and Brun, 1994a and b; Jolivet and Patriat, 1999; Rosenbaum et al., 2002; Bond et al., 2007; Tirel et al., 2009) and eventually as a proof of co-axial deformation from local (Rosenbaum et al., 2003) at crustal scale (Bond et al., 2007). In the southern islands (Kea, Kythnos, Serifos, Ios) the dominant sense of shear top to SW is interpreted either as associated to a SW-dipping extensional detachment (Naxos-Ios: Lister et al., 1984, Ios: Forster and Lister, 2010, Kea, Kythnos, Serifos: Iglseder et al., 2009, Serifos: Brichau et al., 2008) or to SW-directed thrusting (Ios: Huet et al., 2009).

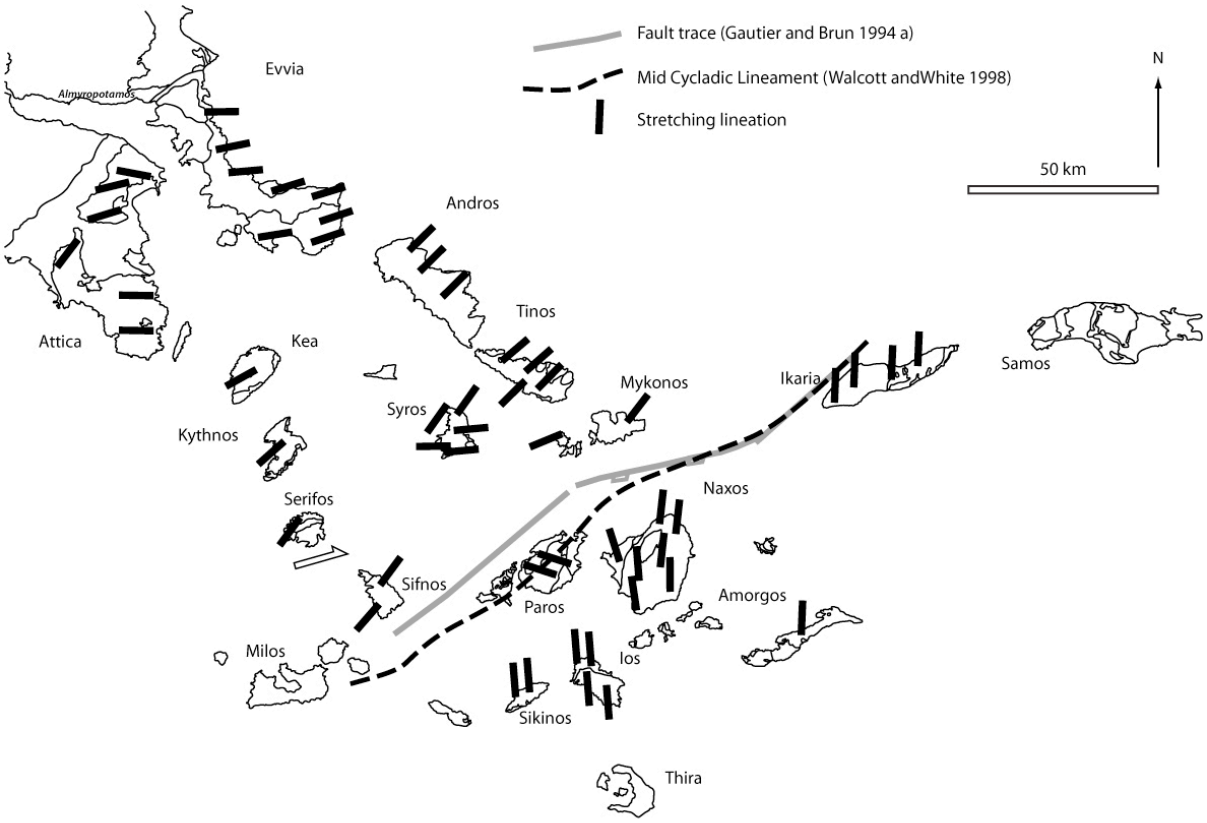

Fig. VIII-7. Map of stretching lineations.

8.3.2 Subduction-related thrusting

Syn-metamorphic thrusting i) occurs at the contact between basement and sediments (Naxos: Katzir et al., 2008, Ios: Van der Marr, and Jansen 1979) and ii) is responsible for emplacement of ophiolitic mélange on top of sediments (Syros: Ridley, 1982; Keiter et al., 2004; Evvia: Shaked et al.,., 2000). In Evvia (Shaked et al., 2000) and in Andros (Ziv et al., 2010), the ophiolitic mélange is thrust on top of a marble-schists sequence and both units are affected by HP metamorphism with a pressure up to 22 kbar. In the Almyropotamos window of Evvia (Shaked et al.,., 2000) as well as in Amorgos and Samos (Rosenbaum and Ring, 2007; Ring et al., 2007) the thrust pile is itself thrust on top of the Eocene numulitic flysch with a lower pressure metamorphism of 10-12 kbar. The above relations between deformation and high-pressure metamorphism indicate that thrusting is related to a subduction that was active until middle Eocene.

8.4. Segmentation of the Cycladic Blueschists Unit since middle Miocene

8.4.1. Regional-scale faults

As shown in figure VIII-8, the Cyclades islands correspond to the highs of faulted blocks segmented by large-scale normal faults trending dominantly NW-SE and strike-slip faults trending NE-SW. The largest of these strike-slip faults accommodates the opening of the pull-apart basins of Ikaria-Samos to the northeast and Myrthes to the southwest that (Fig. VIII-8).

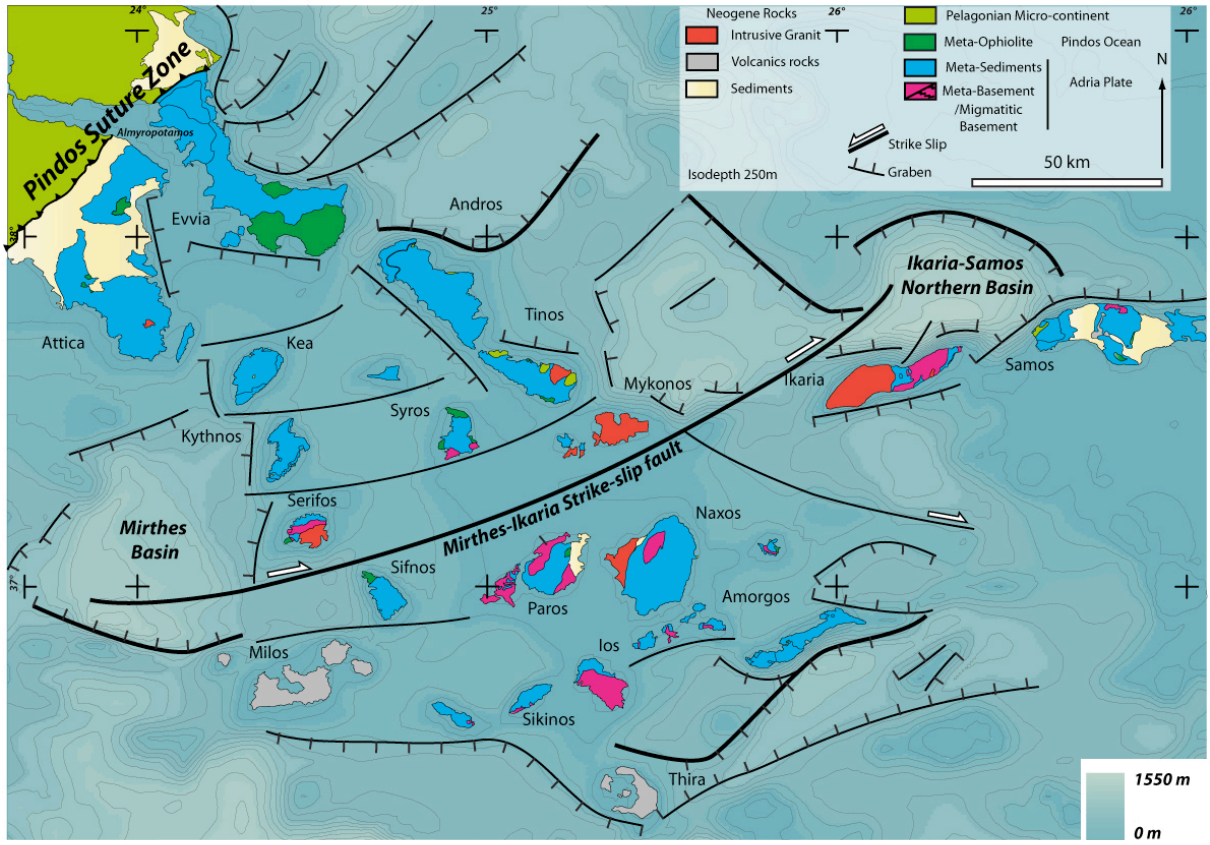

Fig. VIII-8. Pattern of large-scale Neogene faults in and around the Cyclades. Bathymetry is represented with 250 m isodepth contours (data from ETOPO1 1 Arc-Minute Global Relief Model; Amante and Eakins, 2009). The DEM resolution is 120x120 m 2 per pixel.

The oldest sedimentary deposits in the Cyclades basins are Burdigalian/Aquitanian (Btittner and Kowalczyk, 1978; Meulenkamp, 1979; Papanikolaou and Royden, 2007). This indicates that the brittle segmentation of the CBU responsible for the Cyclades archipelago morphology started in Early Miocene. The two sets of NW-SE trending normal faults and NE-SW trending strike-slip faults whose morphological signature is recorded in bathymetry (Fig. VIII-8) controlled the

development of Neogene sedimentary basins over the Cycladic plateau (Mascle and Martin 1990).

8.4.2. Island-scale extensional fault systems

Detailed mapping of brittle extension in Sifnos and Syros exemplifies two main types of kilometer-scale patterns: i) tilted blocks and ii) flat & ramp systems.

Sifnos displays large tilted blocks bounded by WNW-ESE trending faults with a 1.5 to 2.0 km spacing (Fig. VIII-9). Block tilting reaches dip values up to 45°. The normal fault shown in figure 9a roots at the base of the marble series along a flat-lying network showing brittle shear bands marked by breccias and gouges (Fig. VIII-9b). Small-scale shear bands and rolling blocks indicate a top to S sense of shear. This flat-lying contact has been previously interpreted has a major ductile detachment that accommodated the exhumation of metamorphic rocks (Avigad et al., 1992; Trotet et al., 2001a). As illustrated in figure VIII-9 it is a late brittle normal fault originally steeply-dipping and tilted to shallow dip, around 15°.

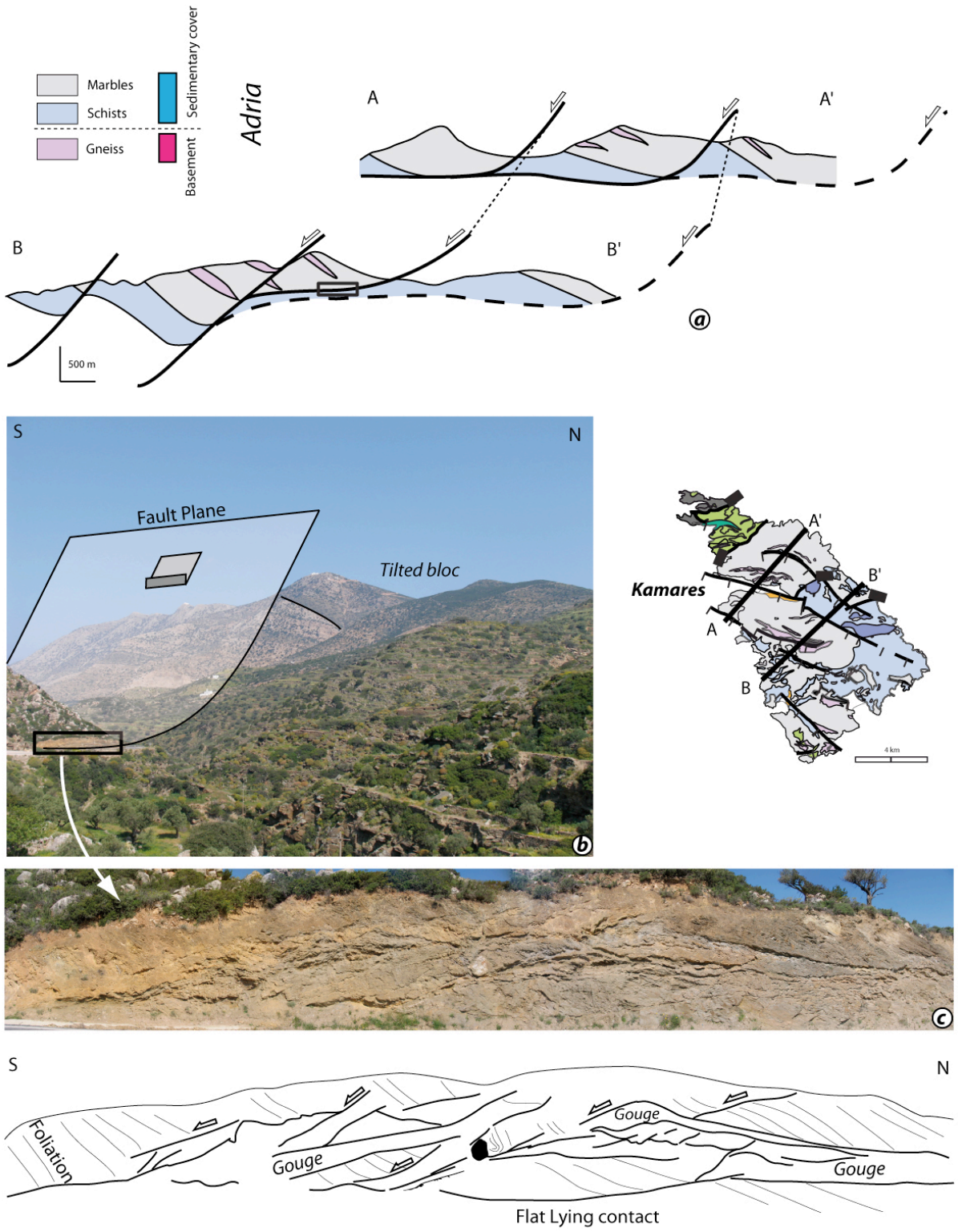

Fig. VIII-9. NE-SW The titled block pattern accommodating a southward displacement in Sifnos: a) NE-SW-trending cross-sections AA' and BB' with map location indicated. b) View looking west of the Kamares normal fault and associated tilted block and c) Outcrop-scale pattern of deformation related to the low-dipping part of the Kamares fault.

Syros displays a major flat & ramp extensional system illustrated by sections AA' and BB' (Fig. VIII-10). In the north of the island, in vicinity of Kambos, the Kastri basal fault is parallel to the foliation-parallel lithological layering of Kastri and Pyrgos marble-schist units that is gently dipping to the north. This part of the displacement surface is the upper décollement of the extensional system. In the southern part of the island, from Hermoupoli to the southern coast the displacement surface cuts down section indicating that it is an extensional ramp. Cross-cutting relationships show that further south the marble-schist hangingwall sequence comes into parallel contact with the underlying basement. This indicates that the movement surface merges into the sedimentary cover-basement contact (Section BB') corresponding to the lower décollement of the extensional system. The hanginwall-footwall relationships, the southward sense of displacement and the associated brittle deformation (breccias) indicate that the Kastri basal fault is a post-metamorphic kilometre-scale extensional system with a flat-ramp geometry whose minimum southward displacement estimated about 7km. Here again, this late brittle extension was previously interpreted as a flat-lying synmetamorphic detachment (Trotet et al., 2001a).

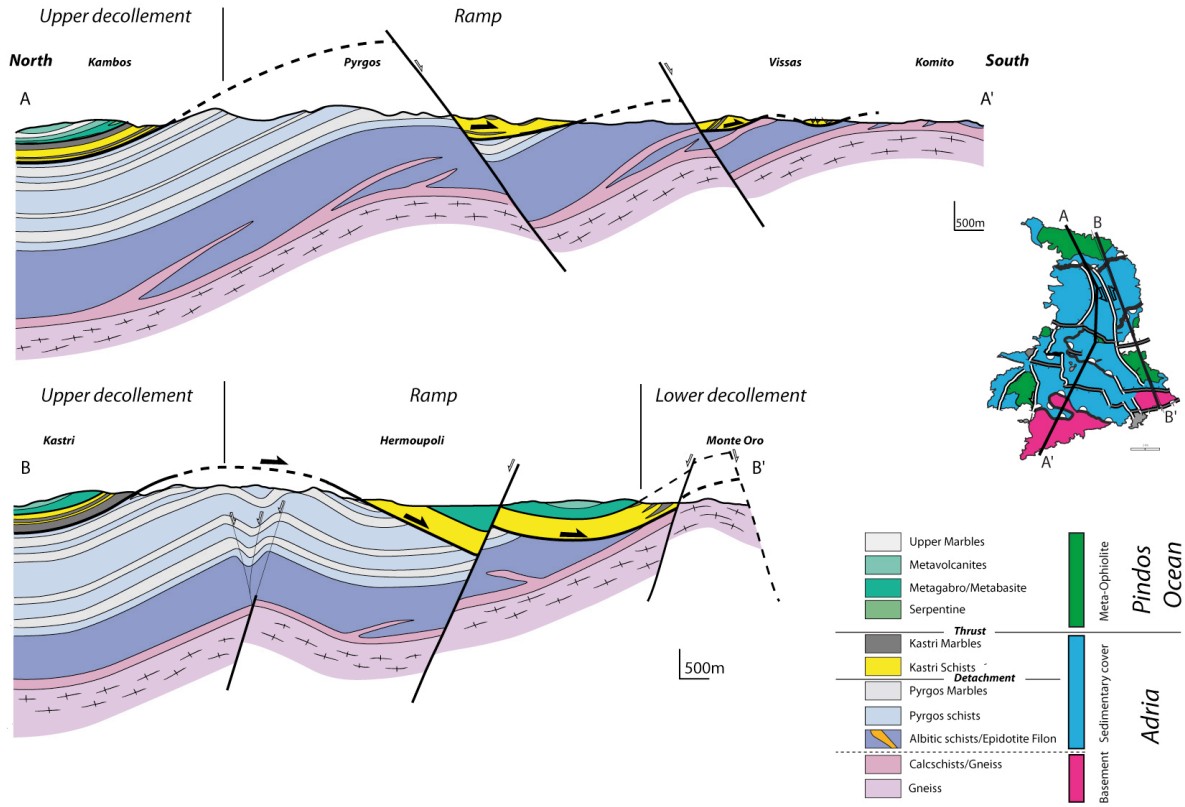

Fig. VIII-10. Sub-meridian cross-sections showing the flat and ramp geometry of the Syros extensional system with a southward displacement.

8.4.3. Folding in the central Cyclades

It has been recognised since long ago that the central Cyclades are affected by folding with axes trending as a N to NE direction (Fig. VIII-11). The Burdigalian sediments of Paros are affected by upright folds with wavelengths in the order of some 100m (Angelier, 1977). In the central part of the island, the metamorphic rocks are also affected in a N-S trending corridor by a train of upright folds (Papanikolaou, 1979, 1980) (Fig. VIII-11 a). For a regional-scale synthesis of folding evidence in the island of Andros (Fig. VIII-11b), Tinos, Paros and Naxos see Avigad and Garfunkel (2001). The Syros island also displays comparable folding of the metamorphic pile from kilometer-scale wavelength in the north to outcrop-scale along the southern coast (Fig. VIII-11 c).

At a larger scale, to the SE of the Myrthes-Ikaria strike-slip fault, the synmetamorphic detachment of Paros and Naxos is folded with N-S trending axes parallel to those observed inside these islands either in metamorphic rocks or in Neogene basin. Therefore, folding mostly occurred after the activity of the synmetamorphic detachment and the deposition of Burdigalian sediments, suggesting a Langhian-Serravalian age. This also shows that the 3D shape of the Paros and Naxos detachment is not original (a-type dome; Jolivet and Goffé, 2000) but results from a middle-Miocene folding of an initially planar detachment that started to develop in late-Oligocene/early-Miocene (Gautier et al., 1993). This implies that the Naxos detachment was not anymore functioning in late-Miocene as interpreted from thermochronological data. Instead, we interpret the FT-ages of 12-8 Ma obtained in Naxos (Brichau et al., 2007) (Fig. VIII-12) as related to folding and associated denudation in Serravalian-Tortonian. To the SE of the Myrthes-Ikaria strike-slip fault, in Andros, Tinos and Syros fold axes trend N30° (Fig. VIII-11, map).

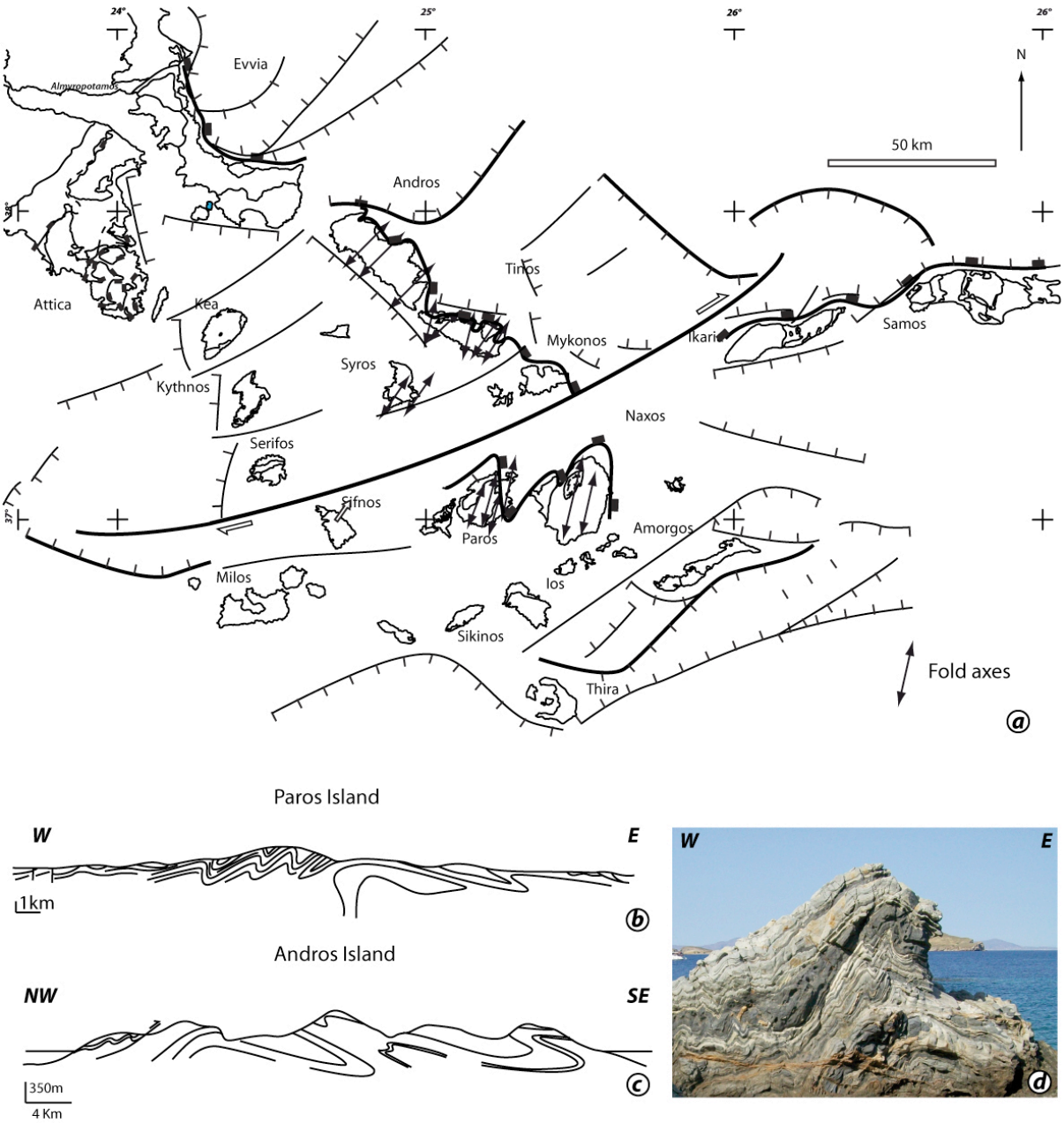

Fig. VIII-11. Folding with N to N30° trending axes in the central Cyclades. a) Map of fold axes in Andros, Tinos, Syros, Paros and Naxosc. b) W-E cross-section showing km-scale folding in Paros (Papanikolaou 1979) c) NW-SE cross-section showing km-scale folding in Andros (Papanikolaou 1980) and d) Example of outcrop-scale folds with N30° trend axes, in south Syros.

8.4.4. Low-T Thermochronology

The late stages of denudation in the Cyclades are illustrated by the available thermochronological data (Apatite and Zircon fission tracks and zircon U-Th/ He) (Fig. VIII-12). The whole set of data gives a rather consistent range of ages from 16 to 5 Ma at regional-scale, if error bars. An even smaller range of ages from 12 to 8 Ma is given by

the zircon fission tracks and the U-Th/ He ratio in zircons that correspond to closure temperatures of 200°C and 60°C, respectively.

The small range of 4 Ma ages at the scale of the whole Cyclades strongly suggests that the late stages of denudation are controlled by: i) distributed extension observed from island-scale, as illustrated in Sifnos (Fig. VIII-9) and Syros (Fig. VIII-10), to the regional-scale (Fig. VIII-8) and ii) coeval folding in particular in Paros and Naxos. This is at variance with denudation attributed to synmetamorphic detachments at the scale of some islands, as recently advocated (Ring et al., 2003; Brichau et al., 2006, 2007, 2008, 2010).

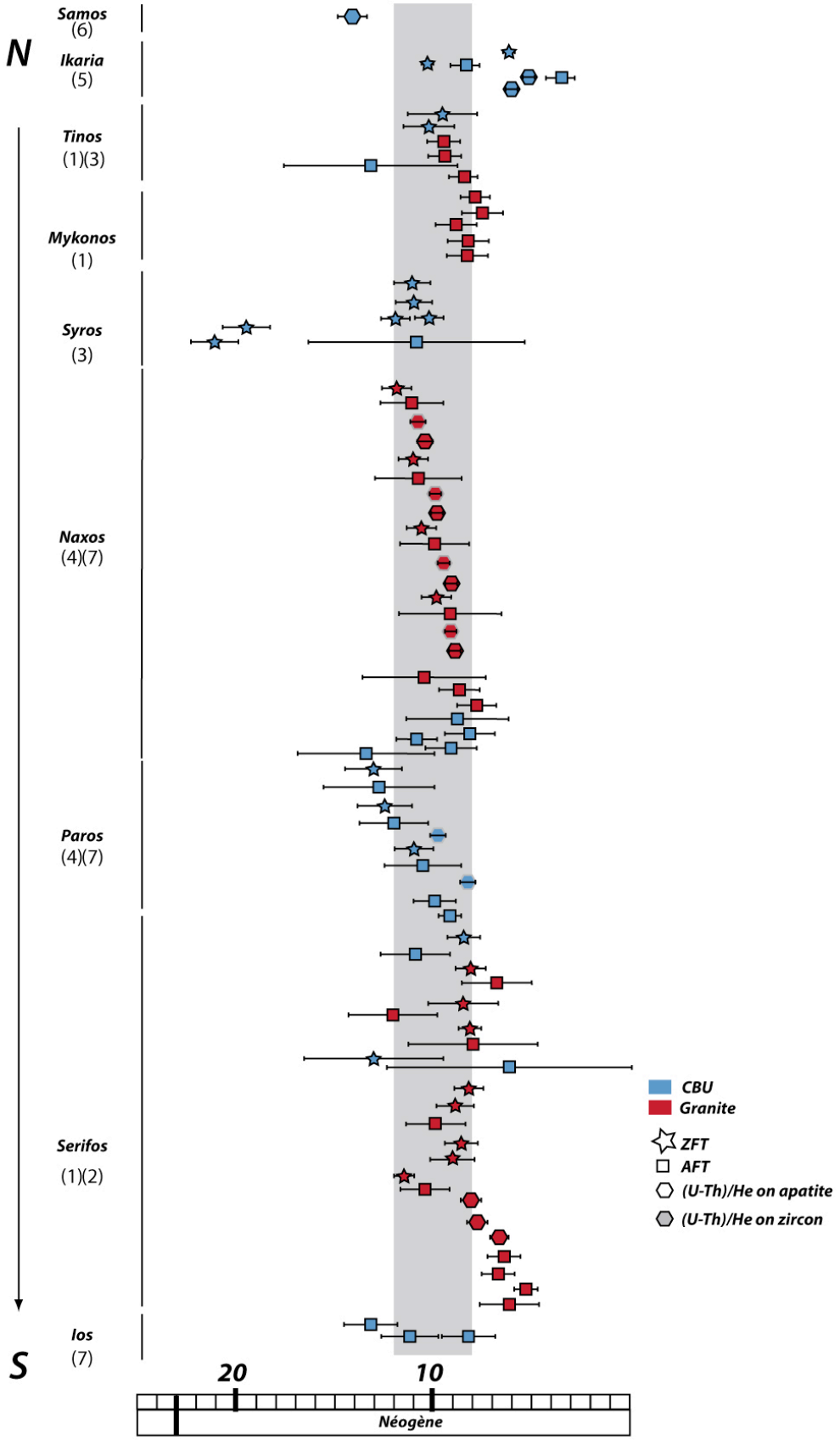

Fig. VIII-12. Low-temperature thermochronological data available for the whole Cycladic Blueschists Unit. Numbers refer to source references (see Tab. 4)

Location	Age (Ma)	uncertainity	Method	Reference	N° in the Fig. 12
Tinos	13,1	4,4	AFT	Hejl et al., 2002	1
Tinos	8,4	0,7	AFT	Hejl et al., 2002	1
Tinos	9,5	0,8	AFT	Hejl et al., 2002	1
Tinos	9,3	0,8	AFT	Hejl et al., 2002	1
Tinos	9,3	0,8	AFT	Hejl et al., 2002	1
Mykonos	8,3	1	AFT	Hejl et al., 2002	1
Mykonos	8,2	1	AFT	Hejl et al., 2002	1
Mykonos	8,9	1	AFT	Hejl et al., 2002	1
Mykonos	7,6	1	AFT	Hejl et al., 2002	1
Mykonos	7,9	0,7	AFT	Hejl et al., 2002	1
Serifos	6,1	1,5	AFT	Hejl et al., 2002	1
Serifos	5,3	0,6	AFT	Hejl et al., 2002	1
Serifos	6,7	0,8	AFT	Hejl et al., 2002	1
Serifos	6,4	0,8	AFT	Hejl et al., 2002	1
Serifos	10,3	1,3	AFT	Brichau et al., 2008	2
Serifos	11,4	0,5	ZFT	Brichau et al., 2008	2
Serifos	8,6	0,8	ZFT	Brichau et al., 2008	2
Serifos	9	1,1	ZFT	Brichau et al., 2008	2
Serifos	9,9	1,8	AFT	Brichau et al., 2008	2
Serifos	8,9	0,9	ZFT	Brichau et al., 2008	2
Serifos	8,2	0,7	ZFT	Brichau et al., 2008	2
Serifos	6,3	6,2	AFT	Brichau et al., 2008	2
Serifos	13	3,6	ZFT	Brichau et al., 2008	2
Serifos	8	3,3	AFT	Brichau et al., 2008	2
Serifos	8,3	0,6	ZFT	Brichau et al., 2008	2
Serifos	12,1	2,2	AFT	Brichau et al., 2008	2
Serifos	8,6	1,8	ZFT	Brichau et al., 2008	2
Serifos	6,7	1,8	AFT	Brichau et al., 2008	2
Serifos	8,1	0,7	ZFT	Brichau et al., 2008	2
Serifos	10,9	1,8	AFT	Brichau et al., 2008	2
Serifos	8,5	0,7	ZFT	Brichau et al., 2008	2
Serifos	8,1	0,5	(U/Th)He on apatite	Brichau et al., 2008	2
Serifos	7,7	0,5	(U/Th)He on apatite	Brichau et al., 2008	2
Serifos	6,6	0,4	(U/Th)He on apatite	Brichau et al., 2008	2
Serifos	7,5	0,3	(U/Th)He on apatite	Brichau et al., 2008	2
Syros	10,7	5,5	AFT	Ring et al., 2003	3
Syros (Vari)	21,2	1,3	ZFT	Ring et al., 2003	3
Syros (Vari)	19,6	1,3	ZFT	Ring et al., 2003	3
Tinos	9,6	1,7	ZFT	Ring et al., 2003	3
Tinos	10,2	1,2	ZFT	Ring et al., 2003	3
Syros	10,1	0,7	ZFT	Ring et al., 2003	3
Syros	11,9	0,6	ZFT	Ring et al., 2003	3
Syros	11	0,9	ZFT	Ring et al., 2003	3
Syros	11,1	0,9	ZFT	Ring et al., 2003	3
Naxos	8,2	1,2	AFT	Brichau et al., 2006	4
Naxos	8,7	2,6	AFT	Brichau et al., 2006	4
Naxos	9,3	2,6	AFT	Brichau et al., 2006	4
Naxos	9,7	0,8	ZFT	Brichau et al., 2006	4
Naxos	9,8	1,8	AFT	Brichau et al., 2006	4
Naxos	10,6	0,8	ZFT	Brichau et al., 2006	4
Naxos	10,7	2,2	AFT	Brichau et al., 2006	4
Naxos	11,1	0,8	ZFT	Brichau et al., 2006	4
Naxos	11,2	1,6	AFT	Brichau et al., 2006	4
Naxos	11,8	0,8	ZFT	Brichau et al., 2006	4
Paros	10,5	2	AFT	Brichau et al., 2006	4
Paros	11	1	ZFT	Brichau et al., 2006	4
Paros	12,1	1,8	AFT	Brichau et al., 2006	4
Paros	12,4	1,4	ZFT	Brichau et al., 2006	4
Paros	12,7	2,8	AFT	Brichau et al., 2006	4
Paros	13,1	1,4	ZFT	Brichau et al., 2006	4
Naxos	8,9	0,3	(U/Th)He on apatite	Brichau et al., 2006	4
Naxos	9,2	0,3	(U/Th)He on zircon	Brichau et al., 2006	4
Naxos	9,1	0,4	(U/Th)He on apatite	Brichau et al., 2006	4
Naxos	9,5	0,3	(U/Th)He on zircon	Brichau et al., 2006	4
Naxos	9,7	0,6	(U/Th)He on apatite	Brichau et al., 2006	4
Naxos	9,8	0,4	(U/Th)He on zircon	Brichau et al., 2006	4
Naxos	10,7	0,5	(U/Th)He on apatite	Brichau et al., 2006	4
Naxos	10,4	0,4	(U/Th)He on zircon	Brichau et al., 2006	4
Paros	8,3	0,4	(U/Th)He on zircon	Brichau et al., 2006	4
Paros	9,8	0,3	(U/Th)He on zircon	Brichau et al., 2006	4
Ikaria	10,3	0,3	ZFT	Ring 2007	5
Ikaria	6,3	0,3	ZFT	Ring 2007	5
Ikaria	8,4	0,8	AFT	Ring 2007	5
Ikaria	5,2	0,9	AFT	Ring 2007	5
Ikaria	6	0,3	(U/Th)He on apatite	Ring 2007	5
Ikaria	3,6	0,2	(U/Th)He on apatite	Ring 2007	5
Samos	14,1	1,2	ZFT	Kumerics et al., 2005	6
Paros	9,9	1,1	AFT	Hejl 2003	7
Paros	9,3	0,6	AFT	Hejl 2003	7
Naxos Granite	7,8	0,8	AFT	Hejl 2003	7
Naxos	13,4	3,5	AFT	Hejl 2003	7
Naxos	9,3	1,3	AFT	Hejl 2003	7
Naxos Granite	10,3	3,1	AFT	Hejl 2003	7
Naxos Granite	8,6	1	AFT	Hejl 2003	7
Naxos	10,9	1	AFT	Hejl 2003	7
Ios	11,2	1,4	AFT	Hejl 2003	7
Ios	8,3	1,1	AFT	Hejl 2003	7
Ios	13,2	1,1	AFT	Hejl 2003	7

Table VIII-4. References concerning the Low temperature thermochronology shown in the figure VIII-12.

8.5. Map restoration of the post-Serravalian deformation

8.5.1. Top to N to NE shear, from late Eocene to Mid-Miocene

From their maximal burial depth to the crustal depths, the HP metamorphic rocks of the CBU have undergone ductile deformation related to exhumation synchronous with retrograde metamorphism. The compilation of geochronological data at regional scale (Fig. VIII-5) shows that the transition from blueschist facies to greenschist facies occurred around 35 Ma, meaning that the CBU was already undergoing exhumation in late Eocene. Therefore, top to N to NE shear that is synchronous to retrograde metamorphism occurred during exhumation of the CBU from mantle depth to crustal depths (Fig. VIII-13).

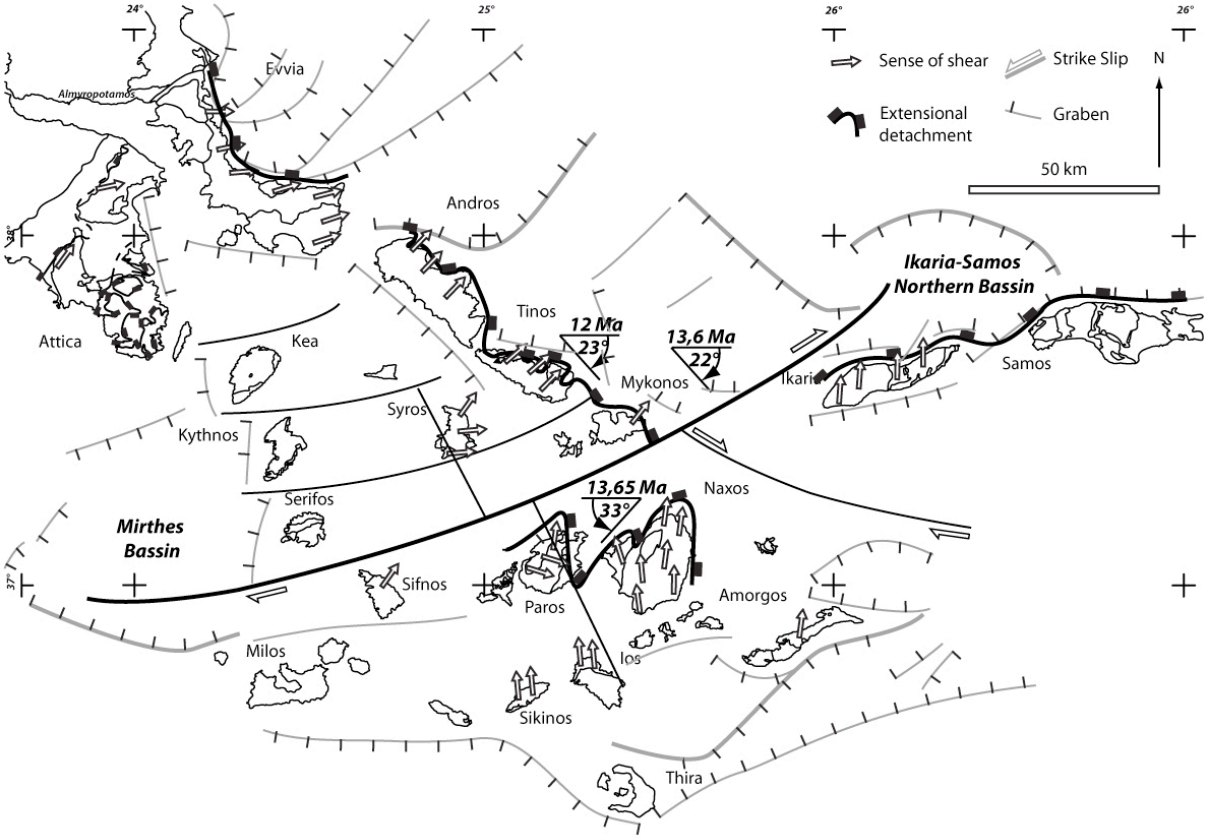

Fig. VIII-13 Top-to-NE sense of shear associated to the north dipping detachments. For source references see Tab. 5.

Location	Reference	N° in the Fig. 13
Evvia	Gautier and Brun 1994 a	1
Attica	Brun and Kostopoulos Pers. Com.	2
Andros	Gautier and Brun 1994 a	3
Tinos	Gautier and Brun 1994 a	4
Mykonos	Gautier and Brun 1994 a	6
Naxos	Gautier et al., 1993	7
Paros	Gautier et al., 1993	8
Amorgos	Rosembaum and Ring 2007	9
Ikaria	Ring 2007	10
Syros	Gautier and Brun 1994 a, Trotet et al., 2001 a	11
Sifnos	Gautier and Brun 1994 a, Trotet et al., 2001 a	12
Sikinos	Gautier and Brun 1994 a	13
Ios	Huet et al., 2009	14

Table VIII-5: References concerning the top to the NE sense of shear shown in the figure VIII-13.

However, the ductile deformation with a top to N to NE sense of shear resulted from two successive deformations events: i) first the exhumation of the whole CBU from its maximum burial depth to deep crustal levels, in the Cyclades but also further to northwest in the Olympus and Ossa mountains, and (ii) second core complex extension synchronous with high temperature metamorphism in the central Cyclades (Naxos/Paros: Gautier et al., 1993 ; Mykonos: Gautier and Brun, 1994 a).

8.5.2 Restoration of block rotation

At Cyclades-scale the trend of stretching lineations defines two distinct domains separated by an offshore discontinuity oriented NE-SW, located between Mykonos and Naxos to the northeast and between Sifnos and Paros toward the southwest (Gautier and Brun, 1994 a). Walcott and White (1998) called "Mid Cycladic Lineament" (MCL) a line with a similar orientation but running through Paros (Fig. VIII-7). In none of these two previous studies the kinematics of this structural discontinuity has been elucidated. In the present study we refer to the Myrthes-Ikaria strike-slip fault that accommodates the opening of pull-apart basins to the northeastern and southwestern ends. However,

the Myrthes-Ikaria fault has not exactly the same direction and is located between located between Mykonos and Naxos to the northeast and between Serifos and Sifnos toward the southwest.

Stretching lineations display NE and N mean trends to the northwest and the southeast of the Myrthes-Ikaria fault, respectively. Paleomagnetic data (Morris and Anderson, 1996) show that these two domains characterized by N and NE trending lineations have undergone significant components of differential vertical axis rotations on the basis of measurements made in Tinos, Mykonos and Naxos. The Northwest and Southeast domains have rotated clockwise by ca. 22° and anticlockwise by ca. 33°, respectively. Therefore the differential angle of rotation between the two domains is 55°. The angle between the lineation trends of the domain is also of the same order c.a. 50°. This indicates that the lineations had the same initial trend before block rotation. This block rotation occurred after 12 Ma as demonstrated by the age of rotated dykes in Tinos (Avigad et al., 1998).

To restore the geometry prior to 12 Ma in map view we proceeded in three stages (Fig. VIII-15). First, the Cyclades were divided in four sub-domains (Evvia-Attica, Andros-Tinos-Mykonos, Paros-Naxos and Ikaria-Samos) with similar amount and sense of rotation and lineation trends (Fig. VIII-13a). The sub-domain boundaries correspond to existing major faults. Second, to remove the displacements accommodated by normal and strike-slip faults in the Andros-Tinos-Mykonos sub-domain, the southern islands have been realigned parallel to the mean trend of the northern islands. Third, the two domains separated by the Myrthes-Ikaria fault, whose rotation was known, have been rotated back by the same angle. This back rotation has been done simultaneously with a sinistral displacement along the Myrthes-Ikaria fault that brought the detachments of Naxos-Paros Andros-Tinos-Mykonos almost in line –i.e. a displacement of about 50km. The Evvia-Attica sub-domain has been slightly rotated to keep the Evvia detachment in line with the one of Andros. The folding of the Paros-Naxos detachment has not been unfolded (Fig. VIII-13b) but, in order to take into account the amount of shortening, the Ikaria-Samos sub-domain has been translated eastward by 40 km.

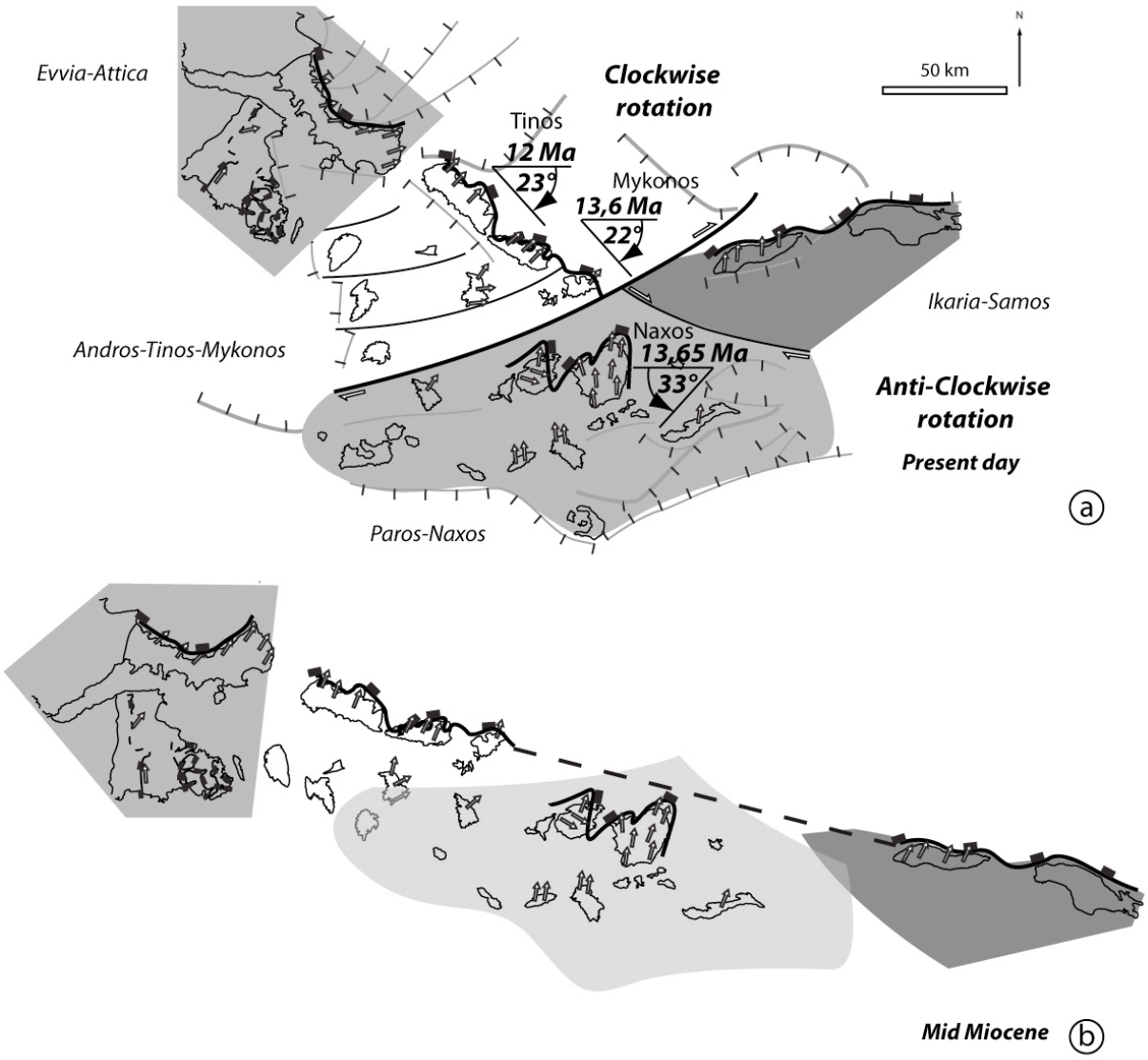

Fig. VIII-14. Restoration of the post-12 Ma segmentation of the Cycladic Blueschist Unit. a) Contours of the five sub-domains considered for the restoration with angles of rotation documented by paleomagnetism. b) The restored geometry is obtained by three operations: 1. removal of displacements accommodated by large regional faults shown in Fig. 8, 2: back-rotation of the Andros-Mykonos and Naxos-Paros domains and 3. eastward translation of the Ikaria-Samos domain. See text for full description of the restoration procedure.

8.5.3. Implications of the restoration

The first outcome of the restoration is the reconstruction of a single detachment for the whole Cyclades, contrary to recent interpretations where multiple and separate detachments are considered (Tirel et al., 2009; Jolivet et al., 2010; Ring et al., 2010). We propose to extend the definition of "North Cycladic Detachment System" (Jolivet et al.,

2010) to this restored geometry that integrates in its original position the Naxos-Paros detachment between Mykonos and Ikaria.

On the restored map, the migmatites and granites define a high temperature (HT) lenticular band along 250 km seated below the North Cycladic Detachment System (Fig. VIII-14) with a maximum width of around 40 km where the HP metamorphic assemblages are more strongly retrogressed in greenschist facies than outside. This structure corresponds to a unique "Central Cyclades Core Complex" whose exhumation occurred in early Miocene as indicated by the age of the Naxos/Paros migmatites is 16-20 Ma (U/Pb on Zircon, Keay, 2001) with a top to NE sense of shear. The late emplacement of the Serifos granite, which is located outside the Central Cyclades Core Complex, is likely favoured by the Myrthes-Ikaria fault.

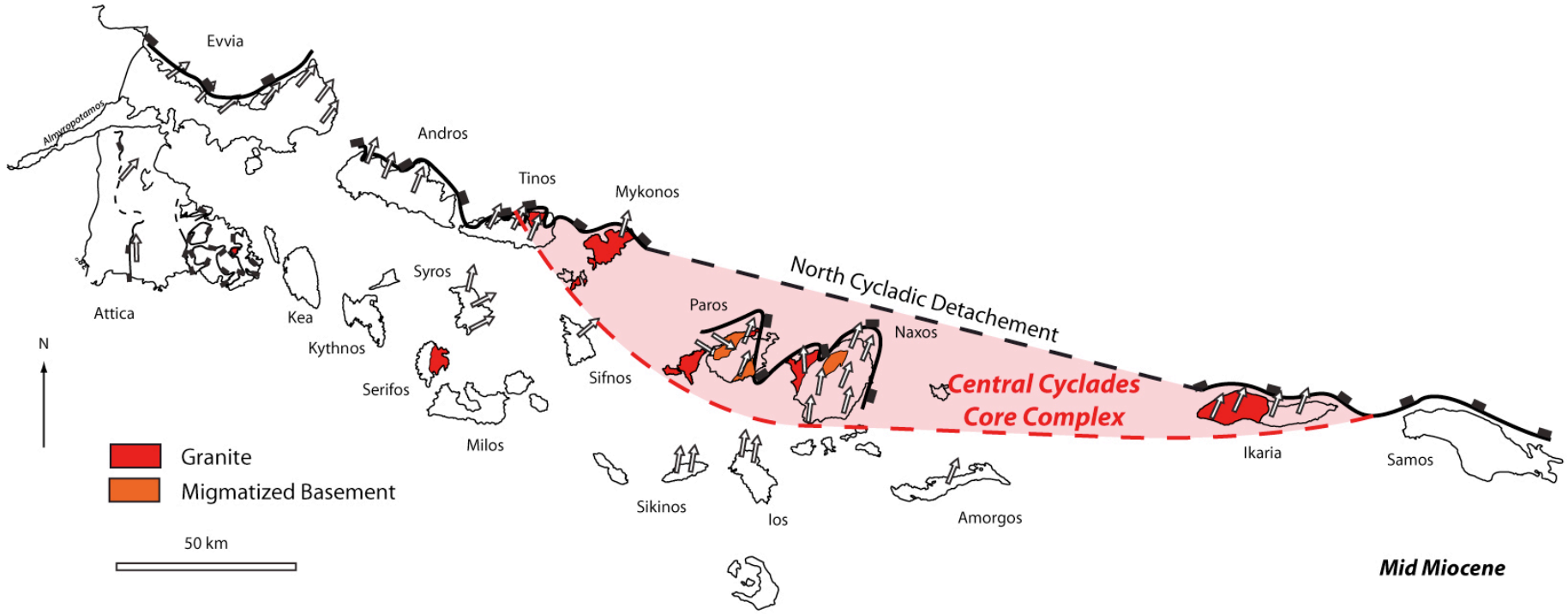

Fig. VIII-15. Restored map of the Cyclades at the end of middle Miocene showing only one detachment and only one core complex: The North Cycladic Detachment and the ***Central Cyclades Core Complex****.*

8.6. Ductile shearing related to subduction

8.6.1. Shearing deformation related to thrusting

Top to S to SW sense of shear is observed in the whole CBU (Fig. VIII-15). In Evvia, Syros, Tinos and Sifnos, this sense of shear is associated to lawsonite pseudomorphs; The preservation of lawsonite pseudomorphs indicates that the lawsonite bearing rocks has not been deformed after the lawsonite breakdown (Keiter et al., 2004; Philippon et al., 2009). As the lawsonite stability field is located on the prograde PT-path of the CBU, the top to S to SW sense of shear associated to lawsonite pseudomorphs corresponds to a deformation synchronous with prograde metamorphism and therefore is related to subduction.

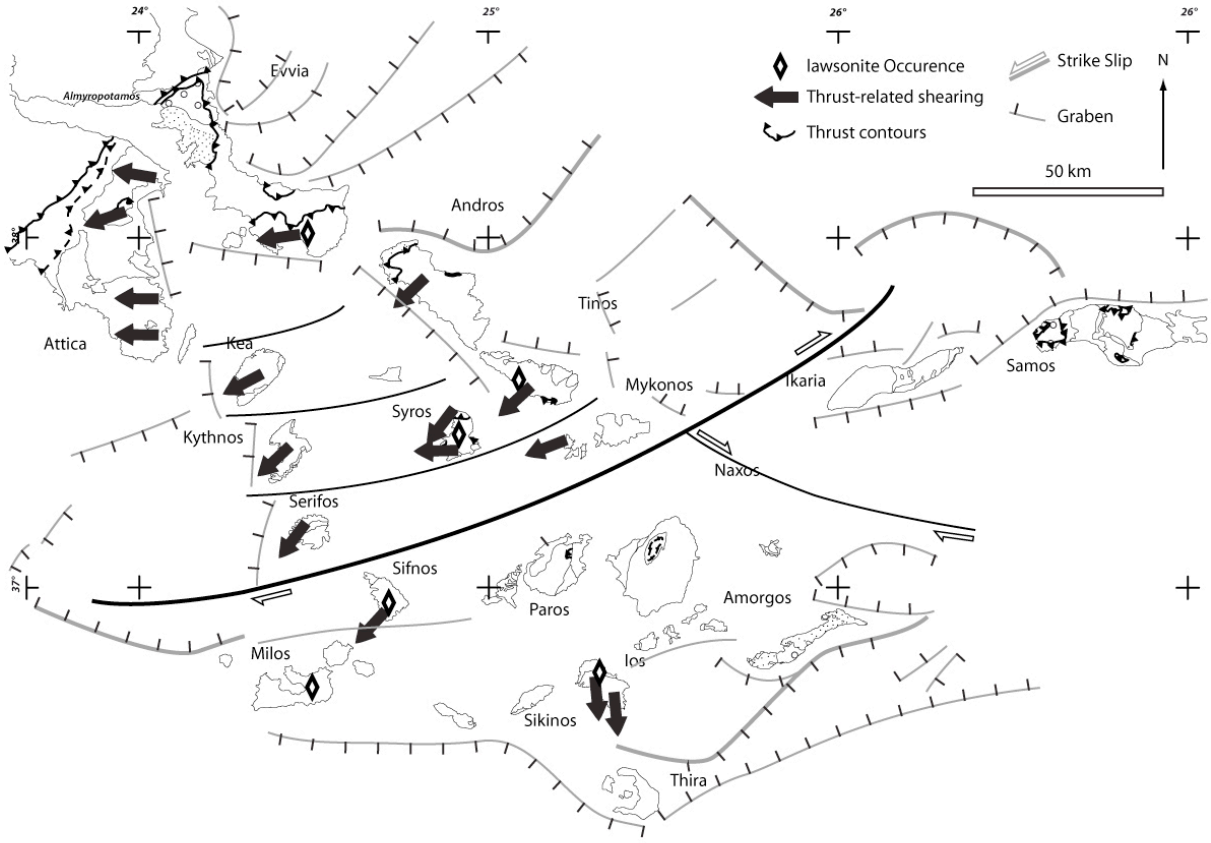

Fig. VIII-16. Map of the Cyclades showing the distribution of early top-to-SW senses of shear, occurrences of lawsonite pseudomorphs and thrusts. For source references see Tab. 6.

Location	Reference	N° in the Fig. 16
Evvia	Gautier and Brun 1994 a	1
Attica	Brun and Kostopoulos Pers. Com.	2
Andros	Gautier and Brun 1994 a	3
Tinos	Gautier and Brun 1994 a	4
Mykonos	Gautier and Brun 1994 a	6
Serifos	Iglseder et al., 2009	7
Kythnos	Iglseder et al., 2009	8
Kea	Iglseder et al., 2009	9
Syros	Gautier and Brun 1994 a, Trotet et al., 2001 a	10
Sifnos	Gautier and Brun 1994 a, Trotet et al., 2001 a	11
Ios	Huet et al., 2009	12

Table 6: References concerning the top to the SW sense of shear shown in the figure VIII-16.

Thrusts evidence within the CBU is regionally associated with top to S to SW shear indicating southwestward thrusting events occurring under blueschists facies conditions. This is responsible for the thrusting of ophiolitic melange on top of the marble-schist sedimentary sequences in particular in Evvia (Shaked et al., 2000), Syros (Bonneau et al., 1980; Ridley, 1982; Keiter et al., 2004), Samos (Ring et al., 2007). This nappe stacking occurred at great depth as indicated by associated metamorphism with pressure up to 20± 2Kbar (Gitahi, 2004; Holley et al., 2004) and ductile deformation. It indicates that the oceanic units have been decoupled from the down-going lithospheric mantle to allow the subduction of the Adria continental margin underneath.

8.6.2. Top to S or SW shear at regional-scale

A plot of the shear senses related to subduction-related thrusting and to exhumation on the restored map of the Cyclades in middle Miocene shows three domains: i) top to NE shear is dominantly represented in the Central Cyclades Core Complex and is early Miocene as it affect the migmatites and granites, ii) top to the SW is dominantly represented in Attica and the southwestern islands (Kea, Kythnos, Serifos) and both senses of shear occurs between the two previous domains (Fig. VIII-16).

In the intermediate domain where both senses of shear are observed the top to SW shear that is associated to lawsonite pseudomorphs corresponds to subduction related thrusting, prior to Lutetian as demonstrated in Almyropotamos window of Evvia

(Shaked et al., 2000). The top to NE shear has two origins. It corresponds first to the exhumation of the CBU from early Eocene to lower Oligocene and second to the Central Cyclades Core Complex exhumation that is accommodated by the North Cycladic Detachment System from early Miocene to middle Miocene. The difference between these two top to NE shearing events is demonstrated by the cross-cutting at right angle of the Pindos suture zone by the North Cycladic Detachment in Evvia (Fig. VIII-1). In addition, the post-12 Ma segmentation of the CBU is accompanied by semi-brittle deformation that can also give top to SW shear. For exemple, in the following settings: i) close to large normal faults dipping to southwest that controlled the development of large faulted blocks and their ultimate dome like geometry (Fig. VIII-17a), like in Andros and Tinos ii) associated to flat-ramp extensional systems with a southward displacement (Fig. VIII-17b), like in Syros (Fig. VIII-10), or at the base of strongly tilted blocks, like in Sifnos (Fig. VIII-9), inside the marble-schist sedimentary sequence of the CBU.

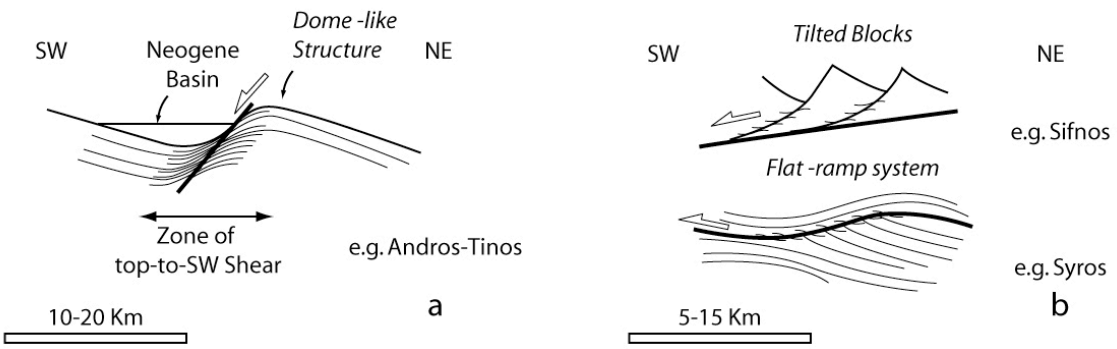

Fig. VIII-17. Post-12 Ma top-to-SW sense of shear that develop a) within dome-like structures, or b) in relation with titled blocks or flat-ramp extensional system.

In the southwestern Cyclades islands and in Attica the top to SW shear is dominant. In Attica it is clearly related to early thrusting as in the Penteli Mountains the basement is thrust on top of the sedimentary cover. In Serifos, two different events are responsible for the top to SW shear. The latest one is coeval with the Serifos granite emplacement at 8 Ma. It corresponds to the post-12 Ma deformation that segmented the CBU (see section 4.2) and displays the same kinematics than those observed in the same period in Syros (Fig. VIII-9) and Sifnos (Fig. VIII-10), that in the restored map are located North of Serifos (Fig. VIII-18). In Kea, Kythnos and Serifos, concerning the deformation prior to granite emplacement, the top to SW shear is not dated. Because these islands

are located between Attica and Ios (Fig. VIII-18) where top to SW shear is clearly related to thrusting, the whole southern domain should represents a part of the CBU that is non affected by top to NE shear related to exhumation and where the subduction-related deformation is still preserved.

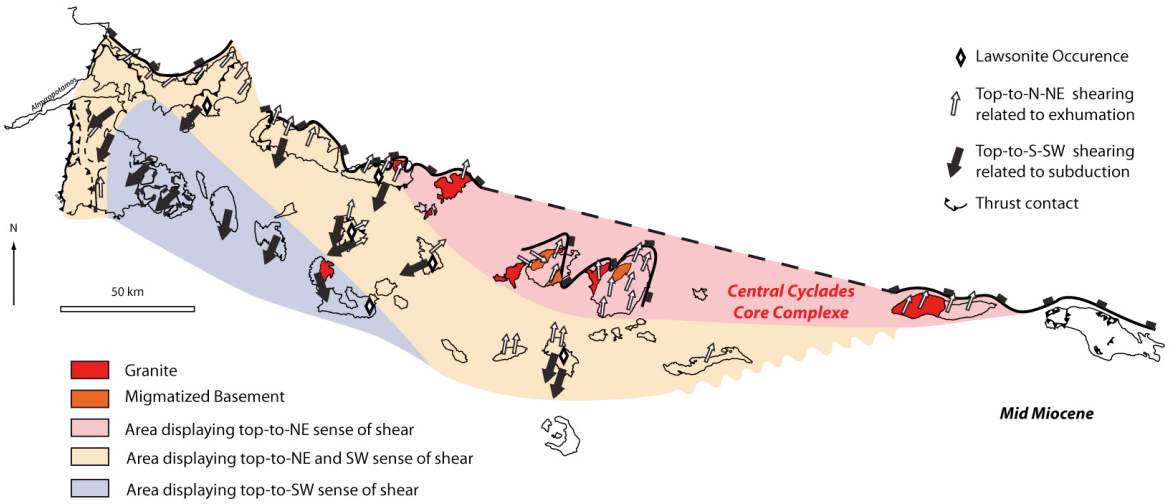

Fig. VIII-18. Restored map of the Cyclades at the end of middle Miocene, showing three domains characterized by only top-to-SW shear (center: Red), only top-to-SW shear (to the SW: blue) and by both senses of shear (Orange).

8.7. Discussion

This regional-scale study of the Cycladic blueschists shows i) that the timing and kinematics of ductile fabrics and their relation with metamorphism have recorded both subduction and exhumation and ii) that exhumation occurred in three major stages (Fig. VIII-19). Some of these outcomes deserve discussion with reference to previous studies.

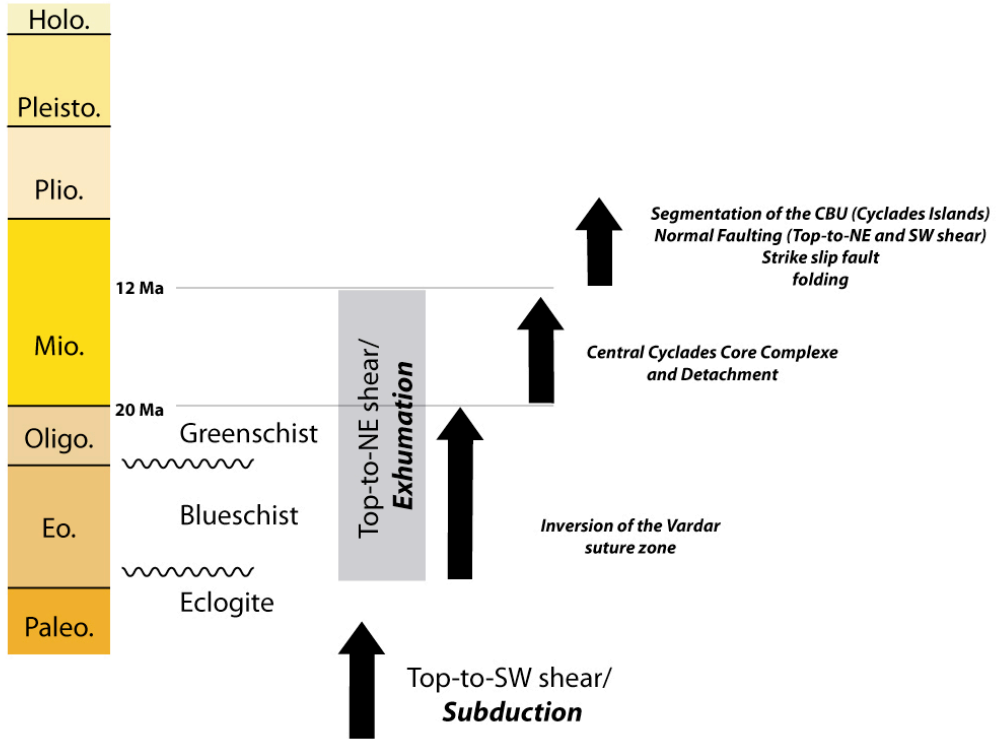

Fig. VIII-19. Synthetic table of the timing and kinematics of the deformation event that affected the CBU from early Eocene to present day.

8.7.1. Senses of shear and their relation to subduction and exhumation

Since more than 15 years most studies have reported evidence for both top to NE and SW shear in the Cycladic blueschists (Gautier and Brun, 1994a and b; Jolivet and Patriat, 1999; Trotet et al., 2001a; Parra et al., 2002; Rosenbaum et al., 2002; Mehl et al., 2005; Bond et al., 2007; Tirel al., 2009). In almost all studies it has been attempted to interpret these deformations with opposite senses of shear in the frame of the CBU exhumation controlled by extensional detachments dipping either to the NE (Gautier et al., 1993; Gautier and Brun 1994 a and b; Ring et al., 2003; Huet et al., 2009) or to the SW (Lister et al., 1984; Forster and Lister, 2010; Iglseder et al., 2009). The superposition of ophiolitic melange or gneissic basement on top of marble-schist sequences and the presence of undeformed lawsonite pseudomorphs show that the CBU has recorded subduction-related thrusting. The associated sense of shear is top to S or SW. Distributed extension that accommodated the segmentation of the CBU between 12 and 8 Ma gave semi-brittle deformation with also top to SW shear. This points out that senses of shear must be handled with care and in particular that relative and absolute

chronological evidence is essential to elaborate kinematic interpretations at either local or regional scales in terms of subduction and exhumation.

Evidence of top to SW shear either due to pre-Lutetian subduction-related thrusting or to post-12 Ma semi-brittle extension has previously been considered synchronous to top to NE shear. Attempts were made to interpret them as conjugate senses of shear in the two flanks of core complexes most often at the scale of given islands. Available chronological data summarized in the present paper show that both top to NE and SW shears developed at different periods, due to either thrusting or extension and from fully ductile to semi-brittle conditions, from Paleocene to late Miocene –i.e. over a time span of 40 Ma.

8.7.2. Two separate stages of top to NE shear related to exhumation

A two-stage exhumation pattern was first revealed by the PT-path recorded in Tinos blueschists (Fig. 14 in Parra et al., 2002). Two decompression events occurred 18 to 10 Kb before 37 Ma and from 10 to 1 Kb between 30 and 20 Ma. In the time interval between these two decompression events (From 37 to 30 Ma), rocks underwent an isobaric temperature increase from 400 to 575°C. This was interpreted as a two-fold exhumation history within an accretionary prism (Fig. 15 in Parra et al., 2002): A first "cold" (syn-orogenic) uplift before 37 Ma followed by a warmer exhumation accommodated by a NE dipping detachment between 30 and 20 Ma.

The evidence for two top to NE shearing events is demonstrated by the cross-cutting at right angle of the Pindos suture zone by the North Cycladic Detachment in Evvia (Fig. VIII-1). The Pelagonian units lying on top of the Pindos suture are also affected by a metamorphism with PT conditions of 10-11 Kb and 500-550°C around 110 Ma (Perraki et al., 2003) and by top to NE shear (Walcott and White, 1998). Therefore, a first top to NE shearing event occurred prior to the onset of the North Cycladic Detachment. Because the CBU is not affected by top to NE shear in its southern part (Fig.1 VIII-18) the Pindos suture has not been reactivated in extension during the first stage of exhumation. It is the inversion in extension of the Vardar suture that accommodated the first stage of the CBU exhumation together with the overlying Pelagonian units (Brun and Faccenna, 2008). This first stage of exhumation likely occurred between 45 (Thrusting above Lutetian flysch in Evvia) and 37 Ma. The North

Cycladic Detachment System started to develop at 30 Ma crosscutting the previous structures and in particular the Pindos suture.

8.7.3. How many detachments? How many core complexes?

The restoration of the CBU geometry prior to the post-12 Ma segmentation shows that the post 30 Ma exhumation history corresponds to a single core complex at Cyclades-scale associated to a single detachment dipping to the NE (Fig. VIII-18).

In many previous studies, two types of interpretations prevailed. Some models considered either several coeval detachments all NE-dipping (Gautier and Brun, 1994a and b; Jolivet et al., 2004, 2010; Tirel et al., 2009) or divergent detachments NE-dipping to the NE and SW-dipping to the SW (Fig. 7 in Ring et al., 2010). As summarized in Fig. VIII-19, top to SW shear is not associated to an extensional detachment but to subduction-related thrusting prior to 45 Ma. Our restoration (Fig. VIII-15) shows that the Naxos-Paros detachment is in fact a part of the North Cycladic Detachment Systems. Finally, some previously invoked detachments are post-12 Ma extensional systems that developed in semi-brittle conditions (Fig. 17b).

Conclusion

The tectonic history of the Cycladic Blueschist Unit can be summarized in five main stages as follow:

1/ Prior to Lutetian, ophiolitic units belonging to the Pindos ocean and metamorphosed in the eclogite facies, were thrust toward the SW on top of the sedimentary cover of the northern Adria continental margin inside a NE-dipping subduction.

Subduction-related thrusting involving the Adria margin units –i.e sedimentary cover and gneissic basement terminated in Lutetian time

2/ A first stage of exhumation from mantle depths to lower crustal levels with a top to NE shear occurred before 37 Ma was accommodated by an extensional inversion of the Vardar suture zone.

3/ A second stage of exhumation from deep crustal levels to near surface still with top to NE shear occurred between 30 and 20 Ma was accommodated by the North Cycladic Detachment. It is during this stage that the Central Cyclades Core Complex exhumed.

4/ After 12 Ma the CBU has been segmented by normal faults. Block rotation and folding with NS-trending axes were dominantly controlled by the Myrthes-Ikaria strike-slip fault in the centre of the Cyclades.

Acknowledgements

The present work was financially supported by the ANR-EGEO project. We are extremely grateful to L. Jolivet for having introduced us to Syros geology and for the field trip that he organised especially for us in Tinos and Mykonos. Discussions at various stages of the project with L. Jolivet, P. Agard, B. Huet, and L. Labrousse, in particular within the framework of the ANR-EGEO project, have been very useful and stimulating. However, the data and interpretations presented here are our entire our own.

References

Altherr R., Schliestedt M., Okrusch M., Seidel E., Kreuzer H., Harre W., Lenz H., Wendt I. and G. A. Wagner (1979), Geochronology of high-pressure rocks on Sifnos (Cyclades, Greece). Contributions to Mineralogy and Petrology 70, 245-255.

Altherr, R., Kreuzer, H., Wendt, I., Lenz, H., Wagner, G.A., Keller, J., Harre, W. and A. Höhndorf. 1982. A late Oligocene/Miocene high temperature belt in the Attic-Cycladic crystalline complex (SE Pelagonian, Greece). Geol. Jb., E23, 67-164.

Amante, C. and B. W. Eakins. 2009. ETOPO1 1 Arc-Minute Global Relief Model: Procedures, Data Sources and Analysis. NOAA Technical Memorandum NESDIS NGDC. 24-19.

Andriessen, P., Boelrijk, N., Hebeba, E., Priem, N., Verdurmen, E. and R. Vershure. 1979. Dating the events of metamorphism and granitic magmatism in the alpine orogen of Naxos (Cyclades, Greece). Contribution to Mineralogy and Petrology 69, 215– 225.

Andriessen, P, Banga, G. and E. H. Hebeda. 1987. Isotopic age study of pre-Alpine rocks in the basal units on Naxos, Sikinos and Ios, Greek Cyclades. Geol. Mijnbouw 66, 3 – 14.

Angelier, J. 1977. Essai sur la néotectonique et les derniers stades tarditectoniques de l'arc Egéen et de l'Egée méridionale. Bulletin de la société géologique de France XIX (3), 651-662.

Avigad, D. and Z. Garfunkel. 1989. Low angle faults above and below a blueschists belt : Tinos Island, Cycaldes, Greece. Terra Nova 1, 182-187.

Avigad, D., Matthews, A., Evan, W. and Z. Garfunkel. 1992. Cooling during the exhumation of a blueschist terrane : Sifnos (Cyclades), Greece. European Journal of Mineralogy 4 (3), 619-634.

Avigad, D., Jolivet, L. and J.M. Azañon. 1997. Back arc extension and dénudation of mediterranean éclogites. Tectonics 16 (6), 924-941.

Avigad, D. 1998. High-pressure metamorphism and cooling on SE Naxos (Cyclades, Greece). Euroepan Journal of Mineralogy 10, 1309-1319.

Avigad, D., Baer, G. and A. Heimann. 1998. Block rotations and continental extension in the central Aegean Sea: palaeomagnetic and structural evidence from Tinos and Mykonos (Cyclades, Greece). Earth and Planetary Science Letters 157, 23-40.

Avigad, D., Ziv, A. and Z. Garfunkel. 2001. Ductile and brittle shortening, extension-parallel folds and maintenance of crustal thickness in the central Aegean (Cyclades, Greece). Tectonics 20 (2), 277-287. doi:10.1029/2000TC001190.

Baldwin, S. L. 1996. Contrasting P-T-t histories for blueschists from the western Baja Terrane and the Aegean; effects of syn-subduction exhumation and backarc extension, in Subduction: Top to bottom. Geophys. Monogr., vol. 96, edited by G. E. Bebout et al., pp. 135 – 141, AGU, Washington, D. C.

Baldwin, S. L., and G. S. Lister. 1998. Thermochronology of the South Cyclades Shear Zone, Ios, Greece; effects of ductile shear in the argon partial retention zone. Journal of Geophysical Research 103, 7315 – 7336. doi:10.1029/97JB03106.

Baziotis, I. 2008. Petrological and Geochemical study of the metamorphic rocks from east Attica. Ph.D. Thesis, National Technical University of Athens, Greece.

Bond, C., Butler, R. and J. Dixon. 2007. Co-axial horizontal streching within extending orogens: the exhumation of HP rocks of Syros (Cyclades) revisited. In: Ries, A., Butler, R. and Graham, R. (Eds), Deformation of the continental crust: The legacy of Mike Coward. Geological Society, London Special Publications 272. pp. 203-222. Doi : 10.1144/GSL.SP.2007.272.01.12.

Bonneau, M., Blake, M.J.C., Gueyssant, J., Kienast, J.R., Lepvrier, C., Maluski, H. and D. Papanikolaou. 1980 a. Sur la signification des séries métamorphiques (schistes bleus) des cyclades (Héllènides, Grèce). L'exemple de l'île de Syros. Comptes rendus de l'académie des sciences Paris 290, 1463-1466.

Bonneau, M., Gueyssant, J., Kienast, J.R., Lepvrier, C. and H. Maluski. 1980 b. Tectonique et métamorphisme Haute pression d'âge Eocène dans les Hellénides : exemple de l'île de Syros (Cyclades, Grèce). Comptes rendus de l'académie des sciences Paris 291, 171-174.

Bonneau, M.B. and J.R. Kienast. 1982. Subduction, collision et schistes bleu: exemple de l'Egée, Grèce. Bulletin de la société Géologique de France 7, 785-791.

Bonneau, M. 1984. Correlation of the Hellenide nappes in the south-east Aegean and their tectonic reconstruction. Geological Society, London, Special Publications 17, 517-527.

Brichau, S., Ring, U., Ketcham, R., Carter, A., Stockli, D. and M. Brunel. 2006. Constraining the long-term evolution of the slip rate for a major extensional fault system in the central Aegean, Greece, using thermochronology. Earth and Planetary Science Letters 241, 293–306. doi:10.1016/j.epsl.2005.09.065.

Brichau, S., Ring, U., Carter, A., Monié, P., Bolhar, R., Stockli, D. et al. 2007. Extensional faulting on Tinos Island, Aegean Sea, Greece: how many detachments? Tectonics 26, TC4009. doi: 10.1029/2006TC001969.

Brichau, S., U. Ring, A. Carter, R. Bolhar, P. Monie, D. Stockli, and M. Brunel. 2008. Timing, slip rate, displacement and cooling history of the Mykonos detachment footwall, Cyclades, Greece, and implications for the opening of the Aegean Sea basin, J. Geol. Soc., 165, 263 – 277, doi:10.1144/0016- 76492006-145.

Brichau, S., Thomson, S. and U. Ring. 2010. Thermochronometric constraints on the tectonic evolution of the Serifos detachment, Aegean Sea, Greece. Int J Earth Sci (Geol Rundsch) 99, 379–393. doi : 10.1007/s00531-008-0386-0.

Bröcker, M., Kreuzer, H., Matthews, A. & Okrusch, M. 1993. 40Ar/39Ar and oxygen isotope studies of polymetamorphism from Tinos Island, Cycladic blueschist belt. Journal of Metamorphic Geology, 11, 223-40.

Bröcker, M. and Franz, L. 1998. Rb-Sr isotope studies on Tinos Island (Cyclades, Greece): additional time constraints for metamorphism, extent of infiltration-controlled overprinting and deformational activity. Geological Magazine, 135 (3), 369 - 382.

Bröcker, M. and M. Enders. 2001. Unusual bulk-rock compositions in eclogite-facies rocks from Syros and Tinos (Cyclades, Greece): implications for U-Pb zircon geochronology. Chemical Geology, 175, 581-603.

Bröcker, M. and L. Franz. 2006. Dating metamorphism and tectonic juxtaposition on Andros Island (Cyclades, Greece): results of a Rb–Sr study. Geological Magazine 143, 609-620.

Bröcker, M. and A. Keasling. 2006. Ionprobe U–Pb zircon ages from the high-pressure/ low temperature mélange of Syros, Greece: age diversity and the importance of pre-Eocene subduction. Journal of Metamorphic Geology 24, 615–631.

Brun, J.P. and C. Faccenna. 2008. Exhumation of high-pressure rocks driven by slab rollback. Earth and Planetary Science Letters 272, 1–7. doi:10.1016/j.epsl.2008.02.038

Brun, J.P. and D. Sokoutis. 2010. 45 m.y. of Aegean crust and mantle fl ow driven by trench retreat. Geology 38 (9), 815–818. doi: 10.1130/G30950.1.

Btittner, D. and G. Kowalczyk. 1978. Late Cenozoic stratigraphy and paleogeography of Greece- A review. In Alps, Apennines and Hellenides. Edited by H. Closs et al., IUCG Sci.

Rep., 38, 494-501.

Bulle, F., Bröcker, M., Gärtner, C. and A. Keasling. 2010. Geochemistry and geochronology of HP mélanges from Tinos and Andros, Cycladic blueschist belt, Greece. Lithos 117 (1-4), 61-81. doi:10.1016/j.lithos.2010.02.004.

Dubois, R. and Bignot G. 1979. Presence d'un "hardground" nummulitique au de la serie crétacée d'Almyropotamos (Eubee meridionale, Grece). Paris, Academie des Sciences Comptes Rendus, 289, 993–5.

Dürr, S.T., Altherr, R., Keller, J., Okrusch, M. and E. Seidel. 1978. The median Aegean Crystaline Belt: Stratigraphy, structure, metamorphism, magmatism, In Alp, Appenines, Hellenides (eds H. Cloos, D. Roeder and K. Schmidt), p. 455–77.

Dürr, S. 1985. Geological Map of Greece, 1:50 000. Amorgos–Donoussa Sheet. Institute of Geological and Mining Research, Athens.

Engels, M. and T. Reischmann. 1999. Geochronology of the Pre-Alpine Basement of the Central Cyclades, Greece. Journal of Conference Abstracts 4, 806, EUG 10.

Faure, M. and M. Bonneau. 1988. Données nouvelles sur I'extension néogène de I'Egée: la déformation ductile du granite miocene de Mykonos (Cyclades, Grèce). Comptes rendus de l'académie des sciences Paris, 307, 1553-1559.

Forster, M. and G. Lister. 2005. Several distinct tectono-metamorphic slices in the Cycladic eclogite–blueschist belt, Greece. Contributions to Mineralogy and Petrology, 150 (5), 523-545. doi: 10.1007/s00410-005-0032-9.

Forster, M.A. and G.S. Lister. 2009. Core complex related extension of the Aegean lithosphere initiated at the Eocene-Oligocene transition. Journal of Geophysical Research (Solid Earth), 114, B02401, 36 PP. doi:10.1029/2007JB005382.

Forster, M.A. and G.S. Lister. 2010. Argon enters the retentive zone: reassessment of diffusion parameters for K-feldspar in the South Cyclades Shear Zone, Ios, Greece. In: Ring, U., Brandon, M.T., Lister, G.S. and Willett, S.D. (Eds). Advances in interpretation of geological processes: refinement of multi-scale data and integration in numerical modelling. Geological Society, London, Special Publication, Geological Society, London, Special Publications, 2010, 332, 17-34. doi: 10.1144/SP332.2.

Fytrolakis, N., Papanikolaou, D. and A. Panagopoulos. 1981. Stratigraphy and structure of Amorgos Island, Aegean Sea. Annales Géologiques des Pays Helléniques, 30, 455–472.

Gautier, P., Ballèvre, M., Brun, J.P. and L. Jolivet. 1990. Extension ductile et bassins sedimentaires mio-pliocenes dans les Cyclades îles de Naxos et Paros). Comptes rendus de l'Académies des Sciences Paris, 310, 147-153.

Gautier, P., Brun, J.P. and L. Jolivet. 1993. Structure and kinematics of Upper Cenoizoic extensional detachment on Naxos and Paros (Cyclades Islands, Greece). Tectonics 12, 1180-1194.

Gautier, P., and J.-P. Brun. 1994a. Crustal-scale geometry and kinematics of late-orogenic extension in the central Aegean (Cyclades and Evvia Island). Tectonophysics 238, 399–424.

Gautier, P., and J. P. Brun. 1994 b. Ductile crust exhumation and extensional detachments in the central Aegean (Cyclades and Evvia islands). Geodinamica Acta 7, 57 – 85.

Gitahi, N. 2004. Geochemistry and metamorphic evolution of éclogites on Syros island, Greece. Extended Abstracts, Seventeenth Annual Keck Research Symposium in Geology Proceedings, Lexington, VA, P.81-4.

Gupta, S., and M. J. Bickle. 2004. Ductile shearing, hydrous fluid channelling and high-pressure metamorphism along the basement-cover contact on Sikinos, Cyclades, Greece, in Flow Processes in Faults and Shear Zones, edited by G. I. Alsop et al., Geol. Soc. Spec.

Publ., 224, 161 – 175, doi:10.1144/GSL.SP.2004.224.01.11.

Hejl, E., Riedl, H., Weingartner H. 2002. Post-plutonic unroofing and morphogenesis of the Attic–Cycladic complex (Aegea, Greece). Tectonophysics 349, 37– 56.

Hejl, E., Riedl, H., Soulakellis, N., Van Den Haute, P. and H. Weingartner. 2003. Young Neogene tectonics and relief development fission-track dating on the Aegean islands of Naxos, Paros and los (Cyclades, Greece). Mitt. Ostern Geol. Ges. ISSN 0251-7493 93 (2000) 105-127 Wien.

Henjes-Kunst, F. and H. Kreuzer. 1982. Isotopic dating of pre-alpidic rocks from the Island of Ios (Cyclades, Greece), Contribution to Mineralogy Petrology 80, 245 – 253, doi:10.1007/BF00371354.

Holley, E.A., Ross, T. and J.T. Cheney. 2004. Pressure-température conditions of metamorphism in eclogites, Syros, Greece. Geological Society of America, Abstracts with Programs 36 (4), 91.

Huet, B., Labrousse, L.,Jolivet, L. (2009) Thrust or detachment? Exhumation processes in the Aegean: Insight from a field study on Ios (Cyclades, Greece). Tectonics, VOL. 28, TC3007, doi:10.1029/2008TC002397.

Iglseder, C., Grasemann, B., Schneider, D. A., Petrakakis, K., Miller, C., Klötzli, U. S., Thöni, M., Zàmolyi, A. and C. Ramboussek. 2009. I and S-type plutonism on Serifos (W-Cyclades, Greece). Tectonophysics 473 (1-2), 69-83. doi:10.1016/j.tecto.2008.09.021.

Jolivet, L. and M. Patriat. 1999. Ductile extension and the formation of the Aegean Sea. Geological Society, London, Special Publications 156, 427-456. doi: 10.1144/GSL.SP.1999.156.01.20.

Jolivet, L. and P. Goffé. 2000. Les dômes métamorphiques extensifs. Comptes rendus de l'académie des Sciences 320, 739-751.

Jolivet, L., Faccenna, C., Goffé, B., Burov, E. and P. Agard. 2003. Subduction tectonics ans exhumation of high-pressure metamorphic rocks in the Mediterranean orogens. American Journal of Science 303, 353- 409.

Jolivet, L., Famin, V., Mehl, C., Parra, T., Aubourg, C., Hébert, R. and P. Philippot. 2004. Progressive strain localisation, boudinage and extensional metamorphic complexes, the Aegean Sea case. In: Whitney, D.L., Teyssier, C., Siddoway, C.S. (Eds.), Gneiss Domes in Orogeny: Geological Society of America Special Paper 380. Geological Society of America, Boulder, Colorado, pp. 185–210.

Jolivet, L., Trotet, F., Monié, P., Vidal, O., Goffé, B., Labrousse, L., Agard, P. and B. Ghorbal. 2009. Along-strike variations of P–T conditions in accretionary wedges and syn-orogenic extension, the HP–LT Phyllite–Quartzite Nappe in Crete and the Peloponnese. Tectonophysics 480 (1-4), 133-148. doi:10.1016/j.tecto.2009.10.002.

Jolivet, L. and J.P. Brun. 2010. Cenozoic geodynamic evolution of the Aegean. International Journal of Earth Sciences 99 (1), 109-138. doi:10.1007/s00531-008-0366-4.

Jolivet, L., Lecomte, E., Huet, B., Denèle, Y., Lacombe, O., Labrousse, L., Le Pourhiet, L. and C. Mehl. 2010. The North Cycladic Detachment System. Earth and planetary Science Letters 289, 87–104. doi:10.1016/j.epsl.2009.10.032.

Katsikatso, G., Migiros, G., Triantafillis, M. and A. Mettos. 1986 a. Geological structure of Internal Hellenides (E. Thessaly — SW Macedonia, Euboa–Attica–Northern Cyclades Islands and Lesvos). Geological and Geophysical Research, Special Issue 191–212.

Katsikatsos, G., Dounas, A. and P. Gaitanakis. 1986 b. Geological Map of Greece, Athinai–Elefsis Sheet 1.50.000, I.G.M.E., Athens.

Katzir, Y., Garfunkel, Z., Avigad, D. and A. Matthews. 2008. Diverse P-T paths for the Cycladic ultramafic rock associations: Constraints on their origin, emplacement and exhumation. IOP Conf. Ser.: Earth Environ. Sci. 2 012018.

Keay, S. 1998. The geological evolution of the Cyclades, Greece: constraints from SHRIMP U–Pb geochronology. Ph.D. thesis, Australian National University, Canberra, pp. 335.

Keay, S., Lister, G. and I. Buick. 2001. The timing of partial melting, Barrovian metamorphism and granite intrusion in the Naxos metamorphic core complex, Cyclades, Aegean Sea, Greece. Tectonophysics 342, 275– 312.

Keiter, M., Piepjohn, K., Ballhaus, C., Lagos, M. and M. Bode. 2004. Structural development of high-pressure metamorphic rocks on Syros Island (Cyclades, Greece). Journal of Structural Geology 26 (8), 1433-1445. doi:10.1016/j.jsg.2003.11.027.

Klein-Helmkamp, U., Reinecke, T.B. Stöckhert. 1995. The aragonite-calcite transition in LT-HP metamorphic carbonatic rocks from S-Evia, Greece: the microstructural and compositional record. Bochumer Geologische und Geotektonische Arbeiten 44, 78-83.

Kreutzer, H., Harbe, W., Lenz, H., Wendt, I.F. Henjes-Kunst. 1978. K/Ar- und Rb/Sr-Daten von Mineralen aus dem polymetamorphen Kristallin der Kykladen-Insel Ios (Griechenland). Fortschr. Miner. 56 (1), 69-70, 1978.

Kumerics, C., Ring, U., Brichau, S., Glodny, J. and P. Monié. 2005. The extensional Messaria shear zone and associated brittle detachment faults, Aegean Sea, Greece. Geological Society of London 162, 701-721.

Lagos M., Münker C., Tomaschek F. and C. Ballhaus (2002), Geochemistry and Lu-Hf geochronology of the metavolcanic Grizzas sequence in northern Syros (Cyclades, Greece). European Journal of Mineralogy 14 (1), 97.

Lagos, M., Scherer, E.E., Tomaschek, F., Münker, C., Keiter, M., Berndt, J. and C. Ballhaus. 2007. High précision Lu-Hf geochronology of Eocene éclogite facies rocks from Syros, Cyclades, Greece. Chemical geology 243 (1-2), 16-35. doi:10.1016/j.chemgeo.2007.04.008.

Liati, A., Skarpelis, N. and G. Pe-Piper. 2009. Late Miocene magmatic activity in the Attic-Cycladic Belt of the Aegean (Lavrion, SE Attica, Greece): implications for the geodynamic evolution and timing of ore deposition. Geological Magazine 146, 732-742.

Lister, G. S., Banga, G. and A. Feenstra. 1984. Metamorphic core complexes of cordilleran type in the Cyclades, Aegean Sea, Greece. Geology 12, 221-225. doi:10.1130/0091-7613(1984)12<221:MCCOCT>2.0.CO,2.

Maluski, H., Vergely, P., Bavay, D., Bavay, P. and G. Katsikatsos. 1981. 39Ar/40Ar dating of glaucophane and phengites in southern Euboa (Greece) geodynamic implications. Bulletin de la Société Geologique de France V, 469–476.

Maluski, H., Bonneau, M., and J.R. Kienast. 1987. Dating the metamorphic events in the Cycladic area: 40Ar/39Ar data from metamorphic rocks of the island of Syros (Greece), Bulletin de la Société géologique de France III, 833-841.

Martin L., Duchêne S., Deloule E. and O. Vanderhaeghe. 2006. The isotopic composition of zircon and garnet: A record of the metamorphic history of Naxos, Greece, Lithos 87, 174–192.

Mascle, J. and L. Martin. 1990. Shallow structure and recent evolution of the Aegean Sea: A synthesis based on continuous reflection profiles. Marine Geology 94, 271–299. doi: 10.1016/0025-3227(90)90060-W.

Matthews, A. and M. Schliestedt. 1984. Evolution of the blueschist and greenschist facies rocks of Sifnos, Cyclades, Greece. Contributions to Mineralogy and Petrology 88, 150–163.

Mehl, C., Jolivet, L. and O. Lacombe. 2005. From ductile to brittle: evolution and localization of deformation below a crustal detachment (Tinos, Cyclades, Greece). Tectonics 24, TC4017. doi:10.1029/2004TC001767.

Mehl, C., Jolivet, L., Lacombe, O., Labrousse, L. and G. Rimmelé. 2007. Structural evolution of Andros island (Cyclades, Greece): a key to the behaviour of a !at detachment within an extending continental crust. In: Taymaz, T., Dilek, Y., Ylmaz, Y. (Eds.), The Geodynamics of the Aegean and Anatolia. Special Publications. Geological Society, London, pp. 41–73. doi:10.1144/SP291.3 0305-8719/07/$15.00.

Meulenkamp, J.E. 1979. The Aegean and the Messinian salinity crisis: Proc. of the VI Coll. On the Geology of the Aegean Region, v. 3, p. 1253- 1263.

Morris, A. and M. Anderson. 1996. First palaeomagnetic results from the Cycladic Massif, Greece, and their implications for Miocene extension directions and tectonic models in the Aegean. Earth and Planetary Science Letters 142 (3-4), 397-408.

Papanikolaou, D. 1978. Contribution to the geology of the Aegean Sea; the island of Andros. Annales Geologiques des Pays Helleniques 29(2), 477–553.

Papanikolaou, D. 1980. Contribution to the geology of Aegean Sea: the island of Paros, Annal. Géol. Pays Helléniques 30 (1), 65–96.

Papanikolaou, D.J. and L.H. Royden. 2007. Disruption of the Hellenic arc: Late Miocene extensional detachment faults and steep Pliocene-Quaternary normal faults—Or what happened at Corinth? tectonics 26, TC5003. doi:10.1029/2006TC002007.

Parra, T., Vidal, O. and L. Jolivet. 2002. Relation between the intensity of deformation and rétrogression in blueschist metapelites of Tinos Island (Greece) evidenced by chlorite–mica local equilibria. Lithos 63, 41– 66.

Pe-Piper, G. and D.J.W . Piper. 2002. The igneous rocks of Greece The anatomy of an orogen. Ed. Beiträge zur Regionalen Geologie der Erde, 573 pp. ISBN 978-3-443-11030-7.

Pe-Piper, G. and D. J. W. Piper. 2007. Neogene back-arc volcanism of the Aegean: new insights into the relationship between magmatism and tectonics. in Cenozoic Volcanism in the Mediterranean Area, edited by L. Beccaluva and G. Bianchini, Geological Society of America, pp. 17–31. doi: 10.1130/2007.2418(1102).

Perraki, M., Hoinkes, G., Mposkos, E. and M. Thoeni. 2003. Early Cretaceous and Tertiary metamorphic events of the Pelagonian Zone in the E. Thessaly area, Greece. Geophysical Research Abstracts 5, 04438.

Philippon, M., Brun, J.P. and F. Gueydan. 2009. Kinematic records of subduction and exhumation in the Ile de Groix Blueschist (Hercynian belt, Western france). Journal of structural geology 31 (11), 1308-1321. doi: 10.1016/j.jsg2009.07.003.

Pohl, J. (1999), Geologie und Hochdruckgesteine der Insel Syros, Griechenland. Diploma thesis, Geologisches Institut, Albert-Ludwigs Universitat, Freiburg, 107 pp.

Putlitz, B., Cosca, M. A. and J.C. Schumacher. 2005. Prograde mica 40Ar/39Ar growth ages recorded in high pressure rocks (Syros, Cyclades, Greece). Chemical Geology 214 (1-2), 79-98. doi:10.1016/j.chemgeo.2004.08.056.

Ridley, J. 1982. Arcuate lineation trends in a deep level, ductile thrust belt, Syros, Greece. Tectonophysics 88 (3-4), 347-360. doi:10.1016/0040-1951(82)90246-3.

Ring, U., Layer, P. W. and T. Reischmann. 2001. Miocene high-pressure metamorphism in the Cyclades and Crete, Aegean Sea, Greece: Evidence for large-magnitude displacement on the Cretan detachment. Geology 29, 395 – 398.

Ring, U. and T. Reischmann. 2002. The weak and superfast Cretan detachment, Greece:

Exhumation at subduction rates in extruding wedges. Journal of the Geological Society, London. 159, 225-228.

Ring, U. and P.W. Layer. 2003. High-pressure metamorphism in the Aegean eastern mediterranean : Underplating and exhumation from the late cretaceous until the Miocene to Recent above the retrreating Hellenic subduction zone. Tectonics 22 (1022), 23 pp. doi:10.1029/2001TC001350.

Ring, U., Thomson, S.N., Bröcker, M. 2003. Fast extension but little exhumation : the Vari detachment in the Cyclades, Greece. Geological magazine, 140, (3), p 245-252. DOI: 10.1017/S0016756803007799.

Ring U. 2007. The Geology of Ikaria Island: The Messaria extensional shear zone, granites and the exotic Ikaria nappe. Journal of the Virtual Explorer 27, Paper 3, doi:10.3809/jvirtex.2007.00171.

Ring, U., Okrusch, M. and T. Will. 2007. Samos Island, Part I: metamorphosed and nonmetamorphosed nappes, and sedimentary basins. Journal of the Virtual Explorer 27, paper 5. doi:10.3809/jvirtex.2007.00180.

Ring, U., and C. Kumerics. 2008. Vertical ductile thinning and its contribution to the exhumation of highpressure rocks: The Cycladic blueschist unit in the Aegean. Tectonics 165 (6), 1019-1030.

Ring, U., Glodny, J., Thomas, W. and S. Thomson. 2010. The Hellenic Subduction System: High-Pressure Metamorphism, Exhumation, Normal Faulting, and Large-Scale Extension. Annual Review of Earth and Planetary Sciences 38, 45-76.

Rosenbaum, G., Avigad, D. and M. Sánchez-Gómez. 2002. Coaxial flattening at deep levels of orogenic belts: evidence from blueschists and eclogites on Syros and Sifnos (Cyclades, Greece). Journal of Structural Geology 24 (9), 1457-1462. doi:10.1016/S0191-8141(01)00143-2.

Rosenbaum, G. and U. Ring. 2007. Structure and metamorphism of Amorgos: a field excursion. Journal of the Virtual Explorer, Volume 27, Paper 7.

Schliestedt, M., Bartsch, V., Carl, M., Matthews, A. and F. Henjes-Kunst. 1994. The P–T path of greenschist-facies rocks from the island of Kithnos (Cyclades, Greece). Chemie Erde 54, 281–296.

Schmädicke, E., and T.M. Will. 2003. Pressure-temperature evolution of blueschist facies rock from Sifnos, Greece, and implications for the exhumation of high-pressure rocks in the central Aegean. Journal of Metamorphic Geology 21, 799 – 811, doi:10.1046/ j.1525-1314.2003.00482.x.

Schumacher, J.C.B., Brady, J., Cheney, J.T. and R.R. Tonnsen. 2008. Glaucophane bearing Marbles on Syros, Greece. Journal of Petrology 49 (9), 1667-1686. doi:10.1093/petrology/egn042.

Shaked, Y., Avigad, D. and Z. Garfunkel. 2000. Alpine high-pressure metamorphism at the Almyropotamos window (southern Evia, Greece). Geological Magazine 137 (4), 367–380.

Stouraiti, C., Mitropoulos, P., Tarney, J., Barreiro, B., McGrath, A.M. and E. Baltatzis. 2010. Geochemistry and petrogenesis of late Miocene granitoids, Cyclades, southern Aegean: Nature of source components. Lithos 114, 337–352.

Tirel, C., Gautier, P., van Hinsbergen, D.J.J., and M.J.R. Wortel. 2009. Sequential development of interfering metamorphic core complexes: numerical experiments and comparison with the Cyclades, Greece. Geological Society, London, Special Publications 311, 257-292.

Tomaschek, F. and C. Ballhaus. 1999. TheVari Unit on Syros (Aegean Sea) and its relation to the Attic-Cycladic Crystalline Complex. Journal of Conference Abstracts 4, 72.

Tomaschek, F., Kennedy, A., Keay, S. and C. Ballhaus. 2001. Geochronological constraints on Carboniferous and Triassic magmatism in the Cyclades: SHRIMP U---Pb ages of zircons from Syros, Greece. Journal of Conference Abstracts 6(1), 315.

Tomaschek, F., Kennedy, A. K., Villa, I.M., Lagos, M. and C. Ballhaus. 2003. Zircons from Syros, Cyclades, Greece. Recrystallization and mobilization of zircon during high-pressure metamorphism. Journal of Petrology 44, 1977-2002.

Trotet, F., Jolivet, L. and O. Vidal. 2001a. Tectono-metamorphic evolution of Syros and Sifnos islands (Cyclades, Greece). Tectonophysics 338, 179-206.

Vandenberg, L.C. and G.S.Lister. 1996. Structural analysis of basement tectonics fromthe Aegean metamorphic core complex of Ios, Cyclades, Greece. Journal of structural geology 18, 1437–1454.

Van der Maar, P., and J. B. H. Jansen. 1983. The geology of the polymetamorphic complex of Ios, Cyclades, Greece and its significance for the Cycladic Massif, Geol. Rundsch. 72, 283 – 299. doi:10.1007/ BF01765910.

van Hinsbergen, D.J.J., Langereis, C.G. and J.E. Meulenkamp. 2005. Revision of the timing, magnitude and distribution of Neogene rotations in the western Aegean region. Tectonophysics 396, 1–34. doi: 10.1016/j.tecto.2004.10.001.

Walcott, C.R. and S.H. White. 1998. Constraints on the kinematics of post-orogenic extension imposed by stretching lineations in the Aegean region. Tectonophysics 298, 155–175. doi : 0040-1951/98/$19.00.

Wijbrans, J. R., and I. McDougall 1986. 40Ar/39Ar dating of white micas from an alpine high-pressure metamorphic belt on Naxos (Greece): The resetting of the argon isotopic system. Contrib. Mineral. Petrol. 93, 187 – 194, doi:10.1007/BF00371320.

Will, T., M. Okrusch, E. Schmädicke, and G. Chen. 1998. Phase relations in the greenschist-blueschist-amphibolite-eclogite facies in the system Na2O-CaO-FeO-MgO-Al2O3-SiO2 – H2O (NCFMASH), with application to metamorphic rocks from Samos, Greece. Contrib. Mineral. Petrol., 132, 85 – 102, doi:10.1007/s004100050406.

Wortel, M.J.R., and W. Spakman. 2000. Subduction and slab detachment in the Mediterranean-Carpathian region. Science 290, 1910–1917, doi:10.1126/science.290.5498.1910.

Ziv, A., Katzir, Y., Avigad, D. and Z. Garfunkel. 2010. Strain development and kinematic significance of the Alpine folding on Andros (western Cyclades, Greece). Tectonophysics 488 (1-4), 248-255.

Chapitre 9: L'extension Egéenne et extrusion de l'Anatolie depuis 15 Ma.

AEGEAN EXTENSION AND ANATOLIA ESCAPE SINCE 15 MA.

Melody Philippon[1], Jean-Pierre Brun[1], Frédéric Gueydan[1] and Dimitrios Sokoutis[2].

[1] Géosciences Rennes UMR 6118 CNRS, Université de Rennes 1, 35042 Rennes cedex, France

[2] Faculty of Earth and Life Sciences, VU (Vrije Universiteit) University Amsterdam, De Boelelaan 1085, 1081 HV Amsterdam, Netherlands

Manuscript in preparation

Abstract

Aegean extension is driven by the slab rollback of the Hellenic subduction since about 45 Ma. The North Anatolian Fault that propagated into the Aegean domain about 5 Ma ago resulted from the westward displacement of Anatolia in late Neogene. However, EW-trending deformation in the centre of Aegean suggests that the interaction between subduction and Anatolia escape started around 12 Ma. Using laboratory experiments, we show that the deformation pattern of Aegean extension depends i) on the ratio of trench retreat and Anatolia escape velocities and ii) on the presence of rheological zones of weakness inherited from the previous tectonic history.

9.1. Introduction

The Aegean region is a natural laboratory for studying lithospheric scale extensional deformation triggered by slab retreat (Mc Kenzie 1972). The active Aegean extension is controlled to the south by the retreat of Hellenic trench (western and southern boundary) at a velocity Vpull= 33 mm.y-1, and, to the east, the latitudinal east to west displacement of the Anatolia at a velocity Vpush= 21 mm.y-1 (McClusky et al., 2000) (Fig. IX-1).

The active Hellenic trench ends laterally at the Kephalonia Fault (KF) that corresponds at surface to the boundary between the downgoing slab and the locked continental collision to the northwest (Papanikolaou and Royden 2007) (Fig. IX-1) and that acts as a pivot around which the trench rotates clockwise. This pivot has migrated southeastward through time from Scutary Peç in Albania in Eocene times (45 to 35 Ma) to Kefalonia, in early Miocene. A clockwise rotation of 30° to 40° of the western Aegean

domain is demonstrated by paleomagnetism (Kissel and Laj 1988). A second pivot is located to the eastern end of the trench against the Rhodes strike-slip fault (RF) that is the shallow expression of the Hellenic slab tearing occurring at depth (Brun and Sokoutis 2010) (Fig. IX-1). Rotation around that pole is estimated to 25° since Miocene (Kissel et al., 2003)

Westward displacement of Anatolia is a response to the Early Miocene Arabia-Eurasia collision (Okay et al., 2010). The North Anatolian Fault resulted from the westward extrusion of Anatolia and is active since Late Miocene (Armijo et al., 1999, Sengor et al., 2005). Oligocene dextral strike-slip faults are described in Turkey in the Uludag Massif showing that extrusion seems to have started earlier and to predate the Arabia-Eurasia collision: (Bozkurt and Oberhansli 2001, Zattin et al., 2005, Okay et al., 2008).

Aegean extension started around 45 Ma in the Rhodope Core complex (Brun & Sokoutis 2007) coeval with the onset of blueschist exhumation in the Cyclades (Brun and Faccenna2008, Jolivet and Brun 2010). A core complex started to develop in the central Cyclades around 20 Ma (Gautier and Brun 1994) (Fig. IX-1). Since late Miocene distributed extension controlled the development of sedimentary basins across the whole Aegean (Mascle and Martin 1990).

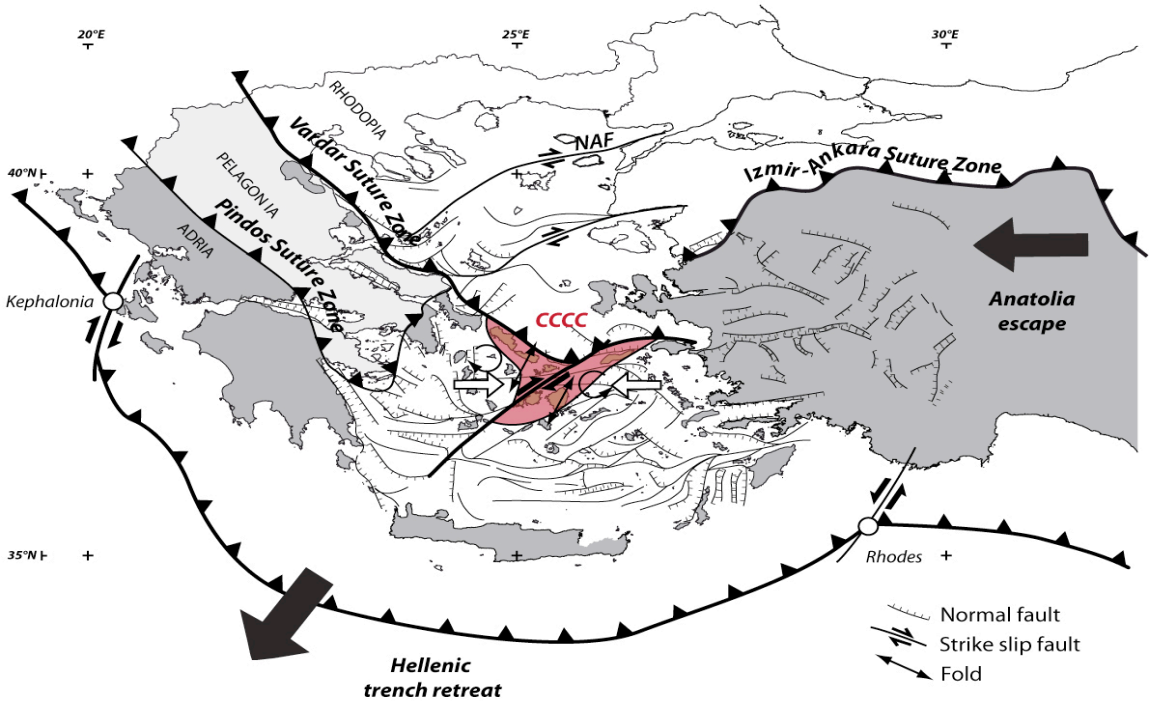

Fig. IX-1. Regional map of Greece showing the mains tectoniques features. Thrust-related strcutrures : sutures zones and present day subduction zone. Extension-related structures : The graben and hosrt network, the strike slip faults, folds and ***The Central Cyclades Core Complex (CCCC)***

Previous models of the gravitational collapse of the Hellenides, where the trench was simulated by a free boundary, showed that Aegean extension occurs prior to Anatolia extrusion (Gautier et al., 1999). In order to investigate the development of the pattern of Aegean extension from middle Miocene to present day, the experiments presented in this paper simulate different combinations of trench retreat and Anatolia escape velocities. Extension is driven by two saloon-type doors pull at constant rate Vpull to simulate the retreating trench. Anatolia escape is simulated by a N-S wall that displaces westward at constant rate Vpush. The Vardar zone that appears as a sharp limit between the north and central Aegean is represented by a weak zone in some models (see Fig. IX-1). The study concerns the relative effects of i) the ratio Vpull/Vpush and its variations in time and ii) the role of a major mechanical discontinuity at lithosphere scale such as the Vardar Suture Zone.

9.2. Effect of Input Parameters

Our experiments have been designed and calibrated in order to obtain a velocity field close to the observed GPS data (Fig. IX-2). The experimental box is 120 cm long and 60 cm wide. For easy comparison, the vertical boundaries of the model represent the North of the Aegean system. Two rotation axes control the rotation of saloon doors along the southern boundary in order to apply an extensional velocity Vpull at 5 cm/h (e.g. 5 cm/a) with an amount of retreat maximum at doors junction and linearly decreasing towards the two rotation axes. These conditions reflect the southward migration of the Hellenic trench since middle Miocene, around two rotating axes (Kephalonia, Rhodes, Fig IX-1). The whole eastern vertical boundary is moving to the west at Vpush, implying also that the eastern rotation axis in the south move toward the western rotation axis at Vpush . These boundary conditions imply that the southern part of the model, where space is created by the rotating trench, is mainly subjected to extension, the central part of the model sustains both extension driven by trench retreat and shortening induced by Anatolia escape. The eastern part is mainly dominated by the deformation related to the Anatolia escape.

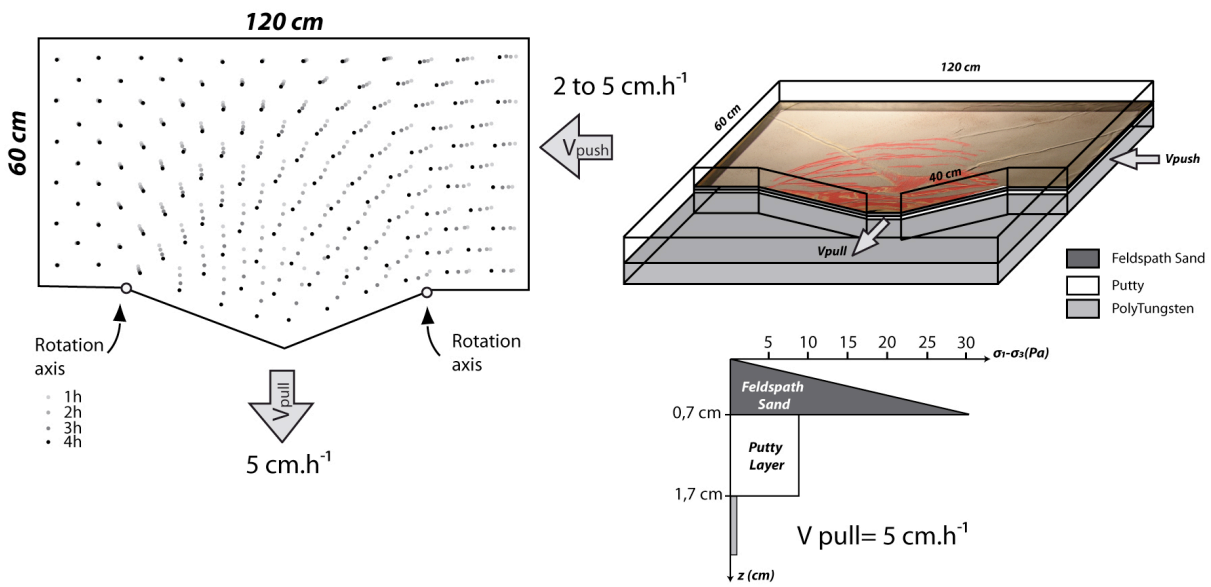

Fig. IX-2. Boundary conditions and velocity field obtain from theses conditions . Apparatus design and model's strength.

The tested parameters are i) the rate of westward Anatolia escape (Vpush) and the time at which escape started ii) the role of the Vardar suture (weak zone) on the pattern of deformation. The geological constraints are i) the overall graben pattern within the Aegean, ii) the geometry of the NAF, and finally iii) the existence of a dextral strike-slip fault zone with N-S km scale en échelon folds in the center of the Cyclades (Fig. IX-1).

If both Anatolia escape and the southward trench retreat started at 25 Ma, deformation is strongly partitioned into thrust, in the East, and strike-slip, in the West, related to Anatolia escape; and limited extension in the South where gravitational spreading occurs due to southward trench retreat. Both thrust and NE-SW strike slip faults lead to the rigid westward migration of Anatolia. If Anatolia escape started at 11 Ma, extensional deformation becomes widespread and the northern rim of the extensional deformed zone is directly related to the position of the two rotation axes. Anatolia escape is accommodated by both major N-S thrusts to the North and dextral strike slip, in the western rim and in the centre of the extensional domain (Fig. IX-3 a and b). Note the space created between the two rotating doors, reflecting a much lower amount of shortening compared to the previous experiments, and hence a smaller displacement of the eastern rotation axis toward the west. If Anatolia escapes since 11

Ma, but at a larger rate (5 cm/h), N-S thrusts faults are more pronounced in the North while the dextral strike-slip fault zone in the centre of the extensional domain is no longer present (Fig. IX-3c). The rate of Anatolia escape thus controls the internal structure of the extensional region: at large Vpush, the large amount of shortening is mostly accommodated in the western border of the entire deformed region; while at lower Vpush, the amount of shortening is accommodated in a wider region.

Widespread extension, with varying graben orientation and dextral strike-slip fault zone are typical of the Cyclades. However, the thrust front to the North is not relevant to the North Aegean. Only the existence of a V-shape weak zone in the center of the model leads to the absence of such major thrusts (Fig. IX-3d).

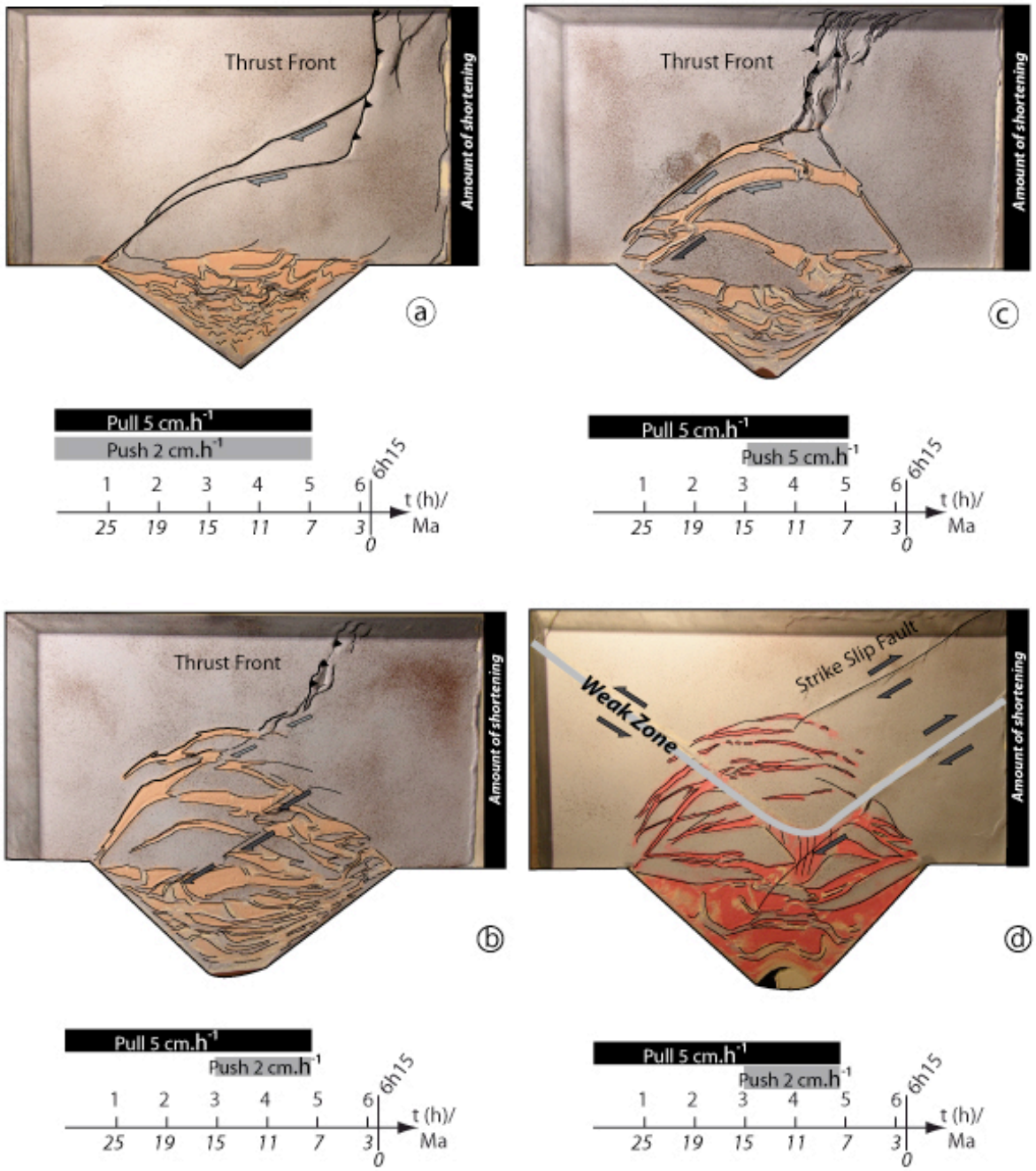

Fig. IX-3. Four differents runs of the experiments. Tested parameters : i) the rate of westward Anatolia escape (Vpush) and the time at which escape started ii) the role of the Vardar suture (weak zone).

The Vardar suture zone (VSZ) and its eastern continuity the Izmir Ankara suture zone (IASZ) are the main lithosphere-scale discontinuities (Fig. IX-1). The late Oligocene position of the VSZ/IASZ is V shaped, as it has been already deformed by the Eocene

rotation around Scutary Peç rotation pole (See Brun and Sokoutis 2010).The Vardar suture is thus modeled by two NW-SE and NE-SW rectilinear branches, connected in the center of the Aegean sea (Fig. IX-1 and IX-3d). In that case, Anatolia escape is mainly accommodated by the reactivation of the weak zone in dextral shear. NE-SW dextral strike slip fault with en echelon N-S folds occurs in the center of the extensional domain and is connected to the weak zone where the two rectilinear branches join. NE-SW strike-slip fault (e.g. North Anatolian Fault) also partly accommodates Anatolia escape in the North Aegean. The orientation of the NAF is here controlled by the geometry of the Vardar suture.

Four top views at different times (16, 12, 4 and 0 Ma, Fig. IX-4) of this experiment reveal the proper timing of extensional, contractional and strike-slip deformation. Before Anatolia escape, at 16 Ma, southward trench retreat that started at 25 Ma leads to widespread extension in the model, north and south of the weak zone. The reactivation of the suture zone in dextral shear is thus active without Anatolia escape in order to accommodate the southward spreading of the model. Ductile extensional deformation is moreover localized in the edge of the suture zone (e.g. Northern Cyclades, Naxos-Paros area). At 12 Ma, Anatolia escape started and is first fully accommodated by a more pronounced dextral shearing of the weak zone. NE-SW trending strike-slip fault also occurs within the stretched part of the suture zone, in the Naxos-Paros area.

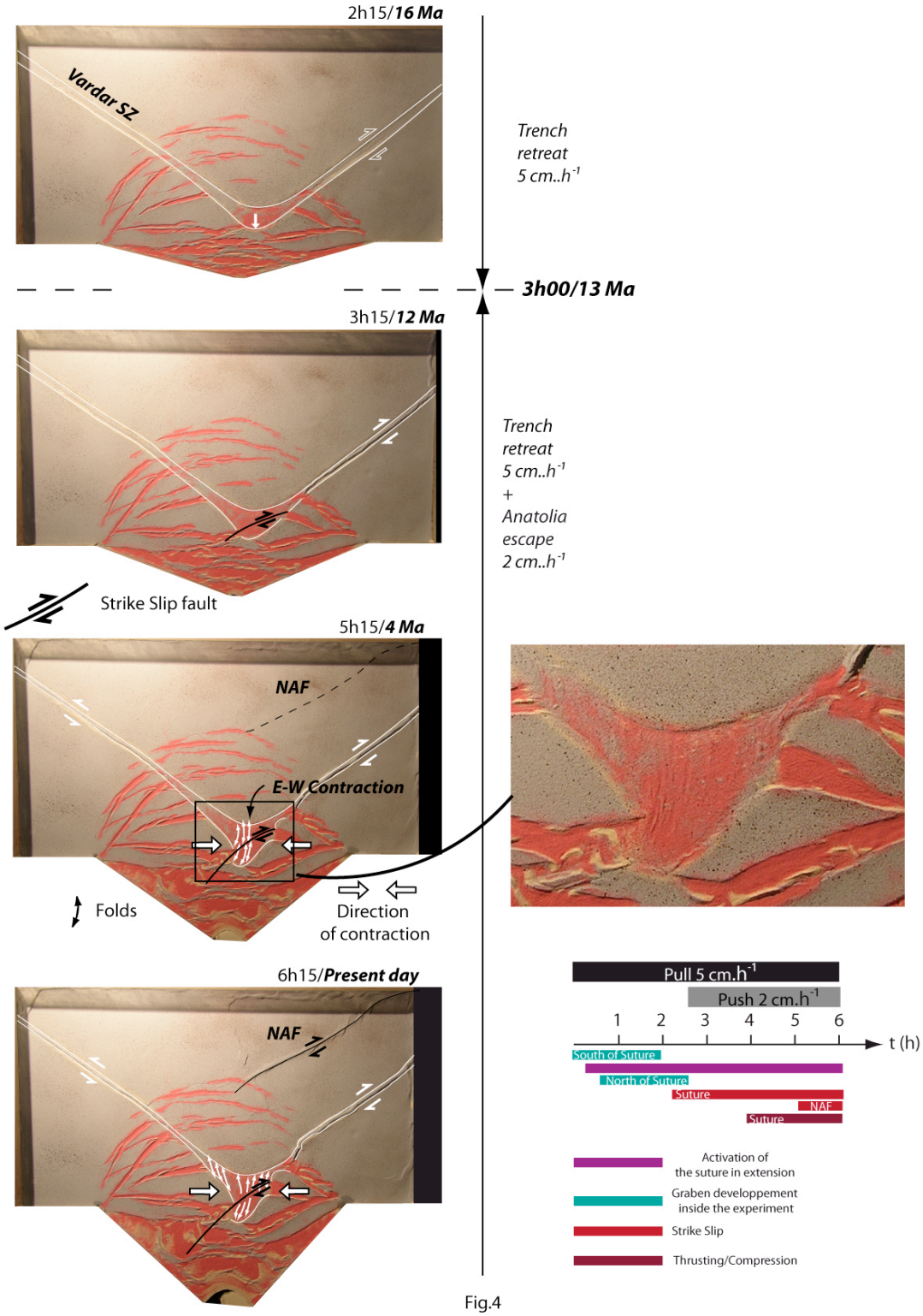

Fig. IX-4. Four steps of a successful experiment. The main tectonic features observed in the field can be identified in the model. Extension-related structures : The graben and hosrt network, the strike slip faults, the folds and The Central Cycaldes Core Complex (CCCC)

At 4Ma, a major NE-SW strike-slip structure has developed from the reactivated suture towards the stretched central Cyclades, and has accommodated both Anatolia escape and trench retreat (Fig. IX-4c). N-S trending en échelon folds occur in the central Cyclades area. Such E-W shortening, localized in the center of the weak zone, is induced by the westward escape of Anatolia. Such evolution of the central Cyclades, and more generally of the Central Cyclades Core Complex, from localized N-S stretching between 25 and 12 Ma to E-W shortening and N-S stretching after 12 Ma is consistent with the well constrained tectonic evolution of the Cyclades. At 4Ma, the increase in the amount of E-W shortening induced the initiation of a NE-SW strike-slip fault, almost parallel to the suture, e. g. the NAF. The NAF is thus a late structure that formed 8 Ma after the onset of Anatolia escape and hence little accommodated the E-W shortening, that is mostly transferred into the dextral shearing along the suture. At present day, the NAF is fully developed and ended within the northern rim of the extended domain.

9.3. Aegean extension since Tortonian

Both the interaction of trench retreat and westward displacement of Anatolia and the effect of weak zones at lithosphere scale –i.e. Vardar Suture Zone- play a major role in the development Aegean extensional pattern since middle Miocene. Trench retreat locked laterally by two pivots (Kephalonia and Rhodes) is primarily responsible for the pattern of graben development in south Aegean, since late Miocene. E-W shortening that gives a large NE-SW trending strike-slip fault (the Myrthes-Ikaria strike-slip fault) and folds with N-S axes in the central Cyclades (Fig. IX-1) can directly be compared with the structures observed in the model of figure IX-4 that resulted from the reactivation of the weak zone representing the Vardar suture. In the central Cyclades this E-W shortening occurred between 12 and 8 Ma. This suggests that Anatolia westward extrusion started to interact with trench retreat earlier than commonly believed. In the model of Fig. 4 the equivalent of the NAF developed at a late stage of evolution. This indicates that the North Anatolian Fault (NAF) is not the major structure resulting from the Anatolia westward escape.

9.4. Appendix

9.4.1. Apparatus

Scaled analogue models were carried out in Plexiglas box, two apparatus have been used to perform the experiments presented in this study. The one door experiment has been designed to study the effect of the rotational retreat of the slab and its impact on the graben pattern development. The saloon-type opening doors experiment is a more evolved one and allows us (i) to model the entire Hellenic subduction zone retreat and the (ii) to monitor the effect of the westward Anatolia escape thank to a leftward moving wall.

9.4.2. Analog materials

From top to bottom, the experiments are made of three layers that represent the upper and lower crust and the astenosphere, respectively. Feldspath sand, behaving as a Mohr-Coulomb material, is a good analogue of the Upper Crust, with a density ρ=1,3, and a coefficient of internal friction μ=0,9. The putty used for these experiment is a homemade material called Feta (which corresponds to a special mix of PDMS, BaSO4, Rodorsil and Oleic Acid). The Feta with a density ρ=1,39, and a viscosity η=1.3.10-4 Pa.s-1 , have a Newtonian behavior and therefore as been choose as an analogue of the Lower Crust. The analogue fluid of the astenopshere is a melt Glycerol and Poly Tungsten, with a density of ρ=1,6. With such densities, the analogue with nature is well approach: the ratio nature /experiment is close to one. For the scaling see Annexe F.

Acknowledgments

The present work was financially supported by the ANR-EGEO project. We are extremely grateful to D. Sokoutis and the Teclab crew for these month spent in Amsterdam.

References

Armijo R., Meyer B., Hubert A. and A. Barka (1999), Westward propagation of the North Anatolian fault into the northern Aegean: timing and kinematics. Geology 27, 267-270.

Bozkurt E., and R. Oberhänsli (2001), Menderes Massif (western Turkey): Structural, metamorphic and magmatic evolution—A synthesis. International Journal of Earth Sciences 89, 679–708. doi: 10.1007/s005310000173.

Brun J.P. and C. Faccenna (2008), Exhumation of high-pressure rocks driven by slab rollback. Earth and Planetary Science Letters 272, 1–7. doi:10.1016/j.epsl.2008.02.038

Brun J.P. and D. Sokoutis (2007), Kinematics of the Southern Rhodope Core Complex (North Greece). International Journal of Earth Sciences 96 (6), 1079-1099. doi:10.1007/s00531-007-0174-2

Brun J.P. and D. Sokoutis (2010), 45 m.y. of Aegean crust and mantle fl ow driven by trench retreat. Geology 38 (9), 815–818. doi: 10.1130/G30950.1.

Gautier P., and J.-P. Brun (1994a), Crustal-scale geometry and kinematics of late-orogenic extension in the central Aegean (Cyclades and Evvia Island). Tectonophysics 238, 399–424.

Gautier P., Brun J.P., Moriceau R., Sokoutis D., Martinod J. and L. Jolivet (1999), Timing, kinematics and cause of Aegean extension: a scenario based on a comparison with simple analogue experiments. Tectonophysics 315 (1-4), 31-72. doi:10.1016/S0040-1951(99)00281-4

Jolivet L. and J.P. Brun (2010), Cenozoic geodynamic evolution of the Aegean. International Journal of Earth Sciences 99 (1), 109-138. doi:10.1007/s00531-008-0366-

4.

Kissel C., Laj C., Poisson A. and N. Görür (2003), Paleomagnetic reconstruction of the Cenozoic evolution of the Eastern Mediterranean. Tectonophysics 362 (1-4), 199-217. doi:10.1016/S0040-1951(02)00638-8

Kissel C. and C. Laj (1988), The Tertiary geodynamic evolution of the Aegean arc: a paleomagnetic reconstruction. Tectonophysics 146 (1-4), 183-201. doi:10.1016/0040-1951(88)90090-X.

Mascle J. and L. Martin (1990), Shallow structure and recent evolution of the Aegean Sea: A synthesis based on continuous reflection profiles. Marine Geology 94, 271–299. doi: 10.1016/0025-3227(90)90060-W.

McClusky S., and 27 others, (2000), Global positioning system constraints on plate kinematics and dynamics in the eastern Mediterranean and Caucasus: Journal of Geophysical Research 105, 5695–5720.

McKenzie D. (1972), Active Tectonics of the Mediterranean Region. Geophysical journal international 30(2), 109-185.

Okay A.I., Satır M., Zattin M., Cavazza W. and G. Topuz (2008), An Oligocene ductile strike-slip shear zone: Uludağ Massif, northwest Turkey—Implications for the westward translation of Anatolia. Geological Society of America Bulletin 120, 893–911. doi: 10.1130/B26229.1.

Okay A.I., Zattin M. and W. Cavazza (2010), Apatite fission-track data for the Miocene Arabia-Eurasia collision. *Geology* 38 (1), 35–38. doi: 10.1130/G30234.1.

Papanikolaou D.J. and L.H. Royden (2007), Disruption of the Hellenic arc: Late Miocene extensional detachment faults and steep Pliocene-Quaternary normal faults—Or what happened at Corinth? tectonics 26, TC5003. doi:10.1029/2006TC002007.

Şengör A.M.C., Tüysüz O., İmren C., Sakınç M., Eyidoğan H., Görür N., Le Pichon X. and C. Rangin (2005), The North Anatolian fault: A new look. Annual Review of Earth and Planetary Sciences 33, 37–112. doi: 10.1146/annurev. earth.32.101802.120415.

Zattin M., Okay A.I., and W. Cavazza (2005), Fissiontrack evidence for late Oligocene and mid-Miocene activity along the North Anatolian fault in south-western Thrace. Terra Nova 17, 95–101. doi: 10.1111/j.1365-3121.2004.00583.x.

Partie 4/ Conclusions générales

Cette thèse, qui a été réalisée dans le cadre du projet ANR/EGEO, concerne l'évolution tectonique de l'Unité des Schistes Bleus Cycladiques, en centre Egée. Elle s'appuie sur trois échelles d'analyse :

- analyse structurale des formations métamorphiques de haute pression de Syros et, partiellement, de Sifnos : cartographie structurale, modélisation 3D des données (GOCAD), étude des relations métamorphisme/déformation

- Restauration cartographique de la segmentation post-métamorphique des Cyclades prenant en compte une synthèse des données pétrologiques, structurales et géochronologiques, les données paléomagnétiques disponibles et une analyse morpho-tectonique de la bathymétrie de l'Egée.

- Modélisation analogique de l'interaction entre retrait de la subduction Hellénique et déplacement vers l'ouest de l'Anatolie, avec une attention particulière concernant le développement de la segmentation des Cyclades en extension et décrochement

Les conclusions de ce travail sont d'une part d'ordre méthodologique, s'agissant plus particulièrement de géologie structurale, et d'autre part concernent l'évolution tectonique du domaine centre Egéen et notamment la distinction entre subduction et exhumation dans la structuration des schistes bleus.

10.1 Méthodologie d'analyse structurale

10.1.1 Les pseudomorphes de Lawsonite : un outil d'identification des déformations progrades dans les roches de haute pression

La lawsonite est un minéral de haute pression basse température qui cristallise sur le chemin métamorphique prograde suivi par les unités lithologiques subductées. Lorsque l'unité sort de son champ de stabilité, en particulier au cours de l'exhumation, la lawsonite se déstabilise en un assemblage de micas blancs, albite, épidote (Fig.X-1a).

Dans un certain nombre de sites répertoriés, les schistes bleus ont conservé malgré leur déstabilisation des pseudomorphes des cristaux de lawsonite, c'est-à-dire la forme des macro-cristaux mais pas la structure cristalline interne. La conservation de pseudomorphes de lawsonite, comme à Syros et dans d'autres iles des Cyclades, implique que la roche hôte n'a subi aucune déformation pénétrative depuis la cristallisation des porphyroblastes de lawsonite.

Une illustration de ceci est donnée par la cartographie en rayons X d'un pseudomorphe de lawsonite de Syros réalisé à la microsonde montrant que celui-ci présente toujours la structure interne « en sablier » primaire d'une lawsonite fraîche. (Fig. X-1b).

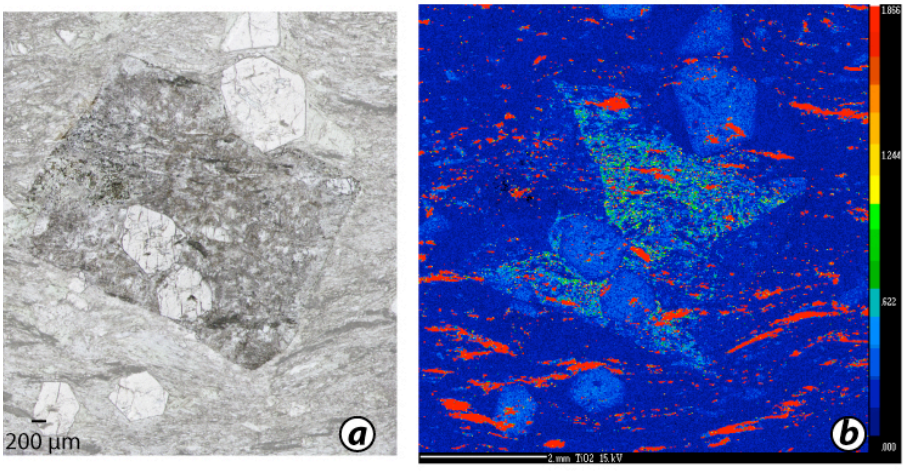

Fig. X-1. Photographie d'une lame mince et carte rayon X de l'élément Ti de cette même lame

A Syros, les lithologies présentant des pseudomorphes de lawsonite conservent un cisaillement vers le Sud (Fig. X-2) qui n'est quasiment pas observé dans les roches sans lawsonite. En outre, les roches à pseudomorphes de lawsonite sont quasiment indemnes de cisaillement vers le NE tandis que les roches sans lawsonite sont le plus souvent affectées par ce cisaillement vers le NE synchrone de la retromorphose en facies schiste vert.

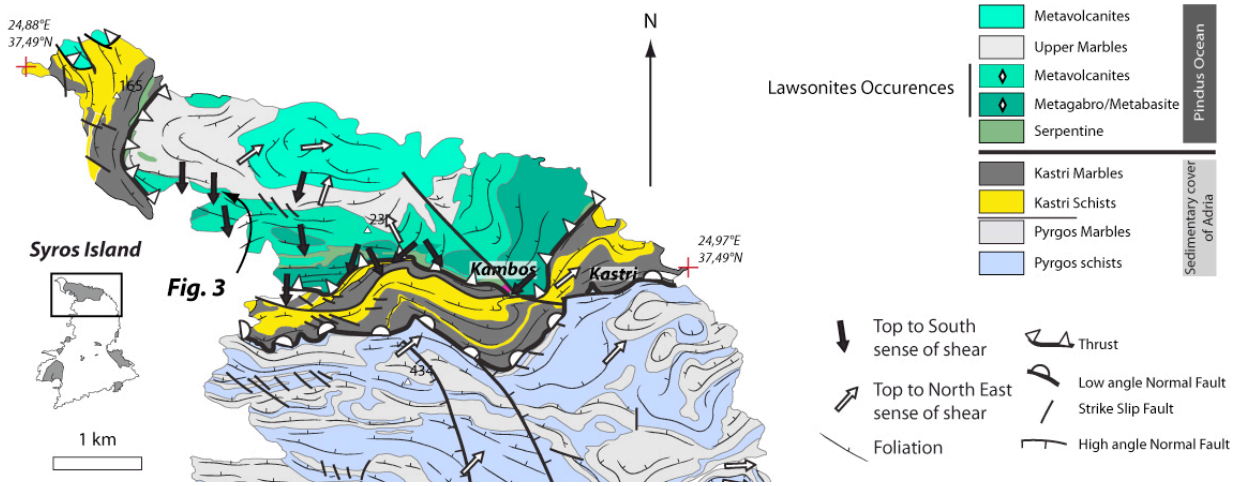

Fig. X-2. Carte structurale du Nord de l'île de Syros montrant les relations entre cisaillement et lithologies à pseudomorphes de lawsonite.

Ces observations faites dans les Cyclades confirment celles réalisées précédemment dans les schistes bleus de l'Ile de Groix (Philippon et al 2009) : Les pseudomorphes de lawsonite peuvent être utilisés en tant que jauges de non-déformation. Ils fournissent donc un outil très utile pour l'identification des déformations synchrones du métamorphisme prograde et, par conséquent, pour la caractérisation cinématique de la subduction.

Dans le cas des Cyclades, les sens de cisaillement relevés dans les roches à pseudomorphes de lawsonite indiquent tous un cisaillement vers le S-SW et donc une subduction à pendage nord. Bien que cette conclusion puisse ne pas surprendre, il est intéressant de noter que jusqu'à présent, il n'avait pas été trouvé d'évidence directe et incontestable des déformations syn-subduction et de leur cinématique.

10.1.2 Systèmes extensifs en plat et rampes dans la croûte fragile

L'élaboration de coupes géologiques nord-sud de l'île de Syros illustre les relations entre les trois unités constitutives de l'île (socle, sédiments et croûte océanique). Elle a permis de mettre en évidence trois surfaces de discontinuités majeurs, de nature différentes (Fig. X-3):

- Un chevauchement de l'unité océanique sur les sédiments de la marge,
- Un système extensif semi-fragile, avec une géométrie en plat et rampe, au sein de la pile sédimentaire,
- Un réseau de failles tardives, recoupant les trois unités constitutives de l'île.

Les critères cinématiques observés sur le terrain montrent que le système extensif en plat et rampe identifié à Syros correspond à un déplacement relatif des unités supérieures vers le Sud. En nous appuyant sur les datations existantes (Ring et al., 2003) l'activité de ce contact tectonique plat est une réponse à une extension N-S débutant au Miocène moyen.

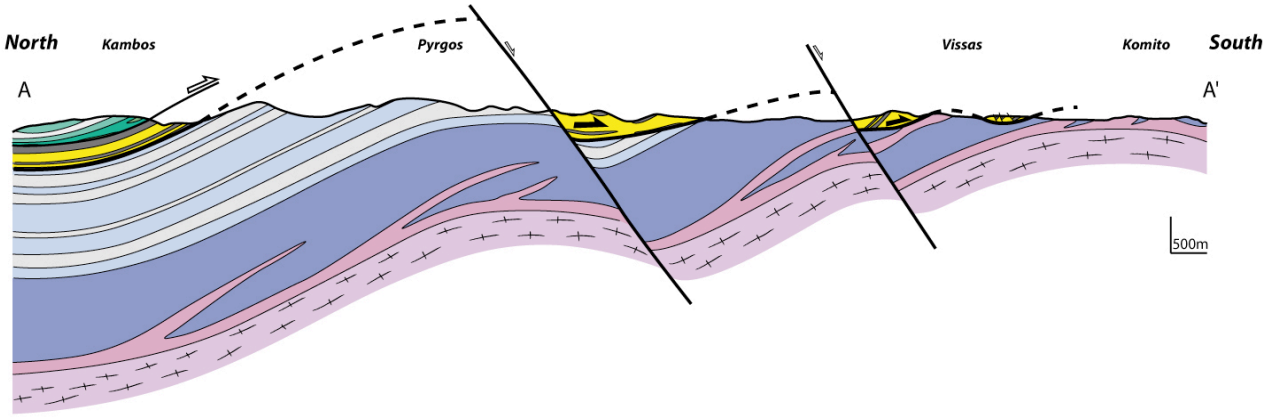

Fig. X-3. Couppe Nord-Sud de l'île de Syros, montrant le Système en plat et rampe.

Il était considéré jusqu'à présent que trois détachements ductiles étaient participaient à l'exhumation différentielle des unités constitutives de Syros sous l'unité supérieure Pélagonienne (Ridley, 1984). L'analyse présentée ici montre que :

1 / le socle de l'unité supérieure Pelagonienne n'affleure pas à Syros. Les gneiss de Vari, dans le SE de l'ile, qui étaient rapportés au Pélagonien font en fait partie du bloc

continental Adria dans la mesure où il est montré que ces gneiss constituent le socle des unités métasédimentaires de Pyrgos et Kastri.

2 /Le système extensif semi-fragile en plat et rampe de Syros, qui est tardif dans l'évolution, ne participe pas à l'exhumation syn-métamorphique des roches de haute pression- basse température.

Dans le cas des Cyclades, de nombreux détachements sont décrits comme étant responsables soit de l'exhumation des roches métamorphiques HT et HP (Gautier et Brun, 1994 a et b ; Jolivet et Goffé, 2000), soit de l'exhumation de des roches métamorphiques HP (Ring et Reischmann, 2003; Forster et Lister, 2008). Les contacts plats observés dans l'unité des Schistes Bleus Cycladiques (SBC), tels celui de Syros, sont internes à l'unité et réactivent en décollement des niveaux lithologiques ou des discontinuités tectoniques qui constituent des zones de faiblesse préexistante. Ces structures extensives d'âge Miocène moyen sont donc postérieures à l'exhumation déjà largement accomplie des SBC.

10.2 Tectonique Egéenne

Pour réaliser l'analyse de l'histoire et la cinématique tectonique enregistrées dans l'Unité des schistes Bleus Cycladiques une étape essentielle consistait à restaurer la segmentation, par failles normales et décrochements, subie par les Cyclades. En voici, le résultats et les implications.

10.2.1 Segmentation post-12 Ma des Cyclades

À l'échelle régionale, les linéations d 'étirement sont orientées N45° au nord ouest et N-S au sud est du domaine Egéen (Fig. X-4). Ces deux domaines d'orientation des linéations d'étirement sont séparés par une discontinuité orientée NE-SW (Gautier et Brun 1994 a) : le « Mid Cycladic Lineament » (MCL) (Walcott and White, 1998).

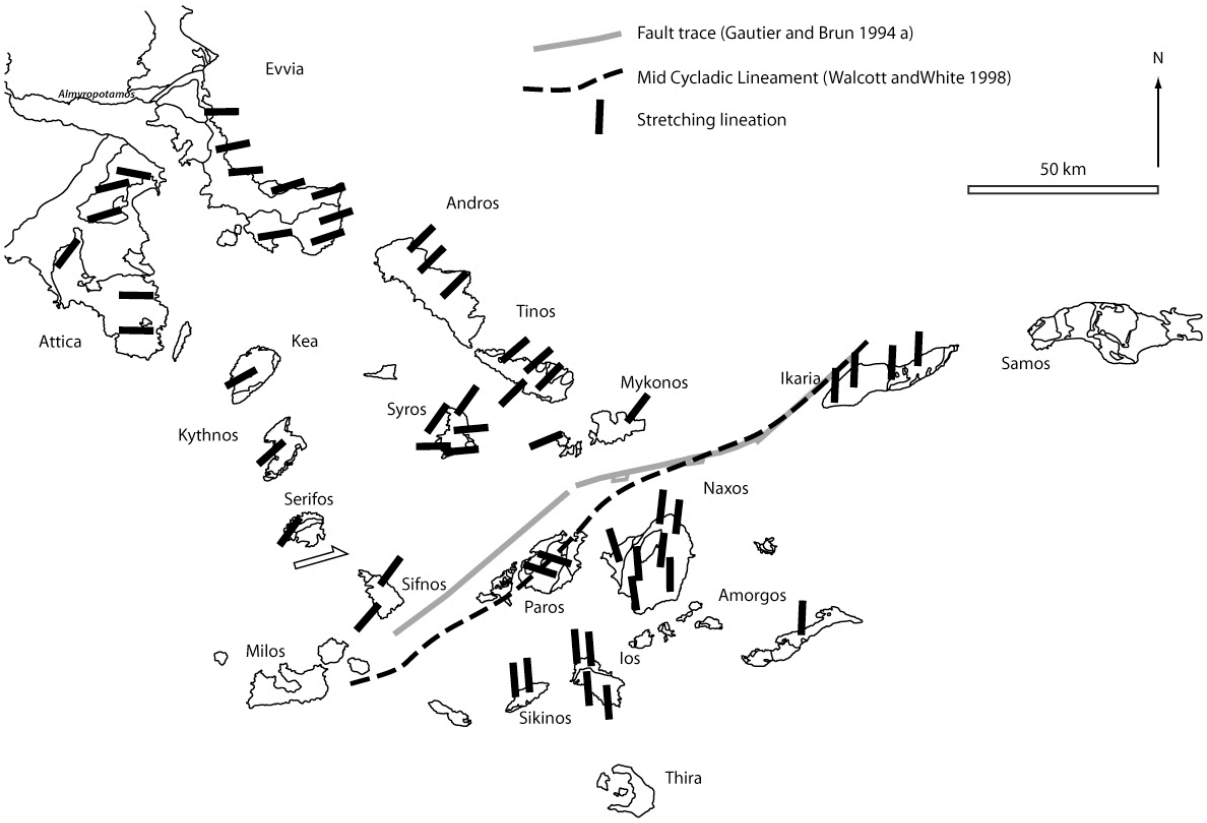

Fig. X-4 : Carte des linéations d'étirement à l'échelle des Cyclades.

A partir d'une interprétation de la bathymétrie et des données existantes concernant les bassins sédimentaires Neogènes (Mascle et Martin 199X), on montre que ce « linéament » est une faille décrochante dextre, accommodant l'ouverture de bassins en pull-apart à ses extrémités nord-est et sud-ouest (Les bassins de Myrthes et Ikaria-Samos)(Fig. X-5).

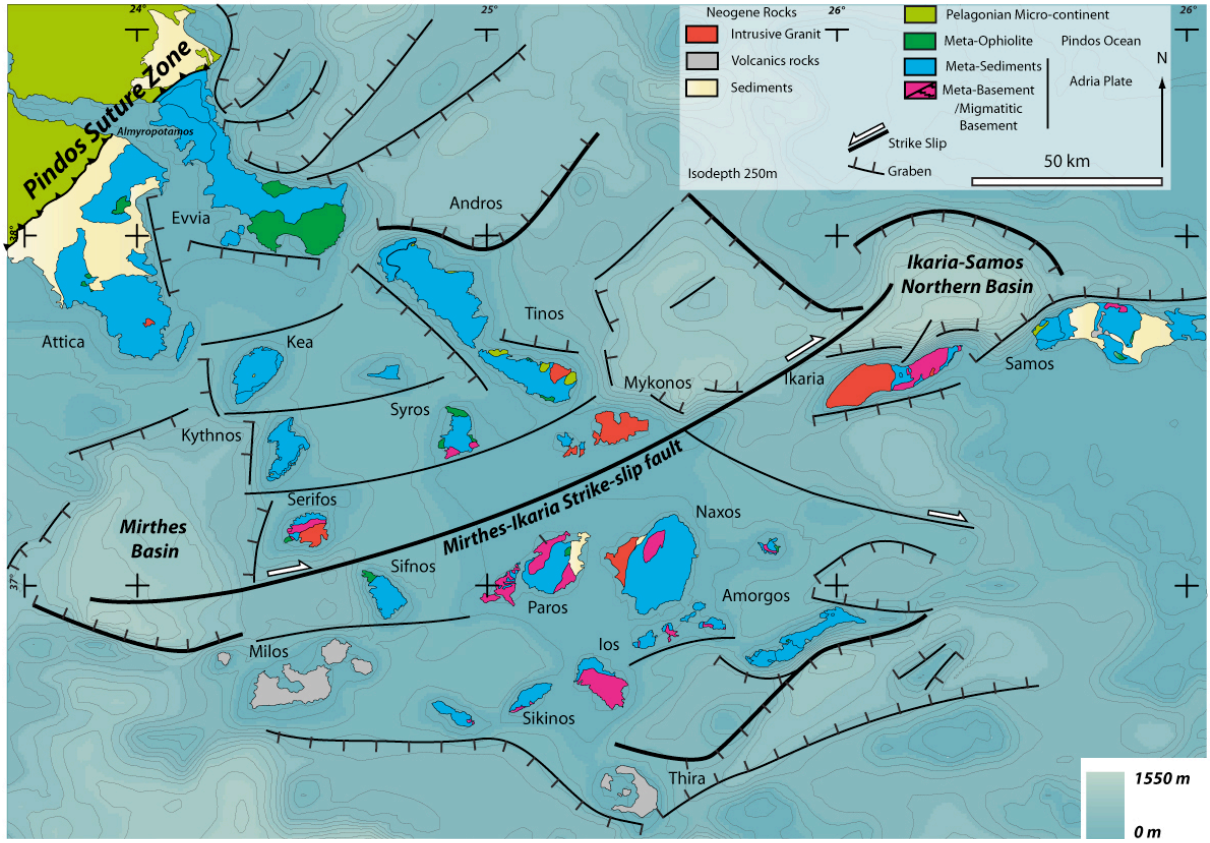

Fig. X-5 : Carte des Cyclades, interprétation de la bathymétrie.

Les données paléomagnétiques montrent que les deux domaines séparés par la Faille de Myrthes-Ikaria ont enregistré des rotations d'axe vertical, respectivement de 22° horaire au NW et 33° anti-horaire au SE (Morris et Anderson 1996). Le différenciel de rotation entre ces deux domaines est de 55°. L'obliquité entre les linéations de ces deux domaines est du même ordre c.a. 50°, montrant que les linéations avaient la même direction avant la rotation des blocs. Cette rotation différentielle a eu lieu à partir de 12 Ma (Avigad et al., 1998).

10.2.2. Restauration en carte de la déformation post-12 Ma

La restauration « en carte » de la géométrie anté-12 Ma, a été réalisée en trois étapes (Fig. X-6).

Premièrement, les Cyclades ont été divisées en cinq domaines i) délimités par les failles majeures, normales et décrochantes qui ont segmenté les Cyclades à partir de 12 Ma et ii) présentant un même sens et une même quantité de rotation autour d'un axe

vertical ainsi qu'une même orientation des linéations (Eubée-Attique, Andros-Tinos-Mykonos, Paros-Naxos et Ikaria-Samos).

Deuxièmement, afin d'annuler le déplacement sur les failles normales et décrochantes dans le sous-domaine Andros-Tinos-Mykonos, les îles du Sud ont été réalignées avec celle du Nord.

Troisièmement, les deux domaines séparés par la faille de Myrthes-Ikaria, dont la rotation différentielle est connue, ont été affectés d'une rotation inverse et de la même valeur angulaire que celle indiquée par le paléomagnétisme. Cette annulation de la rotation est synchrone d'un déplacement dextre le long de la faille de Myrthes-Ikaria. Ce mouvement d'une amplitude d'environ 50 km le long du décrochement, ré-aligne les détachements de Naxos-Paros, et d'Andros-Tinos-Mykonos. Une légère rotation du domaine Eubée-Attique a été réalisé pour aligner la position de son détachement avec celui d'Andros-Tinos-Mykonos. Le détachement de Naxos-Paros n'a pas été déplissé, mais pour prendre en compte la quantité de raccourcissement correspondante, le bloc Ikaria-Samos a été translaté vers l'Est de 40 km.

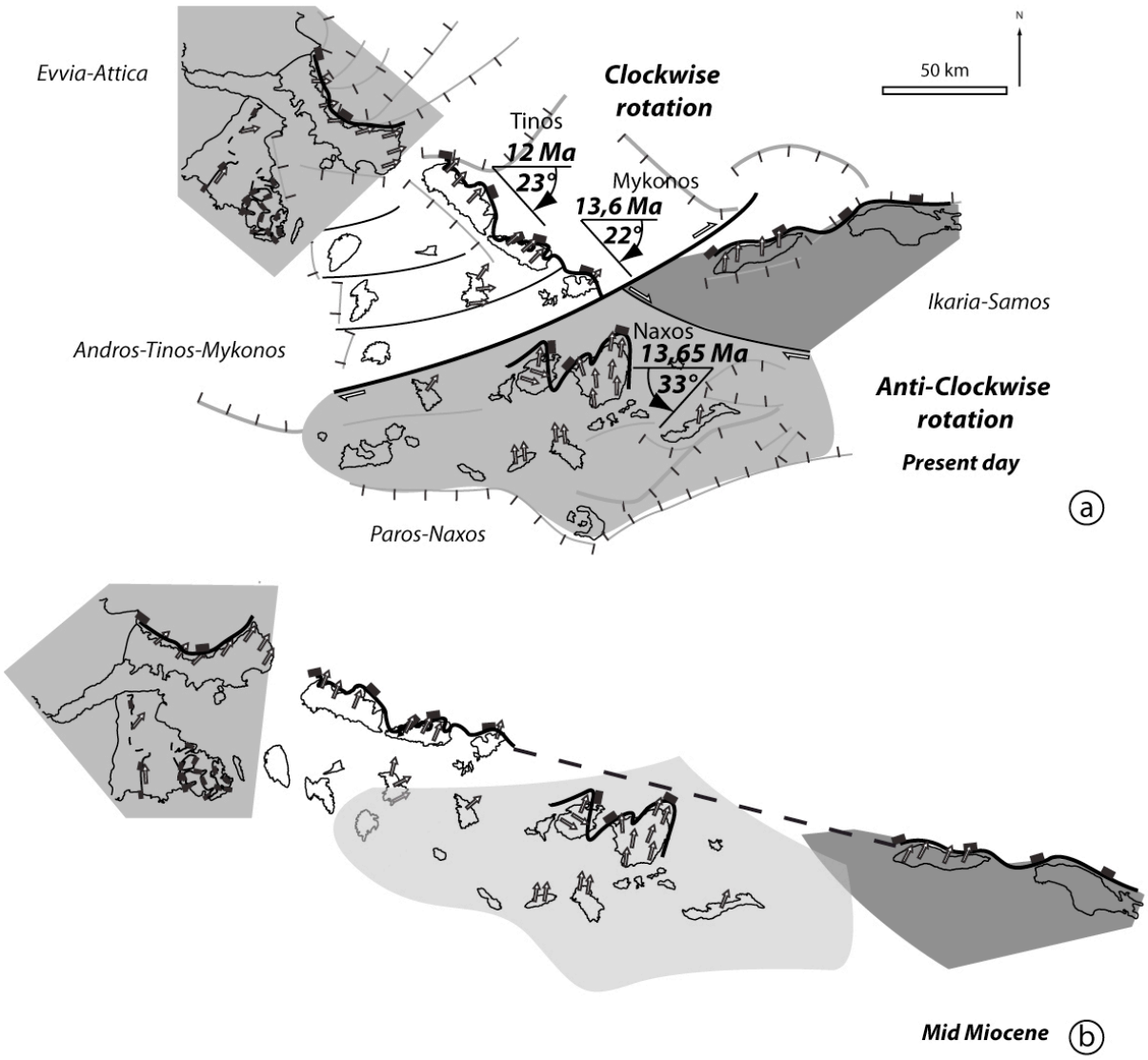

Fig. X-6. Restauration de la déformation post-12 Ma.

- 10.2.3. Structures et cinématique des déformations anté-12 Ma

- Le Core Complexe des Cyclades Centrales

Après restauration, les granites et les migmatites sont alignés sur 250 km de long sous le Détachement Nord Cycladique, définissant une zone de haute température affectée par un détachement à pendage NE (Fig. X-7, aire en rouge). Dans cette zone, les assemblages de haute pression sont fortement rétromorphosés. Cette structure correspond à un dôme métamorphique extensive unique: le « Core Complexe des Cyclades Centrales » dont l'exhumation débute au Miocène inférieur (l'âge des migmatites de Naxos et Paros

est comprise entre 16 et 20 Ma (U/Pb on Zircon, Keay, 2001)), accommodée par le Détachement Nord Cycladique.

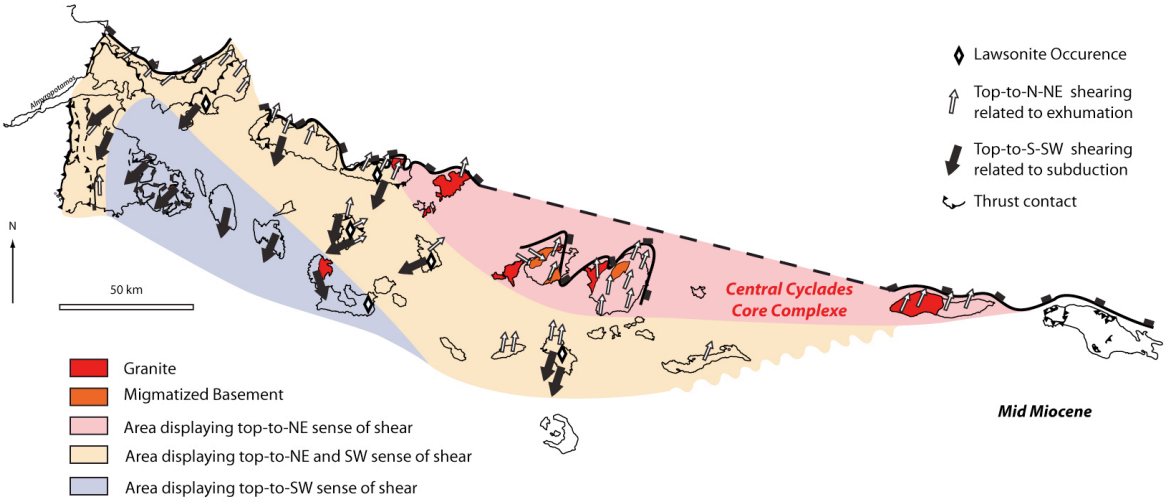

Fig. X-7 Carte des Cyclades, après restauration à 12 Ma, montrant les trois domaines de sens de cisaillement: à cisaillement vers le NE (Rouge), à cisaillement vers le SW et le NE (Orange) et à cisaillement vers le SW (Bleu).

- Les deux étapes de cisaillement vers le NE

Le cisaillement vers le Nord Est a deux origines. Premièrement, Il correspond à l'exhumation des SBC, de l'Eocène inférieur à l'oligocène supérieur, sous la suture du Vardar (zone orange, Fig. X-7) et deuxièmement à l'exhumation du Core Complexe des Cyclades Centrales dont l'exhumation est accommodée par de Détachement Nord Cycladique du Miocène inférieur au Miocène moyen (zone rouge Fig. X-6). Cette distinction de deux sens de cisaillements vers le NE est démontrée à l'échelle cartographique par le fait que le détachement Nord Cycladique recoupe à angle droit la Suture du Pinde.

- Le cisaillement vers le SW et la subduction

Dans le domaine intermédiaire (zone orange, Fig. X-7), deux sens de cisaillements sont observés : haut vers le NE et vers le SW. Le cisaillement vers le SW correspond à du chevauchement d'âge anté-Lutétien. Le fait qu'il soit systématiquement associé à des pseudomorphes de lawsonites permet de l'attribuer à la subduction. Dans le SW des Cyclades, ce cisaillement vers le SW est dominant (En bleu, Fig. X-7) et en Attique et à

Ios, il est clairement lié à une déformation chevauchante. A noter que ce domaine SW des Cyclades correspond à une partie des Schistes bleus Cycladiques non affectés par la déformation cisaillante vers le NE liée à l'exhumation. On dispose ainsi d'une première cartographie de la cinématique de la subduction à l'échelle des Cyclades.

10.2.4. Un modèle d'évolution tectonique des Schistes Bleus Cycladiques

L'histoire tectonique des schistes bleus cycladiques peut ainsi être résumée en cinq étapes(Fig. X-8).:

- Avant le Lutétien, les méta-ophiolites de l'océan du Pinde (Faciès des schistes bleus à éclogites), sont chevauchées vers le Sud sur la couverture sédimentaire de la marge nord d'Adria dans une zone de subduction à pendage NE.
  La subduction des unités de la marge d'Adria –i.e. couverture sédimentaire et socle gneissique- se poursuit jusqu'au Lutétien.
- Pendant l'Eocène supérieur jusqu'à 37 Ma, un premier stade d'exhumation depuis des profondeurs mantelliques jusqu'à la base de la croûte, avec un sens de cisaillement vers le NE, a été accommodé par l'inversion en extension de la suture du Vardar.
- Entre 30 et 20 Ma, un deuxième stade d'exhumation, de la croûte basale à la croûte supérieure, toujours en cisaillement vers le NE, a été accommodé par le Détachement Nord Cycladique. C'est lors de ce stade que s'exhument les unités métamorphiques de haute température du Core Complexe des Cyclades Centrales.
- Après 12 Ma, l'unité des Schistes Bleus Cycladiques a été segmentée par des failles normales et des décrochements. La rotation de blocks et le plissement d'axe N-S sont contrôlés par le décrochement dextre de Myrthes-Ikaria, au centre des Cyclades.

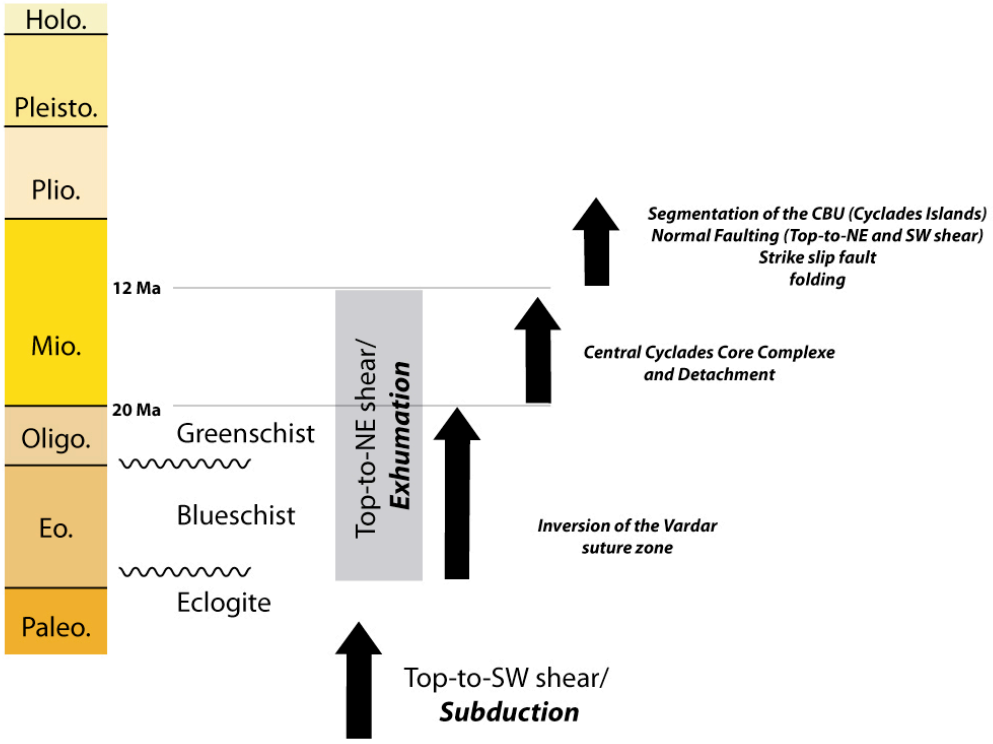

Fig. X-8. Tableau récapitulatif de l'histoire des schistes bleusCycladiques.

10.3. L'extension Egéenne et l'extrusion de l'Anatolie depuis 15 Ma.

La structuration tardive des Cyclades et sa segmentation, avec en particulier un déplacement dextre d'environ 50 km sur le décrochement de Myrthes-Ikaria soulevait le problème de l'interaction entre retrait de la subduction Hellenique vers le sud et extrusion de l'Anatolie vers l'ouest (Fig. X-8). La déformation des Cyclades après 12 Ma suggère en effet une extrusion de l'Anatolie bien avant la propagation de la Faille Nord Anatolienne, estimée à 5 Ma (Armijo et al 1999). Ce problème a été abordé expérimentalement en clôture de de cette thèse.

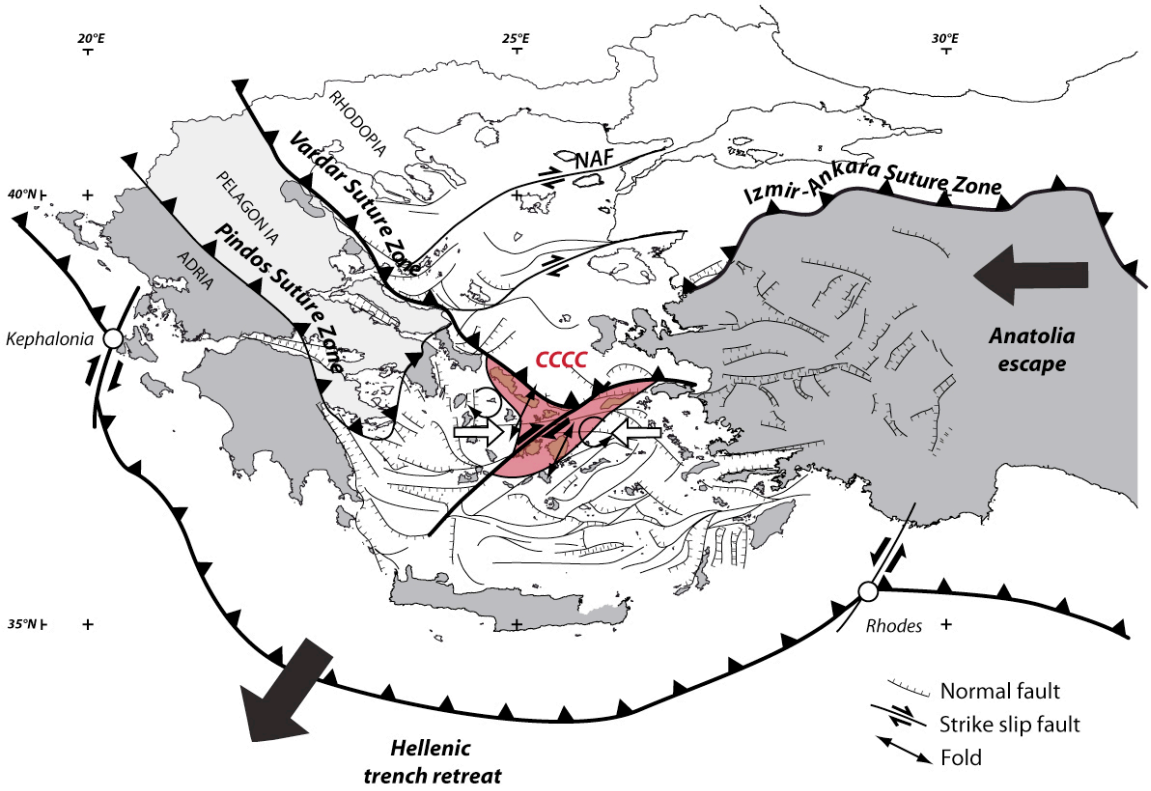

Fig. X-8: Carte tectonique grecque et turque, montrant les conditions aux limites (Extrusion de l'Anatolie et retrait du panneau plongeant).

Une première série d'expériences simulant uniquement l'interaction entre retrait de la subduction Hellenique (Vpull) et extrusion de l'Anatolie (Vpush), a permis de montrer qu'une lithosphère homogène ne permettait pas d'obtenir les structures observées dans le domaine égéen s.l., car un front chevauchant se développait systématiquement dans la partie du modèle correspondant au domaine Nord Egéen.

Comme la suture du Vardar apparaît dans la carte géologique de l'Egée en tant que discontinuité majeure, une zone de faiblesse d'échelle lithosphérique, simulant la géométrie de la suture au Miocène moyen, a été rajoutée dans la procédure expérimentale.

La figure X-9 présente les résultats obtenus à différentes étapes de l'expérience :

- De 25 à 16 Ma, le retrait du panneau plongeant induit une extension distribuée dans l'ensemble du modèle, au nord comme au sud de la zone de faiblesse. Vers l'Est, la suture est réactivée en décrochement dextre, avant que l'Anatolie ait commencé à s'extruder, accommodant l'extension vers le Sud. L'extension ductile se localise à la pointe de la zone de suture (correspondant au domaine Mykonos-Naxos-Paros)(Fig. X-9).
- A 14 Ma, l'extrusion de l'Anatolie commence et est accommodée dans un premier temps par une intensification de la réactivation de la suture en décrochement-extensif dextre. Des failles décrochantes NE-SW se développent dans la zone la plus étirée de la suture (Fig. X-9).
- A 4Ma, un décrochement majeur dextre, orientée NE-SW s'initie dans le prolongement de la suture et se propage vers le centre du modèle, accommodant ainsi l'extrusion de l'Anatolie vers l'ouest et le retrait du panneau plongeant vers le sud. Des plis en échelons N-S, compatibles avec le décrochement dextre, se développent au centre des Cyclades témoignant d'un raccourcissement E-W synchrone de l'extension N-S.

  Cette évolution du centre des Cyclades, et plus particulièrement du Core Complexe des Cyclades Centrales, d'un étirement N-S localisé entre 25 et 12 Ma à un raccourcissement E-W combiné à de l'étirement N-S après 12 Ma, dans le modèle, correspond remarquablement à la segmentation par failles normales et décrochements, observée dans les Cyclades (Fig. X-9).
- Vers 4 Ma, le raccourcissement E-W donne naissance à un décrochement d'orientation NE-SW, parallèle à la suture mais au nord de celle-ci dans un domaine préalablement non-déformé qui est directement comparable à la Faille

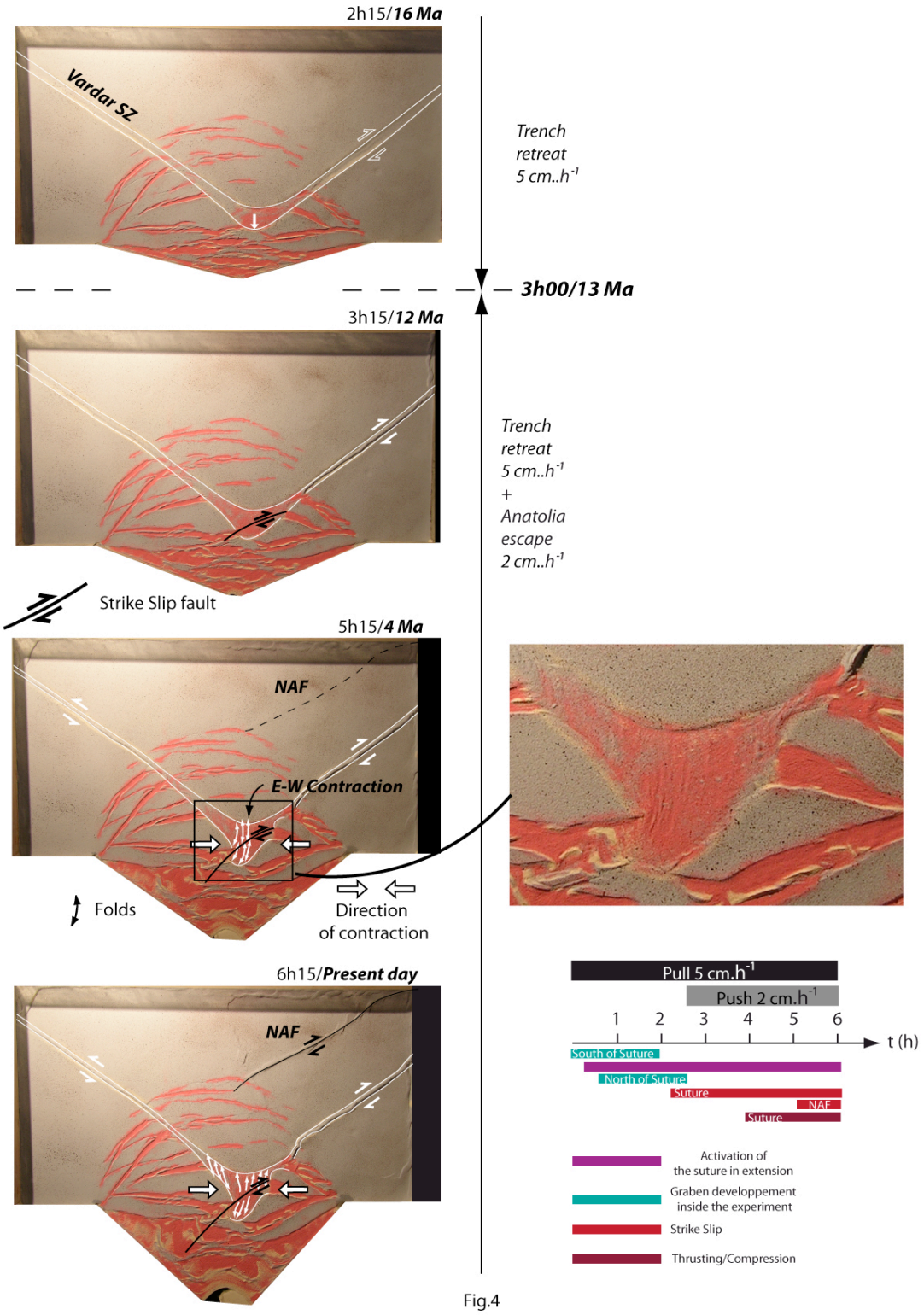

Fig. X-9: Modèle expérimental de la tectonique Egéenne depuis le Miocène moyen montrant l'évolution en quatre étapes de l'interaction entre le retrait de la subduction Hellenique vers le sud et l'extrusion de l'Anatolie vers l'ouest

Nord Anatolienne. Ce décrochement tardif se développe 11 Ma après le début de l'extrusion de l'Anatolie vers l'ouest. La première structure qui ait accommodé l'extrusion de l'Anatolie est donc la suture du Vardar, réactivée en décrochement dextre (Fig. X-9). La faille nord anatolienne apparaît beaucoup plus tardivement en se propageant jusqu'à la bordure nord du domaine étiré (Fig. X-9).

Ce travail de modélisation et sa comparaison, en particulier avec l'évolution des Cyclades, montre que l'interaction entre le retrait de la subduction Hellenique, le déplacement vers l'Ouest de l'Anatolie et l'effet de la Suture du Vardar en tant que zone de faiblesse d'échelle lithosphérique contrôle la structuration de l'Egée depuis le Miocène moyen (Fig. X-9). Le retrait de la subduction en rotation autour des deux pivots de Kephalonia et Rhodes est responsable du développement des grabens en Egée du Sud depuis le début du Miocène. Les grands décrochements NE-SW et le plissement d'axe N-S se développent en réponse au raccourcissement E-W dans le centre Cyclades sont comparables aux structures observées dans le modèle, directement contrôlés par la réactivation la suture du Vardar en décrochement dextre.

Le raccourcissement E-W, dans le centre des Cyclades, est daté entre 12 et 8 Ma (Thermochronologie basse température). Cela suggère que l'extrusion de l'Anatolie vers l'ouest à commence à interagir avec le retrait de la subduction bien plus tôt que communément admis. Dans le modèle, l'équivalent de la Faille Nord Anatolienne se développe très tardivement, indiquant que la Faille Nord Anatolienne n'est pas la structure la plus symptomatique de l'extrusion de l'Anatolie.

En résumé

Malgré la superposition des déformations ductiles lors du cycle enfouissement/exhumation on peut identifier, grâce aux pseudomorphes de lawsonites, les déformations prograde associées à la subduction des déformations rétrogrades liées à l'exhumation.

La suture de l'Océan du Vardar est inversée lors de l'extension syn-convergence causée par le retrait du panneau plongeant. Cette extension est accommodée par l'exhumation des roches de haute pression. Lors de son exhumation, l'unité métamorphique des Cyclades est donc découplée de la plaque plongeante et remonte le long de la suture et devient partie prenante de la plaque supérieure chevauchante.

Le panneau plongeant, qui continue à reculer, induit l'extension arrière arc dans la plaque chevauchante. Le core complexe des Cyclades s'exhume le long de la suture du Vardar à la faveur du Détachement Nord Cycladique en recoupant l'unité des schistes bleus Cycladiques.

L'extrusion de l'Anatolie intervient ensuite en réactivant la branche Est de la suture du Vardar en décrochement dextre et en provoquant le raccourcissement E-W du domaine des Cyclades pendant que se poursuit l'extension égéenne N-S.

Références

Agard P., Yamato P., Jolivet L. and E. Burov (2008), Exhumation of oceanic blueschists and eclogites in subduction zones: Timing and mechanisms. Earth-Science Reviews 92(1-2), 53-79.

Altherr R., Schliestedt M., Okrusch M., Seidel E., Kreuzer H., Harre W., Lenz H., Wendt I. and G. A. Wagner (1979), Geochronology of high-pressure rocks on Sifnos (Cyclades, Greece). Contributions to Mineralogy and Petrology 70, 245-255.

Altherr R., Kreuzer H., Wendt I., Lenz H., Wagner G.A., Keller J., Harre W. and A. Höhndorf (1982), A late Oligocene/Miocene high temperature belt in the Attic-Cycladic crystalline complex (SE Pelagonian, Greece). Geol. Jb., E23, 67-164.

Amante C. and B. W. Eakins (2009), ETOPO1 1 Arc-Minute Global Relief Model: Procedures, Data Sources and Analysis. NOAA Technical Memorandum NESDIS NGDC. 24-19.

Amato J.M., Johnson C., Baumgartner L. and B. Beard (1999), Rapid exhumation of the Zermatt-Saas ophiolite deduced from high-precision Sm–Nd and Rb–Sr geochronology. Earth and Planetary Science Letters 171(3), 425-438.

Andriessen P., Boelrijk N., Hebeba E., Priem N., Verdurmen E. and R. Vershure (1979), Dating the events of metamorphism and granitic magmatism in the alpine orogen of Naxos (Cyclades, Greece). Contribution to Mineralogy and Petrology 69, 215– 225.

Andriessen P, Banga G. and E. H. Hebeda (1987), Isotopic age study of pre-Alpine rocks in the basal units on Naxos, Sikinos and Ios, Greek Cyclades. Geol. Mijnbouw 66, 3 – 14.

Angelier J. (1977), Essai sur la néotectonique et les derniers stades tarditectoniques de l'arc Egéen et de l'Egée méridionale. Bulletin de la société géologique de France XIX (3), 651-662.

Angelier J. (1979), Néoctectonique de l'arc Egéen. Thèse d'état, Univ. Paris VI, Soc. Géol. Nord Pub, 3.

Angelier J., Lyberis N., Le Pichon X., Barrier E. and P. Hucho (1982), The tectonic development of the Hellenic arc and the Sea of Crete: a synthesis. Tectonophysics 86, 159-196.

Aoya M., Uehara S. and S. Wallis (2001), Thermal consequences of a subduction boundary jump: a numerical model for generating subduction-related clockwise P–T paths. Tectonics 21(1), :1004.

Armijo R., Meyer B., Hubert A. and A. Barka (1999), Westward propagation of the North Anatolian fault into the northern Aegean: timing and kinematics. Geology 27, 267-270.

Avigad D. and Z. Garfunkel (1989), Low angle faults above and below a blueschists belt : Tinos Island, Cycaldes, Greece. Terra Nova 1, 182-187.

Avigad D., Matthews A., Evan W. and Z. Garfunkel (1992), Cooling during the exhumation of a blueschist terrane : Sifnos (Cyclades), Greece. European Journal of Mineralogy 4 (3), 619-634.

Avigad D., Jolivet, L. and J.M. Azañon (1997), Back arc extension and dénudation of mediterranean éclogites. Tectonics 16 (6), 924-941.

Avigad D. (1998), High-pressure metamorphism and cooling on SE Naxos (Cyclades, Greece). Euroepan Journal of Mineralogy 10, 1309-1319.

Avigad D., Baer G. and A. Heimann (1998), Block rotations and continental extension in the central Aegean Sea: palaeomagnetic and structural evidence from Tinos and Mykonos (Cyclades, Greece). Earth and Planetary Science Letters 157, 23-40.

Avigad D., Ziv A. and Z. Garfunkel (2001), Ductile and brittle shortening, extension-parallel folds and maintenance of crustal thickness in the central Aegean (Cyclades, Greece). Tectonics 20 (2), 277-287. doi:10.1029/2000TC001190.

Baldwin S. L. (1996), Contrasting P-T-t histories for blueschists from the western Baja Terrane and the Aegean; effects of syn-subduction exhumation and backarc extension, in Subduction: Top to bottom. Geophys. Monogr., vol. 96, edited by G. E. Bebout et al., pp. 135 – 141, AGU, Washington, D. C.

Baldwin S. L., and G. S. Lister (1998), Thermochronology of the South Cyclades Shear Zone, Ios, Greece; effects of ductile shear in the argon partial retention zone. Journal of Geophysical Research 103, 7315 – 7336. doi:10.1029/97JB03106.

Ballhaus C., Tomaschek F. and S. Keay (1999), Stratigraphy and Age Relations on the Island of Syros, Cyclades. Journal of Conference Abstracts 4 (1), 72.

Baziotis I. (2008), Petrological and Geochemical study of the metamorphic rocks from east Attica. Ph.D. Thesis, National Technical University of Athens, Greece.

Bizon G., Bonneau M., Leboulenger P., Matesco S. and F. Thiébault (1976), Sur la signification et l'extension des massifs cristallins externes en Péloponèse méridional et dans l'arc Egéen. Bulletin de la société Géologique de France XVIII, 337-345.

Bond C., Butler R. and J. Dixon (2007), Co-axial horizontal streching within extending orogens: the exhumation of HP rocks of Syros (Cyclades) revisited. In: Ries, A., Butler, R. and Graham, R. (Eds), Deformation of the continental crust: The legacy of Mike Coward. Geological Society, London Special Publications 272. pp. 203-222. Doi : 10.1144/GSL.SP.2007.272.01.12

Bonneau M., Blake M.J.C., Gueyssant J., Kienast J.R., Lepvrier C., Maluski H. and D. Papanikolaou (1980 a), Sur la signification des séries métamorphiques (schistes bleus) des cyclades (Héllènides, Grèce). L'exemple de l'île de Syros. Comptes rendus de l'académie des sciences Paris 290, 1463-1466.

Bonneau M., Gueyssant J., Kienast J.R., Lepvrier C. and H. Maluski (1980 b), Tectonique et métamorphisme Haute pression d'âge Eocène dans les Hellénides : exemple de l'île de Syros (Cyclades, Grèce). Comptes rendus de l'académie des sciences Paris 291, 171-174.

Bonneau M.B. and Kienast, J.R. (1982), Subduction, collision et schistes bleu: exemple de l'Egée, Grèce. Bulletin de la société Géologique de France 7, 785-791.

Bonneau M. (1984) Correlation of the Hellenide nappes in the south-east Aegean and their tectonic reconstruction. Geological Society, London, Special Publications 17, 517-527.

Bousquet R., Goffé B., Henry P., Le Pichon X. and C. Chopin (1997), Kinematic, thermal and petrological model of the Central Alps: Lepontine metamorphism in the upper crust and eclogitisation of the lower crust. Tectonophysics 273(1-2), 105-127.

Bozkurt E., and R. Oberhänsli (2001), Menderes Massif (western Turkey): Structural, metamorphic and magmatic evolution—A synthesis. International Journal of Earth Sciences 89, 679–708. doi: 10.1007/s005310000173.

Brady J. B., Markley M. J., Schumacher J. C., Cheney J. T. and G.A. Bianciardi (2004), Aragonite pseudomorphs in high-pressure marbles of Syros, Greece. Journal of Structural Geology 26 (1), 3-9. doi:10.1016/S0191-8141(03)00099-3

Brichau S., Ring U., Ketcham R., Carter A., Stockli D. and M. Brunel (2006), Constraining the long-term evolution of the slip rate for a major extensional fault system in the central Aegean, Greece, using thermochronology. Earth and Planetary Science Letters 241, 293–306. doi:10.1016/j.epsl.2005.09.065

Brichau S., Ring U., Carter A., Monié P., Bolhar R., Stockli D. et al (2007), Extensional faulting on Tinos Island, Aegean Sea, Greece: how many detachments? Tectonics 26, TC4009. doi: 10.1029/2006TC001969

Brichau S., Ring U., Carter A., Bolhar R., Monié P., Stockli D. and M. Brunel (2008), Timing, slip rate, displacement and cooling history of the Mykonos detachment footwall, Cyclades, Greece, and implications for the opening of the Aegean Sea basin. J. Geol. Soc.165, 263 – 277, doi:10.1144/0016- 76492006-145.

Brichau S., Thomson S. and U. Ring (2010), Thermochronometric constraints on the tectonic evolution of the Serifos detachment, Aegean Sea, Greece. Int J Earth Sci (Geol Rundsch) 99, 379–393. doi : 10.1007/s00531-008-0386-0.

Bröcker M., Kreuzer H., Matthews A. and M. Okrusch (1993): 40Ar/39Ar and oxygen isotope studies of polymetamorphism from Tinos Island, Cycladic blueschist belt. Journal of Metamorphic Geology 11, 223-40.

Bröcker M. and M. Enders (1999), U-Pb zircon geochronology of unusual eclogite-facies rocks from Syros and Tinos (Cyclades, Greece). Geological Magazine 136, 111-118.

Bröcker M. and M. Enders (2001), Unusual bulk-rock compositions in eclogite-facies rocks from Syros and Tinos (Cyclades, Greece): implications for U-Pb zircon geochronology. Chemical Geology 175, 581-603.

Bröcker M. and L. Franz (1998), Rb-Sr isotope studies on Tinos Island (Cyclades, Greece): additional time constraints for metamorphism, extent of infiltration-controlled overprinting and deformational activity. Geological Magazine 135 (3), 369 - 382.

Bröcker M. and L. Franz (2006), Dating metamorphism and tectonic juxtaposition on Andros Island (Cyclades, Greece): results of a Rb–Sr study. Geological Magazine 143, 609-620.

Bröcker M. and A. Keasling (2006), Ionprobe U–Pb zircon ages from the high-pressure/ low temperature mélange of Syros, Greece: age diversity and the importance of pre- Eocene subduction. Journal of Metamorphic Geology 24, 615–631.

Brown M. (2010), Paired metamorphic belts revisited. Gondwana research 18(1), 46-59.

Brun J.P. and J. Van den Driessche (1994), Extensional gneiss domes and detachment fault systems: structure and kinematics. Bulletin de la société géologique de France 6, 519-530.

Brun J.P. and C. Faccenna (2008), Exhumation of high-pressure rocks driven by slab rollback. Earth and Planetary Science Letters 272, 1–7. doi:10.1016/j.epsl.2008.02.038

Brun J.P. and D. Sokoutis (2007), Kinematics of the Southern Rhodope Core Complex (North Greece). International Journal of Earth Sciences 96 (6), 1079-1099. doi:10.1007/s00531-007-0174-2

Brun J.P. and D. Sokoutis (2010), 45 m.y. of Aegean crust and mantle fl ow driven by trench retreat. Geology 38 (9), 815–818. doi: 10.1130/G30950.1.

Btittner D. and G. Kowalczyk (1978), Late Cenozoic stratigraphy and paleogeography of Greece- A review. In Alps, Apennines and Hellenides. Edited by H. Closs et al., IUCG Sci. Rep., 38, 494-501.

Buck RW. (1991), Modes of Continental Lithospheric Extension. Journal of geophysical research 96(B12), 20161, 20178.

Bulle F., Bröcker M., Gärtner C. and A. Keasling (2010), Geochemistry and geochronology of HP mélanges from Tinos and Andros, Cycladic blueschist belt, Greece. Lithos 117 (1-4), 61-81. doi:10.1016/j.lithos.2010.02.004

Burchfield B.C., Nakov R. and T. Tzankov (2003), Evidence from the Mesta halfgraben, SW Bulgaria, for the Late Eocene beginning of Aegean extension in the Central Balkan Peninsula. Tectonophysics 375, 61–76. doi: 10.1016/j.tecto.2003.09.001.

Burov E. (2001), A thermomechanical model of exhumation of HP and UHP methamorphic rocks in Alpine mountain belts. Tectonophysics 342(1-2), 113–136.

Calcagno P., Chiles J.-P., Courrioux G. and A. Guillen (2008), Geological modelling from field data and geological knowledge Part I. Modelling method coupling 3-D potential-field interpolation and geological rules. Physics of the Earth and Planetary Interiors 171 (1-4),147-157.

Carry N, Gueydan F, Brun J.P. and D. Marquer (2009), Mechanical decoupling of high-pressure crustal units during continental subduction. Earth and Planetary Science Letters

278(1-2),13-25.

Caumon, G., Lepage F., Sword C. and J.L. Mallet (2004), Building and Editing a Sealed Geological Model. Mathematical Geology 36 (4), 405-424.

Caumon G., Collon-Drouaillet P., Le Carlier de Veslud C., Viseur S. and J. Sausse (2009), Teachers aide: Surface-based 3D modeling of geological structures. Mathematical Geosciences 41 (8), 927-945.

Caumon G. (2010), Towards Stochastic Time-Varying Geological Modeling. Mathematical geosciences, 42 (5), 555-569. doi: 10.1007/s11004-010-9280-y

Chemenda A.I., Mattauer M., Malavieille J. and N. Bokun A. (1995), A mechanism for syn-collisional rock exhumation and associated normal faulting: Results from physical modelling. Earth and Planetary Science Letters 132(1-4), 225-232.

Chemenda A.I., Mattauer M. and A.N. Bokun (1996), Continental subduction and a mechanism for exhumation of high-pressure metamorphic rocks: new modelling and field data from Oman. Earth and Planetary Science Letters 143(1-4), 173-182.

Chilès J.P., Aug C., Guillen A. and T. Lees (2004), Modelling the geometry of geological units and its uncertainty in 3-D from structural data: The potential field method. In Proc. Orebody Modelling and Strategic Mine Planning, 313-320.

Chopin C. (1984), Coesite and pure pyrope in high-grade blueschists of the Western Alps. A first record and some consequences. Contributions to Mineralogy and Petrology 86, 107–118.

Cloos M. (1982), Flow melanges : Numerical modelling and geologic constraints on their origin in the Franciscan subduction complex, California. Bulletin of the Geological Society of America 93, 330-345.

Cloos M. and R. Shreve (1988a), Subduction-channel model of prism accretion, melange formation, sediment subduction, and subduc- tion erosion at convergent plate margins: Part I,

background and description. Pure and applied geophysics128 (3–4), 455–500.

Cloos M. and R. Shreve (1988b), Subduction-channel model of prism accretion, melange formation, sediment subduction, and subduc- tion erosion at convergent plate margins: Part II, implications and discussion. Pure and applied geophysics128 (3-4), 501-545.

Coleman R.G. and X. Wang (1995), Overview of the geology and tectonics of UHPM. Dans: Ultrahigh Pressure Metamorphism. New York: Coleman, R.G. and Wang, X., p. 1-32.

Coney P.J. and T.A. Harms. (1984), Cordilleran metamorphic core complexes: Cenozoic extensional relics of Mesozoic compression. Geology 12 (9), 550-554.

Cowan E. J., Beatson R. K., Ross H. J., Fright W.R., McLennan T. J., Evans T. R.J., Carr C., Lane R.G., Bright D.V., Gillman A.J., Oshust P.A. and M. Titley (2003), Practical implicit geological modeling. In S. Dominy, editor, Proc. 5th International Mining Conference, Australian Inst. Mining and Metallurgy, pp. 89-99.

Crittenden M.D., Coney P.J. and G.H. Davis (1980), Geologic development of the Cordilleran metamorphic core complexes. Geological society of America. Boudler, C.O.

Davies J.H. and F. von Blanckenburg (1995), Slab breakoff : A model of lithosphere detachment and its test in the magmatism and deformation of collisional orogens. Earth and Planetary Science Letters 129, 85- 102.

Davis G.H. and P.J. Coney (1979), Geologic development of the Cordilleran metamorphic core complexes. Geology 7, 120-124.

De Donatis M. (2001), Three-dimensional visualisation of the Neogene structures of an external sector of the Northern Apennines, Italy. AAPG Bulletin 95, 419-431.

De Kemp E. (2000), 3-D visualization of structural field data: examples from the Archean Caopatina Formation, Abitibi greenstone belt, Québec, Canada. Computers and Geosciences 26, 509-530.

Dewey J. (1988), Cordilleran metamorphic core complexes: Cenozoic extensional relics of Mesozoic compression. Tectonics 7 (6), 1123-1139.

Dixon J. E. and J. Ridley (1987), Syros (field trip excursion). In: Chemical transport in metasomatic processes (ed Helgeson, H. C.) Nato Advanced Study Institutes Series. Series C, pp. 489-500, D. Reidel Publishing Company, Dordrecht.

Drooger C.W. and J.E. Meulenkamp (1973), Stratigraphic contributions to geodynamics in the Mediterranean area: Crete as a case history. Bulletin de la société géologique de Greece 10, 193-200.

Dubois R. and Bignot G. (1979), Presence d'un "hardground" nummulitique au de la serie crétacée d'Almyropotamos (Eubee meridionale, Grece). Paris, Academie des Sciences Comptes Rendus, 289, 993–5.

Duchêne S., Lardeaux J. and F. Albarède (1997), Exhumation of eclogites: insights from depth-time path analysis. Tectonophysics 280 (1-2),125-140.

Dürr S.T., Altherr R., Keller J., Okrusch M. and E. Seidel (1978), The median Aegean Crystaline Belt: Stratigraphy, structure, metamorphism, magmatism, In Alp, Appenines, Hellenides (eds H. Cloos, D. Roeder and K. Schmidt), p. 455–77.

Dürr S. (1985), Geological Map of Greece, 1:50 000. Amorgos–Donoussa Sheet. Institute of Geological and Mining Research, Athens.

Engels M. and T. Reischmann (1999), Geochronology of the Pre-Alpine Basement of the Central Cyclades, Greece. Journal of Conference Abstracts 4, 806, EUG 10.

England P.C. and T.J.B. Holland (1979), Archimedes and the Tauern eclogites: the role of buoyancy in the preservation of exotic eclogite blocks. Earth and Planetary Science Letters 44, 287-294.

Ernst W. (1971), Metamorphic zonations on presumably subducted lithospheric plates from Japan, California, and the Alps. Contributions to Mineralogy and Petrology 34, 43-59.

Ernst W., Maruyama S. and S. Wallis (1997), Buoyancy-driven, rapid exhumation of ultrahigh-pressure metamorphosed continental crust. Proceeding of the Natlonal Academy of Sciences 94, 9532–9537.

Ernst W. (2010), Subduction-zone metamorphism, calc-alkaline magmatism, and convergent-margin crustal evolution. Gondwana Research18 (1), 8-16.

Eskola P.E. (1939) Die metamorphen Gesteine. Dans: Die Entstehung der Gesteine. Berlin: Julius Springer; p. 263-407.

Faure M. and M. Bonneau (1988), Données nouvelles sur I'extension néogène de I'Egée: la déformation ductile du granite miocene de Mykonos (Cyclades, Grèce). Comptes rendus de l'académie des sciences Paris, 307, 1553-1559.

Fernández O., Muñoz J.A., Arbués P., Falivene O. and M. Marzo (2004), Three-dimensional reconstruction of geological surfaces: An example of growth strata and turbidite systems from the Ainsa basin (Pyrenees, Spain). AAPG Bulletin 88, 1049-1068.

Frank T., Tertois A.L. and J.-L. Mallet (2007), 3-D-reconstruction of complex geological interfaces from irregularly distributed and noisy point data. Computers and Geosciences 33, 932-943.

Forster M. and G. Lister (2005), Several distinct tectono-metamorphic slices in the Cycladic eclogite–blueschist belt, Greece. Contributions to Mineralogy and Petrology, 150 (5), 523-545. doi: 10.1007/s00410-005-0032-9.

Forster M.A. and G.S. Lister (2009), Core complex related extension of the Aegean lithosphere initiated at the Eocene-Oligocene transition. Journal of Geophysical Research

(Solid Earth), 114, B02401, 36 PP. doi:10.1029/2007JB005382.

Forster M.A. and G.S. Lister (2010), Argon enters the retentive zone: reassessment of diffusion parameters for K-feldspar in the South Cyclades Shear Zone, Ios, Greece. In: Ring, U., Brandon, M.T., Lister, G.S. and Willett, S.D. (Eds). Advances in interpretation of geological processes: refinement of multi-scale data and integration in numerical modelling. Geological Society, London, Special Publication, Geological Society, London, Special Publications, 2010, 332, 17-34. doi: 10.1144/SP332.2.

Fytikas M., Giuliani O., Innocenti F., Marinelli G. and R. Mazzuoli (1976), Geochronological data on Recent magmatism of the Aegean Sea. Tectonophysics 31, T29-34.

Fytrolakis N., Papanikolaou D. and A. Panagopoulos (1981), Stratigraphy and structure of Amorgos Island, Aegean Sea. Annales Géologiques des Pays Helléniques, 30, 455–472.

Ganne J., Marquer D., Rosenbaum G., Bertrand J. and S. Fudral (2006), Partitioning of deformation within a subduction channel during exhumation of high-pressure rocks: a case study from the Western Alps. Journal of structural Geology, 28(7),1193-1207.

Gautier P., Ballèvre M., Brun J.P. and L. Jolivet (1990), Extension ductile et bassins sedimentaires mio-pliocenes dans les Cyclades îles de Naxos et Paros). Comptes rendus de l'Académies des Sciences Paris, 310, 147-153.

Gautier P., Brun J.P. and L. Jolivet (1993), Structure and kinematics of Upper Cenoizoic extensional detachment on Naxos and Paros (Cyclades Islands, Greece). Tectonics 12, 1180-1194.

Gautier P., and J.-P. Brun (1994a), Crustal-scale geometry and kinematics of late-orogenic extension in the central Aegean (Cyclades and Evvia Island). Tectonophysics 238, 399–424.

Gautier P., and J. P. Brun. (1994 b), Ductile crust exhumation and extensional detachments in the central Aegean (Cyclades and Evvia islands). Geodinamica Acta 7, 57 – 85.

Gautier, P. (1995), Géométrie crustale et cinématique de l'extension tardi-orogénique dans le domaine centre-égéen. Ïles des Cyclades et D'eubée (Grèce). PhD Thesis. Mémoire de Géosciences Rennes 61, 417 pp. ISBN 2-905532-60-2

Gautier P., Brun J.P., Moriceau R., Sokoutis D., Martinod J. and L. Jolivet (1999), Timing, kinematics and cause of Aegean extension: a scenario based on a comparison with simple analogue experiments. Tectonophysics 315 (1-4), 31-72. doi:10.1016/S0040-1951(99)00281-4

Gitahi N. (2004), Geochemistry and metamorphic evolution of éclogites on Syros island, Greece. Extended Abstracts, Seventeenth Annual Keck Research Symposium in Geology Proceedings, Lexington, VA, P.81-4.

Guillot S., Hattori K.H. and J. de Sigoyer (2000), Mantle wedge serpentinization and exhumation of eclogites: Insights from eastern Ladakh, northwest Himalaya. Geology, 28(3),199-202.

Guillot S., Hattori K.H., de Sigoyer J., Nägler T. and A. Auzende (2001), Evidence of hydration of the mantle wedge and its role in the exhumation of eclogites. Earth and Planetary Science Letters193(1-2),115-127.

Guillot S., Hattori K.H., Agard P., Schwartz S. and O. Vidal (2009), Exhumation processes in oceanic and continental subduction contexts: a review. Subduction zone Geodynamics, Frontiers in Earth Sciences, V, 175-205.

Gumiaux C., (2004), Geostatistics applied to the best fit interpolation of orientation data. Tectonophysics 376, 364, 241-259.

Gupta S., and M. J. Bickle (2004), Ductile shearing, hydrous fluid channelling and high-pressure metamorphism along the basement-cover contact on Sikinos, Cyclades, Greece, in Flow Processes in Faults and Shear Zones, edited by G. I. Alsop et al., Geol. Soc. Spec. Publ., 224, 161 – 175, doi:10.1144/GSL.SP.2004.224.01.11.

Hatzfeld D., Kassaras I., Panagiotopoulos D., Amorese D., Makropoulos K., Karakaisis G., et al. (1995), Microseimicity and strain pattern in northwestern Greece. Tectonics 14 (4), 773-785.

Hausmann J.F.L. (1845), Beiträge zur Oriktographie von Syra und ein neues Mineral, der Glaukophan. Gottinger geol Anzeigen, 193-198.

Hecht J. (1984), Geological map of Greece 1:50 000, Syros island. Athens: Institute of Geology and Mineral Exploration.

Hejl E., Riedl H., Weingartner H. (2002), Post-plutonic unroofing and morphogenesis of the Attic–Cycladic complex (Aegea, Greece). Tectonophysics 349, 37– 56.

Hejl E., Riedl H., Soulakellis N., Van Den Haute P. and H. Weingartner (2003), Young Neogene tectonics and relief development fission-track dating on the Aegean islands of Naxos, Paros and los (Cyclades, Greece). Mitt. Ostern Geol. Ges. ISSN 0251-7493 93 (2000) 105-127 Wien.

Henjes-Kunst F. and H. Kreuzer (1982), Isotopic dating of pre-alpidic rocks from the Island of Ios (Cyclades, Greece), Contribution to Mineralogy Petrology 80, 245 – 253, doi:10.1007/BF00371354.

Hermann J., Müntener O. and M. Scambelluri (2000), The importance of serpentinite mylonites for subduction and exhumation of oceanic crust. Tectonophysics, 327 (3-4), 225-238.

Heuret A. and S. Lallemand (2005), Plate motions, slab dynamics and back-arc deformation. Physics of The Earth and Planetary Interiors 149 (1-2), 31-51.

Holley E.A., Ross T. and J.T. Cheney (2004), Pressure-température conditions of metamorphism in eclogites, Syros, Greece. Geological Society of America, Abstracts with Programs 36 (4), 91.

Huet B., Labrousse L. and L. Jolivet (2009), Thrust or detachment? Exhumation processes in the Aegean: Insight from a field study on Ios (Cyclades, Greece). Tectonics 28, TC3007. doi:10.1029/2008TC002397

Huet B. (2010), Rhéologie de a lithosphère continentale l'exemple de la Mer Egée. PhD Thesis. Paris, 422 pp.

Iglseder C., Grasemann B., Schneider D. A., Petrakakis K., Miller C., Klötzli U. S., Thöni M., Zàmolyi, A. and C. Ramboussek. (2009), I and S-type plutonism on Serifos (W-Cyclades, Greece). Tectonophysics 473 (1-2), 69-83. doi:10.1016/j.tecto.2008.09.021

Jolivet L., Dubois R., Fournier M., Goffé B., Michard A. and C. Jourdan (1990), Ductile extension in alpine Corsica. Geology, 18 (10), 1007-1010.

Jolivet L. and M. Patriat. (1999), Ductile extension and the formation of the Aegean Sea. Geological Society, London, Special Publications 156, 427-456. doi: 10.1144/GSL.SP.1999.156.01.20

Jolivet L. and P. Goffé (2000), Les dômes métamorphiques extensifs. Comptes rendus de l'académie des Sciences 320, 739-751.

Jolivet L., Faccenna C., Goffé B., Burov E. and P. Agard (2003), Subduction tectonics ans exhumation of high-pressure metamorphic rocks in the Mediterranean orogens. American Journal of Science 303, 353- 409.

Jolivet L., Famin V., Mehl C., Parra T., Aubourg C., Hébert R. and P. Philippot (2004), Progressive strain localisation, boudinage and extensional metamorphic complexes, the Aegean Sea case. In: Whitney, D.L., Teyssier, C., Siddoway, C.S. (Eds.), Gneiss Domes in Orogeny: Geological Society of America Special Paper 380. Geological Society of America, Boulder, Colorado, pp. 185–210.

Jolivet L., Trotet F., Monié P., Vidal O., Goffé B., Labrousse L., Agard P. and B. Ghorbal

(2009), Along-strike variations of P–T conditions in accretionary wedges and syn-orogenic extension, the HP–LT Phyllite–Quartzite Nappe in Crete and the Peloponnese. Tectonophysics 480 (1-4), 133-148. doi:10.1016/j.tecto.2009.10.002.

Jolivet L. and J.P. Brun (2010), Cenozoic geodynamic evolution of the Aegean. International Journal of Earth Sciences 99 (1), 109-138. doi:10.1007/s00531-008-0366-4.

Jolivet L., Lecomte E., Huet B., Denèle Y., Lacombe O., Labrousse L., Le Pourhiet L. and C. Mehl (2010), The North Cycladic Detachment System. Earth and planetary Science Letters 289, 87–104. doi:10.1016/j.epsl.2009.10.032.

Katzir Y., Avigad D., Matthews A., Garfunkel Z. and B.W. Evans (2000), Origin, HP/LT metamorphism and cooling of ophiolitic mélanges in southern Evia (NW Cyclades), Greece. Journal of metamorphic Geology 18, 699–718.

Katzir, Y., Garfunkel, Z., Avigad, D. and A. Matthews (2008), Diverse P-T paths for the Cycladic ultramafic rock associations: Constraints on their origin, emplacement and exhumation. IOP Conf. Ser., Earth Environ. Sci. 2 012018.

Katsikatso G., Migiros G., Triantafillis M. and A. Mettos (1986 a), Geological structure of Internal Hellenides (E. Thessaly — SW Macedonia, Euboa–Attica–Northern Cyclades Islands and Lesvos). Geological and Geophysical Research, Special Issue 191–212.

Katsikatsos G., Dounas A. and P. Gaitanakis (1986 b), Geological Map of Greece, Athinai–Elefsis Sheet 1.50.000, I.G.M.E., Athens.

Keay S., (1998), The geological evolution of the Cyclades, Greece: constraints from SHRIMP U–Pb geochronology. Ph.D. thesis, Australian National University, Canberra, pp. 335.

Keay S., Lister G. and I. Buick (2001), The timing of partial melting, Barrovian metamorphism and granite intrusion in the Naxos metamorphic core complex, Cyclades, Aegean Sea, Greece. Tectonophysics 342, 275– 312.

Keiter M., Piepjohn K., Ballhaus C., Lagos M. and M. Bode (2004), Structural development of high-pressure metamorphic rocks on Syros Island (Cyclades, Greece). Journal of Structural Geology 26 (8), 1433-1445. doi:10.1016/j.jsg.2003.11.027.

Kissel C., Laj C., Poisson A. and N. Görür (2003), Paleomagnetic reconstruction of the Cenozoic evolution of the Eastern Mediterranean. Tectonophysics 362 (1-4), 199-217. doi:10.1016/S0040-1951(02)00638-8

Kissel C. and C. Laj (1988), The Tertiary geodynamic evolution of the Aegean arc: a paleomagnetic reconstruction. Tectonophysics 146 (1-4), 183-201. doi:10.1016/0040-1951(88)90090-X.

Klein-Helmkamp U., Reinecke T.B. Stöckhert (1995), The aragonite-calcite transition in LT-HP metamorphic carbonatic rocks from S-Evia, Greece: the microstructural and compositional record. Bochumer Geologische und Geotektonische Arbeiten 44, 78-83.

Kreutzer H., Harbe W., Lenz H., Wendt I.F. Henjes-Kunst (1978), K/Ar- und Rb/Sr-Daten von Mineralen aus dem polymetamorphen Kristallin der Kykladen-Insel Ios (Griechenland). Fortschr. Miner. 56 (1), 69-70, 1978.

Kumerics C., Ring U., Brichau S., Glodny J. and P. Monié (2005), The extensional Messaria shear zone and associated brittle detachment faults, Aegean Sea, Greece. Geological Society of London 162, 701-721.

Kounov A., Seward D., Bernoulli D., Burg J.-P. and Z. Ivanov (2004), Thermotectonic evolution of an extensional dome: The Cenozoic Osogovo-Lisets core complex (Kraiste zone, western Bulgaria). International Journal of Earth Sciences 93, 1008–1024. doi: 10.1007/s00531-004-0435-2.

Lagos M., Münker C., Tomaschek F. and C. Ballhaus (2002), Geochemistry and Lu-Hf geochronology of the metavolcanic Grizzas sequence in northern Syros (Cyclades, Greece). European Journal of Mineralogy 14 (1), 97.

Lagos M., Scherer E.E., Tomaschek F., Münker, C., Keiter, M., Berndt, J. and C. Ballhaus, (2007), High précision Lu-Hf geochronology of Eocene éclogite facies rocks from Syros, Cyclades, Greece. Chemical geology 243 (1-2), 16-35. doi:10.1016/j.chemgeo.2007.04.008.

Lallemand S. La subduction océanique. Gordon and Breach Science Publishers; 1999.

Lebayon B. (2005), Évolution structurale et métamorphique d'une croûte continentale subductée (Grand Paradis, Alpes occidentales). PhD Thesis. Mémoire de Géosciences Rennes 121, 385 p. ISBN : 2-914375-43-3

Le Pichon X. and J. Angelier (1979), The Hellenic arc and trench system: a key to the neotectonic evolution of the eastern Mediterranean area. Tectonophysics 60, 1–42.

Liati A. (2005), Identification of repeated Alpine (ultra) high-pressure metamorphic events by U-Pb SHRIMP geochronology and REE geochemistry of zircon: the Rhodope zone of N' Greece. Contributions to Mineralogy and Petrology 150, 608-630.

Liati A., Skarpelis N. and G. Pe-Piper (2009), Late Miocene magmatic activity in the Attic-Cycladic Belt of the Aegean (Lavrion, SE Attica, Greece): implications for the geodynamic evolution and timing of ore deposition. Geological Magazine 146, 732-742.

Liou J.G., Tsujimori T., Zhang R., Katayama I. and S. Maruyama (2004), Global UHP Metamorphism and Continental Subduction/Collision: The Himalayan Model. International Geology Review 46, 1-27.

Lister G. S., Banga G. and A. Feenstra (1984), Metamorphic core complexes of cordilleran type in the Cyclades, Aegean Sea, Greece. Geology 12, 221-225. doi:10.1130/0091-7613(1984)12<221:MCCOCT>2.0.CO,2

Lister G., Forster M. and T.J. Rawling (2001), Episodicity during orogenesis. Geological Society, London, Special Publications 184, 89–113.

Lister G. and M. Forster (2009), Tectonic mode switches and the nature of orogenesis. Lithos

113 (1-2), 274-291.

Malavieille J. (1993), Late orogenic extension in Mountain belts : Insights from the Basin and Range and the Late Paleozoic Variscan belt. Tectonics 12, 1115-1130.

Malavieille J. (2010), Impact of erosion, sedimentation and structural heritage on the structure and kinematics of orogenic wedges : analog models and case studies. Geological Society of America, account GSA Today 20 (1), 4-10.

Mallet J.L. (2002), Geomodeling. Applied Geostatistics. Oxford University Press, New York, NY, 624 p.

Maluski H., Vergely P., Bavay D., Bavay P. and G. Katsikatsos (1981), 39Ar/40Ar dating of glaucophane and phengites in southern Euboa (Greece) geodynamic implications. Bulletin de la Société Geologique de France V, 469–476.

Maluski H., Bonneau M., and J.R. Kienast (1987), Dating the metamorphic events in the Cycladic area: 40Ar/39Ar data from metamorphic rocks of the island of Syros (Greece), Bulletin de la Société géologique de France III, 833-841.

Martin L., Duchêne S., Deloule E. and O. Vanderhaeghe (2006), The isotopic composition of zircon and garnet: A record of the metamorphic history of Naxos, Greece. Lithos 87, 174–192

Mascle J. and L. Martin (1990), Shallow structure and recent evolution of the Aegean Sea: A synthesis based on continuous reflection profiles. Marine Geology 94, 271–299. doi: 10.1016/0025-3227(90)90060-W.

Matmon A., Simhai O., Amit R., Haviv I., Porat N., McDonald E., et al. (2009), Desert pavement–coated surfaces in extreme deserts present the longest-lived landforms on Earth. Geological Society of America Bulletin 121 (5-6), 688-697.

Matthews A. and M. Schliestedt (1984), Evolution of the blueschist and greenschist facies rocks of Sifnos, Cyclades, Greece. Contributions to Mineralogy and Petrology 88, 150–163.

McClay K.R. and A.D. Scott. (1991), Experimental models of hangingwall deformation in ramp-flat listric extensional fault systems. Tectonophysics 188 (1-2), 85-96. doi:10.1016/0040-1951(91)90316-K.

McClusky S., and 27 others, (2000), Global positioning system constraints on plate kinematics and dynamics in the eastern Mediterranean and Caucasus: Journal of Geophysical Research 105, 5695–5720.

McKenzie D. (1972), Active Tectonics of the Mediterranean Region. Geophysical journal international 30(2), 109-185.

McKenzie D.P. (1978), Active tectonics of the Alpine-Himalayan belt: The Aegean Sea and surrounding regions: Royal Astronomical Society Geophysical Journal 55, 217–254.

Mehl C., Jolivet L. and O. Lacombe (2005), From ductile to brittle: evolution and localization of deformation below a crustal detachment (Tinos, Cyclades, Greece). Tectonics 24, TC4017. doi:10.1029/2004TC001767.

Mehl C., Jolivet L., Lacombe O., Labrousse L. and G. Rimmelé (2007), Structural evolution of Andros island (Cyclades, Greece): a key to the behaviour of a !at detachment within an extending continental crust. In: Taymaz, T., Dilek, Y., Ylmaz, Y. (Eds.), The Geodynamics of the Aegean and Anatolia. Special Publications. Geological Society, London, pp. 41–73. doi:10.1144/SP291.3 0305-8719/07/$15.00.

Meulenkamp J.E., (1979), The Aegean and the Messinian salinity crisis. Proc. of the VI Coll. On the Geology of the Aegean Region 3, 1253- 1263.

Mercier J.L., Delibassis N., Gauthier A., Jarrige J.J., Lemeille F., Philip H., Sébrier M. and D. Sorel. (1979), La néotectonique de l'Arc Egéen. Rev. Geol. Dyn. Géogr. Phys. 21, 67-92.

Mercier J. L. (1981), Extensional-Compressional Tectonics Associated with the Aegean Arc:

Comparison with the Andean Cordillera of South Peru - North Bolivia. Phil. Trans. R. Soc. Lond. 300, (1454), 337-355. doi: 10.1098/rsta.1981.0068.

Miller E., Gans P.B. and J. Garing (1983), The snake range décollement: an exhumed mid-tertiary ductile-brittle transition. Tectonics 2 (3), 239-263.

Miyashiro A. (1961), Evolution of metamorphic belts. Journal of petrology 2, 277-311.

Miyashiro A. (1965), Metamorphic Rocks and metamorphic belts. Tokyo: Iwanami-Shoten.

Miyashiro A. (1973), Paired and unpaired metamorphic belts. Tectonophysics 17, 241-254.

Morris A. and M. Anderson (1996), First palaeomagnetic results from the Cycladic Massif, Greece, and their implications for Miocene extension directions and tectonic models in the Aegean. Earth and Planetary Science Letters 142 (3-4), 397-408.

Okrusch, M. and M. Bröcker (1990), Eclogites associated with high grade blueschists in the Cyclades archipelago, Greece: a review. European Journal of Mineralogy 2, 451-478.

Okay A.I., Satır M., Zattin M., Cavazza W. and G. Topuz (2008), An Oligocene ductile strike-slip shear zone: Uludağ Massif, northwest Turkey—Implications for the westward translation of Anatolia. Geological Society of America Bulletin 120, 893–911. doi: 10.1130/B26229.1.

Okay A.I., Zattin M. and W. Cavazza (2010), Apatite fission-track data for the Miocene Arabia-Eurasia collision. *Geology* 38 (1), 35–38. doi: 10.1130/G30234.1.

Papanikolaou D. (1978), Contribution to the geology of the Aegean Sea; the island of Andros. Annales Geologiques des Pays Helleniques 29(2), 477–553.

Papanikolaou D. (1980), Contribution to the geology of Aegean Sea: the island of Paros, Annal. Géol. Pays Helléniques 30 (1), 65–96.

Papanikolaou D.J. and L.H. Royden (2007), Disruption of the Hellenic arc: Late Miocene extensional detachment faults and steep Pliocene-Quaternary normal faults—Or what happened at Corinth? tectonics 26, TC5003. doi:10.1029/2006TC002007.

Parra T., Vidal O. and L. Jolivet (2002), Relation between the intensity of deformation and rétrogression in blueschist metapelites of Tinos Island (Greece) evidenced by chlorite–mica local equilibria. Lithos 63, 41– 66.

Peacock S.M. and K. Wang (1999), Seismic Consequences of Warm Versus Cool Subduction Metamorphism: Examples from Southwest and Northeast Japan. Science 286(5441), 937-939.

Pe-Piper G. and D.J.W . Piper (2002), The igneous rocks of Greece The anatomy of an orogen. Ed. Beiträge zur Regionalen Geologie der Erde, 573 pp. ISBN 978-3-443-11030-7

Pe-Piper G. and D. J. W. Piper (2007), Neogene back-arc volcanism of the Aegean: new insights into the relationship between magmatism and tectonics. in Cenozoic Volcanism in the Mediterranean Area, edited by L. Beccaluva and G. Bianchini, Geological Society of America, pp. 17–31. doi: 10.1130/2007.2418(1102)

Perraki M., Hoinkes G., Mposkos E. and M. Thoeni (2003), Early Cretaceous and Tertiary metamorphic events of the Pelagonian Zone in the E. Thessaly area, Greece. Geophysical Research Abstracts 5, 04438.

Philippon M., Brun J.P. and F. Gueydan (2009), Kinematic records of subduction and exhumation in the Ile de Groix Blueschist (Hercynian belt, Western france). Journal of structural geology 31 (11), 1308-1321. doi: 10.1016/j.jsg2009.07.003.

Platt JP. (1987), The uplift of high pressure-Low temperature metamorphic rocks. Phil. Trans. R. Soc. London A321, 87-103.

Pohl, J. (1999), Geologie und Hochdruckgesteine der Insel Syros, Griechenland. Diploma thesis, Geologisches Institut, Albert-Ludwigs Universitat, Freiburg, 107 pp.

Poli S., and M.W. Schmidt (1995), H2O transport and release in subduction zones—Experimental constraints on basaltic and andesitic systems. Journal of Geophysical Research 100, 22,299–22,314. doi: 10.1029/95JB01570.

Putlitz B., Cosca M. A. and J.C. Schumacher (2005), Prograde mica 40Ar/39Ar growth ages recorded in high pressure rocks (Syros, Cyclades, Greece). Chemical Geology 214 (1-2), 79-98. doi:10.1016/j.chemgeo.2004.08.056.

Ranalli G. (2000), Rheology of the crust and its role in tectonic reactivation. Journal of Geodynamics 30 (1-2), 3-15.

Rawling T.J. and G. Lister (1999), Oscillating modes of orogeny in the Southwest Pacific and the tectonic evolution of New Caledonia. Geological Society, London, Special Publications 154, 109-127.

Ridley J. (1982), Arcuate lineation trends in a deep level, ductile thrust belt, Syros, Greece. Tectonophysics 88 (3-4), 347-360. doi:10.1016/0040-1951(82)90246-3.

Ridley J. (1984), Listric normal faulting and the reconstruction of the synmetamorphic structural pile of the Cyclades. Geological society of London, special publication 17, 755-761.

Ring U., Brandon M., Wiellett S. and G. Lister (1999), Exhumation processes. Geological Society, London, Special Publications 154, 1-27.

Ring U., Layer P. W. and T. Reischmann (2001), Miocene high-pressure metamorphism in the Cyclades and Crete, Aegean Sea, Greece: Evidence for large-magnitude displacement on the Cretan detachment. Geology 29, 395 – 398.

Ring U. and T. Reischmann (2002), The weak and superfast Cretan detachment, Greece: Exhumation at subduction rates in extruding wedges. Journal of the Geological Society, London. 159, 225-228

Ring, U. and P.W. Layer (2003), High-pressure metamorphism in the Aegean eastern mediterranean : Underplating and exhumation from the late cretaceous until the Miocene to Recent above the retrreating Hellenic subduction zone. Tectonics 22 (1022), 23 pp. doi:10.1029/2001TC001350.

Ring U., Thomson S.N. and M. Bröcker (2003), Fast extension but little exhumation : the Vari detachment in the Cyclades, Greece. Geological magazine 140 (3), 245-252. doi: 10.1017/S0016756803007799.

Ring U. (2007), The Geology of Ikaria Island: The Messaria extensional shear zone, granites and the exotic Ikaria nappe. Journal of the Virtual Explorer 27, Paper 3, doi:10.3809/jvirtex.2007.00171.

Ring U., Okrusch M. and T. Will (2007), Samos Island, Part I: metamorphosed and nonmetamorphosed nappes, and sedimentary basins. Journal of the Virtual Explorer 27, paper 5. doi:10.3809/jvirtex.2007.00180

Ring U., and C. Kumerics (2008), Vertical ductile thinning and its contribution to the exhumation of highpressure rocks: The Cycladic blueschist unit in the Aegean. Tectonics 165 (6), 1019-1030.

Ring U., Glodny J., Thomas W. and S. Thomson (2010), The Hellenic Subduction System: High-Pressure Metamorphism, Exhumation, Normal Faulting, and Large-Scale Extension. Annual Review of Earth and Planetary Sciences 38, 45-76.

Roure F., Brun J-P., Colletta B., and J. Van Den Driessche (1992), Geometry and kinematics of extensional structures in the Alpine Foreland Basin of Southeastern France. Journal of Structural Geology, 14 (5), 503-519. doi:10.1016/0191-8141(92)90153-N.

Rosenbaum G., Avigad D. and M. Sánchez-Gómez (2002), Coaxial flattening at deep levels of orogenic belts: evidence from blueschists and eclogites on Syros and Sifnos (Cyclades, Greece), Journal of Structural Geology 24 (9), 1457-1462. doi:10.1016/S0191-

8141(01)00143-2.

Rosenbaum G. and U. Ring (2007), Structure and metamorphism of Amorgos: a field excursion. Journal of the Virtual Explorer, Volume 27, Paper 7.

Schliestedt M., Bartsch V., Carl M., Matthews A. and F. Henjes-Kunst (1994), The P–T path of greenschist-facies rocks from the island of Kithnos (Cyclades, Greece). Chemie Erde 54, 281–296.

Rubatto D. and J. Hermann (2001), Exhumation as fast as subduction? Geology 29, 3-6.

Schmädicke E., and T.M. Will (2003), Pressure-temperature evolution of blueschist facies rock from Sifnos, Greece, and implications for the exhumation of high-pressure rocks in the central Aegean. Journal of Metamorphic Geology 21, 799 – 811, doi:10.1046/ j.1525-1314.2003.00482.x.

Shreve R.L. and M. Cloos (1986), Dynamics of sediment subduction, melange formation and prism accretion. Journal of geophysical research 91(10), 229-10 245.

Schumacher J.C.B., Brady J., Cheney J.T. and R.R. Tonnsen (2008), Glaucophane bearing Marbles on Syros, Greece. Journal of Petrology 49 (9), 1667-1686. doi:10.1093/petrology/egn042

Şengör A.M.C., Tüysüz O., İmren C., Sakınç M., Eyidoğan H., Görür N., Le Pichon X. and C. Rangin (2005), The North Anatolian fault: A new look. Annual Review of Earth and Planetary Sciences 33, 37–112. doi: 10.1146/annurev. earth.32.101802.120415.

Shaked Y., Avigad D. and Z. Garfunkel (2000), Alpine high-pressure metamorphism at the Almyropotamos window (southern Evia, Greece). Geological Magazine 137 (4), 367–380.

Smith DC. (1984), Coesite in clinopyroxene in the Caledonides and its implications for geodynamics. Nature 310, 641–644.

Sobolev N.V. and V.S. Shatsky (1990) Diamond inclusions in garnets from metamorphic rocks. Nature 343, 742–74.

Sotiropoulos S., Kamberis E., Triantaphyllou M.V. and T. Doutsos (2003), Thrust sequences in the central part of the External Hellenides. Geological Magazine 140 (6), 661-668. DOI: 10.1017/S0016756803008367.

Spear F.S. and RR. Parrish (1996), Petrology and Cooling Rates of the Valhalla Complex, British Columbia, Canada. Journal of petrology 37(4), 733-765.

Stoëckert B. and T.V. Gerya (2005), Pre-collisional high pressure metamorphism and nappe tectonics at active continental margins: a numerical simulation. Terra Nova 17(2), 102-110.

Stouraiti C., Mitropoulos P., Tarney J., Barreiro B., McGrath A.M. and E. Baltatzis (2010), Geochemistry and petrogenesis of late Miocene granitoids, Cyclades, southern Aegean: Nature of source components. Lithos 114, 337–352.

Tirel C., Gautier P., van Hinsbergen D.J.J., and M.J.R. Wortel (2009), Sequential development of interfering metamorphic core complexes: numerical experiments and comparison with the Cyclades, Greece. Geological Society, London, Special Publications 311, 257-292.

Tomaschek F. and C. Ballhaus (1999), TheVari Unit on Syros (Aegean Sea) and its relation to the Attic-Cycladic Crystalline Complex. Journal of Conference Abstracts 4, 72.

Tomaschek F., Kennedy A., Keay S. and C. Ballhaus, (2001). Geochronological constraints on Carboniferous and Triassic magmatism in the Cyclades: SHRIMP U---Pb ages of zircons from Syros, Greece. Journal of Conference Abstracts 6(1), 315.

Tomaschek F., Kennedy A. K., Villa I.M., Lagos M. and C. Ballhaus (2003), Zircons from Syros, Cyclades, Greece. Recrystallization and mobilization of zircon during high-pressure metamorphism. Journal of Petrology 44, 1977-2002.

Tomaschek F., Keiter M., Kennedy A.K. and C. Ballhaus (2008), Pre-Alpine basement within the Northern Cycladic Blueschist Unit on Syros Island, Greece. - Zt. dt. Ges. Geowiss. 159 (3), 11 pp. doi: 10.1127/1860-1804/2008/0159-0000.

Trotet F., Jolivet L. and O. Vidal (2001 a), Tectono-metamorphic evolution of Syros and Sifnos islands (Cyclades, Greece), Tectonophysics 338, 179-206.

Trotet F., Vidal O. and L. Jolivet (2001b), Exhumation of Syros and Sifnos metamorphic rocks (Cyclades, Greece). New constraints on the P-T paths. European Journal of Mineralogy 13 (5), 901 – 920. doi: 10.1127/0935-1221/2001/0013/0901.

Tsujimori T., Sisson V.B., Liou J.G., Harlow G.E. and S.S. Sorensen (2006), Very-low-temperature record of the subduction process: A review of worldwide lawsonite éclogites. Lithos 92, 609–624.

Vandenberg L.C. and G.S.Lister (1996), Structural analysis of basement tectonics fromthe Aegean metamorphic core complex of Ios, Cyclades, Greece. Journal of structural geology 18, 1437–1454.

van der Maar P., and J. B. H. Jansen (1983), The geology of the polymetamorphic complex of Ios, Cyclades, Greece and its significance for the Cycladic Massif, Geol. Rundsch. 72, 283 – 299. doi:10.1007/ BF01765910.

van Hinsbergen D.J.J., Langereis C.G. and J.E. Meulenkamp (2005), Revision of the timing, magnitude and distribution of Neogene rotations in the western Aegean region. Tectonophysics 396, 1–34. doi: 10.1016/j.tecto.2004.10.001.

Walcott C.R. and S.H. White (1998), Constraints on the kinematics of post-orogenic extension imposed by stretching lineations in the Aegean region Tectonophysics 298, 155–175. doi : 0040-1951/98/$19.00.

Will T., Okrusch M., Schmädicke E., and G. Chen (1998), Phase relations in the greenschist-blueschist-amphibolite-eclogite facies in the system Na2O-CaO-FeO-MgO-Al2O3-SiO2 –

H2O (NCFMASH), with application to metamorphic rocks from Samos, Greece. Contributions to Mineralogy and Petrology 132, 85 – 102. doi:10.1007/s004100050406.

Wijbrans J. R., and I. McDougall (1986), 40Ar/39Ar dating of white micas from an alpine high-pressure metamorphic belt on Naxos (Greece): The resetting of the argon isotopic system, Contributions to Mineralogy and Petrology 93, 187 – 194. doi:10.1007/BF00371320.

Wijbrans J.R., Schliestedt M. and D. York (1990), Single grain argon laser probe dating of phengites from the blueschist to greenschist transition on Sifnos (Cyclades, Greece). Contribution to mineralogy and petrology 104, 582-593.

Whitney D.L. and P.B. Davis (2006), Why is lawsonite eclogite so rare? Metamorphism and préservation of lawsonite eclogite, Sivrihisar, Turkey. Geology 34 (6), 473–476. doi: 10.1130/G22259.1.

Wortel M.J.R., and W. Spakman (2000), Subduction and slab detachment in the Mediterranean-Carpathian region. Science 290, 1910–1917, doi:10.1126/science.290.5498.1910.

Yamato P., Burov E., Le Pourhiet L., and L. Jolivet (2008), HP-UHP exhumation during slow continental subduction:next term Self-consistent thermodynamically and thermomechanically coupled model with application to the Western Alps. Earth and Planetary Science 271(1-4), 63-74.

Zack T., Rivers T., Brumm R., and A. Kronz (2004), Cold subduction of oceanic crust: Implications from a lawsonite eclogite from the Dominican Republic. European Journal of Mineralogy 16, 909–916. doi: 10.1127/0935-1221/2004/0016-0909.

Zattin M., Okay A.I., and W. Cavazza (2005), Fissiontrack evidence for late Oligocene and mid-Miocene activity along the North Anatolian fault in south-western Thrace. Terra Nova 17, 95–101. doi: 10.1111/j.1365-3121.2004.00583.x.

Ziv A., Katzir Y., Avigad D. and Z. Garfunkel (2010), Strain development and kinematic significance of the Alpine folding on Andros (western Cyclades, Greece). Tectonophysics 488 (1-4), 248-255.

ANNEXES

ANNEXE A : Estimations PT

Estimations PT

a/ Relations texturales dans les schistes bleus à lawsonite.

La lame présente une matrice à glaucophane, sphène, micas blancs, chlorite, épidote et grenats et des amas losangiques contenant de la calcite, du glaucophane, de l'épidote, des micas blancs, des grenats et du sphène. Les amas losangiques correspondent à des porphyroblastes de lawsonites qui ont conservé leur forme malgré la rétromorphose : ce sont des pseudomorphes de lawsonites. En lame mince, la foliation est principalement marquée par l'orientation préférentielle de la glaucophane, des micas blancs, de la chlorite et du sphène. La foliation tourne légèrement autour de ces pseudomorphes de lawsonites, indiquant une croissance syn cinématique des lawsonites. Des grenats et des sphènes se trouvent en inclusion dans les pseudormophes de lawsonites.

L'analyse texturale a mis en évidence deux types de grenats : ceux qui sont en inclusion dans les pseudomorphes de lawsonites et des grenats dans la matrice. Du glaucophane et de l'épidote se trouvent en inclusion dans les grenats de la matrice et des porphyroblastes. Les grenats de la matrice contrairement à ceux contenus en inclusion dans les pseudomorphes présentent des queues de cristallisation à Chlorite.

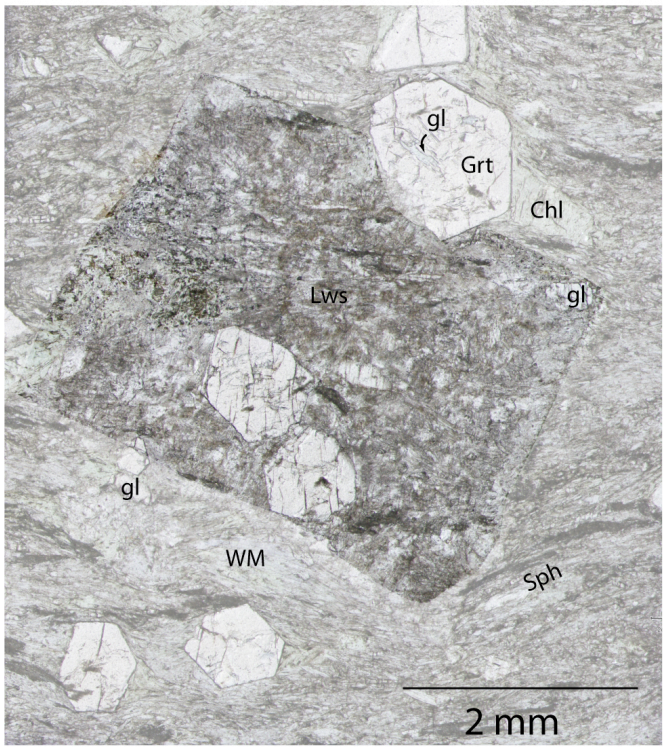

Fig. B-1. Photographie de lame mince montrant les relations entre une pseudomorphose de lawsonite, les grenatset la foliation marquée par le sphène (minéral allongé et sombre), glaucophane et les micas blancs.

b/ Chimie des minéraux.

Les analyses chimiques des minéraux ont été réalisées avec une microsonde électronique Cameca SX 100 (Microsonde Ouest à Brest, sous l'oeil attentif de Marcel Bohn). Les réglages utilisés durant ces mesures étaient de 15 kV, 20 nA et un temps de comptage de 10 sec sur le pic.

-Grenat

Les cartes par rayons X de distribution d'éléments chimiques pour le Ca, Mn, Mg, Fe et Ti montrent 1) que tous les grenats présentent la même zonation qu'ils soient dans la matrice ou bien en inclusion dans les pseudomorphes de lawsonite, et 2) que malgré leur forme automorphe et leurs bordures nettes (au microscope optique), les grenats présentent une zonation chimique au niveau de leurs bordures.

La zonation chimique dans les cœurs des grenats est caractérisée par une décroissance de la teneur en spéssartine (de 11 à 3 mol%) compensée par une augmentation de pyrope (de 9 à 10 mol%) et d'almandin (de 50 à 60 mol%) du cœur vers la bordure (Voir traversée de Grenat,

Fig. XX). La teneur en grossulaire oscille de manière irrégulière entre 26 et 32 mol%. XFe (Fe/(Fe+Mg)) est relativement plat et montre des teneur variant entre 86 et 89 mol%. En bordure de grenat, les tendances s'inversent : on observe une augmentation de grossulaire et spéssartine contre une diminution d'almandin et de pyrope.

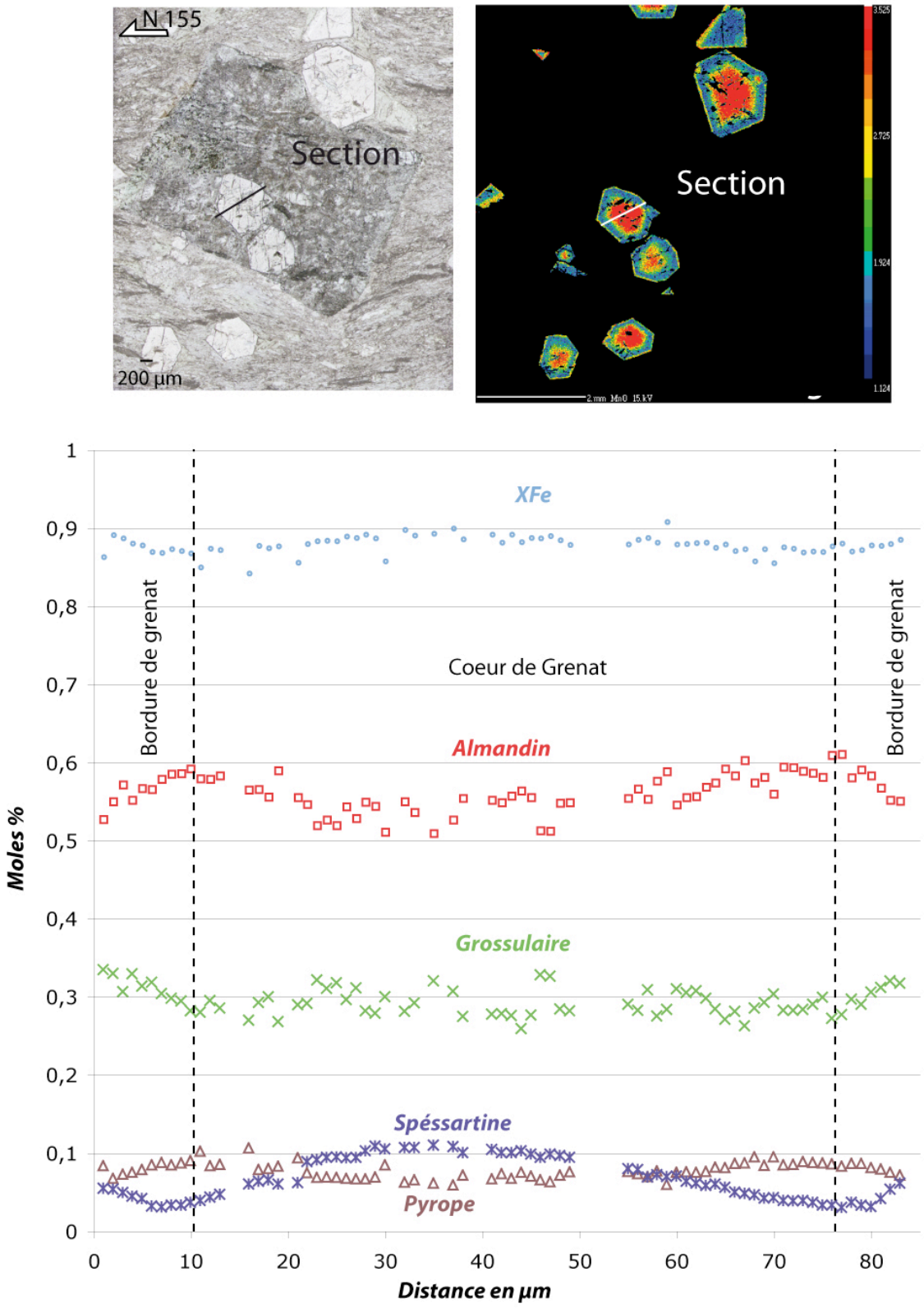

Fig. B- 2. Photographie de lame mince (a) et carte de la concentration en MnO (≈ spessartine) correspondante (b). Profile de grenat (localisé par un trait noir et blanc en (a) et (b), respectivement) montrant l'évolution des teneurs en Almandin (Fe), Grossulaire (Ca), Spéssartine (Mn) et Pyrope (Mg), et la variation de XFe.

- Amphibole bleue

Les amphiboles analysées sont relativement homogènes (sauf pour une amphibole, qui par ailleurs se situe dans la matrice) (Fig. B-3). Ces amphiboles car présentent plus de 1,5 atome de Sodium sur le site M4 (cette proportion varie entre 1,53 et 1,85), elles présentent toutes un (Na+K)/(A) inférieur à 0,5 (compris entre 0,002 et 0,145) sauf l'analyse isolée qui a un (Na+K)/(A) de 0,67. Elles présentent toutes une somme Mg+Fe2+Mn comprise entre 3,12 et 3,47. Ce sont donc des amphiboles sodiques car elles remplissent les conditions suivantes: Na(M4)>1,5 ;(Na+K)/(A)>0,5 et Mg+Fe2+Mn>2,5.

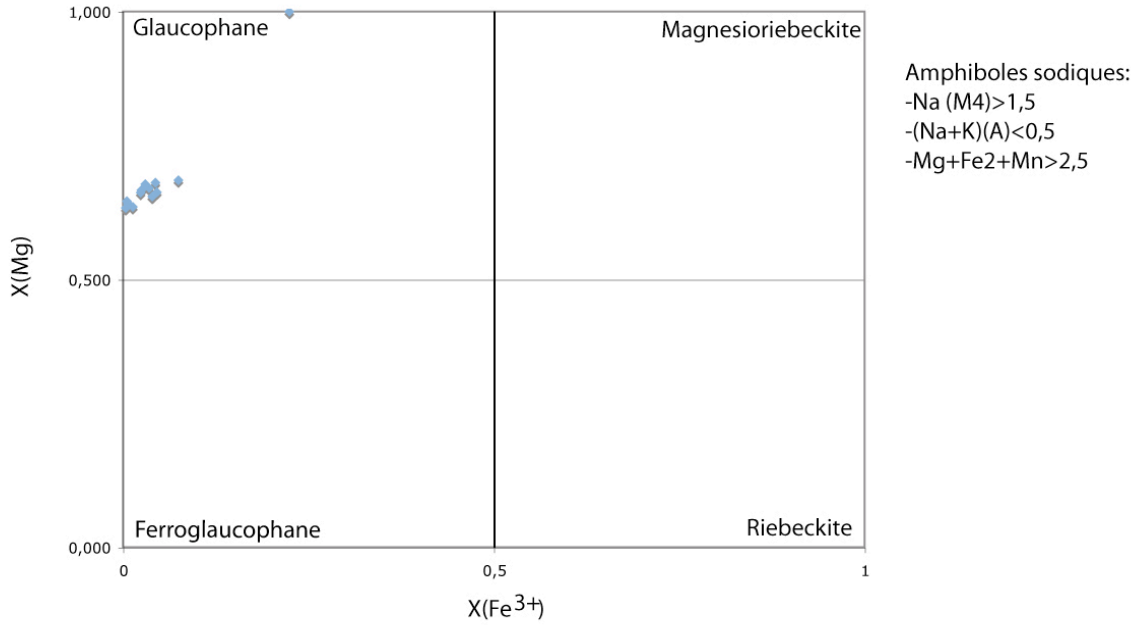

Fig. B- 3. Digramme montrant la composition chimique des amphiboles sodiques de la lame analysée. D'après la classification de Leake et al., (1997).

- Micas Blancs

Les analyses des micas blancs font apparaître que deux types de micas sont spatialement réparties. La paragonite est localisée dans les pseudomorphes de lawsonite alors que la phengite est localisée dans la matrice.

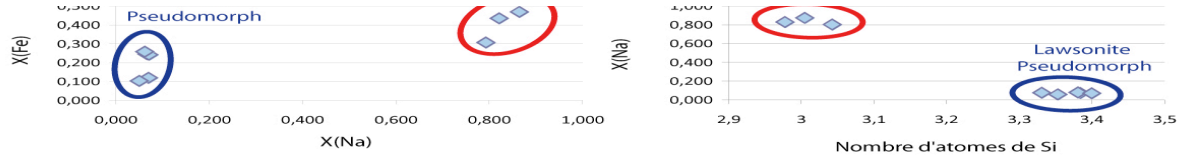

Fig. B- 4. Composition chimique des micas blancs de la lame mince.

Chlorite

La Chlorite uniquement contenue dans la matrice montre une composition chimique relativement homogène (X_{Fe} =0,278-0,342 ; $X_{Al, T2}$=0,57-0,62 ; X_{Mn}=0,0018-0,007).

Sphène

Le sphène est composé de 30.7 mol% de SiO_2, 29,4 mol% de CaO, 39 mol% de TiO_2 et 1,6 mol% de Al_2O_3.

Epidote

Les épidotes sont relativement homogènes, et présentent des rapports X_{Fe} voisins de 1 et sont pauvres en manganèse (X_{Mn}=0,017-0,064, X_{Fe} =0,971-1).

b/ Modèliation numérique des paragénèses à l'équilibre.

- Estimation des conditions P-T moyennes.

La paragénèse retenue, considérée comme étant à l'équilibre se compose de : amphibole, mica blanc, chlorite, épidote, grenat, lawsonite, sphène et quartz. Cette paragénèse permet d'estimer les conditions P-T moyennes atteintes par cet échantillon grâce au mode «average PT» de THERMOCALC. Thermocalc trouve quatre réactions thermodynamiques indépendantes :

1) 9cel + 12clin + 24cz = 9mu + 23py + 16gr + 60H2O
2) 21mu + 37py + 44gr + 60law = 21cel + 18clin + 96cz
3) 21mu + 44gr + 37alm + 60law = 21fcel + 18daph + 96cz
4) 21mu + 90cel + 44gr + 37alm + 60law = 111fcel + 18clin + 96cz

Cet ensemble de quatre réactions se croisent dans un champ restreint correspondant à l'estimation des conditions PT maximales atteintes par l'échantillon qui est de 16,8 kbar ±2,3 et 527 °C ±18 (corrélation de 0,771, sigfit de 1,30).

- Calcul de pseudosection.

Une pseudosection est un diagramme de phases qui représente des paragenèses minérales qu'une roche de composition chimique donnée formerait à différentes pressions et températures. La force d'un tel diagramme est qu'à partir l'analyse texturale de la lame mince, couplée à l'étude de la composition chimique des minéraux et de leur éventuelle zonation, permet l'élaboration d'un chemin pression température. La pseudosection P-T présentée ici a été calculée avec THERMOCALC v. 3.33i (Powell et Holland 1988), en utilisant la base de donnée thermodynamique 5.5 (Holland et Powell, 1998, mise à jour de novembre 2003). La composition chimique de la roche totale est donnée par les analyses réalisées au CRPG de Nancy (Analyse des éléments majeurs par ICP-AES sur poudre, fusion avec $LiBO_2$ et dissolution par HNO_3). La teneur en FeO a été analysée par titration.

L'objectif de ce calcul étant de contraindre la position du chemin prograde des faciès à Lawsonites de l'île de Syros et ainsi de explorer le caractère supposé prograde de la croissance des Lawsonites. La pseudosection a été calculée dans le système NCKFMASHTO (système dont les constituants sont : Na, Ca, K, Fe, Mg, Al, Si, H, Ti, O). On considère l'équilibre chimique à l'échelle de la lame pour la paragénèse retenue est tardive et se compose des: bordures de grenats, glaucophanes, micas blancs, sphène, clinozoïsite de la matrice et cristaux de lawsonites. En effet, le cœur des grenats n'est pas à l'équilibre avec la paragénèse retenue car ils fractionnent beaucoup (ils pompent tout le Mg disponible) et modifient alors la composition de roche totale disponible pour les cristallisations plus tardives.

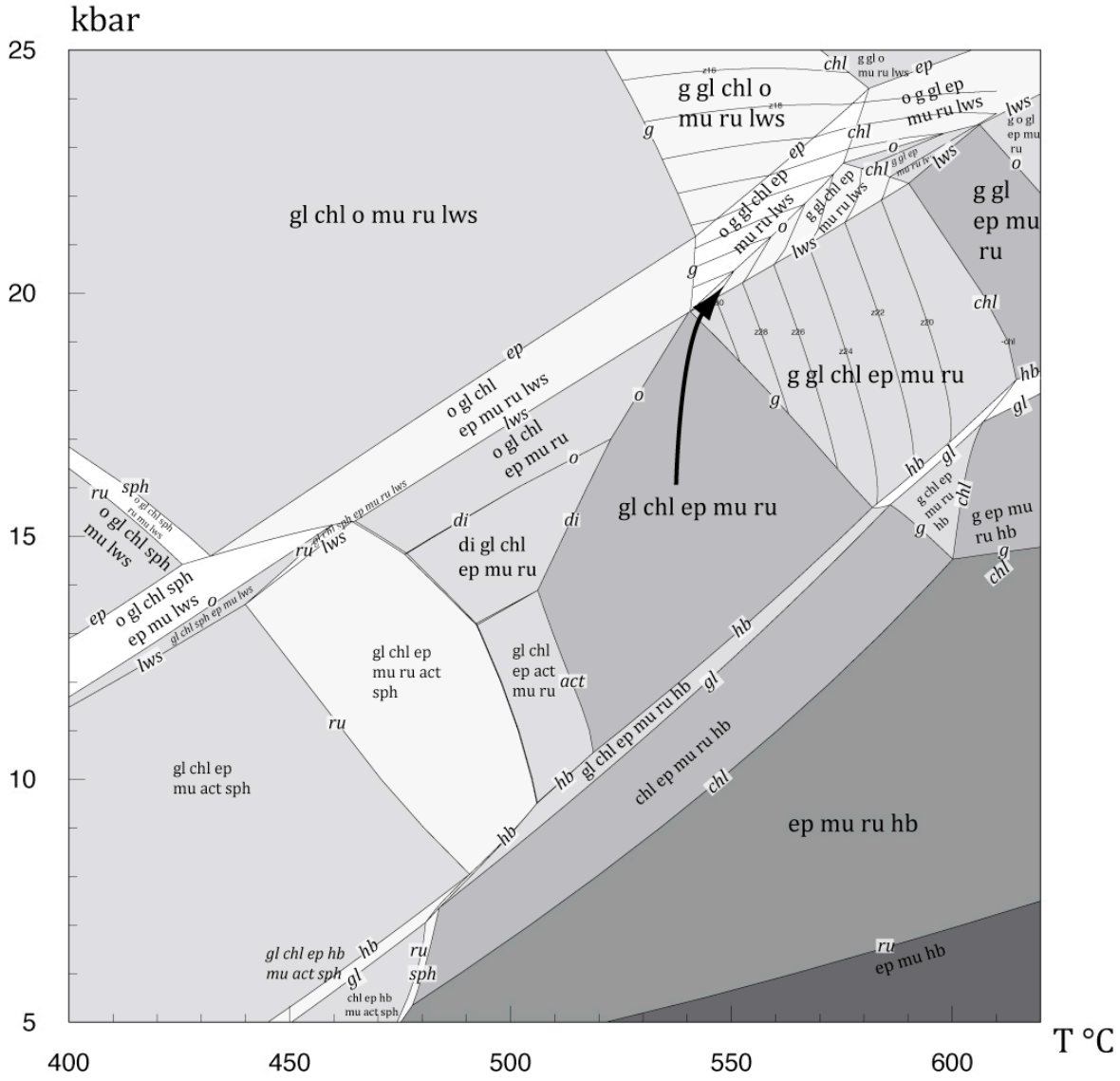

Fig. B-5. Diagramme de phase et chemin pression température déduit des relations texturales.

Les grenats de la lame présentent tous la même zonation chimique à l'intérieur et à l'extérieur des pseudomorphes de lawsonites. Cela indique qu'ils ont eu une croissance commune à l'équilibre avec les minéraux constitutifs de la matrice. La croissance de la lawsonite est tardive par rapport à celle du grenat. La lawsonite cristallise au dépend en partie de la chlorite car les queue de cristallisation autour des grenats ne sont pas conservées lorsqu'ils sont en inclusion dans les porphyroblastes de lawsonite. Cette crsitallisation a lieu en cours de déformation car la foliation tourne légèrement autour des pseudomorphes de lawsonites.

Je déduis de ces relations texturales un chemin prograde (symbolisé par la flèche noire sur le diagramme): les minéraux de la matrice ont cristallisés à l'équilibre : gl+chl+ep+mu+ru, ensuite que la roche est entrée dans le champ de stabilité g gl chl ep mu ru,

c'est à ce moment que le grenats ont cristallisés (avec un z(g) de 0,3 –teneur en grossulaire-). Enfin, elle est passée dans celui lws g gl chl ep mu ru, cristallisant ainsi la lawsonite en fin de trajet prograde.

Le champ de stabilité du sphène calculé ici ne tient pas en compte la teneur en Al du sphène. Or celle ci n'est pas nulle et elle modifie grandement son champ de stabilité. Il est plus probable que le sphène soit encore stable dans les domaines de stabilité précédemment discutés (cela colerais aussi mieux à la paragenèse observée).

ANNEXE B : Tentative de datation des sphènes

Datation des Sphènes pour apporter une contrainte pour le début de l'enfouissement/histoire métamorhpique

Les analyses des sphènes ont été réalisées avec un laser à ablation ICP-MS (ICP-MS Clermont-Ferrand, en collaboration avec Marc Poujol et Jean-Louis Paquett). Les mesures ont été réalisées avec une puissance 8 de mJ, un diamètre d'ablation 58 μm et une fréquence de 5Hz (Résultats, Tableau C-1, correspondance analyses situation dans la lame, Fig. C1).

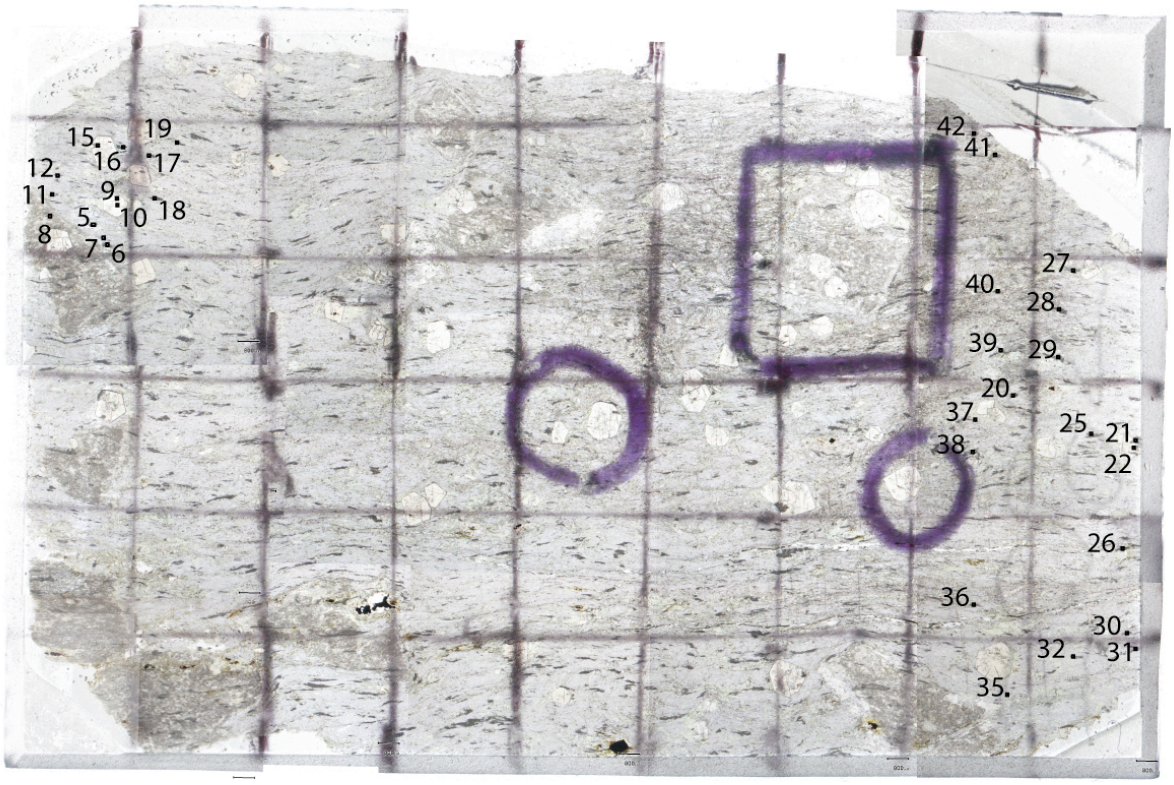

Fig. C-1. Lame mince à Lawsonite avec emplacement des sphènes analysés.

La datation en contexte in situ des Sphènes de cette lame à donné un âge de 59+-140 Ma (Fig. C-2). L'erreur sur cet âge vient du fait que les mesures sont situées au-dessus de la concordia. Cependant, les mesures s'alignent sur une droite de régression mais nettement au-dessus de la concordia. Cela peu s'epxliquer par soit un lessivage U ou bien apport de Pb. Un lessivage linéaire est peu probable. On a donc plus vraisemblablement

un apport de Pb commun très vieux -3 Ga 31±Ma- (est ce que cela signe interaction avec le manteau? Un manteau très «vieux » ?)

Fig. C-2. Diagramme Concordia avec les données.

	Radiogenic Ratios (2σ uncertainties)							Age Ma (1σ uncertainties)					
Analysis_#	$^{206}Pb/^{238}U$	±	$^{207}Pb/^{235}U$	±	$^{207}Pb/^{206}Pb$	±	Rho	$^{207}Pb/^{235}U$	±	$^{206}Pb/^{238}U$	±	$^{207}Pb/^{206}Pb$	±
05051010a	164,36780	4,63964	5,13338	0,17422	0,00208	0,00208	0,65	———	91,55	5186,8	14,24	3067,3	14,28
06051010a	132,01776	2,07968	4,18324	0,10334	0,00137	0,00137	0,65	———	64,27	4965,7	7,94	3044,2	9,53
07051010a	122,59008	2,28800	3,90416	0,10350	0,00157	0,00157	0,65	———	68,02	4891,1	9,4	3036,1	11,02
08051010a	102,94706	1,70080	3,23092	0,08080	0,00151	0,00151	0,65	9298,4	61,56	4715,3	8,31	3059,6	10,44
10051010a	37,33363	0,96634	1,18825	0,03712	0,00287	0,00287	0,65	5048,2	54,67	3702,4	12,8	3037,2	20,01
11051010a	127,09700	2,54870	3,98141	0,10834	0,00169	0,00169	0,65	———	70,1	4927,4	10,1	3062,7	11,59
12051010a	34,16291	0,74260	1,05974	0,02982	0,00253	0,00253	0,65	4658	46,65	3614,8	10,72	3078,4	17,2
15051010a	41,51023	1,82700	1,25760	0,05948	0,00521	0,00521	0,65	5249,3	84,92	3807,4	21,82	3116,2	34,22
16051010a	45,46078	0,71312	1,42425	0,03382	0,00174	0,00174	0,65	5708,5	44,96	3897,7	7,79	3062,7	11,95
17051010a	40,98458	0,85600	1,26943	0,03454	0,00235	0,00235	0,65	5283	49,04	3794,8	10,35	3081	15,91
18051010a	41,00901	0,66792	1,29707	0,03104	0,00181	0,00181	0,65	5361,1	43,54	3795,4	8,07	3047,5	12,61
19051010a	39,97584	1,20104	1,25222	0,04280	0,0033	0,0033	0,65	5233,9	61,24	3770,1	14,88	3063	22,63
20051010a	107,82920	1,83316	3,43551	0,08366	0,00153	0,00153	0,65	9602,9	60,79	4761,9	8,55	3035,9	10,75
21051010a	48,76400	0,82418	1,55473	0,03746	0,0018	0,0018	0,65	6046,4	47,26	3967,4	8,41	3034,8	12,64
22051010a	29,50818	0,59828	0,93840	0,02464	0,00236	0,00236	0,65	4266,6	40,97	3470,6	9,96	3038,9	16,49
25051010a	54,98942	1,24234	1,72938	0,04832	0,00232	0,00232	0,65	6472,7	57,07	4087,1	11,27	3056,8	16
26051010a	34,68888	0,66676	1,10586	0,02790	0,00218	0,00218	0,65	4800,8	42,71	3629,8	9,48	3035	15,24
27051010a	57,96148	3,20024	1,86689	0,10504	0,00519	0,00519	0,65	6789,6	118,08	4139,6	27,56	3018,5	36,54
28051010a	65,44667	1,21802	2,00896	0,04988	0,00194	0,00194	0,65	7101,3	53,43	4261	9,31	3095,5	13,06
29051010a	53,12189	0,91346	1,66096	0,03934	0,00186	0,00186	0,65	6309	47,66	4052,6	8,57	3066,1	12,78
30051010a	39,83007	0,62130	1,26481	0,02842	0,00178	0,00178	0,65	5269,9	40,44	3766,5	7,73	3041,3	12,41
31051010a	108,52059	1,72348	3,44027	0,07806	0,00153	0,00153	0,65	9609,8	56,66	4768,4	7,99	3044	10,66
32051010a	31,65954	0,59250	1,00714	0,02458	0,00217	0,00217	0,65	4491,3	39,47	3539,8	9,21	3038,4	15,19
35051010a	46,43602	0,79156	1,46894	0,03388	0,0019	0,0019	0,65	5826,2	44,23	3918,8	8,47	3047,4	13,18
36051010a	48,07526	1,47604	1,56484	0,05280	0,00307	0,00307	0,65	6071,9	66,36	3953,2	15,27	3001,6	21,94
37051010a	102,44560	1,84334	3,23498	0,07662	0,00173	0,00173	0,65	9304,6	58,32	4710,4	9,05	3050,2	11,97
38051010a	73,87287	1,49386	2,32642	0,05874	0,00201	0,00201	0,65	7747,9	56,91	4382,2	10,13	3054,5	13,89
39051010a	112,71603	3,04276	3,49608	0,10776	0,00232	0,00232	0,65	9690,3	77,25	4806,5	13,58	3078,8	15,73
40051010a	37,16847	0,73668	1,18606	0,02922	0,00224	0,00224	0,65	5041,8	43,08	3698	9,8	3033,4	15,7
41051010a	37,50989	0,96940	1,20747	0,03538	0,00281	0,00281	0,65	5104,6	51,67	3707,1	12,78	3019,3	19,88
42051010a	39,30239	0,75896	1,23945	0,02992	0,00221	0,00221	0,65	5197,3	43,05	3753,3	9,56	3052,2	15,27

Tableau C-1 : Tableau de données LA-ICP-MS *U-Th-Pb*, pour la lame mince étudiée.

ANNEXE C : Philippon et al., 2009

Journal of Structural Geology 31 (2009) 1308–1321

Contents lists available at ScienceDirect

Journal of Structural Geology

journal homepage: www.elsevier.com/locate/jsg

Kinematic records of subduction and exhumation in the Ile de Groix blueschists (Hercynian belt; Western France)

Melody Philippon*, Jean Pierre Brun, Frédéric Gueydan

Géosciences Rennes UMR 6118 CNRS, Université de Rennes 1, 35042 Rennes Cedex, France

ARTICLE INFO

Article history:
Received 20 February 2009
Received in revised form
1 July 2009
Accepted 6 July 2009
Available online 16 July 2009

Keywords:
Subduction/exhumation processes
HP rocks
Shear criteria
Lawsonite

ABSTRACT

Deciphering between deformations related to subduction and exhumation in HP metamorphic rocks represents a challenge for the understanding of the dynamic processes involved and more particularly, the exhumation mechanisms. An analysis of shear criteria in the Ile de Groix blueschists in the Hercynian Belt of southern Brittany (Western France) is carried out in terms of relative chronology and in relation to lithology (mainly micaschists and glaucophane-bearing metabasites). Structural mapping shows that foliations are flat-lying, bearing stretching lineations oriented in a N150°E ± 30° direction. Associated shear criteria are dominantly top-to-northwest and locally, in the southeast part of the island, both top-to-northwest and -southeast. Both shearing deformations lead to intense finite strains as demonstrated by the occurrence of sheath folds and the general orientation of fold axes parallel to the stretching lineation. Detailed mapping in this area showing opposite senses of shear, demonstrates that only top-to-southeast shear is observed in rocks containing well-shaped lawsonite pseudomorphs. In rocks affected by top-to-northwest shear, the lawsonite pseudomorph shape is destroyed by intense stretching. The top-to-southeast shear is coeval with prograde HP metamorphism and precedes a top-to-northwest shear coeval with a retrograde metamorphic path. In the frame of the hercynian belt of southern Brittany, the southeast directed shear is attributed to thrusting related to a northward dipping subduction and the northwest directed shear to exhumation controlled by a northward dipping extensional detachment.

© 2009 Elsevier Ltd. All rights reserved.

1. Introduction

Whereas subduction offers a simple and widely accepted mechanism for the burial of crustal rocks down to mantle depths, the mechanisms invoked to explain the exhumation of HP–UHP rocks remain a debated question (Platt, 1993; Ring et al., 1999; Chopin, 2003). The deformations recorded by HP rocks represent one important set of criteria to be considered in this debate. Any researcher might suspect that during subduction, HP rocks must have undergone some type of thrusting shear, from brittle to ductile conditions, which is either localized or distributed. Then, during exhumation, they must have not only been subjected to metamorphic retrogression, but also deformations related to their rise towards the surface. Therefore, in an ideal case, HP rocks should display the superposition of at least two main sequences of deformation phases. However, what is most commonly described is, in fact, evidence for strong shearing during retrograde metamorphism along extensional detachments, as illustrated in most HP metamorphic belts of the Mediterranean orogens (Jolivet et al., 2003). This would suggest that, most commonly, exhumation related deformation tends to erase previous deformation related to subduction. However, it is likely that, even where the second deformation is intense, remnants of early deformation can be preserved in restricted areas that require particular attention to be detected. For the above reasons, attempting to decipher between the kinematics of ductile deformation related to prograde HP metamorphism (acquired during subduction, on one hand) and to HP rocks retrogression (developed during exhumation, on the other hand) represents a challenge for the understanding of the full subduction–exhumation cycle.

In the above perspective, we re-examine here the kinematics of ductile deformation in the Ile de Groix blueschists (Hercynian belt of southern Brittany; Western France), where a number of previous methodological developments concerning the deformation of HP metamorphic rocks has been carried out. The presence of sheath folds (Quinquis et al., 1978) was interpreted as evidence of progressive shear, possibly related to subduction or obduction. As, at that time, exhumation was always implicitly attributed to erosion, ductile deformation was only interpreted as a result of thrusting-type shear (Quinquis and Choukroune, 1981; Cannat,

* Corresponding author. Tel.: +33 60 364 4740.
E-mail address: melodie.philippon@univ-rennes1.fr (M. Philippon).

0191-8141/$ – see front matter © 2009 Elsevier Ltd. All rights reserved.
doi:10.1016/j.jsg.2009.07.003

1985). Shear bands indicating opposite senses of shear, already identified but not interpreted by Quinquis (1980), were considered to result from a coaxial deformation during exhumation in extension (Shelley and Bossière, 1999). Recent detailed petrological and geochronological studies of the metamorphic history (Bosse et al., 2002, 2005; Ballèvre et al., 2003) offer a precise PTt framework to attempt a new analysis of deformation kinematics.

In this paper, we present a structural analysis of the Ile de Groix metamorphic rocks. A detailed mapping of shear senses is used to establish their relationship with lithology and with prograde and retrograde metamorphism. It is argued that the relationship of shear senses with prograde versus retrograde metamorphism characterizes the deformations related to subduction and exhumation, respectively. Finally, in the frame of the Hercynian belt of Brittany, the results provide a basis to discuss the possible configuration of subduction and the mode of blueschists exhumation.

2. Geological setting

Located to the south of the South Armorican Shear Zone (SASZ), a large HP unit outcrops over more than 300 km from northwest (southern Brittany) to southeast (Vendée; Fig. 1a). It is composed of a lower sub-unit of meta-rhyolites, the so-called "porphyroïdes", with a maximum recorded pressure of 9 kb (Le Hebel et al., 2002) and an upper sub-unit of blueschists outcropping in the Ile de Groix and at Bois de Céné in Vendée (Triboulet, 1974, 1991). In Vendée, the porphyroïdes are thrust onto low grade sediments (Bretignolle locality; Iglesias and Brun, 1976); whereas in southern Brittany, they are separated from underlying middle crust units, mostly micaschists and migmatites, by a Carboniferous extensional detachment (Fig. 1b).

The Ile de Groix metamorphic units consist mostly of micaschists (80%) with minor bodies of metabasites (20%), whose protoliths correspond to oceanic sediments with an occurrence of metacherts and oceanic island basalts (OIB), respectively (Bernard-Griffiths et al., 1986). Since the first mapping by Lamouche (1929), the large-scale structure of the island has often been described as a NW–SE trending upright anticline (Cogné, 1954; Quinquis and Choukroune, 1981; Bosse et al., 2002; Ballèvre et al., 2003). However, the detailed cross-sections of Jeannette (1965) and Boudier and Nicolas (1976) show a succession of west verging inclined folds with a 100–300 m wavelength, instead of a single kilometre-scale anticline. Boudier and Nicolas (1976), argued that i) glaucophane-bearing metabasites are more competent than micaschists and therefore, have preserved evidence of early deformations, ii) in retrogressed metabasites, the so-called prasinites, the development of albite during the greenschist overprint most often erase early deformations and iii) in micaschists, only the latest deformations can be observed. Consequently, they describe the structural history of the Ile de Groix metamorphic rocks as a succession of two main deformation stages. The first stage occurred in the blueschist facies conditions and is responsible for the epidote-glaucophane banding conserved in metabasites. During the second stage, in greenschist facies conditions, micaschists and metabasites layers are deformed in inclined folds that tightened eastward, as previously described by Jeannette (1965). Fold axes that trend N160°–170° are parallel to the glaucophane lineation (Boudier and Nicolas, 1976) and to the stretching direction indicated by sheath fold axes (Quinquis et al., 1978).

A garnet isograd (Fig. 2), trending NNE–SSW (Carpenter, 1976; Quinquis, 1980) divides the island into two parts: with and without garnet to the east and west, respectively. In the eastern part, P and T conditions are estimated as 16–18 kbar and 450 °C (Bosse et al., 2005) from Mn and Mg-rich garnets and as 18–20 kbar, 450 °C (Ballèvre et al., 2003) from lawsonite pseudomorphs in metabasites (Felix, 1972; Felix and Fransolet, 1972). In the western part, P and T conditions are estimated at 12–16 kbar, 450 °C (Bosse et al., 2002). The two metamorphic events are dated as 360–370 Ma for the HP metamorphism and as 345–353 for the greenschist overprint (Rb/Sr on whole rock and $^{40}Ar/^{39}Ar$ dating on phengite and epidote; Bosse et al., 2005). Considering the pressure gap between the two parts and the location of the highest pressure conditions on top of the metamorphic pile, Bosse et al. (2002) interpreted the garnet isograd as a thrust, as previously suggested by Cannat (1985; Fig. 9). On the contrary, Shelley and Bossière (1999) described the whole lithological pile as a unique metamorphic series, retromorphosed from eclogite facies to greenschist facies, without any internal discontinuity.

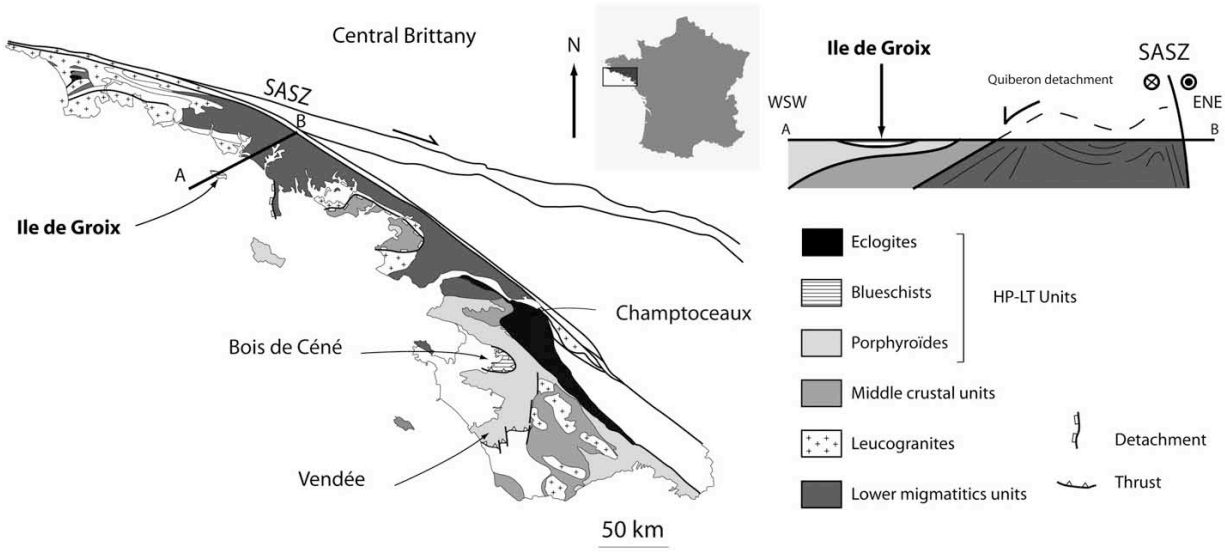

Fig. 1. Geological setting of the Ile de Groix in the frame of the Hercynian belt of southern Brittany. a. Simplified geological map of the metamorphic domain of southern Brittany with the location of the Ile de Groix. SASZ = South Armorican Shear Zone. b. Cross section AB (see location in a) showing the structural position of the Ile de Groix blueschists (modified after Cagnard et al., 2004).

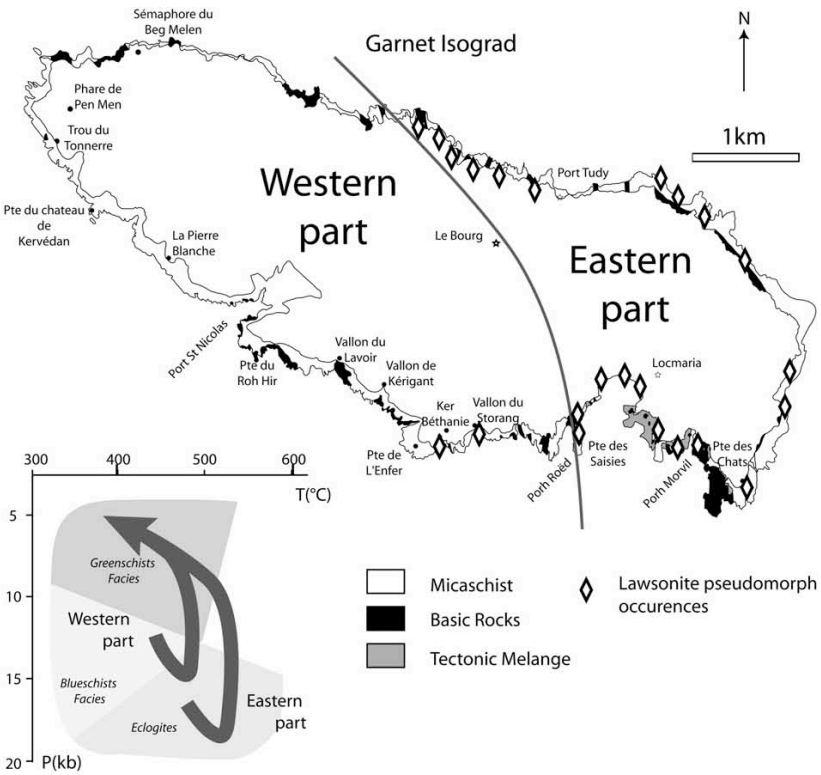

Fig. 2. Metamorphic map of the Ile de Groix showing the location of the garnet isograd (after Quinquis, 1980) and the occurrence of lawsonite pseudomorphs (after Ballèvre et al., 2003). The lithological contours are only shown along the seashore. The PT paths for the western and eastern part of the island are shown in the insert (after Bosse et al., 2002).

The rotation of garnet porphyroblasts, in the stability field of glaucophane, (Quinquis, 1980) and the asymmetry quartz fabrics (Cannat, 1985) indicate a top-to-NW sense of shear attribute to thrusting towards the NW, antithetic to a southward dipping subduction. Top-to-NW and top-to-SE shear criteria observed in equal proportions in thin sections led Shelley and Bossière (1999) to conclude that the whole deformation is co-axial and corresponds to the exhumation of the metamorphic series in extension.

3. Structural setting

3.1. Foliation

The foliation that is generally parallel or close to parallel to lithological boundaries is defined i) in micaschists by the preferred orientation of micas and flattened quartz veins and ii) in metabasites by a metamorphic layering dominantly made of epidote and glaucophane or by chlorite preferred orientation in prasinites. At the island-scale, the foliation that is most often flat lying with an average dip of 15° (stereoplot in Fig. 3a) can locally reach dip values of 70°. From east to west, the foliation attitude defines two main domains to the east and west of Le Trou de l'Enfer (see foliation trajectories in Fig. 3a). To the east, foliation trends are dominantly N–S with eastward dips; whereas, to the west, it trends NW–SE with dips either to the NE or to the SW.

Following the first structural mapping by Lamouche (1929), several studies (Cogné, 1954, 1960; Quinquis, 1980; Bosse et al., 2002) have advocated the presence of an island-scale anticline in the western domain. This could have been suggested by the regular southwestward dip of foliation along the western coastline in the vicinity of Pen Men. However, instead of a large-scale anticline, the high cliffs between Port St Nicolas and the Trou de l'Enfer displays a series of inclined folds underlined by thick layers of metabasites with characteristic wavelengths of about 200–300 m (Fig. 3a), in agreement with previous structural interpretations by Jeannette (1965) and Boudier and Nicolas (1976).

3.2. Lineations

Most rocks display prominent mineral and/or stretching lineations. In metapelites, they are often represented by stretched and corrugated quartz veins. In metabasites that have preserved blueschist parageneses, mineral lineations defined by glaucophane crystals are parallel to the stretching direction given by pressure shadows around garnets porphyroblasts (Quinquis, 1980). In retrogressed metabasistes, the so-called prasinites, stretching lineations are defined by aligned and stretched patches of albite and epidote crystals.

Mineral and stretching lineations are most often shallow plunging with a mean N150°E trend and a dispersion in orientation within a sub-horizontal plane between N–S and N120°E (stereoplot and map in Fig. 3b).

3.3. Shear criteria

In the present study we systematically mapped the sense of shear using C′-type shear bands that are present in all rock types at all scales up to 100 m. However, it was verified that shear senses

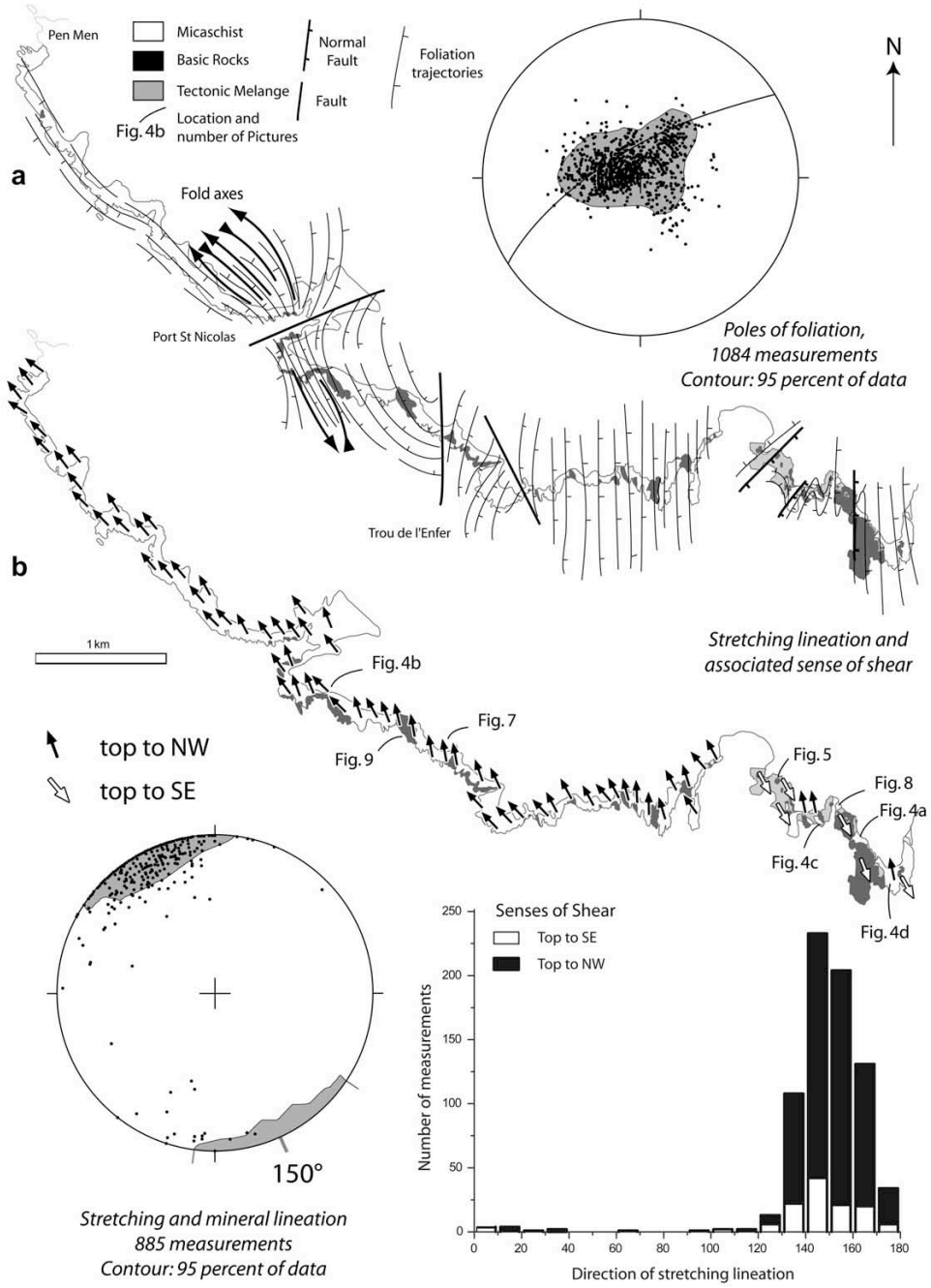

Fig. 3. Structural map of the island's southern coast. a. Foliation trajectories and stereoplot of 1084 foliation measurements b. Stretching lineations and stereoplot of 885 measurements. Associated senses of shear are indicated by black and white arrows for the top-to-northwest and -southeast, respectively. The histogram represents the statistical distribution of lineation directions and senses of shear. Stereoplots: lower hemisphere projection on a Schmidt net with contours for 95% of data.

deduced from shear bands they were consistent with those deduced from rotations of garnet porphyroblasts (Quinquis, 1980) and asymmetrical quartz fabrics (Cannat, 1985). Fig. 4 shows typical aspects of shear bands patterns in micaschists with a dominant sense of shear towards either the southeast (Fig. 4a) or the northwest (Fig. 4b) or with both senses towards the southeast and the northwest (Fig. 4c). In the micaschists, shear bands length and spacing vary according the type of lithology and in particular, as a function of the density of quartz veins (low in Fig. 4b and high in Fig. 4c). In metabasites, where foliation is dominantly marked by glaucophane, the growth of lawsonite crystals is synchronous with SE directed shearing (Fig. 5a). Lawsonites pseudomorphs (Ep–Chl–Ab) have well conserved lozenge shapes even after lawsonite breakdown. At outcrop scale (Fig. 5b, c), in the Amer area,

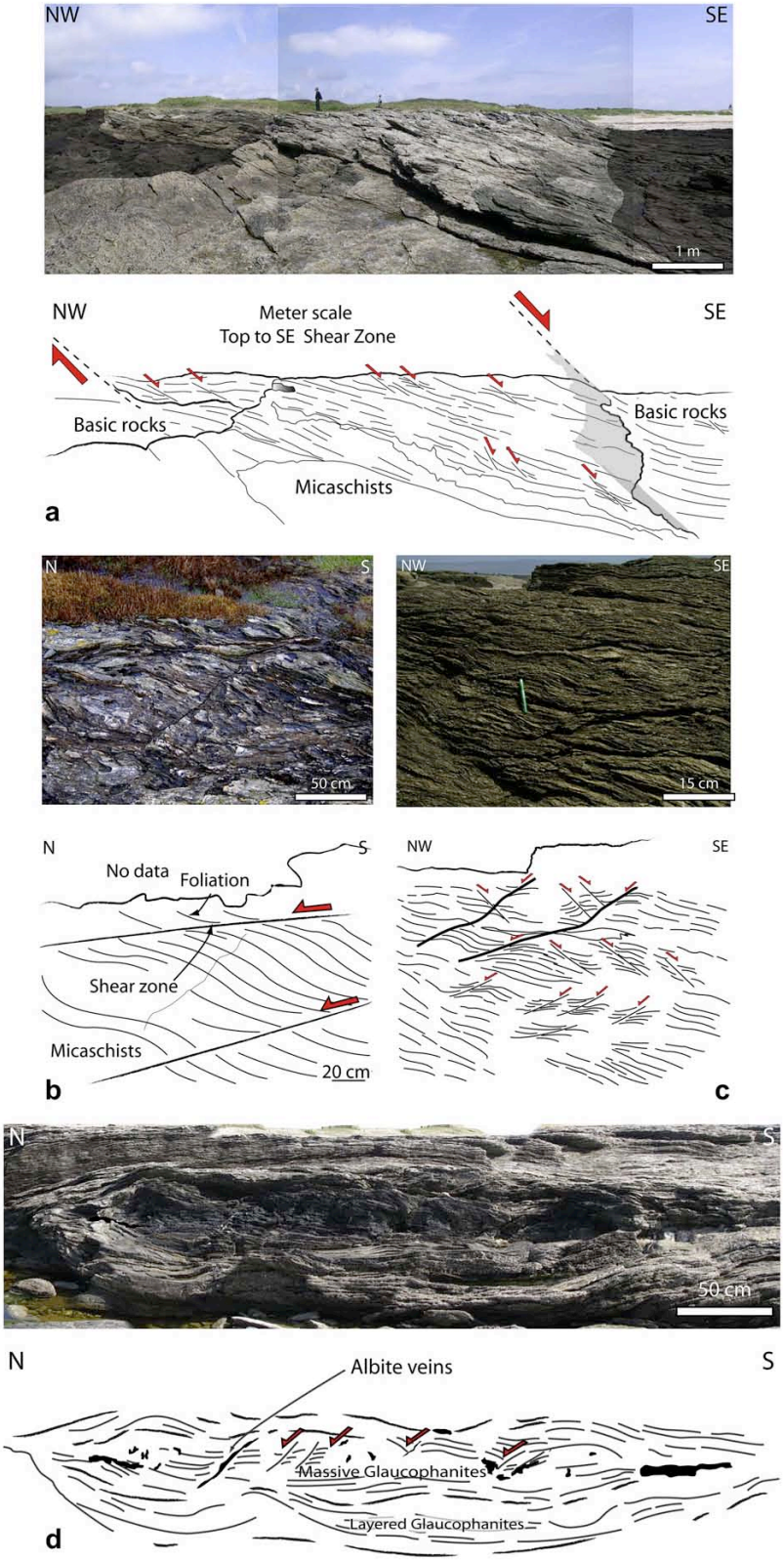

Fig. 4. Examples of shear bands in micaschists. Metre-scale top-to-SE shear bands at (a) the Pointe des Chats and (b) Kerbethanie. Top-to-SE and top-to-NW shear bands at Porh Morvil. d. Photograph and line drawing of a metre-scale glaucophanite boudin in micaschists at the Pointe des Chats.

metabasites show narrow spacing shear bands associated to cm-scale lawsonite pseudomorphs.

Mapping of the senses of shear (Fig. 3b) exemplifies that a top-to-northwest shear is represented in the whole island, whereas a top-to-southeast shear is only observed in the southeast part of the island. From a statistical point of view, a difference of around 10° exists between the mean direction of lineation associated to shearing top-to-northwest and -southeast, respectively (histogram in Fig. 3b). Shear sense indicators close to large reverse to isoclinal folds marked by metabasites inside micaschists were not taken into account to avoid apparent reversal in shear sense in inverted limbs.

4. Relationships between senses of shear and rock types

Detailed geological and structural mapping has been carried out in the southeast part of the island (Fig. 6), between the Pointe des Chats and the Pointe des Saisies, where the two opposite senses of shear are observed. Three kinds of rock types or rock assemblages are distinguished. (1) Metabasites are represented by two main metamorphic facies: glaucophanites (Lawsonite + Glaucophane + Epidote + Garnet) and greenschists, the so-called "prasinites" (Epidote + Albite + Chlorite). The local occurrence of omphacite in the parageneses indicates that the rock has attained the glaucophane-bearing eclogite facies. The presence of lawsonite pseudomorphs gave an estimate of PT conditions at about $P = 18–20$ kbar, $T = 450$ °C. (2) Micaschists, in addition to quartz and white micas, i.e. phengite and paragonite, contain garnet + Chloritoid + rutile ± glaucophane, which provided an estimate of PT conditions at about $P = 16–18$ kbar, $T = 450–500$ °C (Bosse et al., 2002). Retrogressed micaschists characterized by an assemblage containing Albite + Chlorite + Paragonite + Biotite + Ilmenite gave $P = 14–16$ kbar, $T = 400–450$ °C (Bosse et al., 2002). (3) Micaschists containing numerous metre-scale metabasite blocks, or boudins, were mapped as a separate type of rock unit, the so-called tectonic melange in Figs. 2, 3 and 6.

In this area, the foliation (Fig. 6a) is predominantly oriented NS and dips to the east by 0–20°. It is affected by a series of post metamorphic N–S or NE–SW trending normal faults that dip to the east or southeast, and which are also responsible for large open folds.

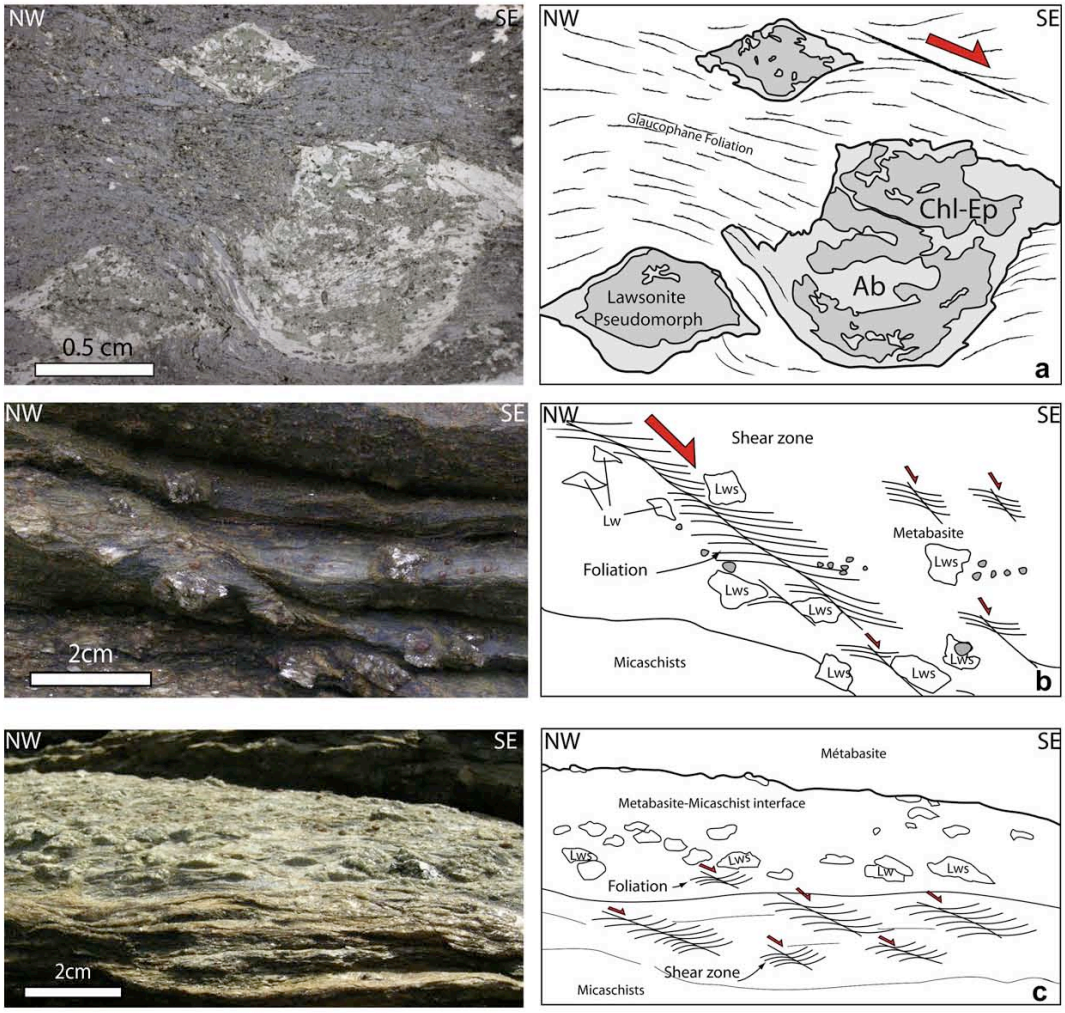

Fig. 5. Lawsonite pseudomorphs in thin section (a) and at outcrop scale (b) in glaucophane-bearing metabasites (a and b) and micaschists (c), between Locmaria and Porh Morvil. Shear bands are top-to-southeast.

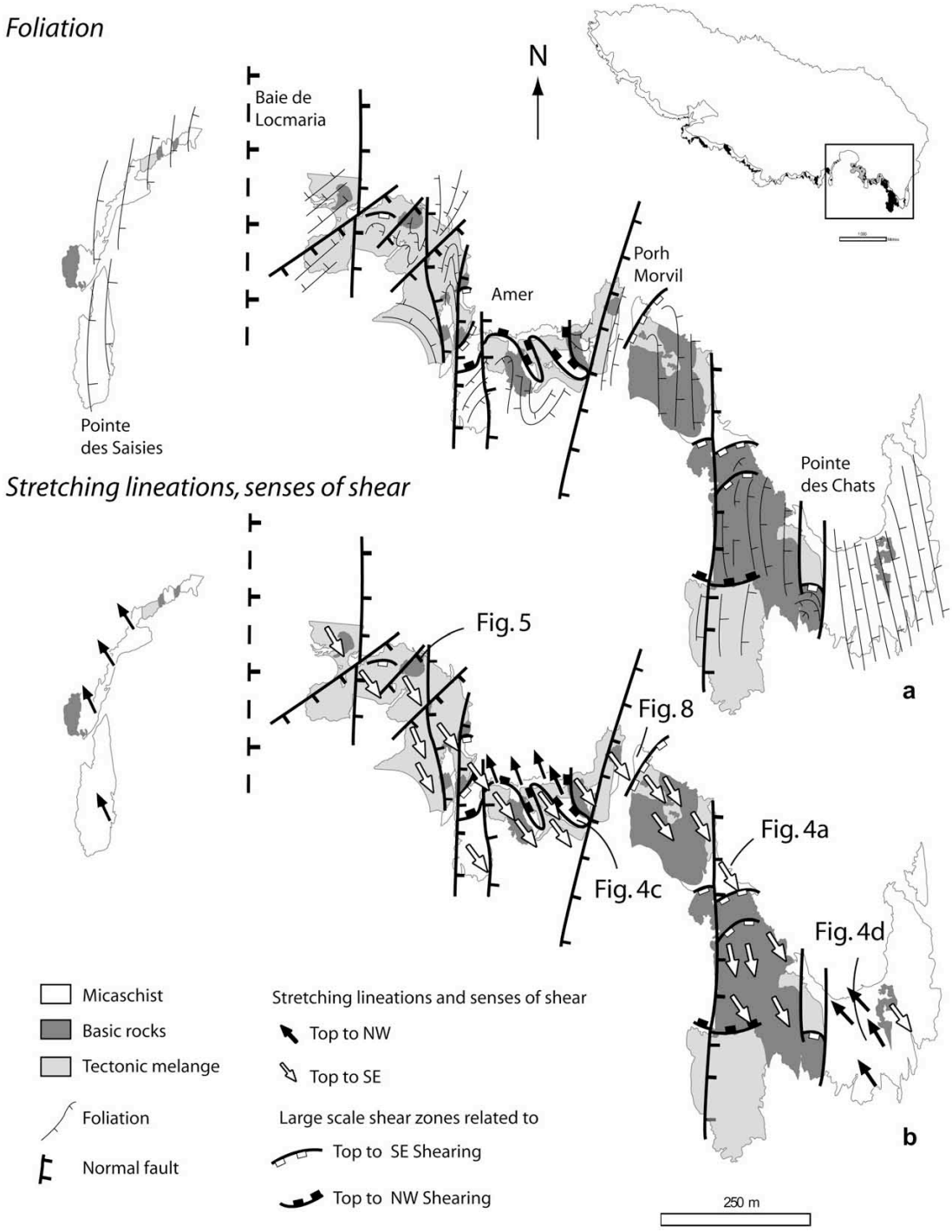

Fig. 6. Detailed structural map of the eastern part of the island between the Pointe des Saisies and the Pointe des Chats. a. Foliation trajectories. b. Stretching lineations. Associated senses of shear are indicated by black and white arrows for the top-to-northwest and -southeast, respectively. The map shows domains of basic rocks or mixed basic rocks and micaschists – i.e. mélange – with only a southeast directed sense of shear.

Lineations have a mean N140°E trend (Fig. 6b). Associated senses of shear show a systematic relation with rock types. A top-to-N140°E sense of shear is observed in all types of mapped units, whereas a top-to-N350°E sense of shear is never observed in metabasites containing lawsonite pseudomorphs (Fig. 6b). Fig. 5 shows an example of a lawsonite pseudomorph closely associated with top-to-N140°E shear bands. Detailed mapping shows the occurrence of shear bands with two senses of shear at 10–100 m

scales. Strong shearing at micaschist–metabasite interfaces is responsible for the mixed lithological pattern, i.e. what is called a tectonic melange in this work (Figs. 4a and 6). It results from the dislocation by boudinage and/or shear zones of large metabasite units and their incorporation inside a micaschist matrix.

The top-to-N350°E sense of shear that affects all types of rocks is observed at the whole island-scale (Fig. 3b). It is synchronous with retrograde metamorphism, as demonstrated by its common association with Ab + Chl + Qz veins in basic rocks and micaschists. Fig. 4d shows Ab + Chl + Qz veins developed within a glaucophanite boudin within a micaschist matrix at the Pointe des Chats, in an area characterized by top-to-N350°E senses of shear. Shear bands are present inside the boudin itself. The lack of clear evidence for N140°E shear criteria at the island-scale suggest that they have likely been erased by a shearing top-to-N350°E. This is in agreement with the lack of lawsonite pseudomorphs in most of the island (Fig. 2). In the Ile de Groix, the existence of lawsonite is only demonstrated by pseudomorphs whose mineral composition is in fact chlorite + epidote + paragonite (Ballèvre et al., 2003; Felix and Fransolet, 1972). However, the shape of lawsonite crystals is locally preserved (Fig. 5a; Felix, 1972). The pseudomorph composition is such that, as soon as they are deformed, they become extremely difficult to identify from their matrix. Consequently, the absence of lawsonite pseudomorphs can be interpreted as a consequence of deformation rather than proof of a non-development of lawsonite. Ballèvre et al. (2003) argued that "lawsonite growth took place at increasing *P* and *T*" and that the lawsonite breakdown recorded "the final part of the history after cessation of the ductile deformation and recording of the earliest stages of exhumation". In agreement with this statement, our structural observations and detailed mapping (Figs. 3b and 6b) show that well-shaped pseudomorphs are closely associated to N140°E shearing (Fig. 5) but, conversely, deformation continued after lawsonite PT breakdown conditions, with a quasi-opposite sense of shear top-to-N350°E. Consequently, the top-to-N140°E sense of shear is associated with the high pressure metamorphism and therefore, precedes the top-to-N350°E sense of shear.

5. Sheath folds

Sheath folds are rather common in all rock types and have been observed at various places in the island (Quinquis and Cobbold, 1978; Quinquis, 1980). Their size directly depends on the thickness of the folded layers. In micaschists, in which they most often affect thin graphitic quartzite layers, they are observed at a 10 cm-scale and their sheath shapes range from symmetrical (Fig. 7a) to asymmetrical (Fig. 7c). In metabasites that represent thick layers embedded in micaschists, the size of sheath folds can reach several tens of metres, parallel to the stretching lineation. The well exposed metabasites of the Vallon du Lavoir display a complex association of symmetrical and asymmetrical sheath folds (Fig. 8).

Sheath folds that develop in a broad spectrum of geological environments (see review in Alsop et al., 2007) generally indicate intense stretching (Cobbold and Quinquis, 1980; Brun and Merle, 1988). As stretching can reach high values in shear zones, they are commonly observed in highly sheared rocks, but shearing is not a necessary condition for their development. It has been suggested long ago that the presence of sheath folds in the Ile de Groix blueschists likely results from intense shearing within a subduction zone (Quinquis et al., 1978). Accordingly, sheath folds have since then been described in many HP metamorphic rocks related to either subduction or exhumation (e.g. Pennine Alps: Lacassin and Mattauer, 1985; Cuba: Stanek et al., 2006; Oman: Searle and Alsop, 2007). However, as argued in the present paper, two superposed events of shearing affect the Ile de Groix blueschists: the top-to-N140°E, related to the prograde HP metamorphism, and the top-to-N350°E, related to the retrograde metamorphism. The present study reveals that sets of sheath folds were generated during both of the shearing events.

To understand the processes of fold axes reorientation that are at the origin of sheath folds, it is especially interesting to examine the geometrical relationships between fold axes and lineations. Fig. 8 presents a metre-scale mapping of fold axes and lineations in metabasites close to the contact with micaschists at Porh Morvil in the southeast of the island (see location in Fig. 6a). Fold axes trend close to N–S (Fig. 8), parallel to the metabasite-micaschist contact, whereas stretching lineations present a strong dispersion in orientation from nearly N–S to E–W (Fig. 8b). E–W trending lineations only occur in relation with folds or boudins close to lithological interfaces. They constitute local and small-scale anomalies with reference to the lineation trend at the kilometre-scale (Fig. 6b). Folds and boudins result from mechanical instabilities due to strong competence contrasts in the contact strain zones between metabasites and micaschists. In fold limbs dipping at a low angle, lineations trend close to N90°E. The geometrical relationship between fold axes and lineations (Fig. 8b, c) indicates that folds likely formed with axes trending roughly N50°E, perpendicular to the N140°E direction of shearing, and rotated towards a N–S direction during progressive shearing. The obliquity that stretching lineations in fold limbs make with the regional trend of lineations indicates that they have undergone the same amount of rotation as the fold axes. Similar rotation of lineations associated with reorientation of fold axes is observed in other examples of sheath folding (see Fig. 10 in Alsop and Carreras, 2007). In the southeast of the island, as exemplified at Porh Morvil, reorientation of fold axes and lineation occurred during the earliest event of the shearing top-to-N140°E (Fig. 6b).

In the western part of the island, metabasite bodies are ductilely deformed during the second top-to-N350°E shearing event and form 100 m-wide reversed folds. The Vallon du Lavoir anticline presents a series of 10 m-scale symmetrical and asymmetrical sheath folds in a core of layered glaucophanite embedded in greenschists (Fig. 9a), whose complex 3D structure has been delineated by detailed mapping (Fig. 9b). A large sheath closure is observed in 3D at the SE extremity of the structure (Fig. 9d). In the core of the structure, sheath folds deform a pre-existing foliation bearing a glaucophane lineation that consequently appears to be strongly dispersed on the stereoplots (Fig. 9c, e). In the sheath closure (labelled l and m in Fig. 9c), the lineation dispersion occurs along a plane oriented N160°E, which is also very close to the mean stretching lineation in the surrounding greenschists (star symbol on the stereoplot). In the fold hinges that define the lateral arms of the large structure (labelled n, o, p and q in Fig. 9) the dispersion is such that no particular locus can be defined (Fig. 9e). In the field, it was observed that, around each individual fold hinge, lineations are dispersed in a plane strongly oblique to the fold axis. On the stereoplot (Fig. 9e), fold axes are close to the mean stretching lineation in the surrounding greenschists, indicating a strong reorientation. In Fig. 9f, we have rotated the fold axes in a direction β_0, perpendicular to the mean stretching direction, which likely represents their initial direction. With the same amount of rotation, most of the lineations become close to the plane of dispersion that is observed in the sheath closure (dotted line in Fig. 9c, f). This indicates that the fold hinges of the glaucophanites are rotated in parallel with the stretching direction without a significant superimposed strain. It also implies that glaucophanites are significantly more competent than the surrounding greenschist matrix.

6. Relation between deformation and metamorphism

As documented in Section 4, well-shaped lawsonite pseudomorphs are closely associated to the N140°E shearing (Fig. 5), but

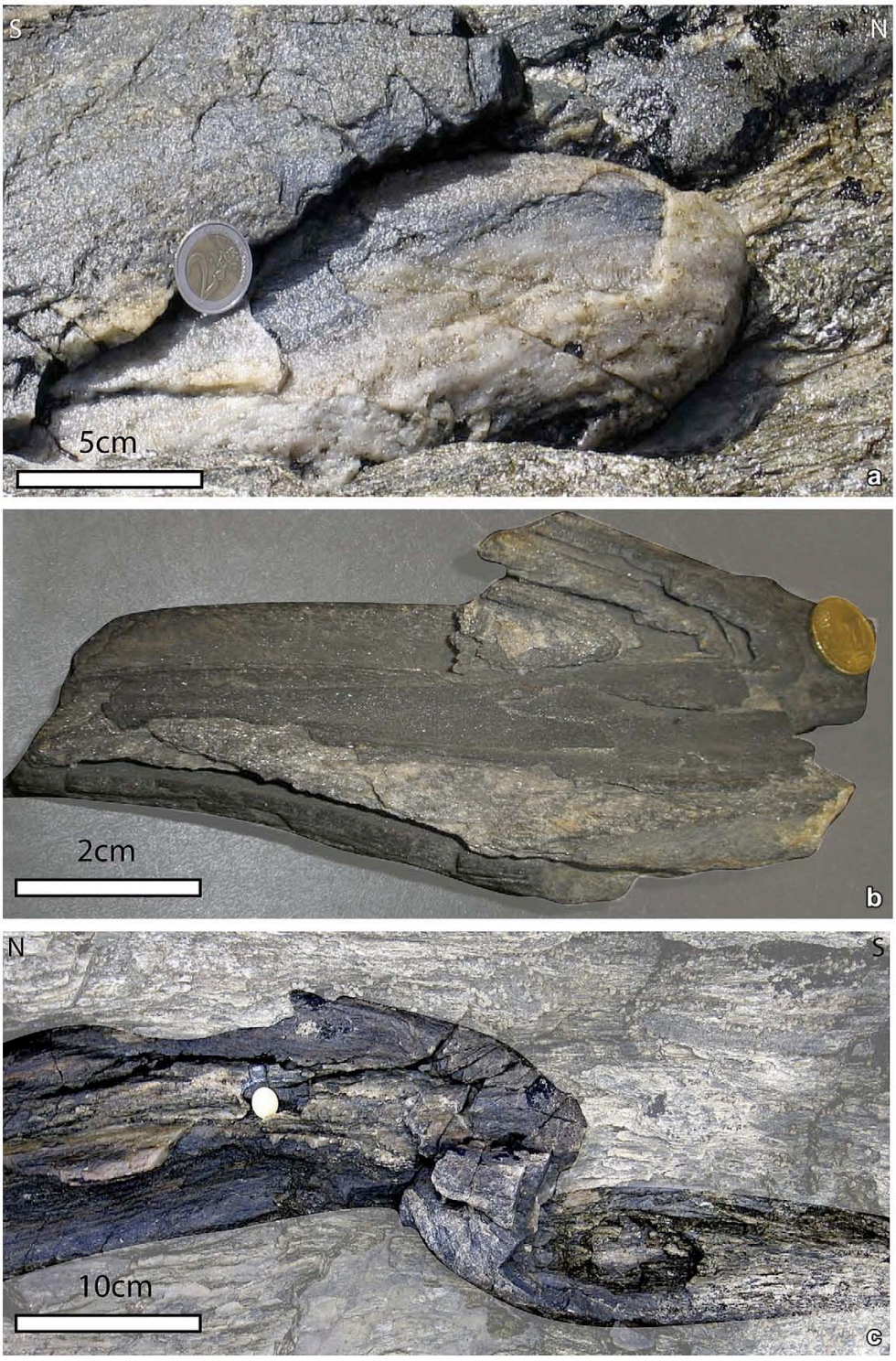

Fig. 7. Sheath folds affecting graphitic quartzite layers in the micaschists of the Vallon de Kerigan (a, c) and sample from Pen Men (b). The shape of sheaths is either symmetrical (a, b) or asymmetrical (c).

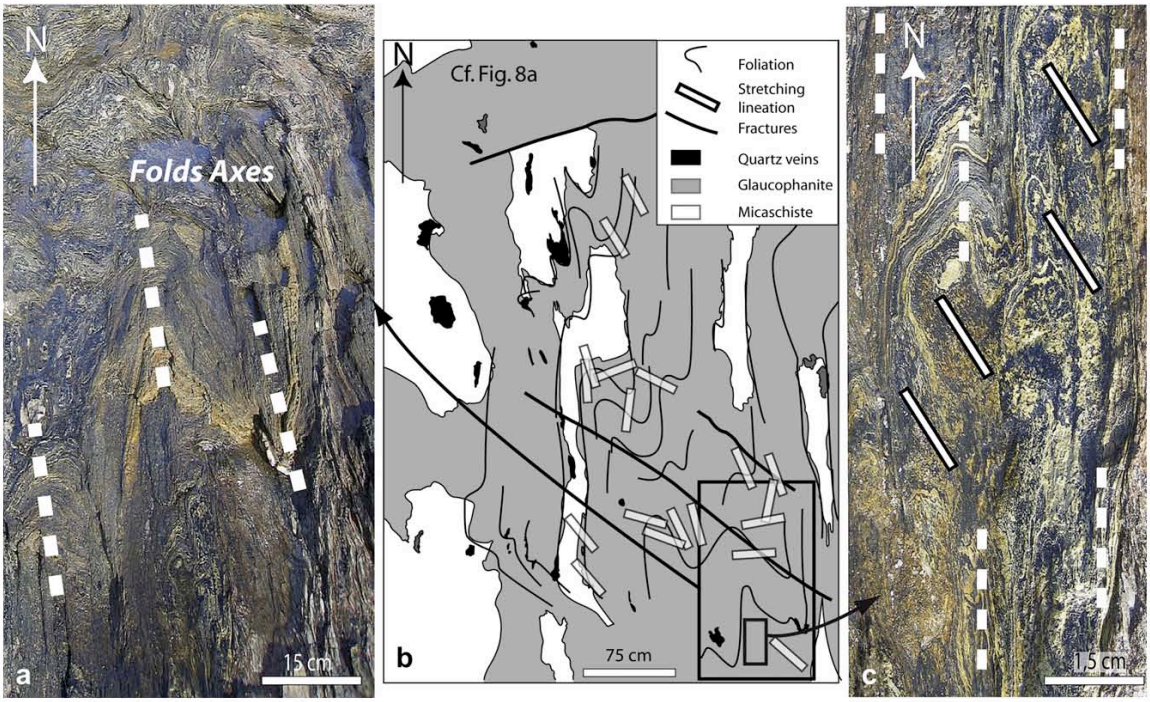

Fig. 8. Reoriented folds axes in glaucophane-bearing metabasites at Porh Morvil. a. Photograph of an outcrop detail. b. Line drawing of the mapped outcrop. c. Photograph of an enlargement of a. White bars in b and c show the orientation of glaucophane lineation. Black thick lines in c underline the fold axes. The location of photographs a and c is shown in b.

deformation continued after lawsonite PT breakdown conditions, with a quasi-opposite top-to-N350°E sense of shear.

In addition to this observation, rock samples that lead to the highest pressure estimates (Bosse et al., 2002) are located in areas characterized by top-to-N140°E senses of shear (samples number 2, 3 and 5* in Fig. 10a). They belong to the prograde part of the PT path and they are located in the stability field of the lawsonite (Fig. 10b). This implies that the top-to-N140°E sense of shear is characteristic of a pressure increase. Conversely, samples 13 and 14 from Bosse et al. (2002), which are strongly retrogressed, are located in areas with a top-to-N350° sense of shear (Fig. 10a). They belong to the retrograde part of the PT path and they are located outside the stability field of the lawsonite (Fig. 10b).

7. Discussion

7.1. Record of subduction and exhumation in the Ile de Groix blueschists

In the Ile de Groix, shear senses deduced from different shear criteria have been interpreted in various ways: both in kinematics terms at the island-scale and in tectonic terms in the frame of the Hercynian belt. Analysis of snowball garnets rotation in thin sections was used by Quinquis (1980) to argue for a top-to-northwest sense of shear. Soon after, the same conclusion was reached by Cannat (1985) from quartz *c*-axes fabrics. Nearly 30 years ago, Quinquis (1980) observed that shear bands had opposite senses of shear but concluded that their significance was too uncertain. More recently, Shelley and Bossière (1999) argued that opposite senses of shear, observed in thin sections, are present in equal proportions and thus, concluded a co-axial deformation.

The rotation of snowball garnets towards the northwest was related by Quinquis and Choukroune (1981) to an "obductive offscrapping" (Moore and Allwardt, 1980) – i.e. a northwest verging thrust associated with a northwest dipping subduction. Quartz *c*-axes fabrics were also interpreted in the frame of a northwestward thrusting by Cannat (1985). However, at the time of these early works, the specific problems related to the exhumation of HP rocks were not clearly identified. All intense deformations and associated ductile fabrics observed in mountain belts were supposed to have resulted from thrusting and therefore, the exhumation of metamorphic rocks was implicitly attributed to erosion. Shelley and Bossière (1999) argued for a pure shear deformation which they attributed entirely to an exhumation in extension, synchronous to a retrogressive sequence from eclogite to greenschists facies. According to this interpretation, the Ile de Groix blueschists were exhumed by crustal thinning.

The detailed mapping of shear senses presented here shows that opposite shear senses are not present in equal amounts, whatever the scale considered, and that a southeast directed shear is only observed in basic rocks in the eastern part of the island, synchronous with a prograde HP metamorphism, and that it precedes the northwest directed shear, synchronous with retrogression (Fig. 12). This is in full agreement with the occurrence of lawsonite pseudomorphs only in rocks showing evidence of southward shearing.

In the frame of the Hercynian belt of South Brittany (Fig. 1), the tectonic interpretation of the kinematic analysis presented here is straightforward. Available field data, in particular from Vendée (see location in Fig. 1), shows that thrust units always root to the north or northeast (Brun and Burg, 1982). In the thrust pile, the upper units that have undergone HP metamorphism – i.e. porphyroïdes (Le Hebel et al., 2002) and the Bois de Céné blueschists (Triboulet, 1991) – are thrust on top of sediments affected only by low grade metamorphism (Iglesias and Brun, 1976). Further north, in the Champtoceaux area (see location in Fig. 1), eclogitic units are thrust on top of low to medium grade metamorphic rocks and also root to

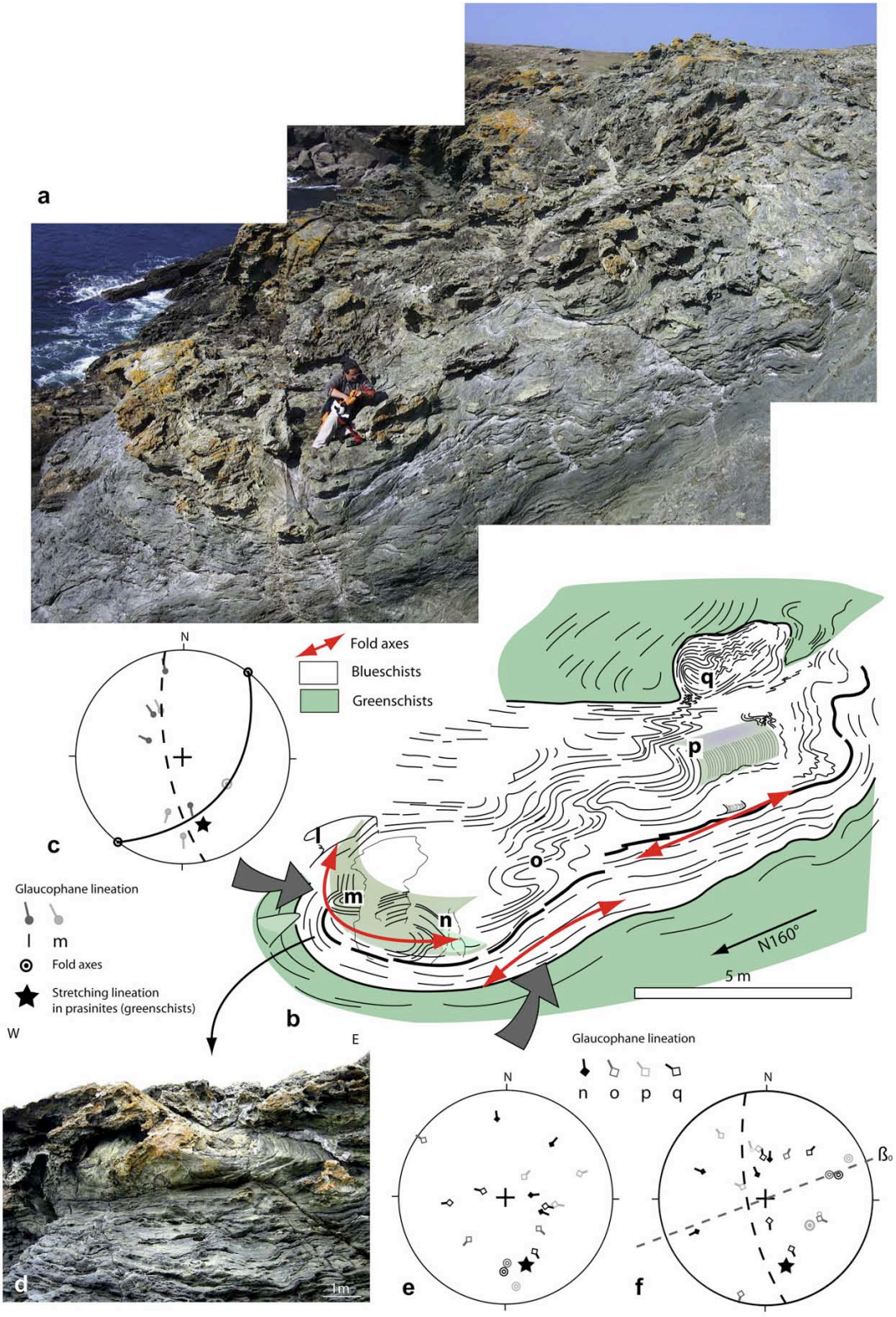

Fig. 9. Pluri-metric sheath fold at the Vallon du Lavoir. a. Photograph showing the bulk structure. b. Line drawing of a. c. Stereplot showing the relative position of fold axes, glaucophane lineations and the direction of shear (star). d. Photograph of the meter-scale eye-type closure affecting an interface between banded glaucophanites and "prasinites" (Greenschists). e. Stereoplot of fold axes and glaucophane lineations. f. Same data as in e restored in their position prior to fold axes reorientation in the shear direction. Stereoplots: lower hemisphere projection on a Schmidt net.

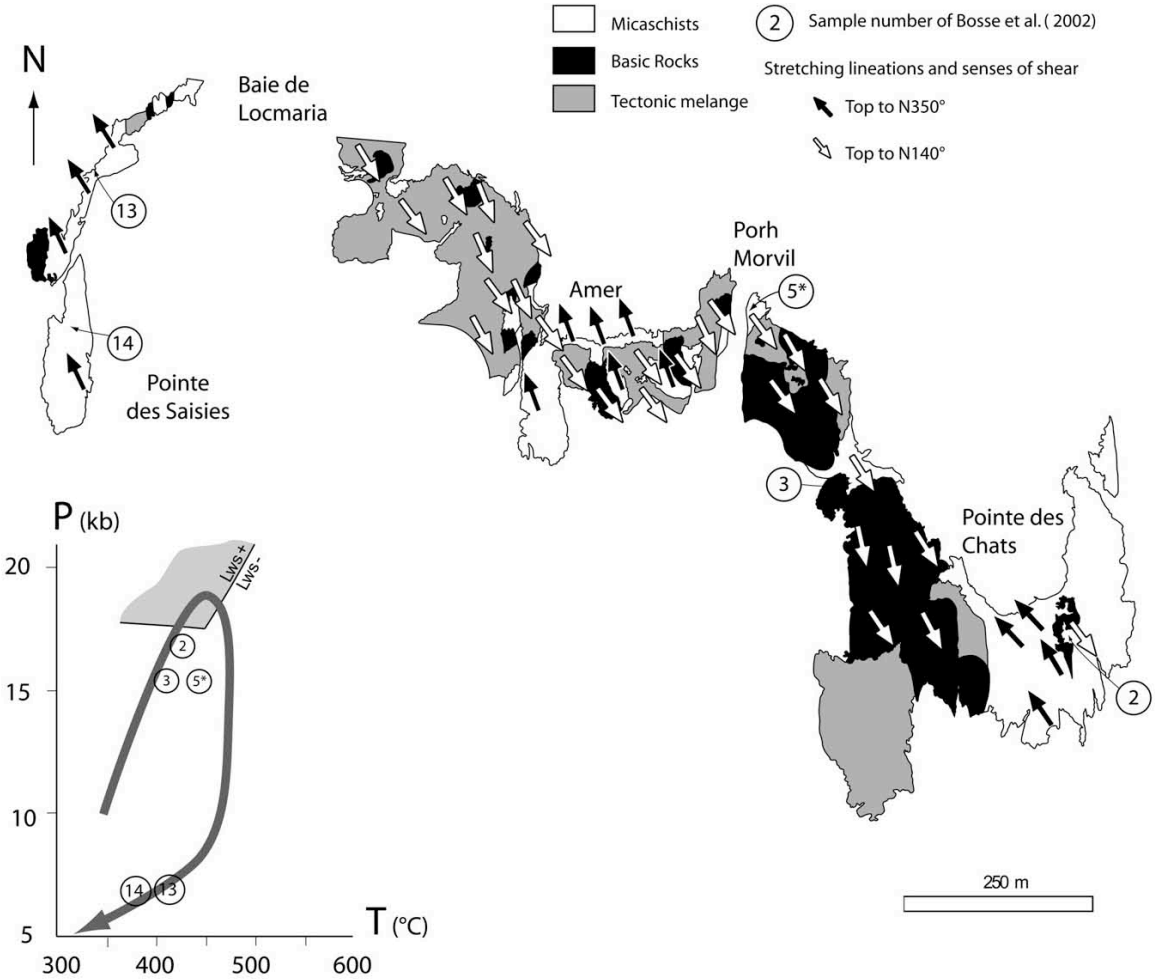

Fig. 10. A map-scale of the relationship between the senses of shear (see Fig. 6) and metamorphism in the southeastern part of the island. Numbers in circles refer to samples analysed by Bosse et al. (2002). The insert shows the position of these samples on the PT path calculated by Ballèvre et al. (2003).

the north and northeast (Ballevre et al., 1987), as clearly imaged by deep seismics (Bitri et al., 2003). At the lithosphere scale, *P*-wave tomography (Judenherc et al., 2003; Gumiaux et al., 2004) has provided evidence for the existence of a northeast-dipping slab remnant below central Brittany. The evidence for a first event of southeastward shearing contemporaneous with HP metamorphism in the Ile de Groix at 358–366 Ma (Bosse et al., 2002) can be interpreted as a result of thrusting within a northward dipping subduction zone (Figs. 11 and 12a). As already stated, the northwestward shearing was previously interpreted as a northward directed thrusting, synchronous with HP metamorphism, but antithetic to a northward dipping subduction (Quinquis and Choukroune, 1981; Cannat, 1985; Fig. 11b). Our study shows that this northwestward shearing is synchronous with retrogressive metamorphic conditions dated at 345–353 Ma (Bosse et al., 2005). As there is no evidence of any major south-dipping thrust to the north of the Ile de Groix and because all units dip northward at a regional-scale, there is no other alternative than to relate this second shearing event to a normal sense detachment dipping northward (Figs. 11c and 12). However, due to the late hercynian extension (Gapais et al., 1993; Cagnard et al., 2004), this early detachment which has accommodated the exhumation of HP units does not outcrop onland (see cross section of Fig. 1b). At the present day level of erosion, the migmatitic core complex of the Morbihan Gulf, controlled by a southwestward dipping detachment, emplaced between the South Armorican Shear Zone and the Ile de Groix (Fig. 1a, b). To some extent, this situation can be compared to the Cyclades, in the Aegean, where the exhumation of HP rocks that are accommodated by an extensional detachment is rapidly followed by the development of a high temperature core complex. The existence of an extensional detachment located on top of the HP units that dips in the same direction as the subduction and brings HP rocks back to the surface in a flat-lying position over a broad area would suggest that, like in the Aegean, exhumation was driven by slab rollback (Brun and Faccenna, 2008).

7.2. Significance of opposite senses of shear in high pressure rocks

The Ile de Groix is not the only example of opposite senses of shear in HP rocks. It is especially relevant to recall the example of HP rocks that belong to the Briançonnais units in the western Alps (Ganne et al., 2006). In this recent orogenic domain, where thrust

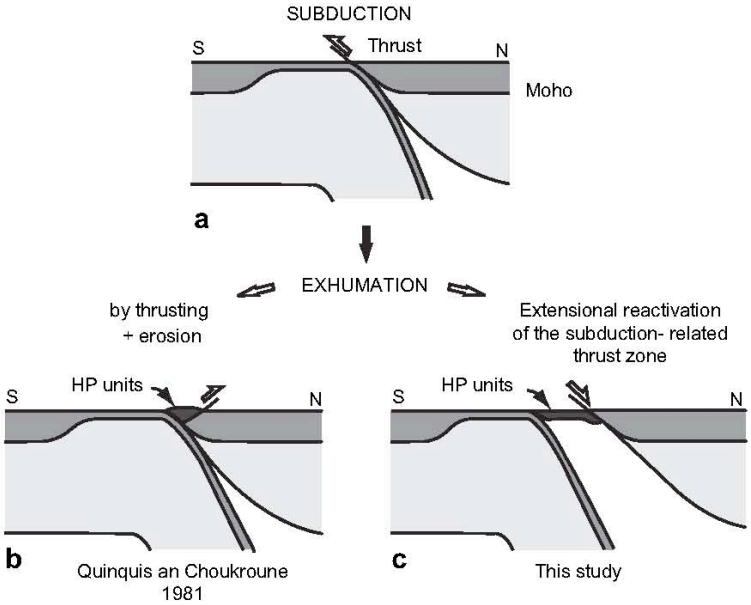

Fig. 11. Sketch summarizing the subduction-exhumation cycle of the Ile de Groix blueschists. a. Northward dipping subduction. Models of exhumation where the northwest sense of shear is interpreted as related to northward thrusting (modified after Quinquis and Choukroune, 1981) (b) or to northward dipping extensional detachment (this work) (c).

units trend north-south, HP rocks display two shear senses: dominantly top to the west in the west and top to the east in the east. Both westward and eastward senses of shear are observed in the same proportion in the transition zone. As Ganne et al. (2006) interpret the two senses of shear as synchronous, they attribute the westward shearing to westward thrusting and eastward shearing to a coeval eastward dipping detachment. Consequently, they propose that the two senses of shear represent the lower and upper parts of a corner flow within a so-called subduction channel. This dynamic interpretation would be acceptable only if the hypothesis concerning the synchronism of the two senses of shear is demonstrated.

In the Cycladic blueschists in Greece, the problem of opposite senses of shear has also been considered. On the islands of Syros and Sifnos, both Rosenbaum et al. (2002) and Bond et al. (2007) argue that opposite senses of shear are contemporaneous and result from pure shear during blueschist exhumation. On the contrary, in this study the analysis of shear criteria at the island-scale indicates that shearing in *H–P* conditions is dominantly top-to-northeast (Trotet et al., 2001). The apparent discrepancy between these two conclusions demonstrates that kinematic analysis is strongly scale-dependant. In fact, strain can be co-axial at a small-scale within a system that is sheared in a uniform sense at a larger scale. In other words, these conclusions are not mutually exclusive.

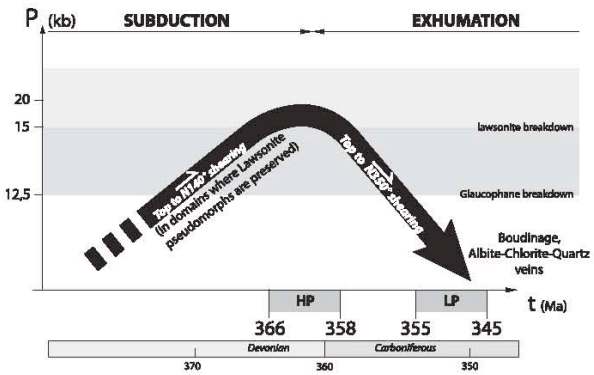

Fig. 12. Summary of the pressure–time evolution of the Ile de Groix blueschists at $T = 450\ ^{\circ}C$.

Regardless of the opinion that one might have about the particular examples above, they illustrate the problem of interpretation opposite shear senses in HP rocks, especially if conclusions are to be drawn at the crust and lithosphere scales.

8. Conclusions

From a regional geological point of view, it is shown that the Ile de Groix blueschists have preserved the kinematic record of both subduction and exhumation as a function of lithology. Shear criteria synchronous with prograde HP and retrograde greenschist metamorphism are directed to the southeast and northwest, respectively. Both shearing deformations lead to intense finite strains as demonstrated by the occurrence of sheath folds and the general orientation of tight fold axes parallel to the stretching lineation. Well conserved lozange shaped lawsonite pseudomorphs occur only in rocks showing only a top-to-southeast sense of shear. In rocks affected by a top-to-northwest shear, the lawsonite pseudomorph shape is destroyed by intense stretching. The pseudomorphs cannot be identified anymore as their constituting minerals are similar to those of the matrix. In the frame of the hercynian belt of southern Brittany, the southeast directed shear is attributed to thrusting related to a northward dipping subduction and the northwest directed shear to an exhumation controlled by a northward dipping extensional detachment.

From a methodological point of view, this study illustrates that deciphering between burial-subduction and the exhumation of HP metamorphic rocks requires not only the analysis of timing and chronology of shear criteria development but also the consideration of their spatial distribution, their relation to lithology and metamorphism and their setting within the regional-scale

structures. In addition, the presence of lawsonite pseudomorphs is especially interesting in this perspective because, as illustrated in the Ile de Groix, rocks where they are conserved have not been deformed during exhumation.

Acknowledgements

We would like to thank our Géosciences Rennes collegues and particularly M. Ballèvre for discussions at various stages of this work and Pavel Pitra for providing the thin section photograph of lawsonite pseudomorphs. Great thanks are also due to the master students Marianne Boix, Nathan Cogné, Aurélia Kerdraon and Irene Mannino for their participation in the field mapping. Thanks to Ian Alsop and Florian Fusseis for very constructive reviews.

References

Alsop, G.I., Carreras, J., 2007. The structural evolution of sheath folds: a case study from Cap de Creus. Journal of Structural Geology 29, 1915–1930.
Alsop, G.I., Holdworth, R.E., McCaffrey, K.J.W., 2007. Scale invariant sheath folds in salt, sediments and shear zones. Journal of Structural Geology 29, 1585–1604.
Ballevre, M., Kienast, J.R., Paquette, J.-L., 1987. The eclogitic metamorphism of the Hercynian Champtoceaux nappe (Armorican Massif). Comptes Rendus de l'Académie des Sciences Paris 305 (2), 127–131.
Ballèvre, M., Pitra, P., Bohn, M., 2003. Lawsonite growth in the epidote blueshists from the ile de groix (armorican massif, France): a potential geobarometer. Journal of Metamorphic Geology 21, 723–735.
Bernard-Griffiths, J., Carpenter, M.S.N., Peucat, J.J., Jahn, B.M., 1986. Geochemical and isotopic characteristics of blueschist facies rocks from the ile de groix, armorican massif (northwest France). Lithos 19, 235–253.
Bitri, A., Ballevre, M., Brun, J.P., Chantraine, J., Gapais, D., Guennoc, P., Gumiaux, C., Truffert, C., 2003. Imagerie sismique de la zone de collision Hercynienne dans le Sud-Est du Massif Armoricain (Projet Armor 2/Programme Géofrance 3D). Comptes Rendus Géoscience Paris 335, 969–979.
Bond, C., Bulter, R.W.H., Dixon, J.E., 2007. Co-axial Horizontal Stretching Within Extending Orogens: The Exhumation of HP Rocks on Syros (Cyclades) Revisited. In: Geological Society of London, Special Publication, vol. 272, pp. 203–222.
Bosse, V., Ballèvre, M., Vidal, O., 2002. Ductile thrusting recorded by the garnet isograd from blueschists-facies metapelites of the Île de groix, armorican massif, France. Journal of Petrology 43, 485–510.
Bosse, V., Féraud, G., Ballèvre, M., Peucat, J., Corsini, M., 2005. Rb-sr and 40ar/39ar ages in blueschists from the Île de groix (armorican massif, France): implication for closure mechanisms in isotopic systems. Chemical Geology 220, 21–45.
Boudier, F., Nicolas, A., 1976. Interprétations nouvelles des relations entre tetonique et métamorphisme dans l'île de groix. bretagne. Bulletin de la Société géologique de France 7 (XVIII), 135–144.
Brun, J.P., Burg, J.P., 1982. Combined thrusting and wrenching in the Ibero-Armorican arc: a corner effect during continental collision. Earth and Planetary Science Letters 61 (2), 319–332.
Brun, J.P., Faccenna, C., 2008. Exhumation of high-pressure rocks driven by slab rollback. Earth and Planetary Science Letters 272 (1–2), 1–7.
Brun, J.P., Merle, O., 1988. Experiments on folding in spreading gliding nappes. Tectonophysics 145 (1/2), 129–139.
Cagnard, F., Gapais, D., Brun, J.P., Gumiaux, C., Van Den Driessche, J., 2004. Late pervasive crustal-scale extension in the south Armorican Hercynian belt (Vendée, France). Journal of Structural Geology 26, 435–449.
Cannat, M., 1985. Quartz microstructures and fabrics in the island of Groix (Brittany, France). Journal of Structural Geology 7, 555–562.
Carpenter, M.S.N., 1976. Petrogenetic Study Of The Glaucophane Schists and Associated Rocks from the Ile De Groix. University of Oxford, Brittany, France.
Chopin, C., 2003. Ultrahigh-pressure metamorphism: tracing continental crust into the mantle. Earth and Planetary Science Letters 212 (1–2), 1–14.
Cobbold, P.R., Quinquis, H., 1980. Development of sheath folds in shear regime in "shear zones in rocks". Journal of Structural Geology 2.
Cogné, J., 1954. L'île deGroix (Morbihan) (feuille ile de Groix au 50.000e). Bulletin du Service de la Carte Géologique de France 239, 41–50.
Cogné, J., 1960. Schistes cristallins et granites en bretagne méridionale: le domaine de l'anticlinal de Cornouaille, Rennes.
Felix, C., 1972. Etude structuro-minéralogique des pseudomorphes de présumée Lawsonite des glaucophanoschistes de l'île de Groix (Bretagne-France): considération sur la possibilité d'une paragénèse à Glaucophane -Lawsonite. Annales de la Société Geologique de Belgique 95, 345–391.
Felix, C., Fransolet, A.M., 1972. Pseudomorphes à épidote s.l., paragonite, muscovite s.l., chlorite, albite.,de porphyroblastes de lawsonite (?) dans les glaucophanites de l'île de groix (bretagne – France). Annales de la Société Geologique de Belgique 95, 323–334.
Ganne, J., Marquer, D., Rosenbaum, G., Bertrand, J.M., Fudral, S., 2006. Partitioning of deformation within a subduction channel during exhumation of high-pressure rocks: a case study from the western alps. Journal of Structural Geology, 1193–1207.
Gapais, D., Lagarde, J.L., Le Corre, C., Audren, C., Jegouzo, P., Casas Sainz, A., Van den driessche, J., 1993. The Quiberon shear zone: evidence for Carboniferous extension in the Variscan belt of South Brittany (France). Comptes Rendus de l'Académie des Sciences 316 (8), 1123–1129.
Gumiaux, C., Judenherc, S., Brun, J.P., Gapais, D., Granet, M., Poupinet, G., 2004. Restoration of lithosphere-scale wrenching from integrated structural and tomographic data (Hercynian belt of Western France). Geology 32, 333–336.
Iglesias, M., Brun, J.P., 1976. Signification des variations et anomalies de la déformation dans un segment de la chaîne hercynienne (les séries cristallogra-phylliennes de la Vendée littorale). Bulletin de la Société Géologique de France 7, 1443–1452.
Jeannette, D., 1965. Etude tectonique de l'île de Groix (Morbihan), Rennes.
Jolivet, L., Faccenna, C., Goffé, B., Burov, E., Agard, P., 2003. Subduction tectonics and exhumation of high pressure metamorphic rocks in the Mediterranean orogens. American Journal of Science 303, 353–409.
Judenherc, S., Granet, M., Brun, J.P., Poupinet, G., 2003. The Hercynian collision in the Armorican Massif: evidence of different lithospheric domains inferred from tomography and anisotropy. Bulletin de la Société Géologique de France 174, 45–57.
Lacassin, R., Mattauer, M., 1985. Kilometre-scale sheath fold at Mattmark and implications for transport direction in the Alps. Nature 316, 739–742.
Lamouche, 1929. Etude tectonique de l'île de Groix. Bulletin de la Société de Sciences Naturelles de l'Ouest 4 (IX), 72–87.
Le Hebel, F., Vidal, O., Kienast, J.R., Gapais, D., 2002. Les "Porphyroïdes" de Bretagne méridionale: une unité de HP-BT dans ka chaîne Hercynienne. Comptes Rendus Géoscience Paris 334, 205–211.
Moore, J.C., Allwardt, A., 1980. Progressive deformation of a tertiary trench slope, Kodiak Islands, Alaska. Journal of Geophysical Research 82 (B9), 4741–4756.
Platt, J.P., 1993. Exhumation of high-pressure rocks: a review of concepts and processes. Terra Nova 5 (2), 119–133.
Quinquis, H., Audren, C., Brun, J.P., Cobbold, P.R., 1978. Intense progessive shear in the île de Groix blueschists and compatibility with subduction or obduction. Nature 273, 43–45.
Quinquis, H., Choukroune, P., 1981. Les schistes bleus de l'île de Groix dans la chaîne Hercynienne: implications cinématiques. Bulletin de la Société Géologique de France 7 (XXIII, no. 4), 409–418.
Quinquis, H., Cobbold, P.R., 1978. Etude de plis noncylindriques résultant d'un cisaillement simple. In: R.A.S.T, p. 327. Lyon.
Quinquis, H., 1980. Schistes bleus et déformation progressive: l'exemple de l'Île de Groix (Massif Armoricain). Université de Rennes 1.
Ring, U., Brandon, M.T., Willet, S.D., Lister, G., 1999. Exhumation Processes. In: Geological Society, London, Special Publication, vol. 154, pp. 1–27.
Rosenbaum, G., Avigad, D., Sánchez-Gómez, M., 2002. Coaxial flattening at deep levels of orogenic belts: evidence from blueschists and eclogites on Syros and Sifnos (Cyclades, Greece). Journal of Structural Geology 24 (9), 1457–1462.
Searle, M.P., Alsop, G.I., 2007. Eye-to-eye with a mega–sheath fold: a case study from Wadi Mayh, northern Oman Mountains. Geology 35 (11), 1043–1046.
Shelley, D., Bossière, G., 1999. Ile de groix: retrogression and structural developments in an extensional régime. Journal of Structural Geology 21, 1441–1455.
Stanek, K.P., Maresch, W.V., Grafe, F., Grevel, C.H., Baumann, A., 2006. Structure, tectonics and metamorphic development of the Sancti Spiritus Dome (Eastern Escambray massif, Central Cuba). Geologica Acta 4 (1–2), 151–170.
Triboulet, C., 1974. Les glaucophanites et roches associéesde l'île de Groix (Morbihan, France): étude minéralogique et pétrologique. Contributions to Mineralogy and Petrology 45, 65–90.
Triboulet, C., 1991. Etude geothermo-barométrique comparée des schistes bleus paléozoïques de l'ouest de la France (Ile de Groix, Bretagne méridionale et bois de Céné, Vendée). Comptes Rendus de l'Académie des Sciences 312 (10), 1163–1168.
Trotet, F., Jolivet, L., Vidal, O., 2001. Tectono-metamorphic evolution of Syros and Sifnos islands (Cyclades, Greece). Tectonophysics 338 (2), 179–206.

Il manquait à cette étude de terrain purement structurale des données pétrologiques en particulier pour affirmer que la Lawsonite avait bien une croissance prograde. Car bien qu'étant un minéral du pic de pression, la Lawsonite aurait pu également cristalliser sur le chemin rétrograde. L'étude de El Khore et al 2009, met en évidence que la croissance des Lawsonites groisillonnes est prograde. L'échantillon GR29 dont le chemin PT est présenté dans la figure suivante provient de la baie de Locmaria (localisation voir Philippon et al 2009, Fig. 6a).

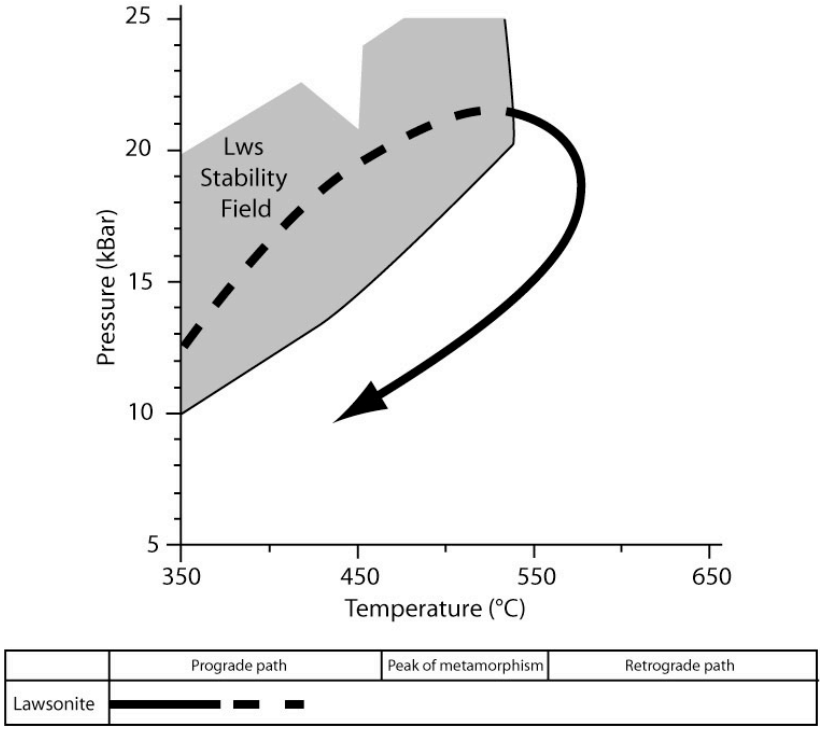

BILAN : Cette étude montre que les schistes bleus de l'île de Groix ont conservés les cinématiques de la subduction et de l'exhumation en fonction de la lithologie. D'un point de vue méthodologique, la distinction entre enfouissement et exhumation des roches métamorphiques de haute pression requiert non seulement l'analyse de la chronologie des sens de cisaillements mais aussi l'analyse de leur distribution spatiale, de leur relation avec la lithologie et le métamorphisme, et de leur configuration par rapport aux structures d'échelle régionale. Cette étude montre que les sens de cisaillements observés ne sont pas synchrones et donc qu'en aucun cas, la déformation est coaxiale. De plus, la présence de pseudomorphes de Lawsonite est particulièrement intéressante. En effet dans les schistes bleus de l'île de Groix, les roches dans lesquelles ils sont conservés n'ont pas été déformées lors de l'exhumation.

ANNEXE D : Carte géologique de l'île de Syros 1 :50000

CARTE GEOLOGIQUE DE L'ÎLE DE SYROS AU 1:50.000

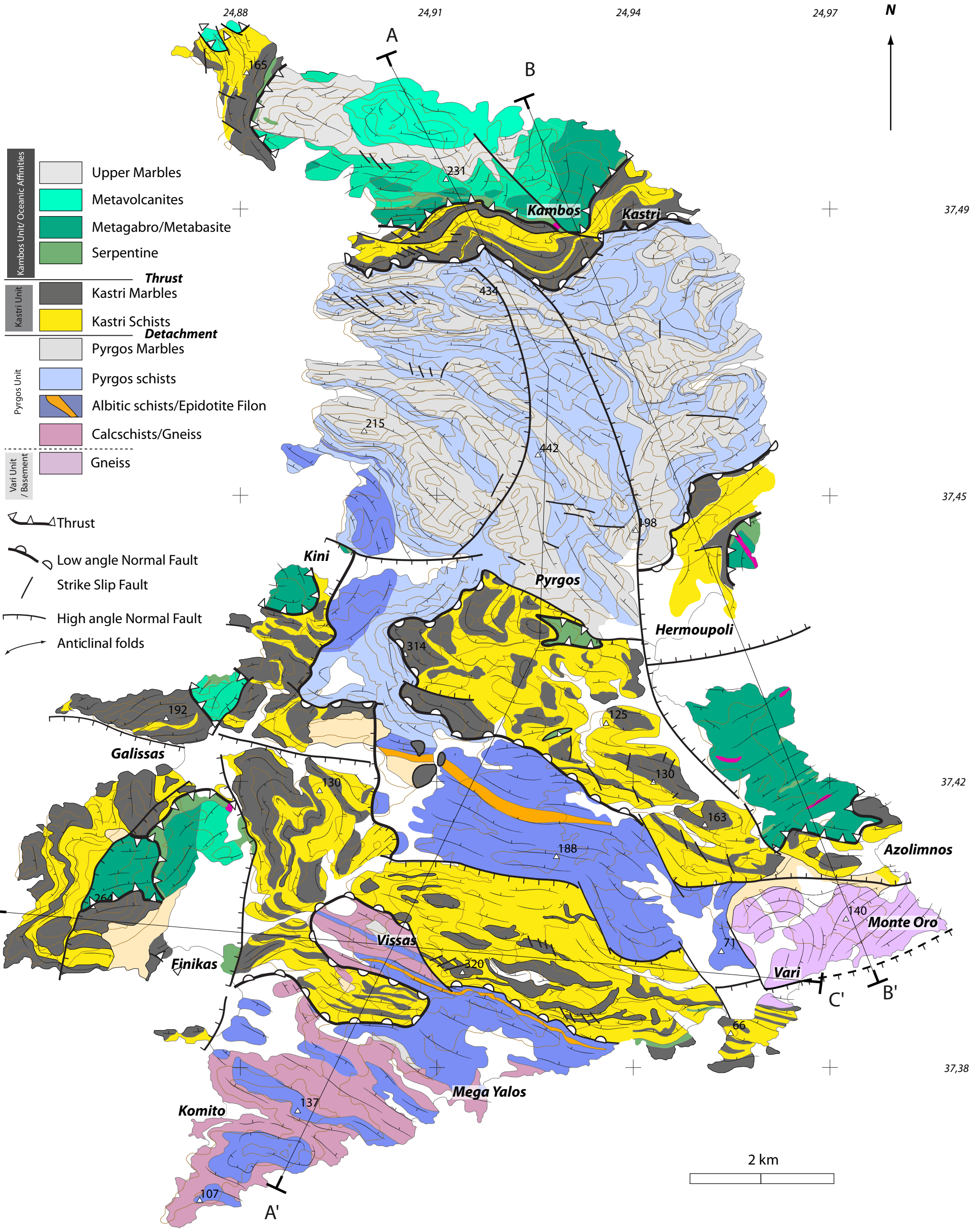

Annexe E : Coupes géologiques de l'île de Syros 1 :50000

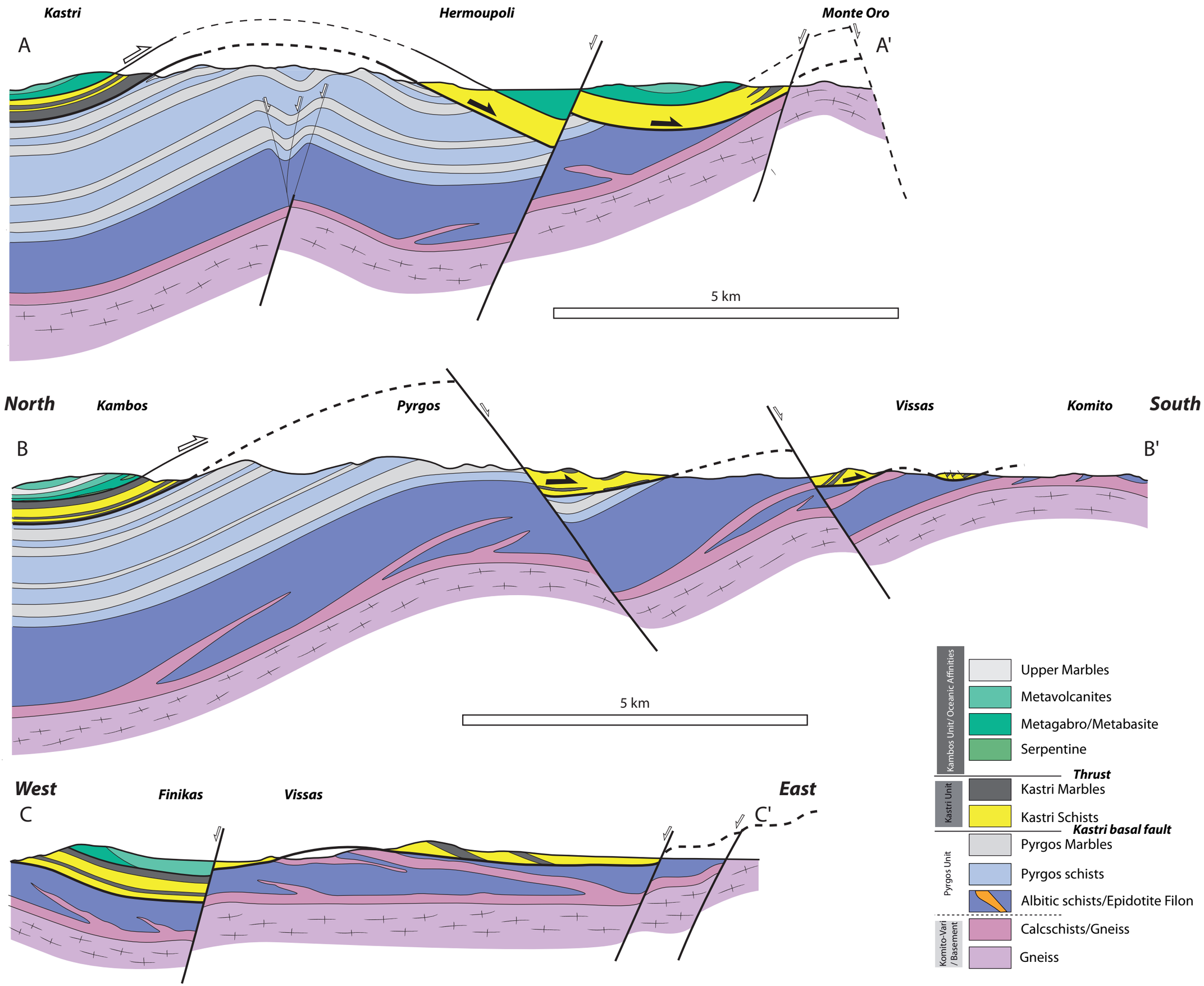
Kastri
Hermoupoli
Monte Oro
A
A'
5 km
North
Kambos
Pyrgos
Vissas
Komito
South
B
B'
5 km
West
Finikas
Vissas
East
C
C'
Kambos Unit/ Oceanic Affinities
Upper Marbles
Metavolcanites
Metagabro/Metabasite
Serpentine
Thrust
Kastri Unit
Kastri Marbles
Kastri Schists
Kastri basal fault
Pyrgos Unit
Pyrgos Marbles
Pyrgos schists
Albitic schists/Epidotite Filon
Komito-Vari / Basement
Calcschists/Gneiss
Gneiss

Annexe F : Dimensionnement des expériences analogiques

		Model	Nature	Dimensionless ratois (model/nature)
Upper crust	Thickness	0.5 cm	7 km	$7.14.\ 10^{-7}$
	Density	1300 $kg.m^{-1}$	2700 $kg.m^{-1}$	0,48
	Coef. of internal Fiction	0.85	0.75	1.1
	Cohesion	15 Pa	6.10^{-7} Pa	$2.5.10^{-7}$
	Strength	77 Pa	$3.3.10^{8}$ Pa	$2.3.\ 10^{-7}$
Lower crust	Tickness	1 cm	18 km	$1.8.\ 10^{-7}$
	Density	1390 kmg^{-3}	3200 kgm^{-3}	0,434375
	Viscosity	$1.3.10^{-4}$	10^{21}	$1.3.10^{-17}$
	Strenght	0,4 Pa	$1.7.10^{6}$ Pa	2,3. 10 -7
	n-Value	1.2		
Lenght		60 cm	600 km	10^{-6}
Strain rate		$14.8.\ 10^{-8} s^{-1}$	$0.825.\ 10^{-13} s^{-1}$	$17.8.\ 10^{-6}$
Time		1s		
Bulk stretching		15 cm	200 km	
Ramberg Number		464	477	0,972746331

Les modèles ont été dimensionnés suivant le principe de la similarité géométrique et dynamique-rhéologique (Ramberg 1981). La similarité géométrique été respectée en réduisant les longueurs par un facteur 10^{-6}, par rapport aux longueurs observées dans la nature. Dans ce but, le modèle à une épaisseur de 1,5 cm afin d'approcher les 25 km d'épaisseur de croûte (Epaisseur moyenne de croûte en Mer Egée Tirel et al., 2004). La distance finale entre le bord fixe de la boîte et les portes est de 75cm et correspond au 750 km observés entre la zone de subduction Héllénique et le Rodhope.

La similiraté dynamique-rhéologique, a été respectée en dimensionnant la pression pression lithostatique, $\sigma^*=\rho^*g\ ^*l^*$, où ρ et g sont respectivement la densité et la constante gravitationnelle. L'astérix indique qu'il s'agît du rapport expérience/nature. Le dimensionnement de l'expérience à été testé en calculant les nombres adimensionnés donnée par le rapport des forces agissant sur le modèle (Ramberg 1981). Pour la déformation ductile, le rapport entre les forces de gravité et la viscosité est donnée par le nombre de Ramberg (qui est proche de 1 pour nos expériences):

$$R_m = (\rho g h^2)/\ \eta\nu$$

Tirel C., Gueydan F., Tiberi C., Brun J.P., (2004), Aegean crustal thickness inferred from gravity inversion. Geodynamical implications. Earth and Planetary Science Letters 228 (3-4), 267-280.

Ramberg H., (1981), Gravity, deformation and the Earth's crust, 2nd ed. Academic Press, London. 452 pp.